DELAY-DIFFERENTIAL MODELS OF CUTTING TOOL DYNAMICS WITH NONLINEAR AND MODE-COUPLING EFFECTS

A Dissertation

Presented to the Faculty of the Graduate School

of Cornell University

in Partial Fulfillment of the Requirements for the Degree of

Doctor of Philosophy

by

Tamás Kalmár-Nagy

January 2002

DELAY-DIFFERENTIAL MODELS OF CUTTING TOOL DYNAMICS WITH NONLINEAR AND MODE-COUPLING EFFECTS

Tamás Kalmár-Nagy, Ph.D.

Cornell University 2002

Advisor: Prof. Francis C. Moon

This Dissertation addresses the problem of the dynamics of machine tool chatter in material removal processes. In particular, this research examines cutting of revolving cylindrical workpieces that introduces time delay into the dynamics equation of motion. The models used in this Dissertation are thus delay-differential equations. The nonlinear dependence of the cutting force on chip thickness (including the dynamic nature of the cutting force) introduces a variety of nonlinear phenomena. The classical single-degree-of-freedom model is analyzed by methods of nonlinear dynamics (Harmonic Balance, Center Manifold Theory, numerical simulations) and the existence of a subcritical Hopf-bifurcation is proved. To obtain the stable upper branch of this bifurcation however, a global motion-limiting nonlinearity (contact loss) is added. In addition, joint experiments were conducted at NIST which provided evidence to validate the above theoretical and numerical results. Another model studied in this Dissertation involves hysteretic cutting force and forcing. The forcing may arise due to rotating imbalance or due to the periodic chip segmentation process. We conjecture that the classical model with nonlinear cutting force and forcing can give rise to complex vibrations. A third-order model

based on a viscoplastic constitutive equation is capable of predicting a stability increase with decreasing rotational speed, while a piecewise linear model predicts quasiperiodic motions below the linear stability boundary. One of the main contributions of this Dissertation is the development of a new three degree-of-freedom lumped-parameter model for oblique cutting. This model shows interesting stability properties, which are partly due to the nonconservative nature of the reduced problem. In particular, this model is shown to exhibit interaction between flutter, divergence and classical delay cutting model instabilities.

Biographical Sketch

Tamás Kalmár-Nagy was born on July 14, 1970 in Budapest, Hungary. He grew up in Budapest and attended Chemical Technical School "Lajos Petrik", where he received a Chemical Technician degree. After graduation from 'Petrik', Tamás went to Bánki Donát Polytechnic, where he was soon overwhelmed with mechanical design courses and honorably discharged himself. He spent the rest of the academic year working as a mailman and preparing for the math and physics entry exams to the Technical University of Budapest. In the Fall of 1990 he started studying mechanical engineering at TUB, majoring in engineering mathematics. He was overwhelmed with mechanical design courses here also, but did not even have time to realize this because of the workload of the other courses. Tamás spent the Spring term of 1994 at the University of Newcastle-upon-Tyne, England as a Tempus fellow, where he worked on modelling particle deposition from turbulent flows. Having liked the adventure abroad, he again left Hungary in the Spring term of 1995 to write his Master Thesis in Trondheim, Norway. This time he worked on Large Eddy Simulation of turbulent plane Couette flows. During his undergraduate years, Tamás submitted five papers for Undergraduate Research Competitions and won numerous awards (two first prizes, two second prizes, one third prize together with a Rector's prize and an extra prize from the Hungarian

Society for Mechanical Engineers).

After graduation (September 1995) Tamás started as a PhD student at the Department of Applied Mechanics of the Technical University of Budapest, under the supervision of Professor Gábor Stépán, working on machine tool vibrations. But he decided to see more of the world and came to Cornell in the Fall of 1996. Since then, he has been a student in the Department of Theoretical and Applied Mechanics working with Professor Francis C. Moon on machine tool vibrations. After finishing his Thesis, Tamás will start a Postdoctoral position with Professor Raffaello D'Andrea in the Department of Mechanical&Aerospace Engineering.

To my family: Pacsmagbéka, Futrinka, Gubacs and to the memory of my grandmother Nagyóca

Acknowledgements

First and foremost, I would like to express my sincere gratitude to Professor Francis C. Moon, my advisor, for his superior guidance through my endeavor. He has always been a constant source of ideas, creative energy and enthusiasm. I have always envied his intuition into engineering problems and I secretly hope that I became endowed with some of it.

I am also greatly indebted to Professors Richard Rand and Raffaello D'Andrea who had the patience to serve on my committee. I learnt a lot on dynamics and control through personal interaction and by their great courses.

Special thanks go to Professors Gábor Stépán and Miklós Farkas at my old school, the Technical University of Budapest, for the solid background in applied mathematics and their encouragement.

The experimental part of this Dissertation was done in collaboration with Dr. Jon Pratt (at NIST, Gaithersburg, MD), for which I am forever grateful.

Professors David Gilsinn, Tim Healey, Herbert Hui, Subrata Mukherjee, Chris Papadopoulos and Steven Yeung provided valuable comments and insights into my research.

I would also like to thank my friends at Cornell, who provided encouragement (not really) and (mostly) criticism. In alphabetical order (that is the only reason

you are not the first one, Wei!) these people are:

Florin "Organic" Bobaru, Matt "Shyguy" Earl, Pritam "BigP" Ganguly, Jayant "Guru" Kulkarni, Cedric "Staplerhand" Langbort, Hsin-man "Cranky" Lu, Basant "Tunaktunaktuntarara" Sharma, Ishan "Your face" Sharma, Mike "Squirrel" Stubna, Wei "Perfect" Zou.

TAM staff Sreemati Mukherjee, Maureen Letteer, Dan Mittler and Peter Brown have always been very helpful and made grad life much easier in the department.

Needless to say, my family was always there in times of need, providing constant support through the years.

Since no one reads acknowledgements, I might as well thank my friends Attila Gali, Zoltán Guttman, Ágnes Jávorszky, Tamás Kálmán, Viktor Lázár, Béla Lindtner, Gábor Molnár, Barnabás Szilágyi and Oszkár Vámosi for being my friends.

Finally, I would like to thank the inventor of Sunshine Mist for providing such a nutritious source of energy that kept me going and the Haunt to provide an outlet for all the excess energy.

Contents

List of Figures

"Basically, a tool is an object that enables you to take advantage of the laws of physics and mechanics in such a way that you can seriously injure yourself. Today, people tend to take tools for granted. If you're ever walking down the street and you notice some people who look particularly smug, the odds are that they are taking tools for granted. If I were you, I'd walk right up and smack them in the face."

Dave Barry, "The Taming of the Screw"

Chapter 1

Introduction

Modern life is unimaginable without manufactured products. The importance of material removal operations is clearly shown by the fact that its associated costs amount to approximately ten percent of the gross national product of industrial nations. Therefore, even minor improvements in productivity would lead to immense savings.

The study of cutting of materials is an old problem, going back 150 years to research in Europe, Japan and North America. The work of 'the father of modern machining' F. W. Taylor (1907) is a prominent example.

Recently, there has been an increased interest in the subject. Higher cutting speeds, new materials and precision machining demand better understanding of the underlying physics. Also, the mathematical and computational tools that are now available opened up new ways to treat this and related problems that were considered intractable even a decade ago. These problems include

- Estimation of the tool vibration amplitude
- Understanding the subcritical instability

- Explanation of small amplitude chaotic vibrations
- Prediction of dynamic chip morphology
- Providing new diagnostics for tool wear
- Suppression of chatter

In this Dissertation we review the development of cutting dynamics modelling in the context of new, low-dimensional nonlinear models and new experimental work in material cutting. Although delay models have been fairly successful in capturing the onset of the large amplitude periodic vibrations, there are also other nonlinear phenomena that require more complex models. A partial list includes (Moon and Kalmár-Nagy, 2001):

- Unsteady chatter vibrations of the cutting tool
- Pre-chatter chaotic or random-like small amplitude cutting vibrations
- Non-regenerative cutting dynamics
- Elasto-thermoplastic instabilities
- Hysteretic effects in cutting dynamics
- Induced electromagnetic voltages at the material-tool interface
- Phase transitions
- Fracture effects

The length of this list serves to suggest that a single degree of freedom regenerative model cannot predict all the important phenomena in cutting dynamics.

However, it is doubtful that a universal model encompassing all the above dynamic problems exist. It is more likely that different models should be used to describe different regimes in cutting. Figure 1.1 shows a *hypothetical* stability chart of a cutting process. The stability boundary shown separates stable and unstable steady-state cutting. For different regimes of the cutting speed-material removal rate parameter space, different physical phenomena might be dominant.

The different (possibly overlapping) boxed domains might be best described by models that include

- Time delay

  The present cut and the one made one revolution earlier might overlap, causing chip thickness (and thus cutting force) variations.

- Friction effects (stick and slip)

  The chip moves along the rake face of the tool, giving rise to friction.

- Thermoplastic instability

  Because of the interplay of thermal softening and strain hardening, periodic chip formation might occur.

- Parametric excitation

  Periodic chip formation may influence the dynamics of the tool.

- Stochasticity

  The tool might be subject to random vibrations due to inhomogeneities in grain structure of the material.

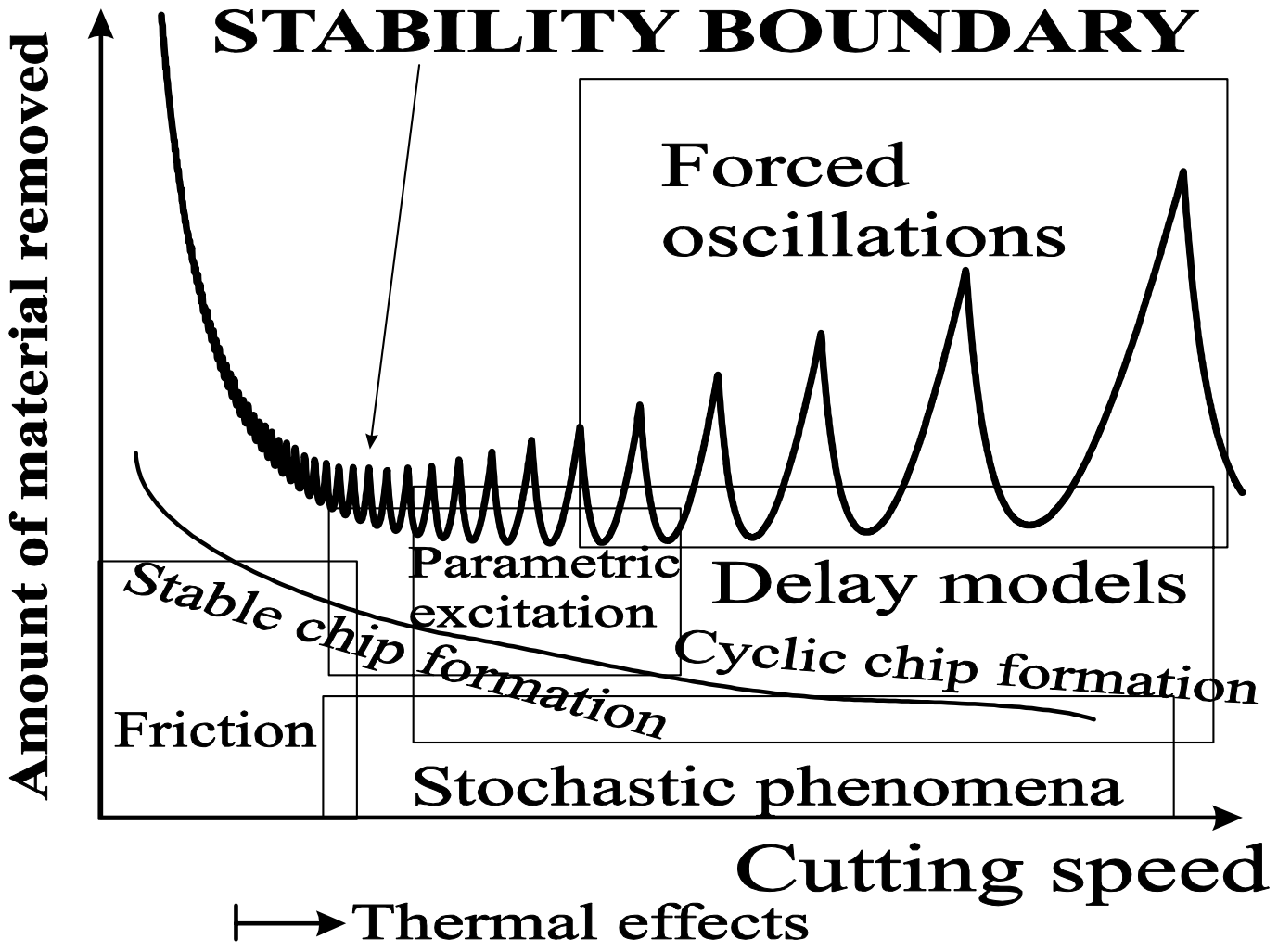

Figure 1.1: *Hypothetical* stability chart and regimes of dominant phenomena.

- Forced oscillations

  Rotating imbalance or misalignment of the workpiece can be a source of excitation.

or combination thereof.

In this Thesis, we focus on models that account for regenerative (time delay) effects and are described by delay-differential equations.

1.1 Contributions

The contributions of the Dissertation can be summarized as:

- New experimental data (in collaboration with NIST)
- Heuristic derivation of the operator equation formulation for delay equations
- General formalism for deriving base functions of the center subspace
- Analysis of the classical 1 DOF tool vibration model

  Harmonic Balance

  Center Manifold Analysis

  Numerical simulations including multiple regenerative effect

- New 1 DOF models

  Harmonically forced nonlinear DDE

  Viscoelastic model

  Piecewise-linear hysteretic cutting force

- Derivation of a new 3 DOF model and its linear analysis

1.2 Organization of the Dissertation

The remaining chapters are organized as follows:

Chapter 2 reviews nonlinear phenomena that have been observed in cutting. Namely, we discuss periodic, quasiperiodic, chaotic and random vibrations that arise in material removal processes. Chapter 3 consists of a survey of existing mathematical models for explaining machine-tool vibrations. These models can be classified as one or two-dimensional, with structural and/or cutting force nonlinearities.

Chapter 4 gives a short tutorial to delay differential equations. Linear stability analysis of these equations is motivated and discussed, including approximations and numerical techniques. Then we present a heuristic argument on how to convert a class of linear delay-differential equations into an operator differential equation on a Banach space, showing how the operator and its adjoint together with the associated bilinear form arises. A simple way of calculating the eigenfunctions of the operator and its adjoint is also described. We then discuss the extension of this argument to nonlinear DDEs in the context of Center Manifold analysis.

A new set of experimental data is presented in Chapter 5. The experiments were done in collaboration with Dr. Jon Pratt at NIST in Gaithersburg, MD, as part of a summer visit in 1998.

The experimental setup is an essentially single-DOF cutting platform. The parameters of the system are identified and the experimental stability boundary is drawn. The cutting force is determined as a function of chip thickness. Experimental data clearly show the existence of subcritical instability (the existence of tool vibrations below the stability boundary). This data also provide the means to verify the correctness of the analysis of the 1 DOF model. Near the intersections

of the stability lobes quasiperiodic tool motions exist. We conclude that delay differential equations (DDEs) are necessary to model machine tool vibrations.

In Chapter 6 we analyze the classical 1 DOF model. Here the structural dynamics of the machine is represented by an equivalent non-linear single-DOF system. The cutting force is assumed to be a function of the chip thickness, which is a function of both the present and delayed displacement of the tool tip. In the first model we consider the cutting force-chip thickness relationship is described as a power law. For the analytic calculations, this function is replaced by its third-order series expansion. First, linear stability is investigated and stability boundaries are drawn. The infinite-dimensional nonlinear delay-differential equation is then represented as an operator differential equation and reduced to a two-dimensional system of ordinary differential equations by the use of Center Manifold Theory at the linear stability boundary. In particular, it is proved that for softening cutting force behavior subcritical Hopf bifurcation exists at the critical value of cutting force coefficient, thus confirming the hysteretic behavior found experimentally. Harmonic Balance approximation is also used to estimate the vibration amplitude. Numerical simulations were also performed, taking contact loss between tool and workpiece into account, giving excellent agreement with experimental results.

Several new one-dimensional delay models are introduced in Chapter 7. First, we analyze the primary resonance of the classical one DOF model with a nonlinear cutting force. Then hysteretic models are developed. One of these is a piecewise-linear cutting force model that has a hysteretic loop depending on the loading-unloading history. Numerical results show that this model exhibits periodic and quasiperiodic oscillations. The other model assumes a viscoelastic constitutive law for the material, thus effectively increasing the order of the classic second-order

model by one. Linear stability of this model is examined.

In Chapter 8 we develop a new 3 degree-of-freedom lumped-parameter model for oblique cutting. One of the equations is stable and uncoupled from the other two, so the stability of the system can be determined by analyzing the other two degrees of freedom.

The Appendices describe mathematical techniques to analyze linear and nonlinear differential equations. We start with a brief discussion of forced linear vibrations, then the Hopf-bifurcation for ordinary differential equations is introduced, then some methods of nonlinear dynamics are summarized.

Chapter 2

Nonlinear Phenomena In Machining

The most common feature of machining operations (such as turning, milling, and drilling) is the removal of a thin layer of material (the chip) from the workpiece using a wedge-shaped tool (Figure 2.1). They also involve relative motion between

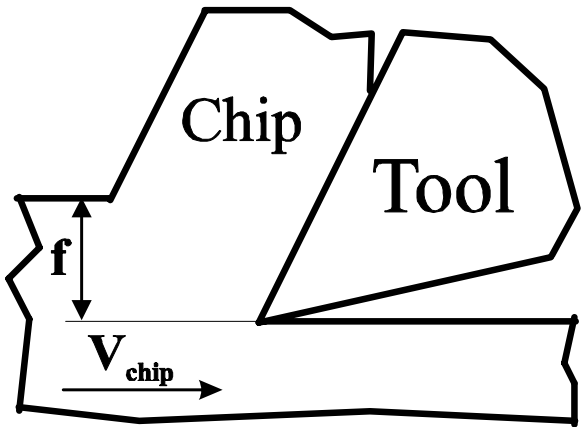

Figure 2.1: Material removal.

the workpiece and the tool. In turning the material is removed from a rotating workpiece, as shown in Figure 2.2.

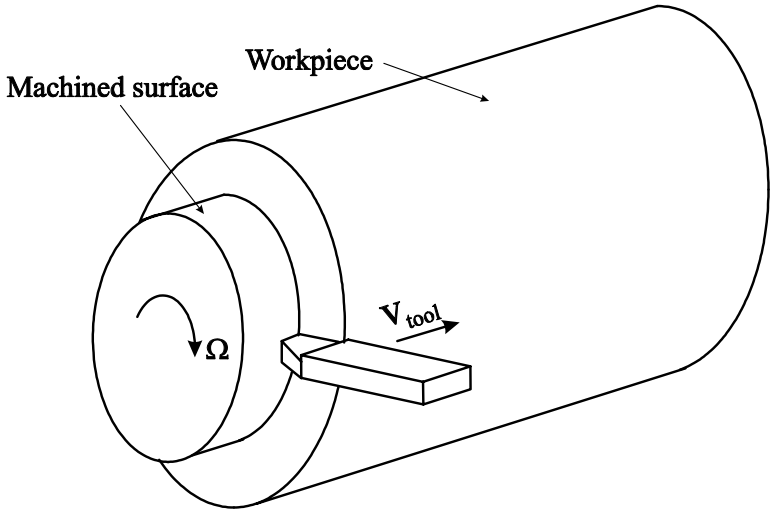

Figure 2.2: Turning.

The cylindrical workpiece rotates with constant angular velocity Ω [rad/s] and the tool is moving along the axis of the workpiece at a constant rate. The feed f is the longitudinal displacement of the tool per revolution of the workpiece, and thus it is also the nominal chip thickness. The translational speed of the tool is then given by

$$v_{tool} = \frac{\Omega}{2\pi} f \tag{2.1}$$

and the chip flow velocity is

$$v_{chip} = \frac{\Omega}{2\pi} r \tag{2.2}$$

where r is the radius of the workpiece.

The interaction between the workpiece and the tool gives rise to vibrations. The phenomenon of the large amplitude vibration of the tool is known as *chatter*. There have been many attempts to describe tool chatter. One of the pioneers of modern machine tool vibrations research, S. A. Tobias (1965) writes

'The machining of metal is often accompanied by a violent relative vibration

between work and tool which is called the chatter. Chatter is undesirable because of its adverse affects on surface finish, machining accuracy, and tool life. Furthermore, chatter is also responsible for reducing output because, if no remedy can be found, metal removal rates have to be lowered until vibration-free performance is obtained.'

Johnson (1996) summarizes several qualitative features of tool vibration

- The tool always appears to vibrate while cutting. The amplitude of the vibration distinguishes chatter from small-amplitude vibrations.
- The tool vibration typically has a strong periodic component which approximately coincides with a natural frequency of the tool.
- The amplitude of the oscillation is typically modulated and often in a random way. The amplitude modulation is present in both the chattering and non-chattering cases.

The nature of the tool vibration can be

- Periodic
- Quasiperiodic (the frequencies of the vibration are incommensurate)
- Chaotic (the frequency spectrum is broadband)
- Stochastic (the signal exhibits noise-like behavior)

These vibrations can further be categorized as self-excited vibrations or vibrations due to external sources of excitation, such as resonances of the machine structure.

A great deal of experimental work has been carried out in machining to characterize and quantify the dynamics of metal cutting (for an overview, see Tlusty (1978)). The source of nonlinearities and chatter mechanisms are also discussed by Wiercigroch and Budak (2001).

2.1 Cutting Force Nonlinearities

The most important characteristics of the cutting process is that the cutting force depends nonlinearly on several cutting parameters and it has a dynamic nature (it can exhibit active hysteresis). In the following we describe some well-known cutting force nonlinearities.

2.1.1 Nonlinear Dependence on Chip Thickness

Taylor (1907) was the first to document nonlinear cutting force dependence on chip thickness. He found the steady-state thrust force to be the function of the cutting parameters such as the chip width w, the chip thickness f, and the cutting speed v. He proposed the simple relationship

$$F = Kwf^n \tag{2.3}$$

where K is a material-dependent constant. In the NIST experiments (see Chapter 5 and also Kalmár-Nagy et al., 1999) the value of n was found to be 0.41 (for aluminium). Oxley and Hastings (1977) present steady state forces as function of chip thickness for carbon steel. However these force measurements are quasi-steady and were taken to be single valued functions of chip thickness and material flow velocity.

2.1.2 Nonlinear Cutting Speed Dependence

Arnold's pioneering experiments (1946) showed that cutting force decreases with increasing cutting speed (Figure 2.3). This phenomenon is analogous to dry friction. Oxley and Hastings (1977) also measured a decrease of cutting force versus material flow velocity in steel. One plausible explanation for this decrease is that with increasing cutting velocity the temperature on the rake face will become high enough to melt the material, thus decreasing friction. Grabec (1986) used this non-

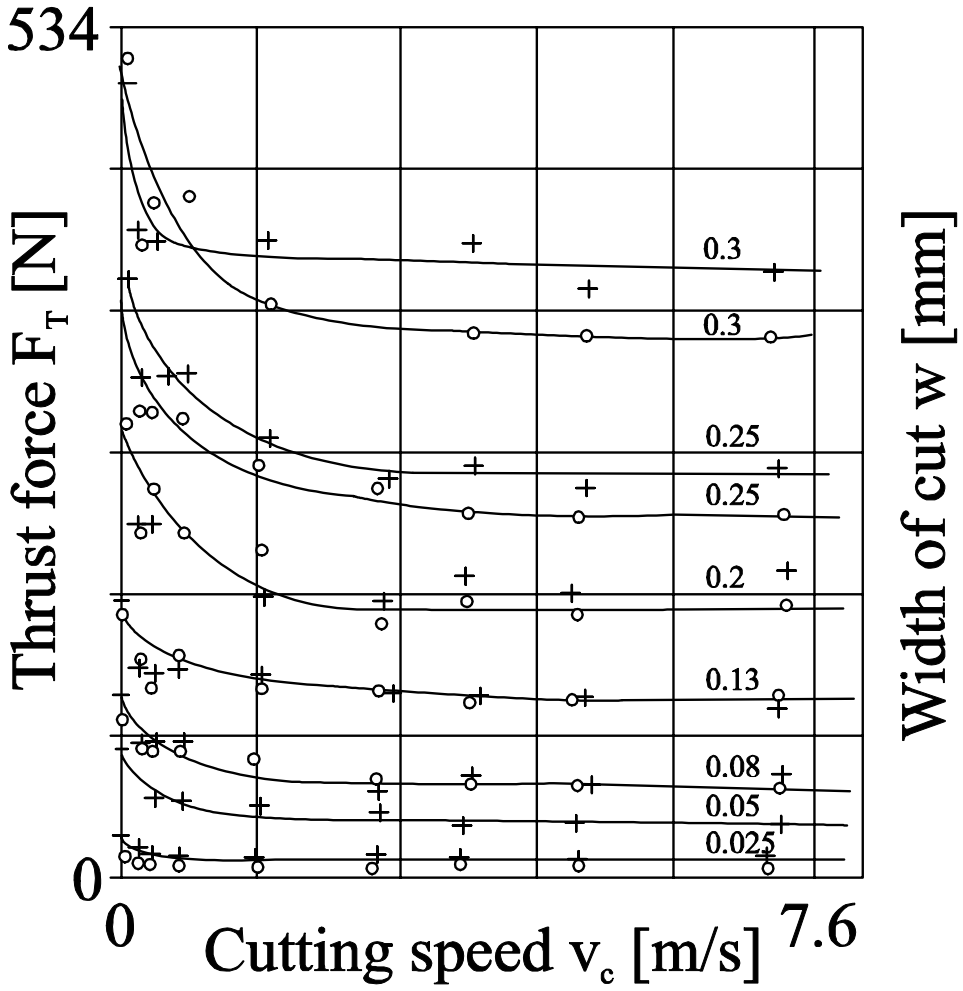

Figure 2.3: Cutting force versus speed. After Arnold (1946).

linearity to show the possibility of chaos in cutting dynamics. His papers sparked a new interest in nonlinear cutting dynamics (see also Wiercigroch and Krivtsov, 2001).

2.1.3 Hysteresis

As shown by Albrecht (1965) and Szakovits and D'Souza (1976) the cutting force-chip thickness relation exhibits hysteresis. This hysteresis depends on the cutting speed, the frequency of chip segmentation, the functional angles of the tool's edges, etc. (Kudinov et al., 1978). Tobias (1965, p. 236) illustrates that F_t, as measured using a vibrating tool, can exhibit a hysteretic dependence on a dynamically varying chip thickness. In Albrecht's experiments (1965) a tubular steel workpiece was orthogonally machined. The tool was mounted on a special two-component dynamometer that could be activated in the feed direction by a hydraulic cylinder. The chip thickness was artificially varied by sinusoidally moving the tool (with frequency of 400 Hz). This gave rise to dynamic response of the cutting forces. The cutting and thrust forces were recorded together with the variation of the chip thickness. Figures 2.4 and 2.5 show the cutting force F_C and the thrust force F_T as functions of chip thickness and tool velocity. The steady-state forces were observed to be much higher than the dynamic ones.

2.2 Time-Delay Effects in Turning

One of the most important effects causing vibrations in a cutting process is due to delay. Because of some external disturbances the tool starts a damped oscillation relative to the workpiece thus making its surface uneven. After one revolution of

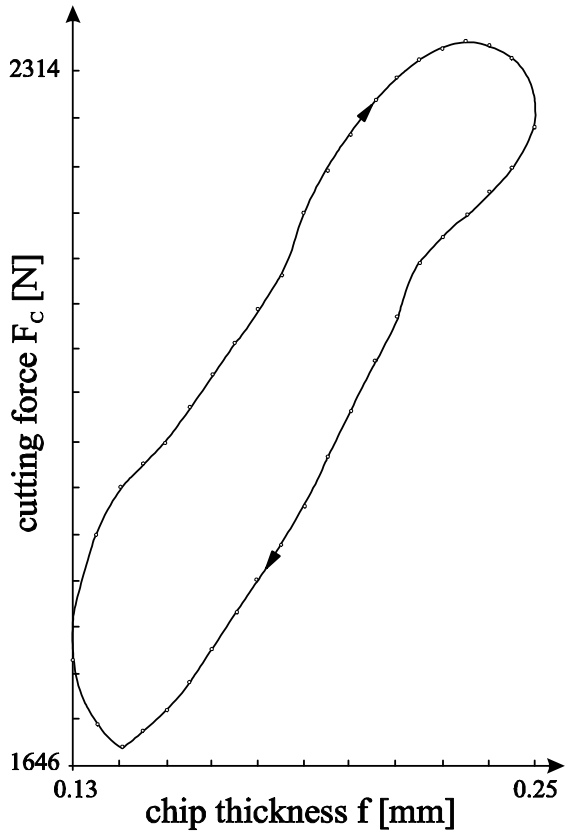

Figure 2.4: Hysteretic behavior of the cutting force. After Albrecht (1965).

the workpiece the chip thickness will vary at the tool (Figure 2.6). This is the so-called *regenerative effect*. The length of this delay is the time-period τ of one revolution of the workpiece

$$\tau = \frac{2\pi}{\Omega} \tag{2.4}$$

In a seminal paper, Hooke and Tobias (1963) described machining experiments in which the tool was hit while turning. A measured time series of the amplitude of the tool oscillation, including the initial disturbance (the hammer blow) is show in Figure 2.7. The tick marks along the horizontal axis correspond to one revolution of the workpiece. The chatter builds up on the same time scale as the time required for one workpiece revolution. This gives strong support to the concept of regenerative

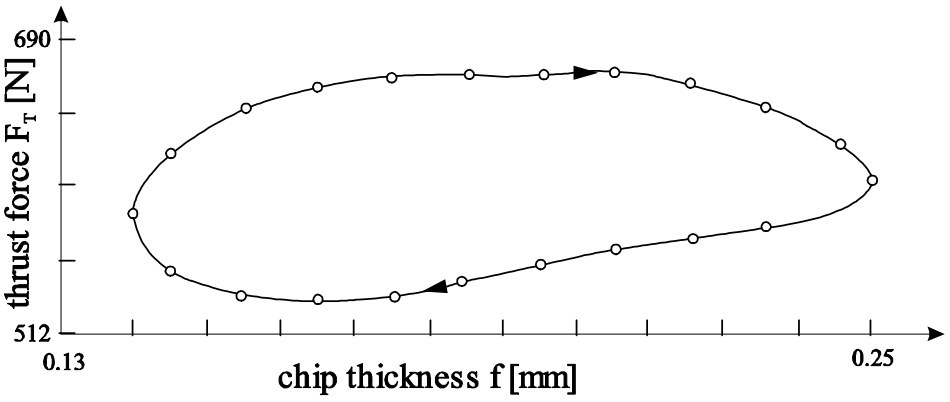

Figure 2.5: Hysteretic behavior of the thrust force. After Albrecht (1965).

chatter.

2.3 Multiple Regenerative Effect

Another important phenomenon is the *multiple regenerative effect*. When the chatter amplitude exceeds a certain value, the contact ceases between the tool and the workpiece and the tool starts a damped vibration until it comes in contact with the workpiece again. When this happens, the uncut chip thickness is affected by the trace of the tool motion even from two or more previous turns before. This process is the culprit for generating chatter marks on the machined surface. Figure 2.8 shows the trace of catastrophic tool vibrations on the machined workpiece surface in thread cutting.

Doi and Kato (1956) performed some beautiful experiments on chatter. They examined the relationship between the undeformed chip thickness and cutting force and found that the lagging of the horizontal cutting force behind the horizontal vibration of the workpiece is the cause of chatter. This so-called *short delay* is much smaller than the time needed for one revolution of the workpiece. These

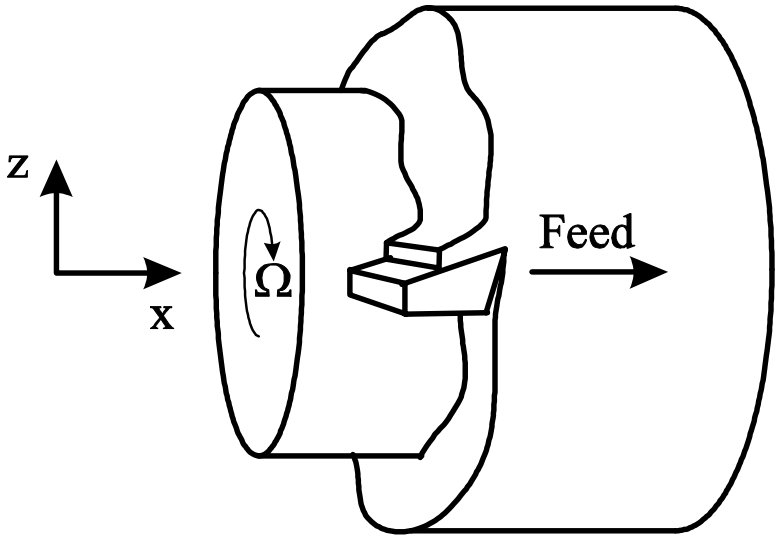

Figure 2.6: Regenerative effect in turning.

researchers presented the earliest nonlinear delay-differential equation model for tool vibrations (see next Chapter).

2.4 Periodic Vibrations

Hooke and Tobias (1963) also demonstrated that perturbations (the hammer blows) might lead to chatter even under normally chatter free cutting conditions. They gradually increased the width of cut and recorded the amplitude of the ensuing vibrations with and without the hammer blow. Their diagram is shown in Figure 2.9. The points along the curves labeled A in this Figure represent experiments without the hammer blow, while those along the curves labelled B correspond experiments with the hammer blow. From the diagram it appears that for a width of cut less than 1.27 mm, the cutting remains stable. However, somewhere between 0.25 and 0.5 mm, the hammer blow induced large amplitude vibrations (hence the term 'finite amplitude instability'). The graph has a striking resemblance to a

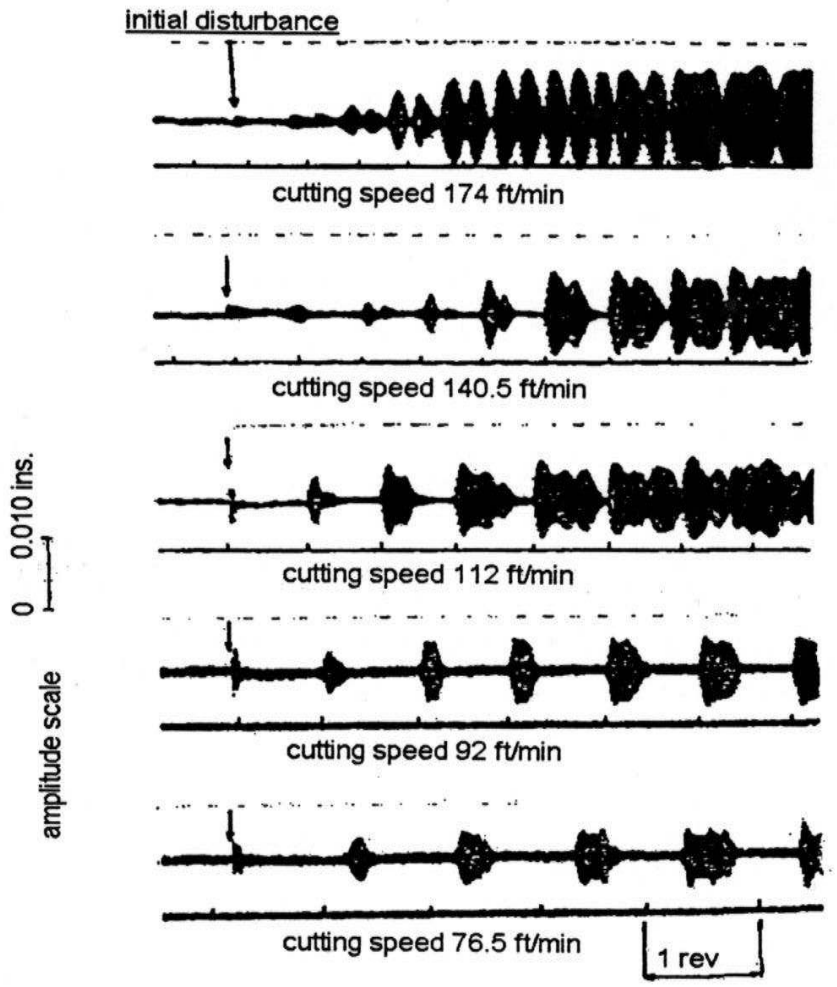

Figure 2.7: Chatter build-up. From Hooke and Tobias (1963).

Hopf bifurcation curve (see Appendix B). In fact these curves might be interpreted as subcritical Hopf bifurcations. While the trivial (steady-state) solution remains stable for the range of widths studied, the hammer blow is sufficient to move the system 'outside' an unstable limit cycle, onto the stable branch B of Figure 2.9.

Figure 2.8: Machined surface after thread cutting. From Stépán (2001).

2.5 Quasiperiodic Tool Vibrations

Several researchers observed quasiperiodic vibrations during machining. Hahn (1953) reported that the vibration of a boring bar "alternately dies out and becomes re-excited", while Saljé (1956) described "low frequency beats" in orthogonal cutting. Thompson (1969) presents strong experimental evidence of amplitude-modulated chatter. Sample time-series are shown in Figure 2.10. Spectral analysis showed two (and in one case three) distinct frequencies with sidebands. While forced vibrations can also result in modulation of chatter amplitude, Thompson argues that the regenerative effect is the cause. The sidebanding can be attributed to the ubiquitous mode-coupling.

Moon (1994) observed quasiperiodic looking vibrations in cutting aluminium alloys. Stépán (2001) measured oscillations during thread cutting (Figure 2.11). The experimentally determined vibration frequencies were compared to the pre-

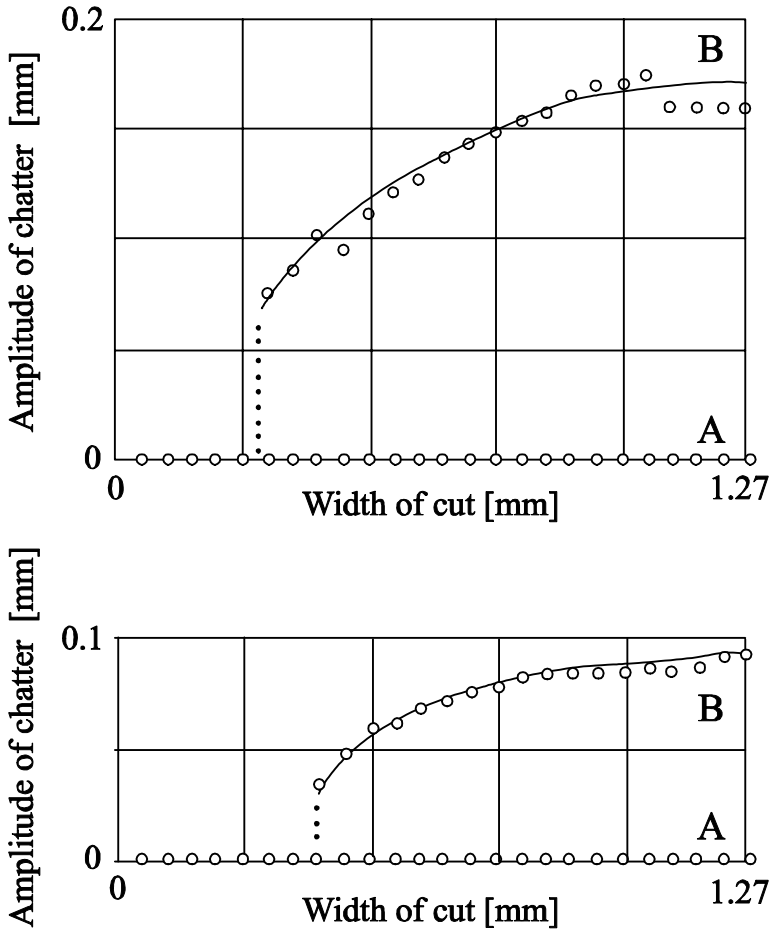

Figure 2.9: Experimental bifurcation diagram of Hooke and Tobias (1963).

diction of the linear theory. The stability chart is shown in Figure 2.12.

As this chart shows, two different frequencies may occur at certain cutting speeds (the lower the cutting speed is, the closer these frequencies are). Quasiperiodic oscillations with slightly different frequencies produce slowly modulating vibrations. These vibrations have been detected experimentally.

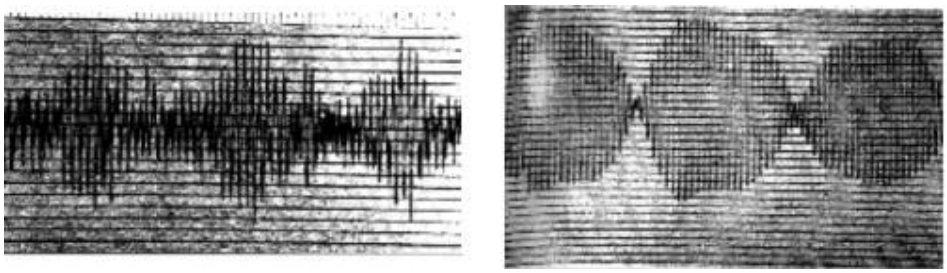

Figure 2.10: Quasiperiodic vibration. From Thompson (1969).

2.6 Complex Vibrations in Nonregenerative Cutting

Complex dynamics can also occur in nonregenerative cutting. An example is shown in Figures 2.13, 2.14, 2.15 for a diamond stylus cutting polycarbonate plates on a turntable (Moon and Callaway, 1997; see also Moon and Kalmár-Nagy, 2001). The width of the cut was smaller than the turning pitch so that there was no overlap and no regenerative or delay effects. The time history of the vibrations of the 16 cm cantilevered stylus holder is shown in Figure 2.14, along with a photo of the cut tracks. The cut tracks appear to be fairly uniform even though the tool vibrations appear to be random or chaotic. When the cutting speed is increased however, the cutting width become highly irregular. And the vibrations become more periodic looking. A FNN of the unsteady vibrations seems to indicate that the dynamics of Figure 2.14 could be captured in a four or five dimension phase space lending evidence that the motion may be deterministic chaos. A summary of these experiments is shown in Figure 2.15 in the parameter plane of stylus dead load versus cutting speed of the turntable.

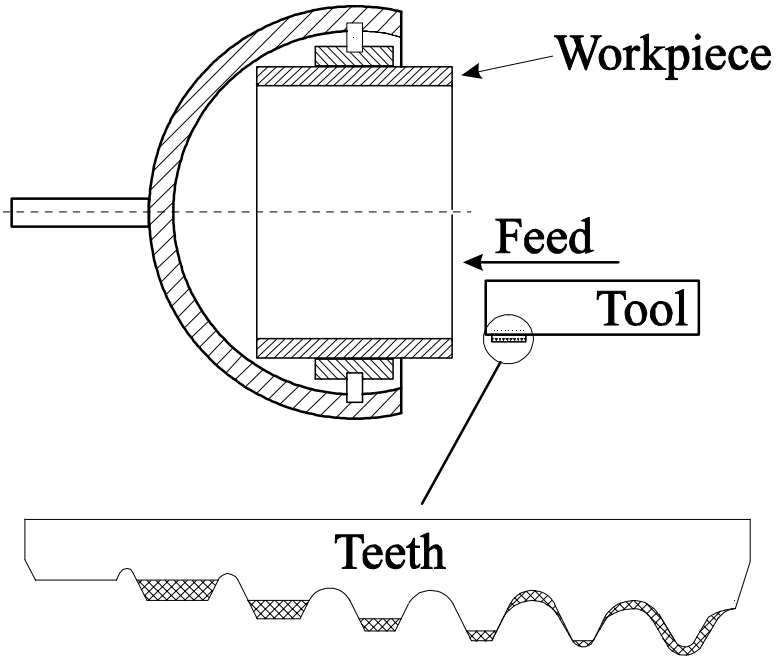

Figure 2.11: Thread cutting. After Stépán (2001).

2.7 Chip Formation

Another possible explanation for complex dynamics is the shear banding instabilities in metals (see for example Komanduri and Brown, 1981). Landberg (1956) investigated periodic chip formation. He determined that the frequency of the process was close to the natural frequency of the tool. Albrecht (1961) also observed cyclic chip formation under normal cutting conditions. His explanation for the chip segmentation is based on cracks developing due to fatigue. This is also supported by the research of Vyas and Shaw (1997). The experiments of Doi and Ohhashi (1992) seem to indicate that chip formation frequency is proportional to the cutting speed. On the other hand, researchers at NIST (Davies, Chou and Evans, 1996) found much higher frequencies (order of 50 kHz, while typical tool frequencies are 1-2 kHz). If this is the case, downloading of energy from high to

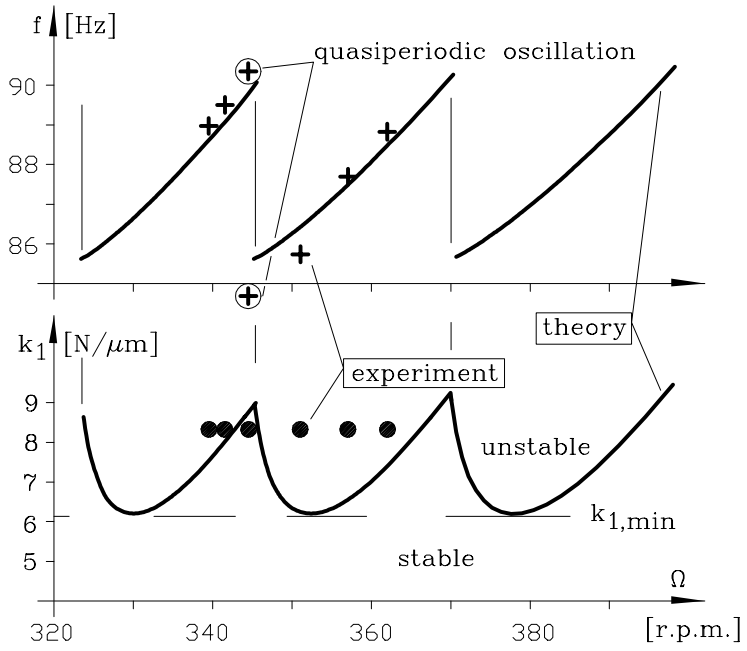

Figure 2.12: Stability chart for thread cutting. From Stépán (2001).

low frequency might be responsible for the observed complex vibrations (Nayfeh and Nayfeh, 1993; see also Tcherniak, 1999).

2.8 Chaos or Randomness?

This Section is based on Moon and Kalmár-Nagy (2001). Recently a number of researchers have provided experimental evidence that tool vibrations in turning may be chaotic (Moon, 1994; Bukkapatnam et al., 1995 and Johnson, 1996). Moon's experiments in the turning of aluminium (using reconstructed phase portraits, probability distribution functions, and Fourier power spectra) showed that tool vibrations are possibly chaotic. Bukkapatnam et al. (1995) applied statistical measures and calculated Lyapunov exponents to verify that dynamic force measurements in the turning of steel exhibit low-dimensional chaotic behavior. Berger

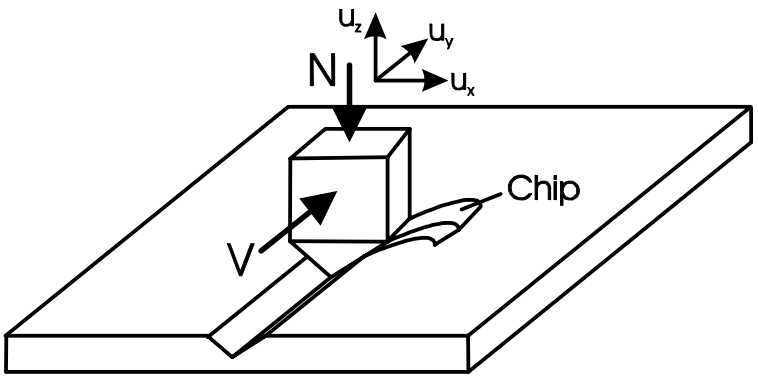

Figure 2.13: Nonregenerative cutting.

Figure 2.14: Time history for cutting of polycarbonate with a diamond stylus and magnification of cut surface (Moon and Callaway, 1999; Moon and Kalmár-Nagy, 2001).

et al. (1995) used the method of false nearest neighbors to show that tool accelerations in the turning of mild steel exhibit low-dimensional chaos and they assert that the chaotic attractor associated with the cutting process can be embedded in a four-dimensional space. Moon and Abarbanel (1995) also used the false nearest neighbors algorithm to show that tool vibrations in the turning of aluminium can be characterized by a low-dimensional attractor, and this attractor can be embedded in a space ranging in dimension from four to six. The above experiments strongly suggest the use of nonlinear dynamics in describing tool vibrations and

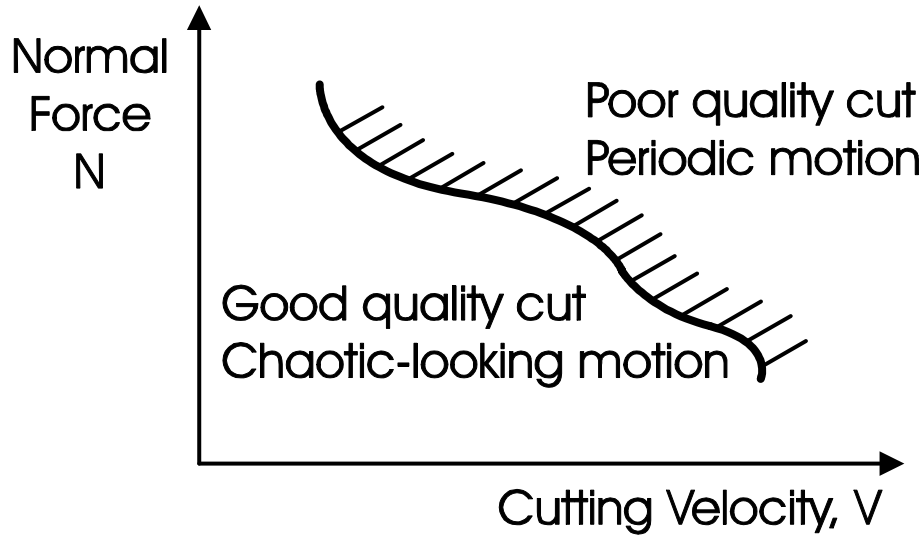

Figure 2.15: Stylus dead load versus cutting speed for diamond stylus on polycarbonate plates (Moon and Callaway).

chatter. These experiments were inspired in part by earlier simulations of a theoretical model by Grabec (1986, 1988) based on a velocity dependent cutting force for which the model exhibited chaotic vibrations.

The time series analysis method has become popular in recent years to analyze many dynamic physical phenomena from ocean waves, heartbeats, lasers and machine tool cutting (see e.g. Abarbanel, 1996). This method is based on the use of a series of digitally sampled data $\{x_i\}$ from which the user constructs an orbit in a pseudo-M-dimensional phase space.

One of the fundamental objectives of this method is to place a bound on the dimension of the underlying phase space from which the dynamic data was sampled. This can be done with several statistical methods involving fractal dimension, false nearest neighbors (FNN), Lyapunov exponents, wavelets and several others.

However, if model based analysis can be criticized for its simplistic models,

then nonlinear time series analysis can be criticized for its assumed generality. Although it can be used for a wide variety of applications, it contains *no physics*. It is dependent on the data alone. Thus, the results may be sensitive to the signal to noise ratio of the source measurement, signal filtering, the time delay of the sampling, the number of data points in the sampling and whether the sensor captures the essential dynamics of the process.

One of the fundamental questions regarding the physics of cutting solid materials is the nature and origin of low level vibrations in so called *normal* or good machining. This is cutting below the chatter threshold. Below this threshold, linear models predict no self excited motion. Yet when cutting tools are instrumented, one can see random-like bursts of oscillations with a center frequency near the tool natural frequency. Work by Johnson (1996) has carefully shown that these vibrations are significantly above any machine noise in a lathe turning operation. These observations have been done by several laboratories and time series methodology has been used to diagnose the data to determine whether the signals are random or deterministic chaos (Berger et al., 1992, 1995; Minis and Berger, 1998; Bukkapatnam et al., 1995a,b, 1999; Moon, 1994; Moon and Abarbanel, 1995; Johnson, 1996; Gradišek et al., 1998).

One of the new techniques for examining dynamical systems from time series measurements is the method of FNN (see Abarbanel, 1996). Given a temporal series of data $\{x_i\}$ one can construct an M dimensional vector space of vectors, $(x_1, \ldots, x_M)$, $(x_2, \ldots, x_{M+1})$, etc., whose topological properties will be similar to the real phase space if one had access to M state variables. The method is used to determine the smallest dimension phase space in which the orbital trajectory does not intersect itself. Thus if the reconstructed phase space is of too low a

dimension, some orbits will appear to cross and some of the points on the orbits will be *false neighbors*. In an ideal calculation, as the embedding dimension M increases, the number of such false neighbors goes to zero. One then assumes that the attractor has been unraveled. This gives an estimate of the dimension of the low order nonlinear model that one hopes will be found to predict the time series.

Using data from low level cutting of aluminum for example, the FNN method predicts a finite dimension for the phase space of between four and five (Moon and Johnson, 1998). This low dimension suggests that these low level vibrations may have a deterministic origin, such as in chip shear band instabilities or chip fracture processes. Minis and Berger (1998) have also used the FNN method in pre-chatter experiments on mild steel and also obtained a dimension between four and five. These experiments and others (Bukkapatnam et al., 1995a,b) suggest that *normal cutting operations may be naturally chaotic*. This idea would suggest that a small amount of *chaos may actually be good in machining*, since it introduces many scales in the surface topology.

In spite of the evidence from time series analysis that normal cutting of metals and plastics may be deterministic chaos, there is no apparent experimental evidence for the usual bifurcations attendant to classic low dimensional nonlinear mappings or flows. However traditional explanations for this low level noise do not seem to fit the observations. It was originally thought that the source of irregularity in chatter is the random resistance of the workpiece when non-homogeneous material with rough surface was cut. However, later experiments showed that chatter exists when machining homogeneous materials with polished surfaces. This indicates that the irregularity of chatter must be attributed to the dynamics of the process itself. Claims that the noise is the result of random grain structure in the material

are not convincing since the grain size in metals is of 10 - 100 microns which would lead to frequencies in the 100 kHz range, whereas the cutting noise is usually in the 1kHz range or lower. Besides the grain structure theory would not apply to plastics as in the above discussion of cutting polycarbonate. Another possible explanation is the shear banding instabilities in metals (see previous Section). But the wavelengths here are also in the 10 micron range and lead to a spectrum with higher frequency content than that observed in cutting noise.

One possible candidate explanation might be tool-chip friction. A friction model was used by Grabec (1986) in his pioneering paper on chaos in machining. However in a recent paper (Gradišek et al., 1998) they now disavow the chaos theory for cutting and claim that the vibrations are random noise (see also Wiercigroch and Cheng, 1997).

So the controversy about the random or deterministic chaos nature of the dynamics of normal cutting of materials remains.

Chapter 3

Physics and Modeling of Metal Cutting

In order to understand and control machine tool vibrations, it is essential to develop accurate models of the machining process. In order to achieve this, the following three major areas should be carefully studied

- Dynamics of the workpiece and machine structure
- Machine tool dynamics
- The coupling between workpiece and tool (cutting forces)

The coupling between the workpiece and the tool occurs because the material of the workpiece is being cut, flowing along the rake face of the tool.

3.1 Physics of Metal Cutting

The Figure below shows a two-dimensional view of orthogonal metal cutting (the chip has a width of w in the third dimension, this is also called the *width of cut*).

The angle α between the face of the tool (the *rake face*) and the vertical through

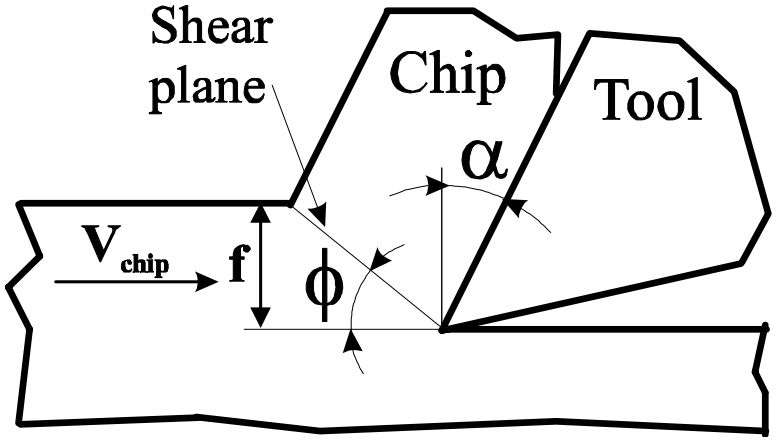

Figure 3.1: Orthogonal cutting.

the tip of the tool is called the *rake-angle*. The so-called primary deformation (or shear) zone extends from the cutting edge to the work surface ahead of the tool. An idealization of this zone is a plane (*shear plane*) which is inclined at an angle φ. The secondary deformation zone lies along the rake face.

A good explanation of the chip forming process is provided by Rogers (1979):

"because of the tool-workpiece geometry in orthogonal cutting, there are two zones of intense shear. The primary shear zone results from the initial deformation of the layer to be removed. The geometry of the metal chip flow is such that, after shearing, the metal in the forming chip is forced to flow normally to the surface of the solid being machined. This flow is also parallel to the rake face of the tool against which the chip is forced with considerable pressure. Frictional heating causes the chip to seize on the rake face. The differential flow between the dead metal at the rake face and the rapidly moving chip takes place over the narrow zone of secondary shear."

The type of chip produced depends on the machined material and the cutting

conditions. Continuous chip is common during machining of most ductile materials (e.g. mild steel, aluminium). If the temperature on the rake face becomes sufficiently high (because of friction), the chip material is welded onto the tool face. Friction is then further increased, and a layered structure of chip material builds up. This structure is usually referred to as a *built-up edge*.

If the work material is brittle (or the cutting speed is sufficiently large), fracture could occur in the primary deformation zone when the chip is only partly formed. The resulting chip is discontinuous. This results in increased tool wear, decreased tool life and degraded surface finish.

A hierarchy of length scales exist in the mechanics of machining. The range of scales vary from the size of dislocation planes ($\sim 10^{-9}$ m) through shear bands ($\sim 10^{-6}$ m) up to the chip size ($\sim 10^{-3}$ m) spanning six orders of magnitude. The implications for modeling are far-reaching. One can naturally ask: how to bridge these scales?

On one hand the analysis should connect the cutting force with cutting speed and tool geometry. This is also the level where the regenerative effect enters the physical picture. A deeper level of analysis addresses stress and strain distributions including strain rate and temperature. This would establish a connection between metallurgy and machining theory with the use of constitutive equations. These equations are relationships between stress, strain, strain rate, temperature and other (hidden) variables concerning the structure and state of the material. Thus the chip formation problem requires the following set of equations

- The continuity equation
- The equation of motion

- The energy balance equation (the first law of thermodynamics)
- Clausius-Duhem inequality (the second law of thermodynamics)
- The constitutive equation of the material

Further, it is necessary to provide initial and boundary conditions.

As it is imperative to have some approximations of the cutting forces, a lot of attention has been focused on chip formation models. In the next Section we take a look at some of these.

3.2 Theories of Chip Formation

The first attempts to explain chip formation were in the 1870's. Piispanen proposed his famous deck-of-cards model in 1937.

The assumptions in these models are usually

- The cutting speed v_C is constant
- The chip thickness f is constant and small compared to the cut width w
- The tool is a perfectly sharp rigid body
- The chip is continuous
- The workpiece material is homogeneous, isotropic and incompressible

3.2.1 Ernst and Merchant Model

The first more complete characterization is due to Ernst and Merchant (1941). Their model is based on the existence of a single shear plane (Figure 3.2).

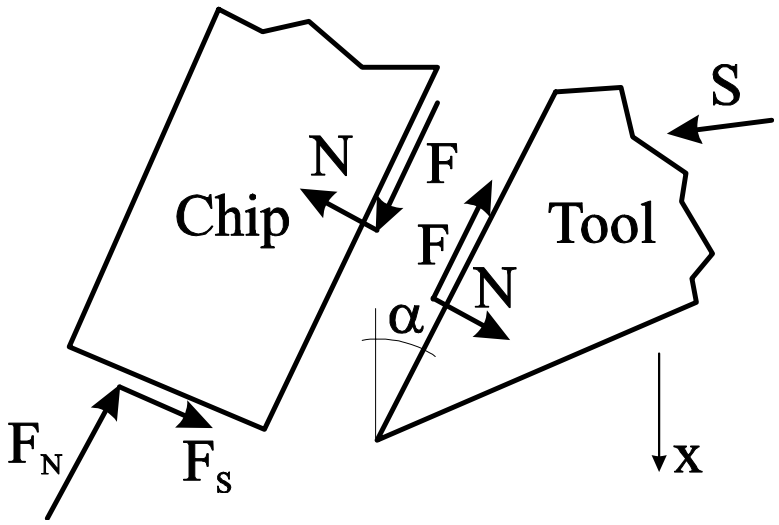

Figure 3.2: The Merchant model.

Each layer of the workpiece material is rigid until it enters the shear plane, where shear occurs instantaneously and the new layer is caused to slide as a rigid body up on the rake face. The chip behaves as a rigid body held in equilibrium by the forces on the chip-tool interface and those of transmitted across the shear plane. Thus linear momentum balance can be written for the sliding block. The stress distribution on the rake face can be resolved into a normal force N, and a friction force F. The resultant force on the tool in the x-direction, known as the thrust force F_t, is given by

$$F_t = -|F|\cos\alpha + |N|\sin\alpha \tag{3.1}$$

where α is the rake angle of the tool. The normal and tangential force components on the shear plane are denoted by F_N and F_S. The friction angle is denoted by λ. Then

$$F_S - \sqrt{F^2 + N^2}\cos(\phi + \lambda - \alpha) = 0 \tag{3.2}$$

where $F_S = \frac{f\tau_y}{\sin\phi}$ with τ_y being the plane strain yield shear stress of the material.

Thus

$$\sqrt{F^2 + N^2} = \frac{f\tau_y}{\sin\phi\cos\left(\phi + \lambda - \alpha\right)} \tag{3.3}$$

The cutting force F_C can then be expressed as

$$F_C = \sqrt{F^2 + N^2}\cos\left(\lambda - \alpha\right) = \frac{f\tau_y \cos\left(\lambda - \alpha\right)}{\sin\phi\cos\left(\phi + \lambda - \alpha\right)} \tag{3.4}$$

Then the following assumptions are made: the shear angle is the one that minimizes F_C (i.e. shear angle takes a value to minimize the work done) and $f\tau_y, \lambda$ is independent of ϕ. To achieve this minimum, $\sin\phi\cos\left(\phi + \lambda - \alpha\right)$ needs to be maximal. Equating the derivative with zero yields

$$\frac{d}{d\phi}\sin\phi\cos\left(\phi + \lambda - \alpha\right) = \cos\left(2\phi + \lambda - \alpha\right) = 0 \tag{3.5}$$

hence

$$2\phi + \lambda - \alpha = \frac{\pi}{2} \tag{3.6}$$

and

$$\frac{d^2}{d\phi^2}\sin\phi\cos\left(\phi + \lambda - \alpha\right)\Big|_{2\phi+\lambda-\alpha=\frac{\pi}{2}} = -2\sin\left(2\phi + \lambda - \alpha\right)|_{2\phi+\lambda-\alpha=\frac{\pi}{2}} = -2 < 0 \tag{3.7}$$

therefore (3.6) really corresponds to the angle minimizing F_C.

This theory was found to give good agreement when cutting synthetic plastics but resulted in inaccurate shear angles for machining steel (Merchant, 1945). Rubenstein (1983) showed that the minimum work hypothesis is erroneous, leading to an unsatisfiable condition.

A modified Merchant model with the assumption that the shear strength of the material increases linearly with increasing shear plane normal stress yields

$$2\phi + \lambda - \alpha = C \tag{3.8}$$

3.2.2 Lee and Shaffer model

Lee and Shaffer (1951) applied plasticity theory to orthogonal cutting (slip-line field theory to analyze the deformation of a rigid-perfectly plastic solid under conditions of plane strain) with the following assumptions:

- Material is rigid-plastic
- Rate independent material behavior
- No temperature effects
- No inertia effects

3.2.3 Burns and Davies Model

Our recent understanding of segmented chip formation can concisely summarized as (Shaw, 1954): "chip segmentation is due to the onset of instability in the cutting process, resulting from competing thermal softening and strain hardening mechanisms in the primary shear zone".

In the last several years several dynamic models have examined basic material nonlinearities including thermal softening (see Davies et al., 1996; Davies and Burns, 2001).

Burns and Davies (1997) treated cutting as a nonlinear dynamical system that includes a mechanism for thermomechanical feedback in the region where the tool-tip and workpiece material are in contact. The model is based on the shear-plane assumption together with the one that there is a local deformation zone (it is based on the observation that the tool distributes a load in the workpiece a certain distance back from the primary shear zone). This deformation process is treated as

local compression. The elastic stress Σ is proportional to the strain ε as

$$\Sigma = E\varepsilon \tag{3.9}$$

where E is the modulus of elasticity. The strain arises because the tool is capable of pushing or pulling on the chip (b is the chip thickness)

$$\varepsilon = \frac{\Delta u}{b} = \frac{u_{tool} - u_{chip}}{b} \tag{3.10}$$

A differential equation for the elastic stress can be obtained by differentiating (3.9) and using (3.10)

$$\frac{d\Sigma}{dt} = E\frac{d\varepsilon}{dt} = \frac{E}{b}\left(v_{tool} - v_{chip}\right) \tag{3.11}$$

As the stress evolves it causes the shear stress τ to build up in the primary shear zone. To see this balance of forces (we ignore the inertial terms) can be written for the Free Body Diagram shown in Fig 3.3.

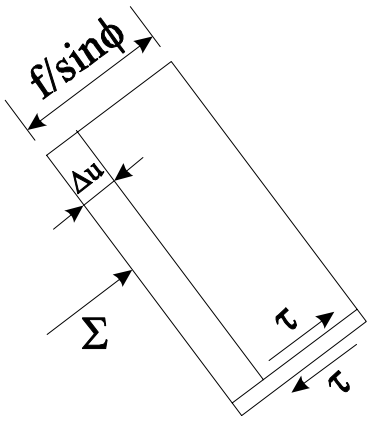

Figure 3.3: Chip formation model of Burns and Davies.

$$\Sigma L w - \tau w b = 0 \tag{3.12}$$

where L is the contact length and w is the chip width (accordingly, Lw is the contact area). Differentiating (3.12) w.r.t time (and assuming that L is constant) leads to

$$\frac{d\tau}{dt} = \frac{L}{b}\frac{d\Sigma}{dt} = \frac{El}{b^2}\left(v_{tool} - v_{chip}\right) \tag{3.13}$$

The initial shear stress elastically deforms the material in the primary shear zone ($v_{chip} = 0$) but after a while it exceeds the yield stress τ_y resulting in plastic deformation ($v_{chip} > 0$). The change in chip velocity gives rise to a plastic strain rate $\dot{\gamma}^p = \frac{v_{chip}}{h}$. This strain rate will be responsible for dissipating the shear energy. Also heat balance equation can be written for the shear zone. After nondimensionalizing this heat balance equation and (3.13) the following system of equations is obtained

$$\frac{d\tau}{dt} = 1 - \Phi \tag{3.14}$$

$$\frac{dT}{dt} = -\xi T + \eta\tau\Phi \tag{3.15}$$

And finally a constitutive equation is needed that specifies the irreversible plastic flow response of the material. One choice is to use Arrhenius kinetics

$$\Phi\left(\tau, T\right) = \exp\frac{\tau - (1 - \nu T)}{\epsilon\left(1 + T\right)} \tag{3.16}$$

Here, ϵ is the strain-rate sensitivity of the material, ν is the thermal softening parameter.

The resulting mathematical model shares many similarities with models of open chemical reactors. In fact, as the cutting speed is increased, a supercritical Hopf bifurcation (see Appendix B) from steady-state to oscillatory behavior occurs in computer simulations of the model, which is consistent with the experimentally observed change from continuous to segmented chip formation.

To obtain an analytical criterion for the material and cutting conditions at which this bifurcation occurs, the researchers developed a related but simpler lumped-parameters model. In another paper, Burns and Davies (1997) demonstrated that a Hopf bifurcation provides a dimensionless group of parameters directly proportional to the cutting speed that predicts the onset of discontinuous chip formation, and is consistent with experimental observations on hardened steel and copper.

3.3 Modeling Machine Tool Vibrations

The sources of nonlinearity in machine tool dynamics are

- Structural nonlinearities
- Cutting force nonlinearities

The principal nonlinear effects on cutting forces include

- Material constitutive relations (stress vs. strain, strain rate and temperature)
- Friction at the tool-chip interface
- Loss of tool-workpiece contact
- Influence of machine drive unit on the cutting flow velocity

The vibrations of the machine tool can be categorized as self-excited vibrations or vibrations due to external sources of excitation, such as resonances of the machine structure. Self-excited vibrations may be due to

- Regenerative effects

- Coupling between modes of the system (coupled mode chatter)
- Parametric excitation caused by chip formation
- Friction effects

These instabilities can be likened to other phenomena such as fluid-structure flutter, rail-wheel instabilities, stick-slip friction vibrations, etc. However, the regenerative model seems to be unique to material processing systems. It appears in turning, drilling, milling, grinding and rolling operations.

3.3.1 Modeling Surface Regeneration

The principle of regenerative chatter in face turning is illustrated in Figure 3.4. In regenerative chatter, the surface generated by the tool on one pass becomes

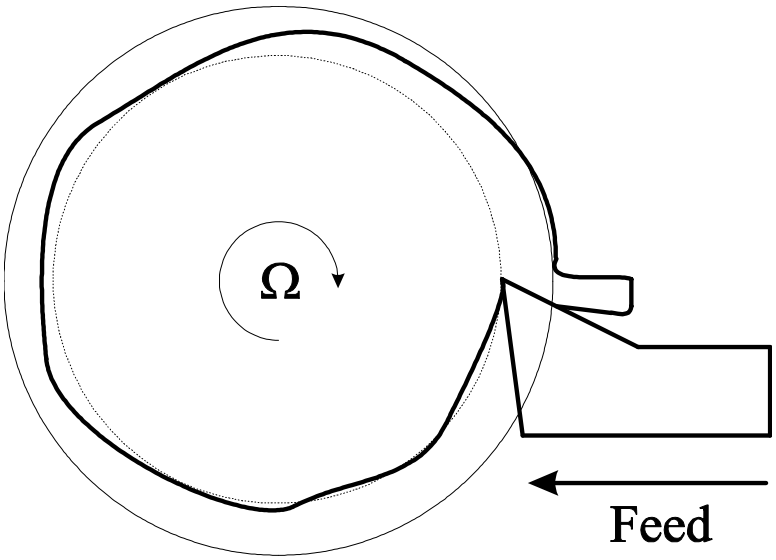

Figure 3.4: Surface regeneration in face cutting.

the upper surface of the subsequent pass. Thus, the thickness of the chip depends

upon the location of the tool now, and the location one revolution ago. The delay is the time required for the workpiece to complete one revolution.

The chip thickness can thus be written as a departure from the steady chip thickness f_0, i.e.

$$f = f_0 + \Delta f \tag{3.17}$$

where the chip thickness variation Δf is expressed as

$$\Delta f = x\left(t - \tau\right) - x\left(t\right) \tag{3.18}$$

The time delay τ is the time of revolution of the workpiece. It is directly related to the angular rate Ω, i.e.

$$\tau = 2\pi/\Omega \tag{3.19}$$

If the tool does not vibrate, the chip thickness is equal to the nominal feed rate f_0.

3.3.2 Modeling the Machine Tool

Figure 3.5 shows a 1 DOF lumped mechanical model of the regenerative machine tool vibration in the case of the so-called orthogonal cutting. The tool is characterized by the mass m, damping c and stiffness k. The model is the simplest one which still explains the basic stability problems and nonlinear vibrations arising in cutting (Tlusty and Spacek, 1954; Stépán, 1989; Stépán, 1997). Sometimes nonlinear stiffness terms are added to the tool stiffness (Hanna and Tobias, 1974). In practice however, these nonlinear terms are very small, even in a cantilevered boring bar. The corresponding Free Body Diagram (ignoring horizontal forces) is also shown in Figure 3.5. Here $\Delta l = l - l_0 + x\left(t\right)$ where l, l_0 are the initial spring length and spring length in steady state cutting, respectively. The zero value of

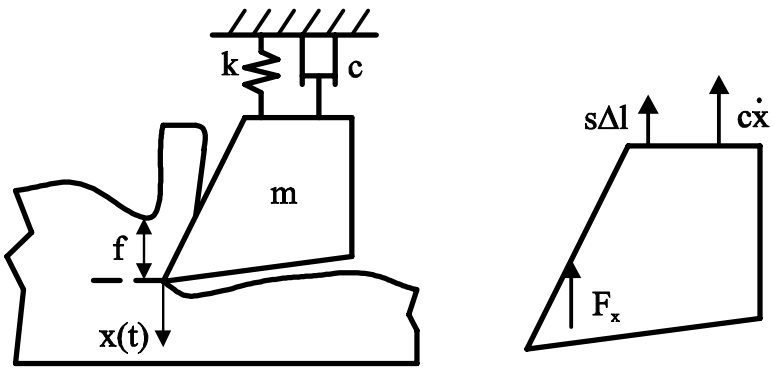

Figure 3.5: 1 DOF mechanical model.

the general coordinate $x(t)$ of the tool edge position is set in a way that the x component F_x of the cutting force F is in balance with the spring force when the chip thickness f is just the prescribed value f_0 (steady state cutting).
The equation of motion of the tool is clearly

$$m\ddot{x} = -s\Delta l - F_x - c\dot{x} \tag{3.20}$$

In steady state cutting ($x = \dot{x} = \ddot{x} = 0$)

$$0 = -s(l - l_0) - F_x(f_0) \Rightarrow F_x(f_0) = -s(l - l_0) \tag{3.21}$$

i.e., there is pre-stress in the spring. If we write $F_x = F_x(f_0) + \Delta F_x$ then Equation (3.20) becomes

$$m\ddot{x} + c\dot{x} + kx = -\Delta F_x \tag{3.22}$$

which can also be written as

$$\ddot{x} + 2\zeta\omega_n\dot{x} + \omega_n^2 x = -\frac{1}{m}\Delta F_x \tag{3.23}$$

Here $\omega_n = \sqrt{s/m}$ is the natural angular frequency of the undamped free oscillating system, and $\zeta = c/(2m\omega_n)$ is the so-called relative damping factor.

The calculation of the cutting force variation ΔF_x requires an expression of the cutting force as a function of the technological parameters, primarily as a function of the chip thickness f which depends on the position x of the tool edge.

3.3.3 Cutting Force Models

The fundamental nonlinearities in material processing usually involve nonlinear relations between stress and strain, or stress and temperature or chemical kinetics and solid state reactions in the material. There is a long history of force measurements in the literature over the past century. Many of these data are based on an assumption of a steady process. Thus, in most cutting force measurements the speed and depth of cut are fixed and the average force is measured as a function of steady material speed and cutting depth. However, this begs the question as to the real dynamic nature of the process. In a dynamic process what happens when the cutting depth instantaneously decreases? Does one follow the average force-depth curve or is there an unloading path similar to elastoplastic unloading? Average force measurements filter out the dynamic nature of the process.

Of course, there have been attempts to characterize dynamic cutting forces (see Chapter 2). These experiments suggest that the cutting force can indeed depend on the loading history.

Stationary Cutting Force Models

The steady-state cutting force (thrust force) F is often expressed as an empirical function of the technological parameters like the chip width w, the chip thickness f, and the cutting speed v. A simple but empirical way to calculate the cutting force is using a curve fitted to data obtained from cutting tests. One popular

steady cutting force versus chip thickness relationship is that proposed by Taylor (1907)

$$F = Kwf^n \tag{3.24}$$

where w is the chip width and K is a material-dependent constant. For aluminium the value of n was found to be 0.41 (see Chapter 5 and also Kalmár-Nagy et al., 1999). Equation (3.24) is a softening force law.

Shi and Tobias (1984) gave a third-order polynomial fit for the cutting force (similar to Figure 3.6). The coefficient of the second order term is negative which

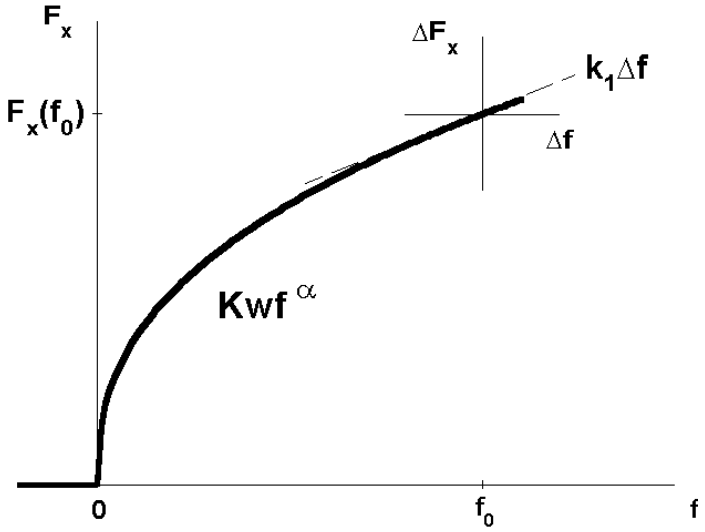

Figure 3.6: Cutting force and chip thickness relation.

is consistent with Taylor's finding of a simple power law with exponent less than 1.

In recent years more complete studies have been published, such as Oxley and Hastings (1977). In this work they present steady state forces as function of chip thickness and cutting velocity for carbon steel. For example, they measured a decrease of cutting force versus material flow velocity in steel. They also measured

the cutting forces for different tool rake angles. However the force measurements themselves are quasi-steady and were taken to be single valued functions of chip thickness and material flow velocity. Kalpakjian (1984, p. 488) observed in the turning of cold-rolled steel that, for rake angles between 10° and 40°, and chip thickness less than 0.15 mm, the thrust force F_t is nearly proportional to the chip thickness f. Tobias (1965, p. 236) found similar relation in the turning of steel. Johnson's (1996) experiments also showed that F_t is approximately proportional to the chip width.

Hysteretic Cutting Force Models

There have only been a few attempts to derive tool vibration models with hysteretic cutting forces. As mentioned in Chapter 2, there have been several investigations into the dynamic nature of the cutting force. Saravanja-Fabris (1972; see also Saravanja-Fabris and D'Souza, 1974) incorporates hysteretic effects into the classical tool vibration model (using the experimental results of Albrecht, 1965) and performs nonlinear stability analysis by means of the describing function method. Similar analysis is given in Chiriacescu (1990). Hysteretic cutting force models will be discussed in Chapter 7.

3.3.4 Putting it All Together: Mathematical Models for Tool Vibrations

Sokolovskii (1946) and Arnold (1946) were one of the first researchers who recognized the importance of nonlinearities describing tool chatter. They considered a non-linear, velocity dependent cutting force to explain negative damping. Arnold

proposed the nonlinear differential equation

$$M\ddot{x}(t) - [A + Bx(t) - \phi(x(t))]\dot{x}(t) + F'x(t) = K \tag{3.25}$$

where M, A, B, F' and K are constants, and $\phi(x)$ is an unspecified function which represents the dependence of the system damping on the tool motion $x(t)$.

Doi and Kato (1956) proposed the following model for tool vibrations

$$m\ddot{x} + c\dot{x} + kx + \mu x(t - \tau) = 0 \tag{3.26}$$

where μ is the overlap factor.

Even when the thrust force depends nonlinearly on the chip thickness, the chip thickness variation is usually small compared to the nominal thickness f. These observations provide some motivation for expanding the function F_t in a Taylor series about f_0 and retaining only the linear term.

After linearizing the cutting force variation (ΔF) at some nominal chip thickness the linearized equation of motion of classical regenerative chatter becomes (see e.g. Stépán, 1989)

$$\ddot{x} + 2\zeta\omega_n\dot{x} + \omega_n^2 x = \frac{k_1}{m}(x - x_\tau) \tag{3.27}$$

where x_τ denotes the delayed value of $x(t)$. The cutting force coefficient k_1 is the slope of the cutting force at the nominal chip thickness. In nondimensional form

$$\ddot{x} + 2\zeta\dot{x} + x = p(x - x_\tau) \tag{3.28}$$

where

$$p = \frac{k_1}{m\omega_n^2} \tag{3.29}$$

This equation will be referred to as the *classical linear model*.

Another early delay model was developed by Tobias and Fishwick (1958)

$$m\ddot{x} + c\dot{x} + kx + z_c k_1 \left(x - x\left(t - \tau\right) + \sigma_1 \dot{x}\right) = 0 \tag{3.30}$$

where σ_1 is the penetration factor (the sign discrepancy with (3.28) is due to the opposite orientation of the coordinate system). The book of Tobias (1965) provides several other examples of linear delay equations used as models for chatter in milling, drilling and turning. The disadvantage of these kind of equations in modelling self-sustained tool vibrations was pointed out by Lin and Weng (1991):

"many efforts have been made to predict the stability boundaries using the linear theory of chatter. As far as the linear theory is concerned, the amplitude of chatter ought to increase indefinitely once the width of cut exceeds a certain critical value, the process becomes unstable. However, the linear theory cannot provide exhaustive information about the properties of well developed chatter."

Hanna and Tobias (1969) considered non-linear structural responses as well. As they pointed out the static stiffness of joints in machine tools and the dynamic response of guideways show non-linear characteristics. Their experimental findings show that small nonlinearity might be present in the structure. Hanna and Tobias (1974) introduced the following nonlinear delay differential equation to describe regenerative chatter in face milling

$$\ddot{x} + \frac{hp^2}{\lambda\omega}\dot{x} + \lambda\left(x + \beta_1 x^2 + \beta_2 x^3\right) = -k_1\left[\Delta f + C_1 \Delta f^2 + C_2 \Delta f^3\right] \tag{3.31}$$

The constants $p, b, \lambda, \omega, \beta_1, \beta_2, k_1, C_1$ and C_2 all relate to a lumped parameter one degree of freedom model.

Other groups have used nonlinear dynamics methodology to study cutting chatter (Moon, 1994; Bukkapatnam et al., 1995; Wiercigroch and Cheng, 1997; Stépán

and Kalmár-Nagy, 1997; Litak et al., 1997; Nayfeh et al., 1998; Minis and Berger, 1998; Moon and Johnson, 1998, 2001).

3.4 2 DOF Models

Generally, a 2 DOF model for tool vibration can be written as

$$\ddot{x} + 2\zeta\dot{x} + x = -dF_x \tag{3.32}$$

$$\ddot{y} + 2\omega_y\zeta_y\dot{y} + y = -dF_y$$

Nigm, Sadek, and Tobias (1977) derived expressions for the chip-thickness ratio and the force ratio in terms of the rake angle, cutting speed, and feed by using dimensional analysis. In a companion paper (1977b) they considered oscillation of the shear plane caused by variation in the cutting parameter. They derived the following expressions for the incremental force components

$$dF_x = wk_s\left[C_1\left(x - x_\tau\right) + \frac{C_2}{v_0}\dot{x} + \frac{C_3}{v_0}\left(\dot{x} - \dot{x}_\tau\right)\right]$$
$$dF_y = wk_s\left[T_1\left(x - x_\tau\right) + \frac{T_2}{v_0}\dot{x} + \frac{T_3}{v_0}\left(\dot{x} - \dot{x}_\tau\right)\right]$$

where the constants C_i, T_i are determined from the geometry of the cut.

Wu and Liu (1985) derived a dynamic shear-angle relation based on Merchant's equations. This relationship is basically a first order approximation for shear-angle oscillations about the mean cutting condition. By assuming a constant length shear plane they arrive at

$$F_x = -2w\tau\left(x_0 - x\right)\left[A_x - C_x v_0 + B_x\left(\dot{x} - \dot{x}_0\right)\right] - f_p$$

$$F_y = 2w\tau\left(x_0 - x\right)\left[A_y - C_y v_0 + B_y\left(\dot{x} - \dot{x}_0\right)\right] \tag{3.33}$$

where the ploughing force f_p is approximated as

$$f_p = \frac{Kw}{v_0}\dot{x} \tag{3.34}$$

Lin and Weng (1991) considered a 2 DOF model with a multiple regenerative effect. They applied the orthogonal cutting model to a description of the nonlinear dependence of cutting forces on the variation of the shear angle when the feed rate changes. Then they analyzed numerical results using phase plane and spectral distributions. The dynamic cutting force generated in the material removal process oscillates the structure and it varies the actual depth of cut. They obtained a third-order expansion for the shear-angle variation and thus obtained the force increments

$$\begin{aligned} dF_x = A_x b\left(x_\tau - x\right) + b\left(f + x_\tau - x\right)\left\{\frac{B_x}{v_0}\left(\dot{x} - \dot{x}_\tau\right) + \right. \\ +C_x\left(\frac{\dot{x}_\tau - \dot{x}}{v_0}\right)^2 + B_x\frac{\dot{x}_\tau\dot{y}_\tau - \dot{x}\dot{y}}{v_0^2} + B_x\frac{\dot{x}_\tau^3 - \dot{x}^3 - 3\left(\dot{x}_\tau\dot{y}_\tau^2 - \dot{x}\dot{y}^2\right)}{3v_0^3} - \\ \left. -C_x\frac{2\left(f + x_\tau - x\right)\left(\dot{x}_\tau\dot{y}_\tau - \dot{x}\dot{y}\right)}{v_0^3} - D_x\left(\frac{\dot{x}_\tau - \dot{x}}{v_0}\right)^3\right\} \end{aligned} \tag{3.35}$$

and dF_y is the same as dF_x with the subscripts x changed to y.

$A_x,\ B_x,\ C_x,\ D_x,\ A_y,\ B_y,\ C_y,\ D_y$ are constant parameters, v_0 is the cutting speed, f is the nominal feed rate, and b is the chip width. Lin and Weng's original model allows for the tool to leave the workpiece, while (3.32) is a simplified version which assumes the tool does not loose contact with the workpiece.

Setting $A_x = \frac{k_s}{m}$ and $B_x = C_x = D_x = A_y = B_y = C_y = D_y = 0$ restricts the model to one degree of freedom and eliminates all nonlinearities, thus reducing this model to the classic one for regenerative chatter for the particular case of $\omega_0 = 1$.

Berger, Rokni and Minis (1992) considered a system with two degrees of free-

dom, denoted by $x_1(t)$ and $x_2(t)$, as a model for vibrations in turning

$$\dot{x}_1 = v_1$$

$$\dot{x}_2 = v_2 \tag{3.36}$$

$$\dot{v}_1 = (x_1 - x_{1\tau})\left[a_3(v_2 - v_{2\tau}) - a_2(v_1 - v_{1\tau})\right] - a_8 x_1 - a_7 v_1 + a_1 x_{1\tau} - \\ - a_{11} v_1^3 \tag{3.37}$$

$$\dot{v}_2 = (x_1 - x_{1\tau})\left[a_6(v_2 - v_{2\tau}) - a5(v_1 - v_{1\tau})\right] - a_4 x_1 - a_{10} x_2 - a_9 v_2 - \\ - a_4 x_{1\tau} - a_{12} v_2^3$$

where the twelve constants depend on the cutting conditions. This model can also be reduced to the classic one by setting $a_1 = a_2 = a_3 = a_{11} = 0$, $a_7 = 2\zeta\omega_0$, $a_8 = \omega_0^2$, $k_s b/m = -1$.

Empirical relations derived from the work of Hastings, Mathew, and Oxley (1980) were used by Grabec (1986, 1988) to propose a nonregenerative, two degree of freedom model for cutting that predicted chaotic dynamics. He assumes that the thrust force is related to the main cutting force through a friction coefficient μ

$$F_x = \mu F_y$$

He also assumes cutting force dependence on the cutting speed and chip thickness as

$$F_y = F_{y0}\frac{s}{s_0}\left[C_1\left(\frac{v}{v_0} - 1\right)^2 + 1\right]$$

where F_{y0} is the steady-state main cutting force at the nominal cutting condition. The friction coefficient is

$$\mu = K_0\left(C_2\left(\frac{v_f R}{v_0} - 1\right)^2 + 1\right)\left(C_2\left(\frac{s}{s_0} - 1\right)^2 + 1\right)$$

where $K_0 = F_{x0}/F_{y0}$, v_f is the friction velocity. The chip thickness ratio is also assumed to be a function of the cutting speed

$$\rho = \rho_0 \left[C_4 \left(\frac{v}{v_0} - 1 \right)^2 + 1 \right]$$

Finally, he makes the following substitutions

$$s = s_0 - x$$

$$v = v_0 - \dot{y}$$

$$v_f = \frac{v}{\rho t} - \dot{y}$$

Grabec's model contains no regenerative terms.

3.4.1 Mode Coupling

Tlusty (1985) considered a system consisting of two orthogonal modes of vibration (Figure 3.7). The cutting force variations can be expressed as

$$dF_x = F \cos(\theta - \psi) \tag{3.38}$$

$$dF_y = F \cos\left(\frac{\pi}{2} + \psi - \theta \right) \tag{3.39}$$

with the linear cutting force

$$F = k_1 w (x_\tau - x) \tag{3.40}$$

the equations of motion can be written as (ε is the ratio of natural frequencies)

$$\ddot{x} + 2\zeta_x \dot{x} + x = p \cos(\theta - \psi) \left[\cos\psi (x_\tau - x) + \sin\psi (y_\tau - y) \right] \tag{3.41}$$

$$\ddot{y} + 2\zeta_y \varepsilon \dot{y} + \varepsilon^2 y = p \sin(\psi - \theta) \left[\cos\psi (x_\tau - x) + \sin\psi (y_\tau - y) \right]$$

If $\psi = \theta = 0$ we recover the 1 DOF classical model (3.28). Pratt (1996) showed that the coupling influence the location of the lobes. Recently Milisavljevich et

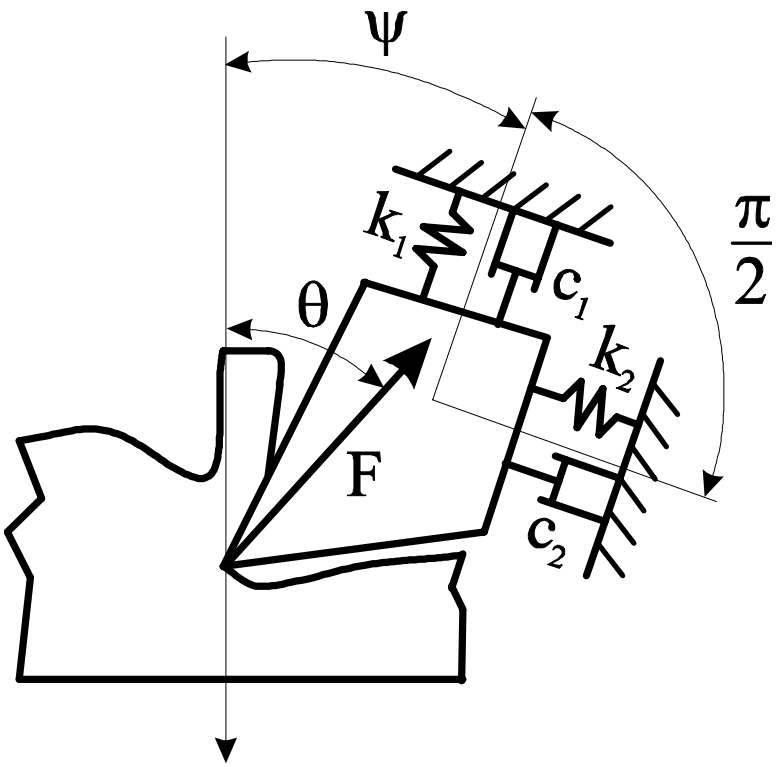

Figure 3.7: Mode-coupled tool vibrations.

al. (2000) studied a 2-DOF mode-coupled model with cutting force nonlinearity. Their model however does not contain delay.

3.5 Short Delay

Most dynamic models deal with concentrated forces acting on the tool. These forces are the components of the resultant of the distributed force system along the rake face of the tool (Figure 3.8).

Following Stépán (1998) the thrust force is expressed as the x component of the resultant of the force system

$$F(f) = \int_0^l P_x(f, s)\mathrm{d}s\,. \tag{3.42}$$

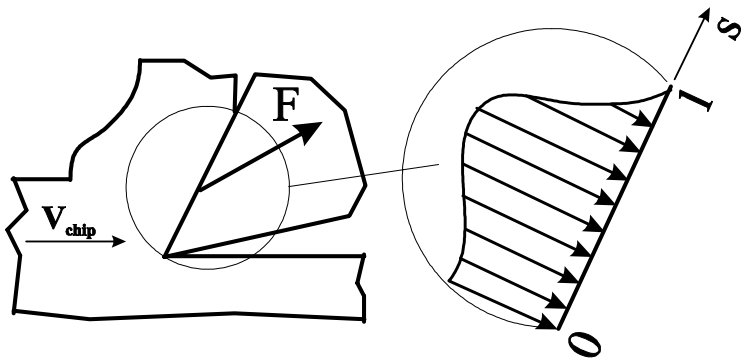

Figure 3.8: Distributed force system on the tool.

where s is the local coordinate, measuring distance from the tooltip ($s = 0$) to the point where the chip curls away from the tool ($s = l$). With the help of a shape (weight) function $W(s)$, the distributed force system is decomposed as

$$P_x(f, s) = \tilde{F}(f)W(s)\,, \quad s \in [0, l] \tag{3.43}$$

where $\tilde{F}(f)$ is an approximation of the cutting force (a power law, for example).

The shape function is normalized, so that

$$\int_0^l W(s)\mathrm{d}s = 1\,. \tag{3.44}$$

In steady state cutting, we find the cutting force for a particular value of the nominal chip thickness as

$$F(f_0) = \int_0^l P_x(f_0, s)\mathrm{d}s = \tilde{F}(f_0)\int_0^l W(s)\mathrm{d}s = \tilde{F}(f_0)\,, \tag{3.45}$$

showing that this decomposition is the generalization of the conventional single-point cutting force models.

The time needed for a differential volume of the chip to move up on the tool face is then

$$h = \frac{l}{v_{chip}}. \tag{3.46}$$

where the chip flow velocity is (r is the radius of the workpiece)

$$v_{chip} = \frac{\Omega}{2\pi} r \tag{3.47}$$

This introduces another timescale to the problem. Recall that τ, the timescale of the regenerative effect can be expressed as

$$\tau = 2\pi/\Omega \tag{3.48}$$

The ratio of h and τ is constant

$$q = \frac{h}{\tau} = \frac{l}{r} \tag{3.49}$$

As this ratio is very small, h will be referred to as the *short delay.*

The chip thickness is written as in (3.17). Since the chip thickness on the tool face has to be expressed as a function of time, a 'local time' θ is introduced to account for the motion of the chip.

$$\theta = s/v \tag{3.50}$$

and the stress distribution function w can be expressed as

$$w(\theta) = vW(v\theta) \quad \Rightarrow \quad \int_0^h w(\theta)\mathrm{d}\theta = 1\,. \tag{3.51}$$

The equation of motion (for more details consult Stépán, 1998) is the linear DDE

$$\ddot{x}(t) + 2\zeta\dot{x}(t) + x(t) = p\int_0^h x(t-\theta)w(\theta)\mathrm{d}\theta - p\int_{-\tau-h}^{-\tau} x(t+\theta)w(\tau+\theta)\mathrm{d}\theta \tag{3.52}$$

If the contact length l is negligible relative to the radius of the workpiece, then the weight function can be chosen as the Dirac delta

$$w(\theta) = \delta(\theta) \tag{3.53}$$

and the resulting equation is the classical linear model (3.28).

Chapter 4

Delay-Differential Equations

Delay-differential equations (DDEs) describe systems where the present rate of change of state depends on a past value (or history) of the state. Many excellent texts can be found on this topic (Bellman and Cooke, 1963; El'sgolt's and Norkin, 1973; Hale, 1977; Kolmanovskii and Nosov, 1986; Stépán, 1989; Hale and Lunel, 1993). The theory of DDEs is a generalization of the theory of ordinary differential equations (ODE) into infinite dimensional phase spaces. This generalization is not a trivial task, though, and it uses the mathematical tools developed for functional differential equations (Hale, 1977; Kuang, 1993).

This Chapter serves as a light introduction to DDEs, as the interested reader can always consult the many technical books and papers on this topic. Also, most results are not accessible to the engineering community, as they are usually mentioned in the context of operator and semigroup theory. Our approach here is more geometric.

A simple linear DDE is the scalar equation

$$\dot{x} = -px\left(t - \tau\right) \tag{4.1}$$

This equation admits the trivial fixed point $x = 0$.

As with linear constant coefficient ordinary differential equations, a necessary and sufficient condition for the asymptotic stability of the trivial solution of (4.1) is that all roots of the characteristic equation have negative real part (Hake, 1977). The *characteristic equation* associated with (4.1) is obtained just as in ODEs, by substituting the trial solution $x(t) = ce^{\lambda t}\,,\ c, \lambda \in \mathbb{C}$ into (4.1) and dividing by $ce^{\lambda t}$

$$\lambda + pe^{-\lambda\tau} = 0 \tag{4.2}$$

This so-called *exponential polynomial* has infinitely many solutions for the complex characteristic roots $\lambda_j\,,\ j = 1, 2, \ldots$.

The transcendental nature of this equation makes characterization of the roots more complicated than those of the polynomial characteristic equations associated with linear constant coefficient ordinary differential equations (Pontryagin, 1955, 1958; Avellar and Hale, 1980; Bellman and Cooke, 1963; Hale and Lunel, 1993).

4.1 Stability

In this section we determine stability of the linear delay differential equation

$$\dot{x} = -px\left(t - \tau\right) \qquad p > 0 \tag{4.3}$$

Assuming the solution in the form

$$x\left(t\right) = ce^{\lambda t} \tag{4.4}$$

the characteristic equation of (4.3) is

$$D\left(\lambda\right) = \lambda + pe^{-\lambda\tau} = 0 \tag{4.5}$$

This transcendental equation cannot be solved explicitly. However, we only want to know where the system goes unstable, and that happens when roots of this equation cross the imaginary axis from the left. It occurs when λ is a pure imaginary number, i.e.,

$$\lambda = i\omega \tag{4.6}$$

Plugging this into the characteristic equation (4.5) we get

$$i\omega + pe^{-i\omega\tau} = 0 \tag{4.7}$$

which can be expanded as

$$i\omega + p\left(\cos\omega\tau - i\sin\omega\tau\right) = 0 \tag{4.8}$$

Separating the real and imaginary parts we have

$$\cos\omega\tau = 0 \tag{4.9}$$

$$\omega - p\sin\omega\tau = 0 \tag{4.10}$$

The first positive solution to (4.9) is

$$\omega = \frac{\pi}{2\tau} \tag{4.11}$$

Equation (4.10) then reduces to

$$\omega = p \tag{4.12}$$

The last two equations give

$$\tau p = \frac{\pi}{2} \tag{4.13}$$

or equivalently

$$p = \frac{\pi}{2\tau} \tag{4.14}$$

It is easy to show (see 6.26) that at this value of τp a pair of complex roots cross the imaginary axis with positive velocity (i.e. from the left) and all other roots have negative real part. That means that the system loses stability at $\tau p = \frac{\pi}{2} \simeq 1.57$.

Equation (4.14) is the so-called *stability curve* on the parameter plane (τ, p). On this curve the characteristic equation has a pair of purely imaginary root. Figure 4.1 shows this stability curve, and also shows numerically determined stability (see Section 4.4.2) of the fixed point of (4.3). Dark points correspond to stable, while light ones correspond to unstable behavior.

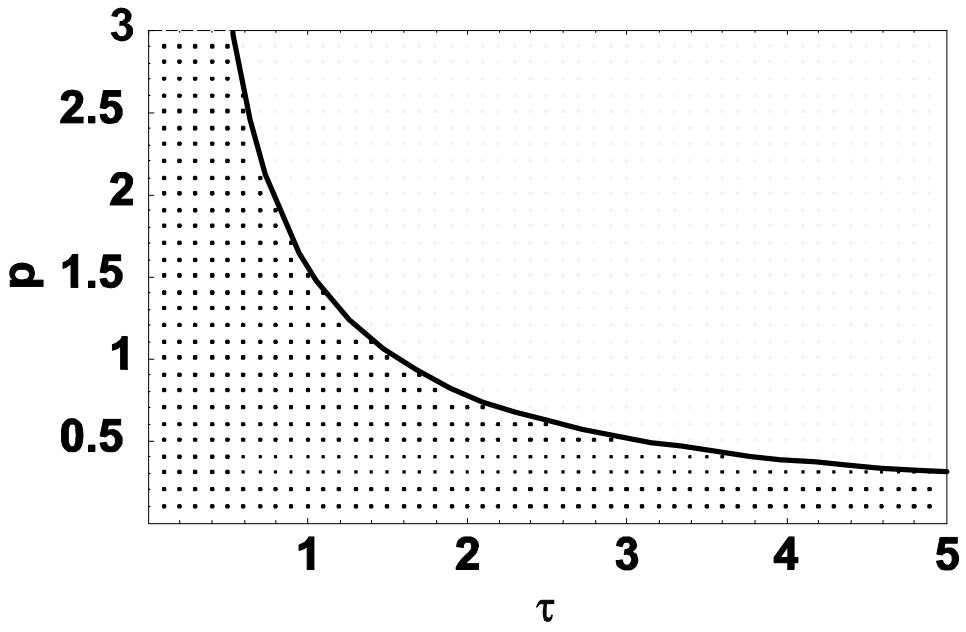

Figure 4.1: Stability chart for equation (4.3). Dark points show stable behavior.

4.2 Stability by Approximation

Several researchers have pointed out the pitfalls of trying to determine stability of DDEs by various approximations, like using the series expansion of $x(t-\tau)$

(Driver, 1977; Fofana, 1993; Insperger, 1999). Most of these methods replace the DDE with a system of ODEs. Even though convergence can be proved in some cases, the stability of the resulting system of ODEs usually depend on the number equations.

Here we will show, how such an approximation can lead to an erroneous result. We aim to find a method with which we could reduce the delay-differential equation

$$\dot{x} = f\left(x\left(t\right), x\left(t-\tau\right)\right) \tag{4.15}$$

to a system of ordinary differential equations (Copeland and Rand, private communication). To this end, we define

$$y = x\left(t-\tau\right) \tag{4.16}$$

and take its Laplace transform

$$\mathcal{L}\left(y\left(t\right)\right) = \mathcal{L}\left(x\left(t-\tau\right)\right) = e^{-s\tau}\mathcal{L}\left(x\left(t\right)\right) \tag{4.17}$$

Assuming small τ we replace the exponential with its $(1,1)$ Padé-approximation

$$e^{-s\tau} \approx \frac{2-s\tau}{2+s\tau} = \frac{4}{2+s\tau} - 1 \tag{4.18}$$

Then (4.17) can be written as

$$2\left(\mathcal{L}\left(y\right) - \mathcal{L}\left(x\right)\right) + \tau s\left(\mathcal{L}\left(y\right) + \mathcal{L}\left(x\right)\right) = 0 \tag{4.19}$$

Taking the inverse Laplace transform of this equation results in

$$2\left(y-x\right) + \tau\left(\dot{y}+\dot{x}\right) = 0 \tag{4.20}$$

We can express $\dot{y}$ as

$$\dot{y} = \frac{2}{\tau}\left(x-y\right) - \dot{x} = \frac{2}{\tau}\left(x-y\right) - f\left(t,x,y\right) \tag{4.21}$$

so the reduced system is

$$\dot{x} = f(x, y) \tag{4.22}$$

$$\dot{y} = \frac{2}{\tau}(x - y) - f(t, x, y) \tag{4.23}$$

Since $f(x, y) = -ky$ equations (4.22, 4.23) become

$$\dot{x} = -ky \tag{4.24}$$

$$\dot{y} = \frac{2}{\tau}(x - y) + ky = \frac{2}{\tau}x + \left(k - \frac{2}{\tau}\right) y \tag{4.25}$$

In matrix notation

$$\frac{d}{dt}\begin{pmatrix} x \\ y \end{pmatrix} = \begin{pmatrix} 0 & -k \\ \frac{2}{\tau} & k - \frac{2}{\tau} \end{pmatrix}\begin{pmatrix} x \\ y \end{pmatrix} \tag{4.26}$$

The eigenvalues of this system are

$$\lambda_{1,2} = \frac{1}{2\tau}\left(k\tau - 2 \pm \sqrt{(k\tau - 6)^2 - 32}\right) \tag{4.27}$$

Clearly, for $k\tau < 2$ the pair of complex eigenvalues has negative real part, indicating asymptotic stability. Thus the error of the approximation is 27%. Also, no matter how small τ is this error prevails.

4.3 Stability Charts

A *stability chart* shows disjunct domains in the space of chosen system parameters (the parameter space) where the equilibrium point of the DDE is stable or unstable. On the boundaries of these domains the characteristic equation has purely imaginary parts. One of the methods for constructing stability charts is the method of D-partitions (Stépán, 1989). The *D-curves* are determined in the parameter space (often plane) by the parametric equations

$$R(\omega) = \operatorname{Re} D(\mathrm{i}\omega) = 0, \quad S(\omega) = \operatorname{Im} D(\mathrm{i}\omega) = 0, \quad \omega \in \mathbb{R}^+ \tag{4.28}$$

where D is the characteristic function of the system. In general, these curves separate infinitely many disjunct domains, and we need some criterion to select the ones which correspond to asymptotic stability.

Given that the roots of the characteristic equation depend continuously on the parameters in the characteristic equation, a necessary condition for the real part of a root to change sign must involve crossing one of these hyper-surfaces in the parameter space. Once the parameter space is partitioned by these hyper-surfaces, one need only determine the number of roots with positive real part on either side of these surfaces. The easiest case to visualize is a two-dimensional parameter space, and the corresponding boundaries are curves in the plane along which the characteristic equation has purely imaginary part. Various tests (see Stépán, 1989) can then be used to determine the number of roots with positive real part in each region partitioned by these curves.

Stépán (1989) uses the infinite dimensional version of the Routh-Hurwitz criterion to analyze the zeros of the characteristic functions of DDEs. If we define the real functions

$$R(\omega) = \operatorname{Re} D(\mathrm{i}\omega)\,, \quad S(\omega) = \operatorname{Im} D(\mathrm{i}\omega)\,, \quad \omega \in [0, \infty)\,, \tag{4.29}$$

and the real zeros of R are denoted by $\rho_1 \geq \ldots \rho_r \geq 0$, i.e.

$$R(\rho_k) = 0\,, \quad k = 1, \ldots, r$$

then the equilibrium of the linear delayed mechanical system of n DOF is asymptotically stable if and only if

$$S(\rho_k) \neq 0\,,\ k = 1, \ldots, r \tag{4.30}$$

$$\sum_{k=1}^{r} (-1)^k \operatorname{sgn} S(\rho_k) = (-1)^n n \tag{4.31}$$

hold. In case of n DOF systems, the dimension of the phase space is $2n$, i.e. always even. The above mentioned stability criterion has a somewhat more complicated form for DDEs with odd dimensions (like (4.1) — see further details in Stépán 1989).

The classical 1 DOF model for tool vibrations can be written as (see Chapter 3)

$$\ddot{x}(t) + 2\zeta\dot{x}(t) + x(t) + p(x - x_\tau) = 0 \tag{4.32}$$

The trivial solution of (4.32) refers to the stationary cutting. When its stability is investigated, the D-curves coming from the characteristic function

$$D(\lambda) = \lambda^2 + 2\zeta\lambda + 1 + pD_0(\tau\lambda) \tag{4.33}$$

$$D_0(\tau\lambda) = 1 - e^{-\lambda\tau} \tag{4.34}$$

should be calculated as defined in (4.29):

$$R(\omega) = -\omega^2 + 1 + pR_0(\psi) = 0 \tag{4.35}$$

$$R_0(\psi) = 1 - \cos(\psi) \tag{4.36}$$

$$S(\omega) = 2\zeta\omega + pS_0(\psi) = 0 \tag{4.37}$$

$$S_0(\psi) = \sin(\psi) \tag{4.38}$$

where the new parameter $\psi = \tau\omega$ is introduced and all the transcendental expressions are separated in the formulas of R_0 and S_0. Eliminating p from (4.37, 4.35)

$$\omega(\psi) = -\zeta\frac{R_0(\psi)}{S_0(\psi)} + \sqrt{1 + \left(\zeta\frac{R_0(\psi)}{S_0(\psi)}\right)^2} \tag{4.39}$$

$$\tau(\psi) = \frac{\psi}{\omega\left(\psi\right)} \tag{4.40}$$

$$p(\psi) = -2\zeta\frac{\omega(\psi)}{S_0(\psi)} \tag{4.41}$$

Since

$$\frac{R_0(\psi)}{S_0(\psi)} = \frac{1-\cos\psi}{\sin\psi} = \tan\frac{\psi}{2}\,, \tag{4.42}$$

the parameter ψ can be eliminated from (4.39), and the D-curves can be expressed as a function of ω. The stability charts are traditionally constructed in the plane of the dimensional quantities k_1 (the cutting force coefficient, see Chapter 3) and angular velocity Ω of the workpiece (Figure 4.2). The values $m = 50$ kg, $\zeta = 0.05$, and $\omega_n = 775$ rad/s were used. Stability of the domains can be determined by

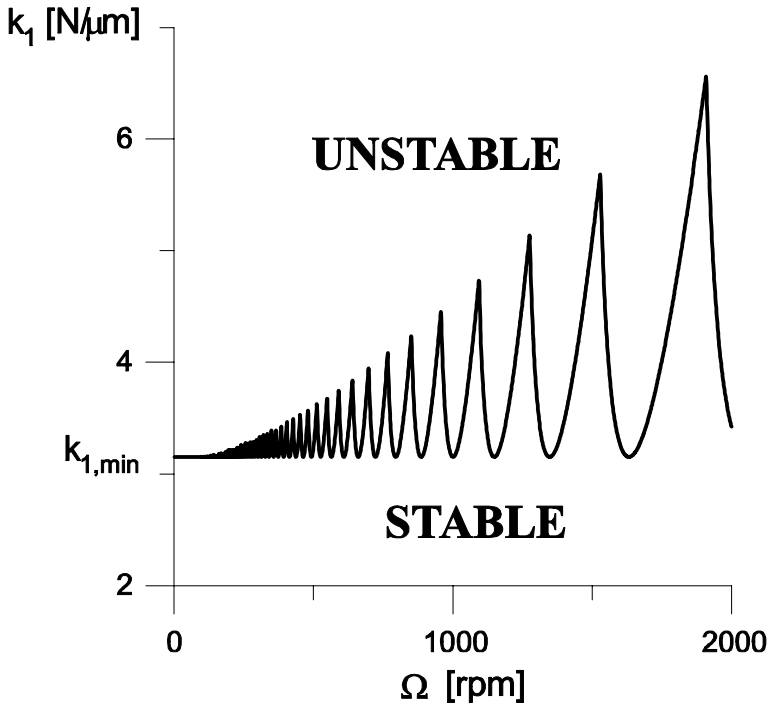

Figure 4.2: Stability chart for the classical model.

using criteria (4.30, 4.31) (see Stépán, 1989) or by using Rouché's theorem (see Appendix D). In Figure 4.2 the stable region corresponds to asymptotic stability of the fixed point. Because of its widespread use, this figure is often referred to as the *classical stability chart*.

4.4 Numerical Stability Analysis

In most of the cases, analytical form of the D-curves can not be obtained. Then we have to resort to numerical methods. Engelborghs and Roose (1999) proposed a numerical algorithm to compute the rightmost (the stability determining) roots of the characteristic equation associated with the DDE. In this Section two numerical methods are employed to draw stability charts. The first one calculates points on the D-curves, while the second determines stability at a given point in the parameter space.

4.4.1 The Method of Chen, Ulsoy and Koren

Chen, Ulsoy and Koren (1997) proposed the following method for numerically finding points that lie on D-curves. First define the following matrix and function

$$\mathbf{A}(v) := \mathbf{L} + e^{-2\pi v i}\mathbf{R} \tag{4.43}$$

$$\text{gap}(v) := \left\{ \text{Re}(\lambda) | \quad \mathbf{A}(v)\,\mathbf{s} = \lambda \mathbf{s},\ |\text{Re}(\lambda)| = \min_i |\text{Re}(\lambda_i)| \right\} \tag{4.44}$$

where

$$2\pi(m+v) = \tau\omega \quad m \in \mathbb{N} \tag{4.45}$$

It is easy to see that $\text{gap}(v) = 0 \Leftrightarrow \lambda = i\omega$. For a given matrix $\mathbf{A}$ we have to find zeros of $\text{gap}(v)$ in $v \in \left[0, \frac{1}{2}\right]$. Then

$$\tau = \begin{cases} \frac{2\pi(m+v)}{|\text{Im}\,\lambda(v)|} & \text{Im}\,\lambda(v) \geq 0 \\ \frac{2\pi(m+1-v)}{|\text{Im}\,\lambda(v)|} & \text{Im}\,\lambda(v) < 0 \end{cases} \tag{4.46}$$

and (τ, p) (or $(1/\tau, p)$) can be plotted. To obtain the numerical D-curves a Mathematica code was written. The zeros of $\text{gap}(v)$ are determined by stepping through

the interval $\left[0, \frac{1}{2}\right]$ with a given stepsize (usually 0.001) and using bisection to zoom in on the root if different signs of the function are found.

The matrices

$$\mathbf{L} = \begin{pmatrix} 0 & 1 \\ -(1+p) & -2\zeta \end{pmatrix}, \qquad \mathbf{R} = \begin{pmatrix} 0 & 0 \\ p & 0 \end{pmatrix} \tag{4.47}$$

correspond to the classical model (4.32). In Figure 4.3 we show the analytical D-curves and numerical solutions together for $\zeta = 0.01$.

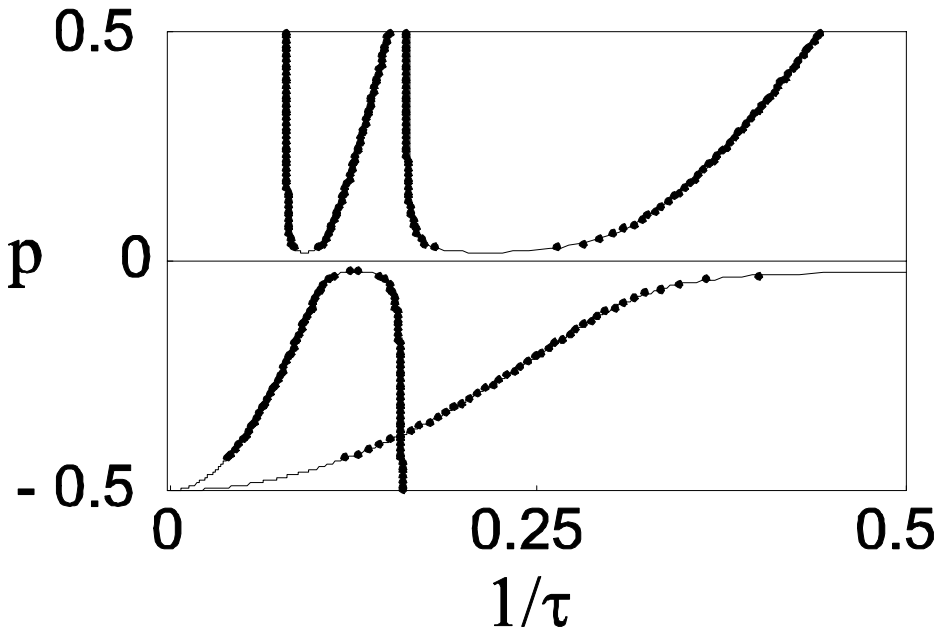

Figure 4.3: Analytical and numerical stability chart for the classical model.

To determine the stability of a region it is sufficient to check the stability of one point inside it (care must be taken since the computation might not find all the D-curves).

4.4.2 Stability by Numerical Integration

Another way to create stability charts is by direct numerical integration of the linear DDE on a grid in the parameter space. The method is illustrated in Figure 4.4. For every point on the grid the DDE is integrated (using Mathematica's fifth

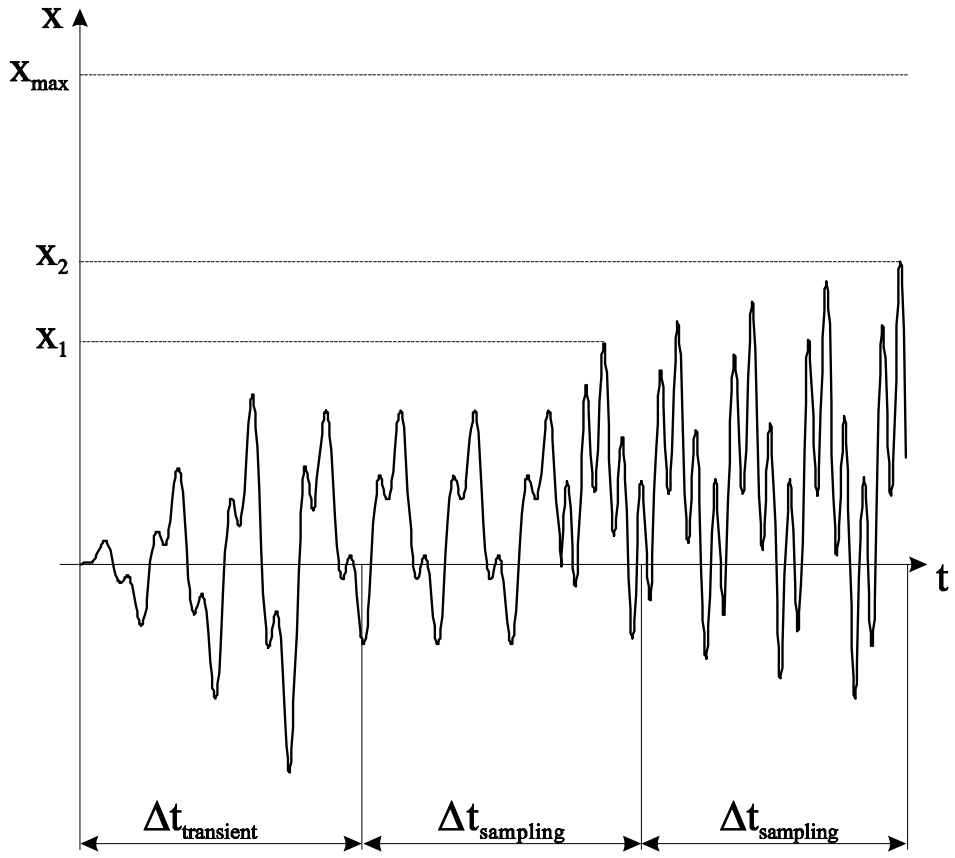

Figure 4.4: Determining stability by integration.

order Runge-Kutta-Fehlberg solver) with a constant initial function (the amplitude does not matter, since we are investigating stability of a unique fixed point of a linear equation). After discarding some initial transients (of length $\Delta t_{transient}$), the maximum amplitudes (x_1 and x_2) of the state variables on two equal length sampling periods (of length $\Delta t_{sampling}$) are determined. If the amplitude is bigger

on the second sampling period than on the first one, the fixed point is deemed unstable, otherwise it is stable. To speed up calculations we consider the fixed point unstable if the state variables become larger than some predetermined bound $x_{\max}$ (which is taken much larger than the amplitude of the initial function) at any $t > 0$. Figure 4.5 shows the stability curves of the classical model together with colored points indicating stability (dark points) or instability (light points). The transient period and both sampling periods were taken 3τ long.

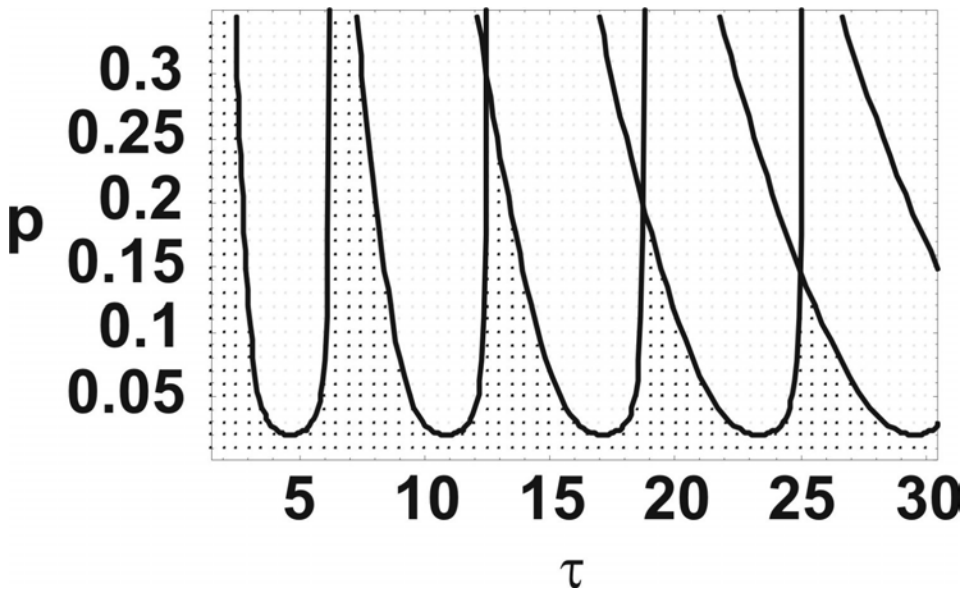

Figure 4.5: Analytical and numerical (by numerical integration) stability chart of the classical model.

4.5 Operator Equation Formulation for DDEs

The theory of delay differential equation has received much attention since the 60's. Most of the theory, however, requires highly mathematical background (Hale, 1977). In preparation for the operator differential equation approach and center

manifold analysis of Chapter 6, we will show an analogy between ordinary and delay differential equations. This will motivate the definitions of the differential operator, its adjoint and the bilinear form used to investigate Hopf bifurcation in delay equations without heavy mathematical artillery. In particular it is shown that the time-delay problem leads to an operator that is the generalization of the defining matrix in a system of ODE's with constant coefficients.

The formal adjoint and the bilinear form provide the basis for a geometry in which it is possible to develop a projection using the basis eigenvectors of the formal adjoint (just as in Hopf bifurcation analysis for ODEs). The significance of this projection is that the critical delay system has a two-dimensional attractive subsystem (the center manifold) and the solutions on this manifold determine the long time behavior of the full system. The mathematically inclined can study Hale (1977).

Let us first consider a scalar autonomous delay differential equation (and the corresponding initial function) of the form

$$\dot{x}(t) = \mathrm{L}x(t) + \mathrm{R}x(t-\tau) + \mathrm{f}(x(t), x(t-\tau)) \tag{4.48}$$

$$x(t) = \phi(t) \quad t \in [-\tau, 0)$$

where L, R are scalars. The first goal is to put equation (4.48) into a form similar to the ODE

$$\dot{\mathbf{x}}(t) = \mathbf{A}\mathbf{x}(t) + \mathbf{f}(\mathbf{x}(t)) \tag{4.49}$$

Here an attempted numerical solution could give a clue. Discretizing equation (4.48) leads to

$$\frac{dx_i}{d\vartheta} \approx \frac{1}{d\vartheta}(x_{i-1} - x_i) \quad i = 1, \ldots, N$$

$$\left.\frac{dx_i}{d\vartheta}\right|_{\vartheta=0} = \mathrm{L}x_0 + \mathrm{R}x_N + \mathrm{f}(x_0, x_N)$$

where $d\vartheta$ is the stepsize of discretization. Taking the limit $d\vartheta \to 0$, and defining the 'shift of time' as

$$x_t(\vartheta) = x(t+\vartheta)$$

we have the following

$$\frac{d}{d\vartheta}x_t(\vartheta) = \frac{d}{d\vartheta}x_t(\vartheta) \quad \vartheta \in [-\tau, 0)$$
$$\left.\frac{d}{d\vartheta}x_t(\vartheta)\right|_{\vartheta=0} = \mathrm{L}x_t(0) + \mathrm{R}x_t(-\tau) + \mathrm{f}(x_t(0), x_t(-\tau))$$

This motivates our definition of the linear differential operator $\mathcal{A}$

$$\mathcal{A}u(\vartheta) = \begin{cases} \frac{d}{d\vartheta}u(\vartheta) & \vartheta \in [-\tau, 0) \\ \mathrm{L}u(0) + \mathrm{R}u(-\tau) & \vartheta = 0 \end{cases} \tag{4.50}$$

and the nonlinear operator $\mathcal{F}$

$$\mathcal{F}(u)(\vartheta) = \begin{cases} 0 & \vartheta \in [-\tau, 0) \\ \mathrm{f}(u(0)) & \vartheta = 0 \end{cases} \tag{4.51}$$

Since $\frac{d}{d\vartheta} = \frac{d}{dt}$, we can rewrite equation (4.48) as

$$\frac{d}{dt}x_t(\vartheta) = \dot{x}_t(\vartheta) = \mathcal{A}x_t(\vartheta) + \mathcal{F}(x_t)(\vartheta)$$

This operator formulation can be extended to multidimensional systems as well

$$\dot{\mathbf{x}}_t(\vartheta) = \mathcal{A}\mathbf{x}_t(\vartheta) + \mathcal{F}(\mathbf{x}_t)(\vartheta) \tag{4.52}$$

This form is very similar to the system of ODEs (4.49). There is one very important difference, though. Equation (4.52) represents an infinite dimensional system. However, the infinite dimensional phase space of its linear part can also be split into stable, unstable and center subspaces corresponding to eigenvalues having positive, negative and zero real part. If we focus our attention to the case where

the operator has imaginary eigenvalues, it means that $\mathcal{A}$ has a pair of complex conjugate *eigenfunctions* $\mathbf{s}$, $\bar{\mathbf{s}}$ corresponding to $\pm i\omega$ satisfying

$$\mathcal{A}\mathbf{s}(\vartheta) = i\omega\mathcal{I}\mathbf{s}(\vartheta) \tag{4.53}$$

$$\mathcal{A}\bar{\mathbf{s}}(\vartheta) = -i\omega\mathcal{I}\bar{\mathbf{s}}(\vartheta) \tag{4.54}$$

where the identity operator $\mathcal{I}$ (this seemingly superfluous definition is intended to make our life easier as a bookkeeping device) is defined as

$$\mathcal{I}\mathbf{u}(\theta) = \begin{cases} \mathbf{u}(\theta) & \theta \neq 0 \\ \mathbf{u}(0) & \theta = 0 \end{cases}$$

Note that equations (4.53, 4.54) represent a boundary value problem (because of the definition of $\mathcal{A}$).

Introducing the real functions

$$\mathbf{s}_1(\vartheta) = \operatorname{Re}\mathbf{s}(\vartheta)$$

$$\mathbf{s}_2(\vartheta) = \operatorname{Im}\mathbf{s}(\vartheta)$$

Equations (4.53, 4.54) can be rewritten as

$$\mathcal{A}\mathbf{s}_1(\vartheta) = -\omega\mathcal{I}\mathbf{s}_2(\vartheta)$$

$$\mathcal{A}\mathbf{s}_2(\vartheta) = \omega\mathcal{I}\mathbf{s}_1(\vartheta)$$

The two functions $\mathbf{s}_1(\vartheta)$, $\mathbf{s}_2(\vartheta)$ span the center subspace which is tangent to the two-dimensional center manifold embedded in the infinite dimensional phase space.

We start by defining the new coordinates

$$y_1(t) = (\mathbf{n}_1(\vartheta), \mathbf{x}_t(\vartheta))$$

$$y_2(t) = (\mathbf{n}_2(\vartheta), \mathbf{x}_t(\vartheta)) \tag{4.55}$$

where $\mathbf{n}$ satisfies

$$\mathcal{A}^{*}\mathbf{n} = -i\omega\mathbf{n} \tag{4.56}$$

The evolution of the new coordinate y_1 would then be given by

$$\dot{y}_1(t) = (\mathbf{n}_1(\vartheta), \dot{\mathbf{x}}_t(\vartheta)) = (\mathbf{n}_1(\vartheta), \mathcal{A}\mathbf{x}_t(\vartheta) + \mathcal{F}(\mathbf{x}_t)(\vartheta)) =$$

$$= (\mathcal{A}^{*}\mathbf{n}_1(\vartheta), \mathbf{x}_t(\vartheta)) + (\mathbf{n}_1(\vartheta), \mathcal{F}(\mathbf{x}_t)(\vartheta))$$

Two questions arise immediately: how shall we define the pairing $(.,.)$ and what is the adjoint operator $\mathcal{A}^{*}$? To answer the first question we can first try to use the usual inner product in the space of continuously differentiable functions on $[-\tau, 0)$

$$(\mathbf{u}(\vartheta), \mathbf{v}(\vartheta)) = \int_{-\tau}^{0} \mathbf{u}^{*}(\vartheta)\,\mathbf{v}(\vartheta)\,d\vartheta \tag{4.57}$$

However, we also want to include the boundary terms at $\vartheta = 0$ from equations (4.50, 4.51) so we try to modify (4.57) as

$$(\mathbf{u}(\vartheta), \mathbf{v}(\vartheta)) = \int_{-\tau}^{0} \mathbf{u}^{*}(\vartheta)\,\mathbf{v}(\vartheta)\,d\vartheta + \mathbf{u}^{*}(0)\,\mathbf{v}(0) \tag{4.58}$$

Now we try to find the adjoint operator from the definition

$$(\mathcal{A}^{*}\mathbf{u}, \mathbf{v}) = (\mathbf{u}, \mathcal{A}\mathbf{v})$$

$$(\mathcal{A}^{*}\mathbf{u}, \mathbf{v}) = \int_{-\tau}^{0} \mathcal{A}^{*}\mathbf{u}\mathbf{v}d\vartheta + [\mathcal{A}^{*}\mathbf{u}(0)]^{*}\,\mathbf{v}(0) \tag{4.59}$$

$$(\mathbf{u}, \mathcal{A}\mathbf{v}) = \int_{-\tau}^{0} \mathbf{u}^* \mathcal{A}\mathbf{v} d\vartheta + \mathbf{u}^*(0)\mathcal{A}\mathbf{v}(0) \overset{by\ parts}{=}$$

$$= -\int_{-\tau}^{0} \frac{d}{d\vartheta}\mathbf{u}^*\mathbf{v} d\vartheta + \mathbf{u}^*(\vartheta)\mathbf{v}(\vartheta)|_{-\tau}^{0} + \mathbf{u}^*(0)[\mathbf{L}\mathbf{v}(0) + \mathbf{R}\mathbf{v}(-\tau)] =$$

$$= -\int_{-\tau}^{0} \frac{d}{d\vartheta}\mathbf{u}^*\mathbf{v} d\vartheta + \mathbf{u}^*(0)\mathbf{v}(0) - \mathbf{u}^*(\vartheta)\mathbf{v}(\vartheta)|_{-\tau} +$$

$$+\mathbf{u}^*(0)\mathbf{R}\mathbf{v}(-\tau) + \mathbf{u}^*(0)\mathbf{L}\mathbf{v}(0) =$$

$$= \int_{-\tau}^{0} \left(-\frac{d}{d\vartheta}\right)\mathbf{u}^*\mathbf{v} d\vartheta + [(\mathbf{I} + \mathbf{L})^*\mathbf{u}(0)]^*\mathbf{v}(0) -$$

$$-\mathbf{u}^*(-\tau)\mathbf{v}(-\tau) + \mathbf{u}^*(0)\mathbf{R}\mathbf{v}(-\tau) \tag{4.60}$$

The first two terms of equation (4.60) are similar to those in equation (4.59) so we seek to eliminate $\mathbf{u}^*(0)\mathbf{R}\mathbf{v}(-\tau) - \mathbf{u}^*(-\tau)\mathbf{v}(-\tau)$. Since this term is usually nonzero, we can try to modify equation (4.58) to get

$$\mathbf{u}^*(0)\mathbf{R}\mathbf{v}(-\tau) - \mathbf{u}^*(\tau - \tau)\mathbf{R}\mathbf{v}(-\tau) = 0 \tag{4.61}$$

instead. This can be achieved with the modification

$$(\mathbf{u}(\vartheta), \mathbf{v}(\vartheta)) = \int_{-\tau}^{0} \mathbf{u}^*(\vartheta + \tau)\mathbf{R}\mathbf{v}(\vartheta) d\vartheta + \mathbf{u}^*(0)\mathbf{v}(0) \tag{4.62}$$

Using Equation (4.62)

$$(\mathbf{u}, \mathcal{A}\mathbf{v}) = -\int_{-\tau}^{0} \frac{d}{d\vartheta}\mathbf{u}^*(\vartheta + \tau)\mathbf{R}\mathbf{v}(\vartheta) d\vartheta + [\mathbf{L}^*\mathbf{u}(0) + \mathbf{R}^*\mathbf{u}(\tau)]^*\mathbf{v}(0)$$

Defining $\gamma = \vartheta + \tau$

$$(\mathbf{u}, \mathcal{A}\mathbf{v}) = (\mathcal{A}^*\mathbf{u}, \mathbf{v}) =$$

$$= \int_{0}^{\tau} \left(-\frac{d}{d\gamma}\right)\mathbf{u}^*(\gamma)\mathbf{R}\mathbf{v}(\gamma - \tau) d\gamma + [\mathbf{L}^*\mathbf{u}(0) + \mathbf{R}^*\mathbf{u}(\tau)]^*\mathbf{v}(0)$$

gives the definition of the adjoint operator

$$\mathcal{A}^*\mathbf{u}\left(\gamma\right) = \begin{cases} -\frac{d}{d\gamma}\mathbf{u}\left(\gamma\right) & \gamma \in (0,\tau] \\ \mathbf{L}^*\mathbf{u}\left(0\right) + \mathbf{R}^*\mathbf{u}\left(\tau\right) & \gamma = 0 \end{cases}$$

with the two complex conjugate eigenfunctions

$$\mathcal{A}^*\mathbf{n}(\gamma) = -i\omega\mathcal{I}\mathbf{n}(\gamma) \tag{4.63}$$

$$\mathcal{A}^*\bar{\mathbf{n}}(\gamma) = i\omega\mathcal{I}\bar{\mathbf{n}}(\gamma) \tag{4.64}$$

Introducing the real functions

$$\mathbf{n}_1\left(\gamma\right) = \mathrm{Re}\,\mathbf{n}(\gamma)$$

$$\mathbf{n}_2\left(\gamma\right) = \mathrm{Im}\,\mathbf{n}(\gamma)$$

Equations (4.63, 4.64) can be rewritten as

$$\mathcal{A}^*\mathbf{n}_1(\gamma) = \omega\mathcal{I}\mathbf{n}_2(\gamma)$$

$$\mathcal{A}^*\mathbf{n}_2(\gamma) = -\omega\mathcal{I}\mathbf{n}_1(\gamma)$$

Since equation (4.62) requires functions from two different spaces ($C^1_{[-1,0]}$ and $C^1_{[0,1]}$) it is a *bilinear form* instead of an inner product. The vectors $\mathbf{n}_i$, $\mathbf{s}_i$ are aligned (this corresponds to orthonormality in the finite dimensional case)

$$(\mathbf{n}_1, \mathbf{s}_1) = (\mathbf{n}_2, \mathbf{s}_2) = 1$$

$$(\mathbf{n}_2, \mathbf{s}_1) = (\mathbf{n}_1, \mathbf{s}_2) = 0$$

The new coordinates y_1, y_2 can be found by the projections (instead of equation (4.55))

$$y_1(t) = y_{1t}(0) = \left(\mathbf{n}_1, \mathbf{x}_t\right)|_{\vartheta=0}$$

$$y_2(t) = y_{2t}(0) = \left(\mathbf{n}_2, \mathbf{x}_t\right)|_{\vartheta=0}$$

Now $\mathbf{x}_t(\vartheta)$ can be decomposed as

$$\mathbf{x}_t(\vartheta) = y_1(t)\mathbf{s}_1(\vartheta) + y_2(t)\mathbf{s}_2(\vartheta) + \mathbf{w}(t)(\vartheta) \tag{4.65}$$

And the operator differential equation (4.52) can be transformed into the 'canonical form'

$$\dot{y}_1 = (\mathbf{n}_1, \dot{\mathbf{x}}_t)|_{\vartheta=0} = (\mathbf{n}_1, \mathcal{A}\mathbf{x}_t + \mathcal{F}(\mathbf{x}_t)\,)|_{\vartheta=0} =$$

$$= (\mathbf{n}_1, \mathcal{A}\mathbf{x}_t)|_{\vartheta=0} + (\mathbf{n}_1, \mathcal{F}(\mathbf{x}_t)\,)|_{\vartheta=0} =$$

$$= (\mathcal{A}^*\mathbf{n}_1, \mathbf{x}_t)|_{\vartheta=0} + (\mathbf{n}_1, \mathcal{F}(\mathbf{x}_t)\,)|_{\vartheta=0} =$$

$$= \omega\,(\mathbf{n}_2, \mathbf{x}_t)|_{\vartheta=0} + (\mathbf{n}_1, \mathcal{F}(\mathbf{x}_t)\,)|_{\vartheta=0} = \omega y_2 + \mathbf{n}_1^{\mathrm{T}}(0)\,\mathbf{F}$$

$$\dot{y}_2 = (\mathbf{n}_2, \dot{\mathbf{x}}_t)|_{\vartheta=0} = -\omega y_1 + \mathbf{n}_2^{\mathrm{T}}(0)\,\mathbf{F}$$

where $\mathbf{F} = \mathcal{F}(y_1(t)\mathbf{s}_1(0) + y_2(t)\mathbf{s}_2(0) + \mathbf{w}(t)(0))$ was used and

$$\dot{\mathbf{w}} = \frac{d}{dt}(\mathbf{x}_t - y_1\mathbf{s}_1 - y_2\mathbf{s}_2) = \mathcal{A}\mathbf{x}_t + \mathcal{F}(\mathbf{x}_t) - \dot{y}_1\mathcal{I}\mathbf{s}_1 - \dot{y}_2\mathcal{I}\mathbf{s}_2 =$$

$$= \mathcal{A}(y_1\mathbf{s}_1 + y_2\mathbf{s}_2 + \mathbf{w}) + \mathcal{F}(\mathbf{x}_t) - \dot{y}_1\mathcal{I}\mathbf{s}_1 - \dot{y}_2\mathcal{I}\mathbf{s}_2 =$$

$$= y_1(-\omega\mathcal{I}\mathbf{s}_2) + y_2(\omega\mathcal{I}\mathbf{s}_1) + \mathcal{A}\mathbf{w} + \mathcal{F}(\mathbf{x}_t) -$$

$$-\left(\omega y_2 + \mathbf{n}_1^{\mathrm{T}}(0)\,\mathbf{F}\right)\mathcal{I}\mathbf{s}_1 - \left(-\omega y_1 + \mathbf{n}_2^{\mathrm{T}}(0)\,\mathbf{F}\right)\mathcal{I}\mathbf{s}_2 =$$

$$= \mathcal{A}\mathbf{w} + \mathcal{F}(\mathbf{x}_t) - \mathbf{n}_1^{\mathrm{T}}(0)\,\mathbf{F}\mathcal{I}\mathbf{s}_1 - \mathbf{n}_2^{\mathrm{T}}(0)\,\mathbf{F}\mathcal{I}\mathbf{s}_2 =$$

$$\begin{cases} \frac{d}{d\vartheta}\mathbf{w} - \mathbf{n}_1^{\mathrm{T}}(0)\,\mathbf{F}\mathbf{s}_1 - \mathbf{n}_2^{\mathrm{T}}(0)\,\mathbf{F}\mathbf{s}_2 & \vartheta \in [-\tau, 0) \\ \mathbf{L}\mathbf{w}(0) + \mathbf{R}\mathbf{w}(-\tau) + \mathbf{F} - \mathbf{n}_1^{\mathrm{T}}(0)\,\mathbf{F}\mathbf{s}_1(0) - \mathbf{n}_2^{\mathrm{T}}(0)\,\mathbf{F}\mathbf{s}_2(0) & \vartheta = 0 \end{cases}$$

4.6 Center Subspace of the Critical DDE

In this Section we show a general method for finding the projection vectors needed in Chapter 6 for the center manifold reduction of a nonlinear DDE whose linear part is ($\mathbf{L}$, $\mathbf{R}$ are real matrices)

$$\dot{\mathbf{x}}(t) = \mathbf{L}\mathbf{x}(t) + \mathbf{R}\mathbf{x}(t-\tau) \tag{4.66}$$

Let us define the characteristic matrix as

$$\mathbf{D}(\lambda) = \lambda\mathbf{I} - \mathbf{L} - \mathbf{R}\mathrm{e}^{-\lambda\tau} \tag{4.67}$$

and the characteristic function

$$D(\lambda) = \det\left(\mathbf{D}(\lambda)\right) \tag{4.68}$$

At a Hopf bifurcation point there is a pair of purely imaginary roots of the characteristic function (6.15) at the critical value of the bifurcation parameter. This is a codimension-1 bifurcation. However, it is possible that there are two pairs of purely imaginary roots (at the intersection of two stability lobes). This is a codimension-2 bifurcation point. In the following calculations we assume that there are either one or two pairs of purely imaginary roots of (6.15)

$$D(i\omega_m) = 0 \qquad m = 1, 2 \tag{4.69}$$

We also suppose that these roots cross the imaginary axis transversally, that is $\mathrm{Re}\,\frac{\mathrm{d}\lambda(p)}{\mathrm{d}p} \neq 0$ and the other roots have negative real part (thus satisfying the requirements of the Hopf-bifurcation Theorem).

As shown previously the linear delay-differential equation (4.66) can be written as the operator equation

$$\dot{\mathbf{x}}_t = \mathcal{A}\mathbf{x}_t \tag{4.70}$$

$$\mathbf{x}_t(\varphi) = \mathbf{x}(t+\varphi)\,, \quad \varphi \in [-\tau, 0] \tag{4.71}$$

where the linear operator $\mathcal{A}$ is defined as

$$\mathcal{A}\mathbf{u}\left(\vartheta\right) = \begin{cases} \frac{\mathrm{d}}{\mathrm{d}\vartheta}\mathbf{u}\left(\vartheta\right) & \vartheta \in [-\tau, 0) \\ \mathbf{L}\mathbf{u}\left(0\right) + \mathbf{R}\mathbf{u}\left(-\tau\right) & \vartheta = 0 \end{cases} \tag{4.72}$$

while the adjoint operator $\mathcal{A}^*$ is given by

$$\mathcal{A}^*\mathbf{v}(\sigma) = \begin{cases} -\frac{\mathrm{d}}{\mathrm{d}\sigma}\mathbf{v}(\sigma) & \sigma \in (0,\tau] \\ \mathbf{L}^*\mathbf{v}(0) + \mathbf{R}^*\mathbf{v}(\tau) & \sigma = 0 \end{cases} \tag{4.73}$$

together with the bilinear form

$$(\mathbf{v},\mathbf{u}) = \mathbf{v}^*(0)\mathbf{u}(0) + \int_{-\tau}^{0} \mathbf{v}^*(\xi+\tau)\mathbf{R}\mathbf{u}(\xi)\mathrm{d}\xi \tag{4.74}$$

The center subspace is spanned by the real and imaginary parts of the complex eigenfunctions $\mathbf{s}_m(\vartheta)$ of $\mathcal{A}$ corresponding to the critical characteristic roots $i\omega_m$. The complex eigenfunctions $\mathbf{s}_m(\vartheta)$ and the eigenfunctions $\mathbf{n}_m(\sigma)$ of the adjoint operator $\mathcal{A}^*$ can be found from

$$\begin{aligned} \mathcal{A}\mathbf{s}_m(\vartheta) &= i\omega_m\mathcal{I}\mathbf{s}_m(\vartheta) \\ \mathcal{A}^*\mathbf{n}_m(\sigma) &= -i\omega_m\mathcal{I}^*\mathbf{n}_m(\sigma) \end{aligned} \tag{4.75}$$

where the identity operator $\mathcal{I}$ is defined as

$$\mathcal{I}\mathbf{u}(\theta) = \begin{cases} \mathbf{u}(\theta) & \theta \neq 0 \\ \mathbf{u}(0) & \theta = 0 \end{cases} \tag{4.76}$$

By defining the 'characteristic operator' as $\mathcal{D}(\lambda) = \lambda\mathcal{I} - \mathcal{A}$ equations (4.75) can also be written as

$$\begin{aligned} \mathcal{D}(i\omega_m)\mathbf{s}_m &= 0 \\ \mathcal{D}^*(i\omega_m)\mathbf{n}_m &= 0 \end{aligned} \tag{4.77}$$

The general solutions to (4.77) are found in the form

$$\begin{aligned} \mathbf{s}_m(\vartheta) &= \mathbf{c}_m e^{i\omega_m\vartheta} \\ \mathbf{n}_m(\sigma) &= \mathbf{d}_m e^{i\omega_m\sigma} \end{aligned} \tag{4.78}$$

The constants $\mathbf{c}_m$, $\mathbf{d}_m$ are found by using the boundary conditions ($\theta = 0$) embedded in the operator equations (4.77)

$$\mathbf{D}(i\omega_m)\mathbf{c}_m = \left(i\omega_m\mathbf{I} - \mathbf{L} - e^{-i\omega_m\tau}\mathbf{R}\right)\mathbf{c}_m = \mathbf{0} \tag{4.79}$$

$$\mathbf{D}^*\left(i\omega_m\right)\mathbf{d}_m = \left(\mathbf{d}_m^*\mathbf{D}\left(i\omega_m\right)\right)^* = \left(-i\omega_m\mathbf{I} - \mathbf{L}^{\mathrm{T}} - e^{i\omega_m\tau}\mathbf{R}^{\mathrm{T}}\right)\mathbf{d}_m = \mathbf{0} \tag{4.80}$$

The vectors $\mathbf{s}$, $\mathbf{n}$ should satisfy the 'orthonormality' conditions

$$(\mathbf{n}_l, \mathbf{s}_k) = \begin{cases} 0 & l \neq k \\ 2 & l = k \end{cases} \tag{4.81}$$

Using (6.52)

$$\begin{aligned} (\mathbf{n}_l, \mathbf{s}_k) &= \mathbf{n}_l^*(0)\mathbf{s}_k(0) + \int_{-\tau}^{0} \mathbf{n}_l^*(\xi+\tau)\mathbf{R}\mathbf{s}_k(\xi)\mathrm{d}\xi = \\ &= \mathbf{d}_l^*\mathbf{c}_k + \mathbf{d}_l^*\mathbf{R}\mathbf{c}_k e^{-i\omega_l\tau}\int_{-\tau}^{0} e^{i\xi(\omega_k-\omega_l)}\mathrm{d}\xi = \\ &= \begin{cases} \mathbf{d}_l^*\left(\mathbf{I} + \frac{i\left(e^{-i\omega_k\tau} - e^{-i\omega_l\tau}\right)}{\omega_k-\omega_l}\mathbf{R}\right)\mathbf{c}_k & l \neq k \\ \mathbf{d}_l^*\left(\mathbf{I} + \tau e^{-i\omega_l\tau}\mathbf{R}\right)\mathbf{c}_l & l = k \end{cases} \end{aligned} \tag{4.82}$$

This can also be rewritten in terms of the characteristic matrix (4.67) as

$$(\mathbf{n}_l, \mathbf{s}_k) = \begin{cases} \mathbf{d}_l^*\left(\frac{\mathbf{D}(i\omega_l) - \mathbf{D}(i\omega_k)}{i\omega_l - i\omega_k}\right)\mathbf{c}_k & l \neq k \\ \lim\limits_{k\to l}(\mathbf{n}_l, \mathbf{s}_k) = \mathbf{d}_l^*\left.\frac{\mathrm{d}\mathbf{D}(\lambda)}{\mathrm{d}\lambda}\right|_{\lambda=i\omega_l}\mathbf{c}_l & l = k \end{cases} \tag{4.83}$$

Note, that $(\mathbf{n}_l, \mathbf{s}_k)_{l\neq k} = 0$ is automatically satisfied because of (4.79, 4.80). To summarize, the vectors $\mathbf{c}$, $\mathbf{d}$ are found from the following equations

$$\mathbf{D}\left(i\omega_m\right)\mathbf{c}_m = \left(i\omega_m\mathbf{I} - \mathbf{L} - e^{-i\omega_m\tau}\mathbf{R}\right)\mathbf{c}_m = \mathbf{0} \tag{4.84}$$

$$\mathbf{D}^*\left(i\omega_m\right)\mathbf{d}_m = \left(i\omega_m\mathbf{I} + \mathbf{L}^{\mathrm{T}} + e^{i\omega_m\tau}\mathbf{R}^{\mathrm{T}}\right)\mathbf{d}_m = \mathbf{0} \tag{4.85}$$

$$\mathbf{d}_l^*\frac{\mathrm{d}\mathbf{D}\left(i\omega_l\right)}{\mathrm{d}\lambda}\mathbf{c}_l = \mathbf{d}_l^*\left(\mathbf{I} + \tau e^{-i\omega_l\tau}\mathbf{R}\right)\mathbf{c}_l = 2 \tag{4.86}$$

Since $\mathbf{D}(i\omega)$ is rank-1 ($D(i\omega) = 0$) there are $3n$ independent complex equations for $4n$ complex unknowns.

4.6.1 Example

For the classical model (3.28)

$$\mathbf{L} = \begin{pmatrix} 0 & 1 \\ -(1+p) & -2\zeta \end{pmatrix}, \quad \mathbf{R} = \begin{pmatrix} 0 & 0 \\ p & 0 \end{pmatrix}. \tag{4.87}$$

Equations (4.84, 4.85) result in (here c_{m1}, d_{m2} are complex!)

$$\mathbf{c}_m = \begin{pmatrix} 1 \\ i\omega_m \end{pmatrix} c_{m1} \tag{4.88}$$

$$\mathbf{d}_m = \begin{pmatrix} 2\zeta - i\omega_m \\ 1 \end{pmatrix} d_{m2} \tag{4.89}$$

Then from (4.86)

$$c_{m1} d_{m2}^* \left(2\zeta + p\tau e^{-i\tau\omega_m} + 2i\omega_m\right) = 2 \tag{4.90}$$

We have the freedom to fix n unknowns, so we choose $c_{m1} = 1$ which in turn yields

$$d_{m2} = \frac{2}{2\zeta + \tau\left(1 + p - \omega_m^2\right) - i2\omega_m\left(1 + \zeta\tau\right)} \tag{4.91}$$

or separating real and imaginary parts

$$d_{m2} = \delta_m \left(2\zeta + \tau\left(1 + p - \omega_m^2\right) + i2\omega_m\left(1 + \zeta\tau\right)\right) \tag{4.92}$$

$$\delta_m = \frac{2}{4\omega_m^2\left(1 + \zeta\tau\right)^2 + \left(2\zeta + \tau\left(1 + p - \omega_m^2\right)\right)^2} \tag{4.93}$$

Then we have

$$\mathbf{d}_m = \delta_m \begin{pmatrix} 2\left(\omega_m^2 + 2\zeta^2 + \zeta\tau\left(1 + p\right)\right) + i\omega_m\left(4\zeta^2\tau + 2\zeta - \tau\left(1 + p - \omega_m^2\right)\right) \\ \left(2\zeta + \tau\left(1 + p - \omega_m^2\right)\right) + i2\omega_m\left(1 + \zeta\tau\right) \end{pmatrix} \tag{4.94}$$

And the real functions $\mathbf{s}_{m1}$, $\mathbf{s}_{m2}$ span the $2n$ dimensional center manifold

$$\mathbf{s}_{m1} = \mathrm{Re}\,\mathbf{s}_m = \begin{pmatrix} \cos(\omega_m t) \\ -\omega_m \sin(\omega_m t) \end{pmatrix}, \qquad \mathbf{s}_{m2} = \mathrm{Im}\,\mathbf{s}_m = \begin{pmatrix} \sin(\omega_m t) \\ \omega_m \cos(\omega_m t) \end{pmatrix} \quad (4.95)$$

Chapter 5

Machining Experiments

This part presents a series of tool vibration measurements in the single point turning of aluminium. The experiments were performed at NIST in collaboration with Dr. Jon Pratt. Some of the results have already been published (Kalmár-Nagy et al., 1999; Pratt et al., 1999) and this chapter is loosely based on these papers.

The motivation behind this work was to gather a consistent set of data to validate theoretical results on the classical single-DOF model for tool vibrations. A dynamic test fixture (1 DOF flexible tool holder with actuators and sensors for dynamic cutting measurements) was developed to explore cutting dynamics (see also Peters and Van Brussel, 1996). In addition, analog feedback control has been incorporated to modify the fixture dynamics. With this active tool-holder, one can explore methodologies for determining machine-tool and cutting process response functions, validate cutting process stability analysis and simulations. Experiments were performed on a diamond turning lathe equipped with a 1.1 kW air-bearing spindle capable of speeds between 0 and 1500 rpm. Its manual slides position unidirectionally within 5 μm; the backlash is about 40 μm.

5.1 Experimental Setup

The dynamic test fixture (Figure 5.1) consists of a right hand cutting tool with a triangular tungsten carbide insert (rake angle=5°, clearance angle=11°, manufactured by), held in a standard tool post mounted to a rigid steel plate.

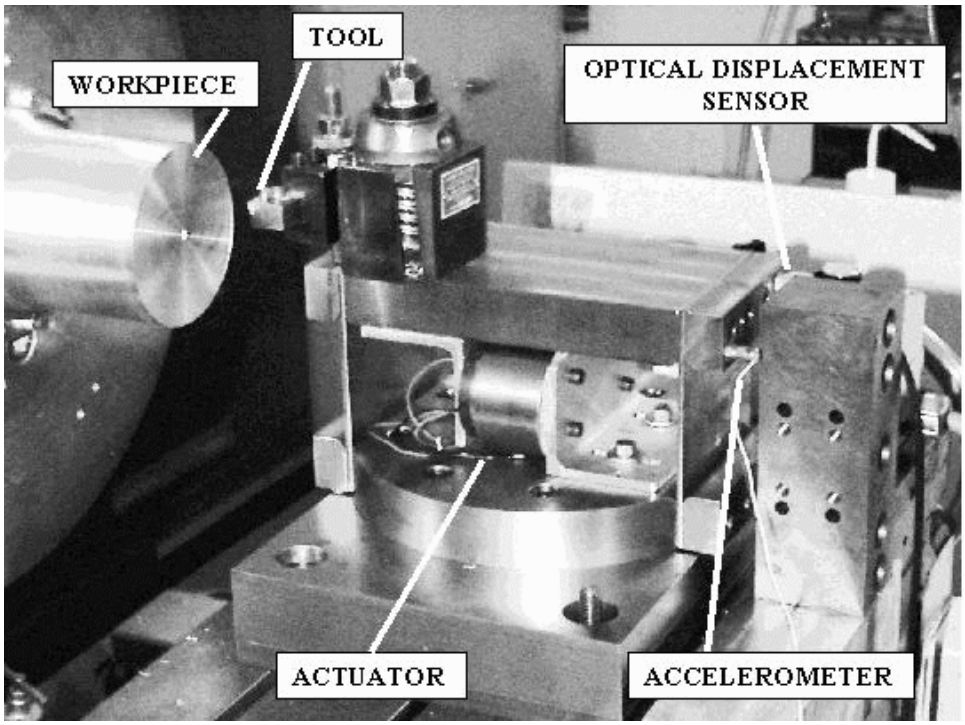

Figure 5.1: Experimental apparatus.

This plate is supported at both ends by thin steel plates thus creating a table structure having high stiffness in the directions perpendicular to the feed direction. This structure is rigidly mounted to the cross slide. Between the two thin plates, two voice coil actuators are placed. The pole pieces are grounded to the cross-slide, while the coils move with the table. Forces can be exerted on the flexible structure by varying the current in the coils. These actuators were used in a chatter control experiment (Pratt et al., 2000).

The workpieces are flanged aluminium cylinders with nominal diameter of 100 mm. These were given a finishing before each set of measurements so that the surface was smooth. The voice coil actuators were used to damp out unwanted vibrations during the finishing procedure. The cylinders are rigidly mounted to the spindle and assumed rigid compared to the tool. The relative displacement between the tool and the workpiece is measured by the table deflection using an optical displacement sensor. An accelerometer is also used to characterize tool motions.

5.2 System Identification

In order to adequately model the fixture's dynamic behavior, both the structural response and the cutting process must be identified. Tounsi and Otho (2000) proposed a method to identify the structural dynamics of a machine-tool-workpiece system by means of interrupted cutting (machining a gear-like workpiece that provides pulse-like cutting force). As derived in Chapter 3 the equation of motion for a SDOF tool can be written as

$$\ddot{x} + 2\zeta\omega_n\dot{x} + \omega_n^2 x = -\frac{1}{m}\Delta F_x \tag{5.1}$$

The mass of the apparatus was found to be

$$m = 10 \text{ kg} \tag{5.2}$$

5.3 Structural Response

The frequency response function (FRF) of a system under test can be determined by conducting a swept-sine test. The tool was sinusoidally excited by means of the

voice coil actuators. With fixed amplitude, the frequency of the signal was varied and the output was measured at different frequencies. The amplitude ratio (output over input) of the peak-to-peak or rms value is determined at each frequency. The machine-tool response function is plotted in Figure 5.2

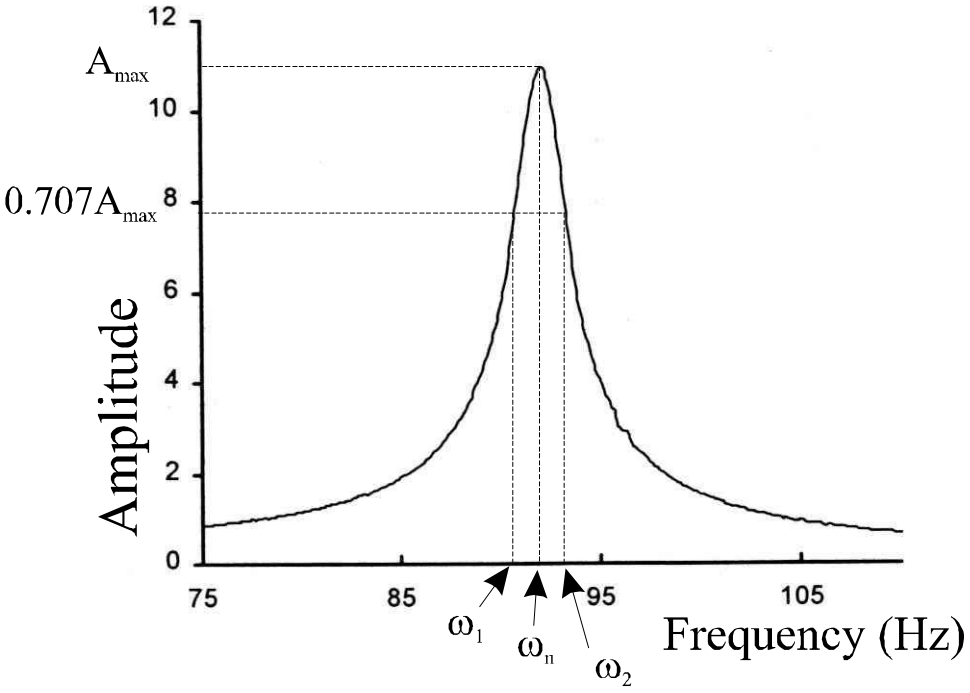

Figure 5.2: Frequency response function.

The modal frequency is simply taken as the frequency of the peak. To estimate damping ratio from the FRF, the *half-power point method* is used. At 70.7% of the magnitude of the modal peak there are the two half-power points with corresponding frequencies ω_1 and ω_2.

The damping ratio can then be calculated as

$$\zeta = \frac{\omega_2 - \omega_1}{2\omega_n} \tag{5.3}$$

The following parameters are identified

$$\omega_n = 92 \text{ Hz} = 578 \text{ rad/s} \tag{5.4}$$

$$\omega_1 = 90.6 \text{ Hz} \qquad \omega_2 = 93.1 \text{ Hz} \tag{5.5}$$

$$\zeta = 0.0136 \tag{5.6}$$

The damping here is only structural damping. It does not include damping that arise from the cutting process (see Chapter 7).

5.4 Nonlinear Cutting Force

As observed by several researchers (Hanna and Tobias 1974; Shi and Tobias 1984), the nonlinear variation of the cutting force as a function of chip thickness can have a dramatic effect on the process stability. Early evidence of the nonlinear dependence of cutting force on feed can be found in the seminal work of Taylor (1907), who felt the characterization of this dependence was of no practical worth, but nonetheless made some of the most carefully controlled measurements to be found in the vast cutting literature. Here we measured the thrust force component of the static cutting force as a function of feed at a fixed cutting speed by replacing the dynamic cutting fixture with a three-component force dynamometer. We note, as a matter of interest, that Taylor inferred the value of the 'cutting pressure' from measurements of the power consumption, while our contemporary practice makes use of modern, high-stiffness dynamometry.

Because of the orientation of the dynamic fixture, we measure only the thrust component of the static cutting force as a function of feed at a fixed cutting speed. The dynamometer output voltage is low-pass filtered at 2 Hz, to eliminate high-frequency content resulting from random excitations. After every cut, the tool was

let to cool to room temperature.

Figure 5.3 shows the results of static cutting force measurements.

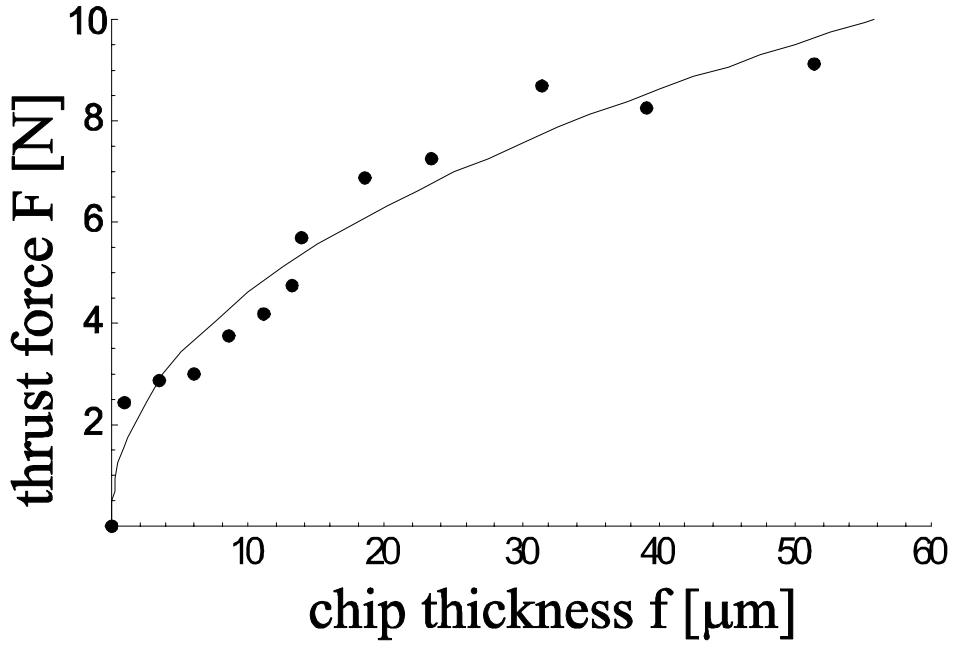

Figure 5.3: Nonlinear cutting force-chip thickness dependence. Solid dots represent experimental data, while the solid line represents equation (5.7).

The thrust force in Newtons is plotted as a function of the feed per revolution (chip thickness) in micrometers for a rotational speed of $\Omega = 836$ rpm (with radius $r = 50$ mm, the cutting velocity is $v_C = 4.375$ m/s) and a nominal width of cut $w_0 = 0.25$ mm (the cutting force was insensitive for small variations in Ω, see also Section 2.1). The force dependence is modeled by a power law (Taylor, 1907), rather than the cubic polynomials of Hanna and Tobias (1974) and Shi and Tobias (1984)

$$F_x(f) = 553 f^{0.41} \text{ [N]} \tag{5.7}$$

where $f = f_0 + \Delta f$ is in meters and $\Delta f = x - x_\tau$ is the chip thickness variation. For

static measurements $\Delta f = 0$ m, since the tool assumes an average static deflection that balances the average cutting force. The cutting coefficient at the nominal feed $f_0 = 36$ μm (and $w_0 = 0.25$ mm) can be calculated as

$$k_1 = \left.\frac{dF_x}{df}\right|_{f_0} = 105000 \frac{\text{N}}{\text{m}} \tag{5.8}$$

Observe that this is the local slope of the cutting force characteristic. Historically, this term has been used to characterize the dynamic cutting force (Tobias, 1965).

5.5 Experimental Stability Chart

A lobe of the stability boundary is traced in a series of experiments. All cutting measurements are made at the same feedrate $s = 508$ μm/s. The feed per revolution f_0 varies by 11% between the smallest and largest rotational rates. Beginning with a small stable cut at a fixed speed, the width of cut w is increased in 25 μm increments using the manual slide in a ramp and hold fashion. The experiment is stopped and recorded when self-sustaining oscillations are observed in the accelerometer voltage monitored on a digital oscilloscope. The test is repeated at different speeds until the lobe is mapped. The experimental stability chart 5.4 shows stability as a function of rotational rate and width of cut w. The analytical curves are drawn (see Sections 4.3 and 6.2) by using the identified parameter values

$$m = 10 \text{ kg}, \zeta = 0.0136, \omega_n = 578 \text{ rad/s} \tag{5.9}$$

Material removal can be increased between 840 rpm and 925 rpm, since w grows from approximately 200 μm to 800 μm over this range.

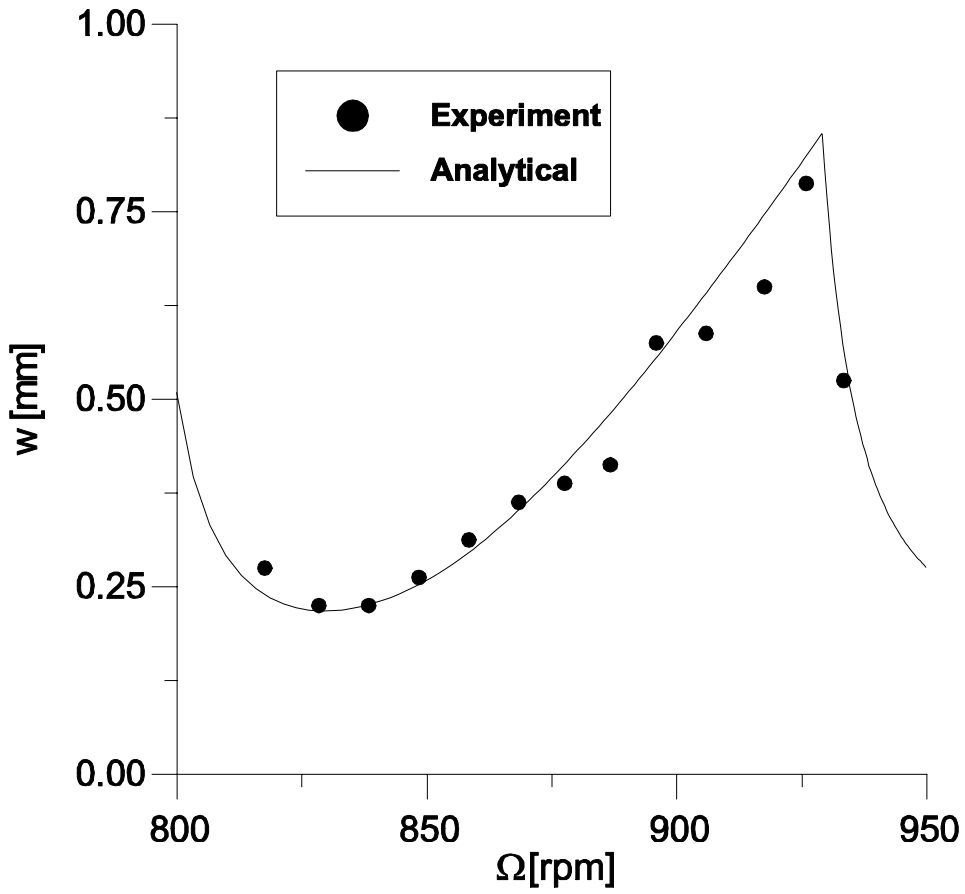

Figure 5.4: Experimental stability chart. The maximal chip width w for which the system is stable shown (for increasing w).

5.6 Experimental Bifurcation Diagram

Next, an experimental bifurcation diagram is generated for the tool system at fixed Ω and s. The bifurcation diagram records the root-mean-square (rms) tool vibration amplitude as a function of w. The response is recorded for both forward and backward sweeps of the control parameter in order to reveal the nonlinear behavior. Tool position measurements are compensated for backlash at the reversal. A nominal speed of 836 rpm is selected corresponding to the minimum of the previously mapped lobe. The spindle speed is not well controlled, and is observed to

decrease $\approx$ 2 rpm as the chip load is increased. Fortunately, the stability along the base of the lobe appears fairly insensitive to this variation.

To create the bifurcation diagram the width of cut w is swept as for the lobe determination, except that the ramp and hold increments are 10 μm and the outputs of the displacement and acceleration signals are continuously recorded. At each increment, the tool cuts for about 5 seconds, these intervals being logged on a separate channel of the scope via a manual switch. The forward sweep is executed first, then the part is remachined to a smooth surface, and the backward sweep is conducted. A variation in the mean surface speed, due to the reduction in the part diameter between forward and backward sweeps, is about 3 percent. The resulting experimental bifurcation diagram is shown in Figure 5.5.

This hysteretic behavior occurs in many practical machining operations, and has been observed by other researchers (Hanna and Tobias, 1974; Shi and Tobias, 1984). In the case shown here, the region of the subcritical instability makes up nearly 40% of the predicted chatter free operating regime. Within this region, disturbances, as might be caused by deviations in the workpiece, jamming up of chips, etc. can push the system into unstable vibrations.

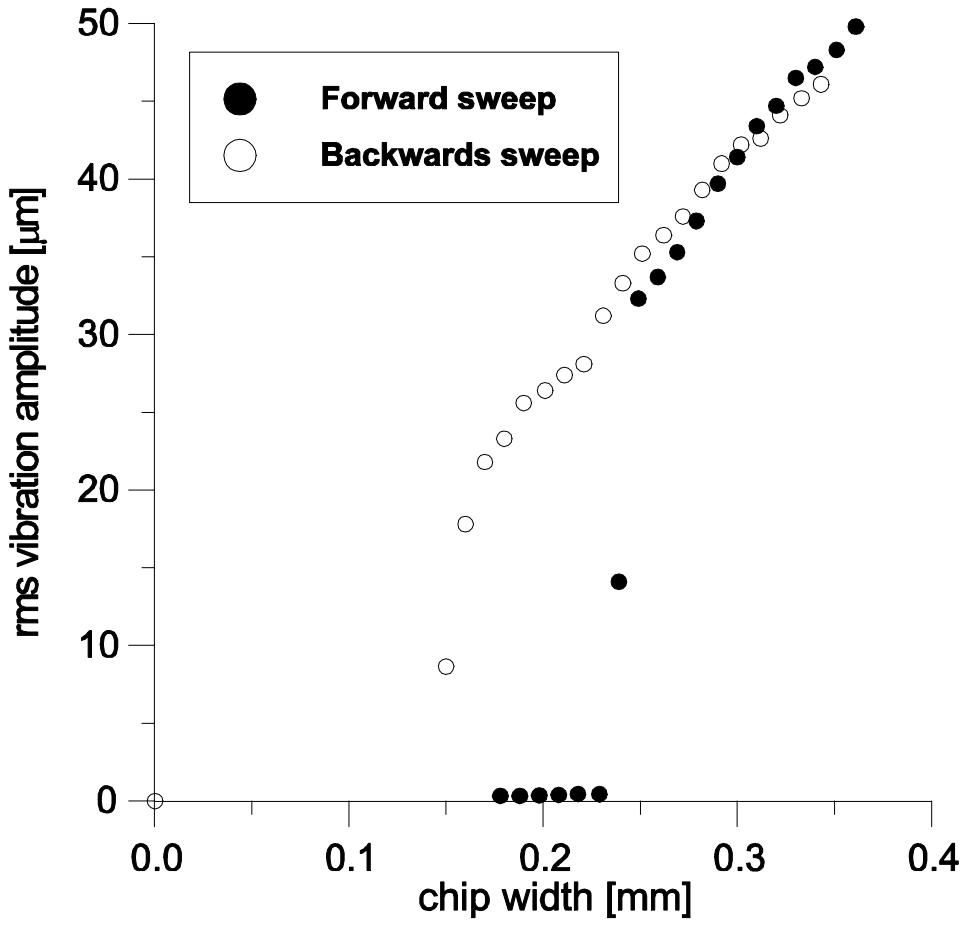

Figure 5.5: Experimental bifurcation diagram. Rms vibration amplitude versus chip width w.

Chapter 6

The Classical Model: Periodic Vibrations

Some of these results have already been published (Stépán and Kalmár-Nagy, 1997; Kalmár-Nagy et al., 1999; Kalmár-Nagy et al., 2001; Kalmár-Nagy et al., 2002) and the Chapter is based on these papers.

The equation of motion for the classical 1 DOF model of tool vibration is given by equation (7.34)

$$\ddot{x} + 2\zeta\omega_n\dot{x} + \omega_n^2 x = -\frac{1}{m}\Delta F_x \tag{6.1}$$

where $\omega_n = \sqrt{k/m}$ is the natural angular frequency of the undamped free oscillating system, and $\zeta = c/(2m\omega_n)$ is the so-called relative damping factor.

The cutting force variation ΔF_x is considered to be the function of the chip thickness variation Δf which depends on both the current position x of the tool edge and its position one revolution ago.

A simple but empirical way to estimate the cutting force is the use of a curve fitting to data obtained from quasi-steady cutting tests. Here we will use the

formula given by Taylor (1907). According to this, the cutting force F_x depends on the chip thickness as

$$F_x(f) = Kwf^{\frac{3}{4}} \tag{6.2}$$

where the parameter K depends on further technological parameters considered to be constant in the present analysis. This is a quasi-static approximation of the cutting force, that does not account for dynamic changes of the chip thickness (dynamic effects will be studied in the next Chapter). The analysis can be extended for power laws with exponent α, see Kalmár-Nagy et al. (1999) and Kalmár-Nagy et al. (2002). Expanding F_x into a power series form around the desired chip thickness f_0 and keeping terms up to order 3 yields

$$F_x(f) \approx Kw \left(f_0^{\frac{3}{4}} + \frac{3}{4}(f-f_0) f_0^{-\frac{1}{4}} - \frac{3}{32}(f-f_0)^2 f_0^{-\frac{5}{4}} + \frac{5}{128}(f-f_0)^3 f_0^{-\frac{9}{4}} \right) \tag{6.3}$$

Or equivalently, we can express the cutting force variation $\Delta F_x = F_x(f) - F_x(f_0)$ as the function of the chip thickness variation $\Delta f = f - f_0$, like

$$\Delta F_x(\Delta f) \approx Kw \left(\frac{3}{4} f_0^{-\frac{1}{4}} \Delta f - \frac{3}{32} f_0^{-\frac{5}{4}} \Delta f^2 + \frac{5}{128} f_0^{-\frac{9}{4}} \Delta f^3 \right) \tag{6.4}$$

The coefficient of Δf on the right hand side of equation (6.4) is usually called the *cutting force coefficient* and denoted by k_1 ($k_1 = \frac{3}{4} K w f_0^{-\frac{1}{4}}$). Note, that k_1 is linearly proportional to the width w of the chip, so in the upcoming calculations it will serve as a bifurcation parameter. Then equation (6.4) can be rewritten as

$$\Delta F_x(\Delta f) \approx k_1 \Delta f - \frac{1}{8} \frac{k_1}{f_0} \Delta f^2 + \frac{5}{96} \frac{k_1}{f_0^2} \Delta f^3 \tag{6.5}$$

Although first only the local bifurcation at $f = f_0 \Leftrightarrow \Delta f = 0$ will be investigated, the case when the tool can leave the material will be taken up in Section 6.8.

The chip thickness variation Δf can easily be expressed as the difference of the present tool edge position $x(t)$ and the delayed one $x(t-\tau)$ in the form

$$\Delta f = x(t) - x(t-\tau) = x - x_\tau \tag{6.6}$$

where the delay $\tau = 2\pi/\Omega$ is the time period of one revolution with Ω being the constant angular velocity of the rotating workpiece. By bringing the linear terms to the left hand side of the equation of motion (6.1) becomes

$$\begin{aligned} &\ddot{x} + 2\zeta\omega_n\dot{x} + \left(\omega_n^2 + \frac{k_1}{m}\right)x - \frac{k_1}{m}x_\tau = \\ &= \frac{k_1}{8f_0 m}\left((x-x_\tau)^2 - \frac{5}{12f_0}(x-x_\tau)^3\right) \end{aligned} \tag{6.7}$$

6.1 Nondimensionalization

Let us introduce the nondimensional time $\tilde{t}$ and displacement $\widetilde{x}$

$$\tilde{t} = \omega_n t \quad \widetilde{x} = \frac{5}{12f_0}x \tag{6.8}$$

and the nondimensional bifurcation parameter

$$p = \frac{k_1}{m\omega_n^2} \tag{6.9}$$

Dropping the tilde (note that the nondimensional time delay is $\tilde{\tau} = \omega_n\tau$) we arrive at

$$\ddot{x} + 2\zeta\dot{x} + x = -p\,(x - x_\tau) + p\delta\left((x-x_\tau)^2 - (x-x_\tau)^3\right) \tag{6.10}$$

where for this particular form of the cutting force

$$\delta = 3/10 \tag{6.11}$$

For any polynomial approximation of the cutting force that is a function of the chip thickness only, the lengthscale can be chosen so that the right hand side will

be exactly as in equation (6.10). If the structure is nonlinear (such as in Hanna and Tobias, 1974), nonlinear terms of x will appear on the left hand side.

The second order equation (6.10) is transformed into a 2 dimensional system by introducing

$$\mathbf{x}(t) = \begin{pmatrix} x_1(t) \\ x_2(t) \end{pmatrix} = \begin{pmatrix} x(t) \\ \dot{x}(t) \end{pmatrix} \tag{6.12}$$

and we obtain the delay-differential equation

$$\dot{\mathbf{x}}(t) = \mathbf{L}(p)\mathbf{x}(t) + \mathbf{R}(p)\mathbf{x}(t-\tau) + \mathbf{f}(\mathbf{x}(t), \mathbf{x}(t-\tau), p) \tag{6.13}$$

where the dependence on the bifurcation parameter p is also emphasized:

$$\begin{aligned} \mathbf{L}(p) &= \begin{pmatrix} 0 & 1 \\ -(1+p) & -2\zeta \end{pmatrix} \\ \mathbf{R}(p) &= \begin{pmatrix} 0 & 0 \\ p & 0 \end{pmatrix} \\ \mathbf{f}(\mathbf{x}(t), p) &= \frac{3p}{10} \begin{pmatrix} 0 \\ (x_1(t) - x_1(t-\tau))^2 - (x_1(t) - x_1(t-\tau))^3 \end{pmatrix} \end{aligned} \tag{6.14}$$

6.2 Linear Stability Analysis

The characteristic function of equation (6.13) can be obtained by substituting the trial solution $\mathbf{x}(t) = \mathbf{c}\exp(\lambda t)$ into its linear part:

$$\begin{aligned} D(\lambda, p) &= \det(\lambda\mathbf{I} - \mathbf{L}(p) - \mathbf{R}(p)\mathrm{e}^{-\lambda\tau}) = \\ &= \lambda^2 + 2\zeta\lambda + (1+p) - p\mathrm{e}^{-\lambda\tau} \end{aligned} \tag{6.15}$$

The necessary condition for the existence of a non-zero solution is

$$D(\lambda, p) = 0 \tag{6.16}$$

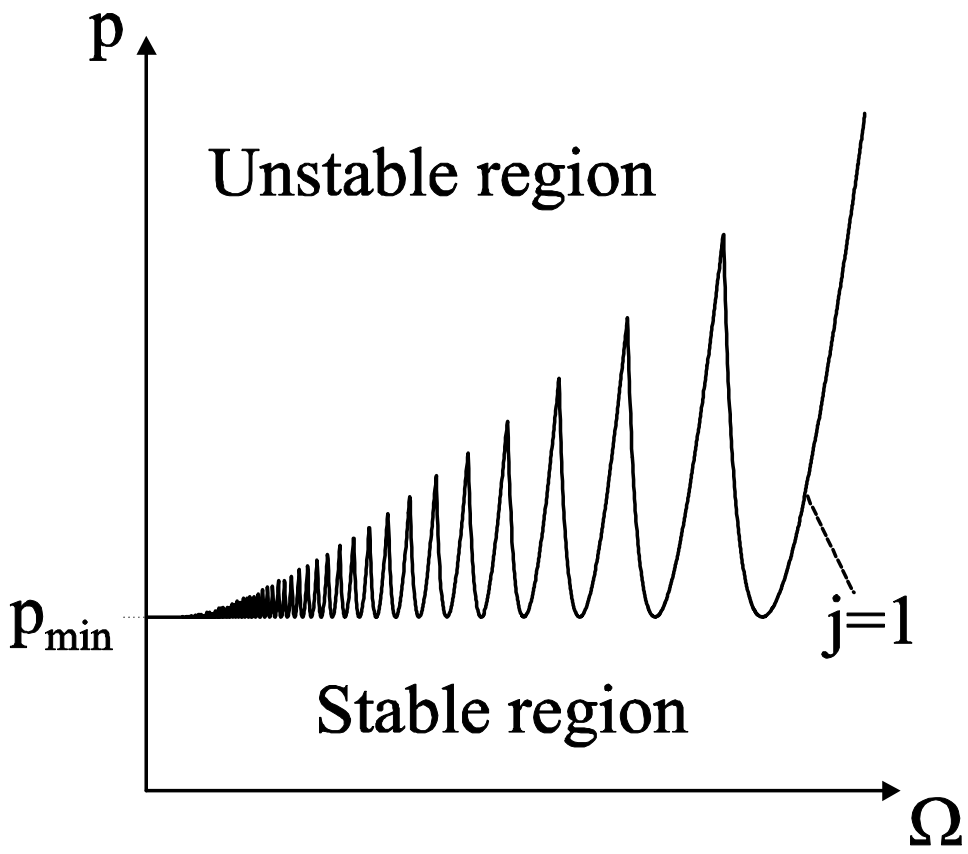

Figure 6.1: Stability chart for the classical model ($\Omega = 2\pi/\tau$)

On the stability boundary shown in Figure 6.1 the characteristic equation has one pair of pure imaginary roots (except the intersections of the lobes, where it has two pairs of imaginary roots). To find this curve, we substitute $\lambda = i\omega$, $\omega > 0$ into equation (6.15).

$$D(i\omega, p) = 1 + p - \omega^2 - p\cos\omega\tau + i\,(2\zeta\omega + p\sin\omega\tau) = 0 \tag{6.17}$$

This complex equation is equivalent to the two real equations

$$1 - \omega^2 + p\,(1 - \cos\omega\tau) = 0 \tag{6.18}$$

$$2\zeta\omega + p\sin\omega\tau = 0 \tag{6.19}$$

The trigonometric terms in equations (6.18, 6.19) can be eliminated to yield

$$p = \frac{\left(1-\omega^2\right)^2 + 4\zeta^2\omega^2}{2\left(\omega^2-1\right)} \tag{6.20}$$

Since $p > 0$ (this is so because the cutting force coefficient is positive, the more material is removed, the higher the cutting force is) this also implies $\omega > 1$.

With the help of the trigonometric identity

$$\frac{1-\cos\omega\tau}{\sin\omega\tau} = \tan\frac{\omega\tau}{2} \tag{6.21}$$

τ can be expressed from equations (6.18, 6.19) as

$$\tau = \frac{2}{\omega}\left(j\pi - \arctan\frac{\omega^2-1}{2\zeta\omega}\right) \quad j = 1, 2, \ldots \tag{6.22}$$

where j corresponds to the jth 'lobe' (parameterized by ω as both τ and p are functions of ω) from the right in the stability diagram (j must be greater than 0, because $\tau > 0$).

And finally

$$\Omega = \frac{2\pi}{\tau} = \frac{\omega\pi}{j\pi - \arctan\frac{\omega^2-1}{2\zeta\omega}} \quad j = 1, 2, \ldots \tag{6.23}$$

At the minima ('notches') of the stability boundary ω, p, Ω assume particularly simple forms. To find these values $\frac{dp}{d\omega} = 0$ has to be solved. Then we find

$$\omega = \sqrt{1+2\zeta}$$

$$p_{\min} = 2\zeta\left(\zeta+1\right) \tag{6.24}$$

$$\tau = \frac{2\left(j\pi - \arctan\frac{1}{\sqrt{1+2\zeta}}\right)}{\sqrt{1+2\zeta}} \quad j = 1, 2, \ldots \tag{6.25}$$

$$\Omega = \frac{\sqrt{1+2\zeta}\pi}{j\pi - \arctan\frac{1}{\sqrt{1+2\zeta}}} \quad j = 1, 2, \ldots$$

To simplify calculations we present results obtained at these parameter values (the calculations can be carried out in general along the stability boundary, see Kalmár-Nagy et al., 1999 and Kalmár-Nagy et al., 2002).

The location of the characteristic roots has now to be established.

A heuristic argument is as follows (this can rigorously proved with Rouché's Theorem, see Appendix D): for $p = 0$ equation (6.15) has only two roots ($\lambda_{1,2} = -\zeta \pm i\sqrt{1-\zeta^2}$) and these are located in the left half plane. Since the delay term makes the phase space infinite dimensional, we might say that apart from these two roots, there are infinitely many more, these being at the north pole of the Riemann-sphere (minus complexinfinity). Increasing the value of p results in characteristic roots 'swarming out' from minus complexinfinity, but for small enough p they do not leave the left half plane.

The necessary condition for the existence of periodic orbits is that by varying the bifurcation parameter (p) the critical characteristic roots cross the imaginary axis with non-zero velocity, that is $\mathrm{Re}\,\frac{\mathrm{d}\lambda(p_{cr})}{\mathrm{d}p} \neq 0$. The characteristic function (6.15) has two zeros $\lambda = \pm i\sqrt{1+2\zeta}$ at the notches.

The change of the real parts of these critical characteristic roots can be determined via implicit differentiation of the characteristic function (6.15) with respect to the bifurcation parameter p

$$\frac{\mathrm{d}D(\lambda(p),p)}{\mathrm{d}p} = \frac{\partial D(\lambda(p),p)}{\partial p} + \frac{\partial D(\lambda(p),p)}{\partial \lambda}\frac{\mathrm{d}\lambda(p)}{\mathrm{d}p} = 0 \tag{6.26}$$

$$\frac{\mathrm{d}\lambda(p_{cr})}{\mathrm{d}p} = -\left.\frac{\frac{\partial D(\lambda(p),p)}{\partial p}}{\frac{\partial D(\lambda(p),p)}{\partial \lambda}}\right|_{\lambda = i\sqrt{1+2\zeta}} \tag{6.27}$$

$$\gamma\colon = \mathrm{Re}\,\frac{\mathrm{d}\lambda(p_{cr})}{\mathrm{d}p} = \frac{1}{2(1+\zeta)^2(1+\zeta\tau)} \tag{6.28}$$

Since γ is always positive and all the characteristic roots but the critical ones of (6.15) are located in the left half complex plane, the conditions of an infinite dimensional version of the Hopf Bifurcation Theorem given in Hassard, Kazarinoff and Wan (1981) are satisfied. γ will later be used in the estimation of the vibration amplitude.

6.3 Solution By Harmonic Balance

The equation studied here is

$$\ddot{x} + 2\zeta\dot{x} + x = -p\,(x - x_\tau) + p\delta\left((x - x_\tau)^2 - (x - x_\tau)^3\right) \tag{6.29}$$

We seek the solution in the form (Mickens, 1996; Nayfeh and Mook, 1979)

$$x\,(t) = A\cos\,(\omega t) + B \tag{6.30}$$

Note, that the constant term is necessary because of the asymmetrical nonlinearity.

Substituting this into (6.29) results

$$C_0 + C_1\cos\,(\omega t) + C_2\sin\,(\omega t) + HOH = 0 \tag{6.31}$$

where HOH stands for higher order harmonics. We require that the C_i's vanish, yielding the following system of equations

$$B - A^2\,p\,\delta + A^2 p\delta\cos\,(\tau\omega) = 0 \tag{6.32}$$

$$2\,\zeta\,\omega + p\,\sin(\tau\,\omega) + \frac{3}{2}A^2\,p\,\delta\,\left(1 - \cos(\tau\,\omega)\right)\,\sin(\tau\,\omega) = 0 \tag{6.33}$$

$$1 - \omega^2 + p\,\left(1 - \cos(\tau\,\omega)\right) + \frac{3p\delta A^2}{2}\left(1 - \cos(\tau\,\omega)\right)^2 = 0 \tag{6.34}$$

Note that setting $A = B = 0$ we recover the linear stability criteria (6.18, 6.19). equation (6.32) immediately results

$$B = A^2\,p\,\delta\,(1 - \cos(\tau\,\omega)) \tag{6.35}$$

Solving (6.33) for A^2 gives

$$A^2 = \frac{2}{3}\frac{p + \frac{2\,\zeta\,\omega}{\sin(\tau\,\omega)}}{p\,\delta\,\left(\cos(\tau\,\omega) - 1\right)} \tag{6.36}$$

Substituting this for A^2 in (6.34) results

$$1 - \omega^2 - 2\zeta\omega \tan\left(\frac{\tau\omega}{2}\right) = 0 \tag{6.37}$$

Note that the frequency ω is not a function of the amplitude, only that of the time delay τ. So we can conveniently use the value of ω on the stability boundary. As was established earlier, on the stability boundary (see equations (6.18, 6.19))

$$\sin(\tau\,\omega) = -\frac{2\,\zeta\,\omega}{p_{cr}} \tag{6.38}$$

$$\cos(\tau\,\omega) = 1 + \frac{1-\omega^2}{p_{cr}} \tag{6.39}$$

We perturb the bifurcation parameter off of the stability boundary as

$$p = p_{cr}\,(1+\varepsilon) \tag{6.40}$$

Using (6.38, 6.39, 6.40) in (6.36) yields

$$A = \sqrt{\frac{2\varepsilon p_{cr}}{3\delta\,(1+\varepsilon)\,(1-\omega^2)}} \tag{6.41}$$

And from (6.35)

$$B = -\frac{2p_{cr}\varepsilon}{3} \tag{6.42}$$

These simple expressions are due to the fact that the constant term cancels in the expressions involving $x - x_\tau$. Since $\delta > 0$, $\omega > 1$ the perturbation ε has to be negative for a limit cycle to exist, that is the limit cycle only exist *below* the stability boundary.

To test this result, we compare the approximate amplitude with numerically obtained ones at the first notch, where

$$\omega = \sqrt{1+2\zeta} \tag{6.43}$$

The delay-differential equation (6.29) was integrated with initial functions of the

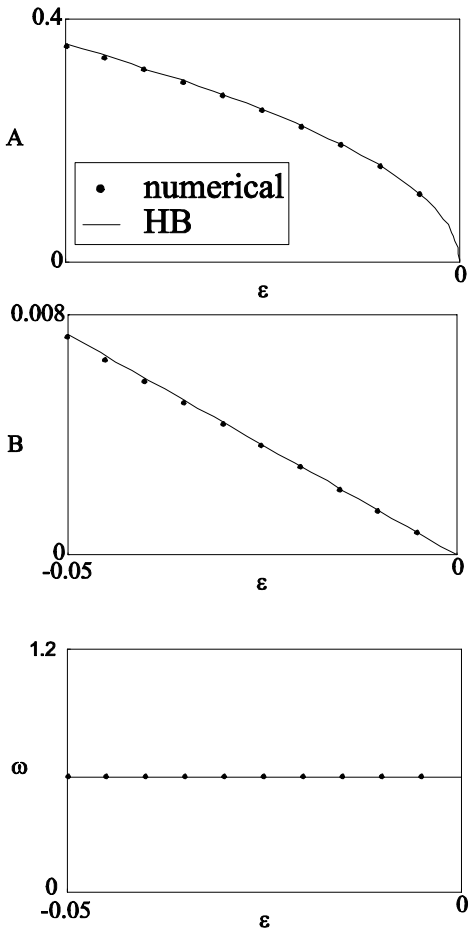

Figure 6.2: Comparison of Harmonic Balance (HB) and numerical solutions.

form $a\cos(\omega t)$. The integration was carried out for 15τ intervals of which the first 5τ intervals were discarded. Stability was determined by whether the amplitude of the solution grew or decayed. A simple bisection algorithm was then employed to find the value of a that resulted in the least growth or decay of the amplitude. Let t_1 and t_2 denote the times where the first and third zeros of the numerical solution $\tilde{x}(t)$, $t \in [5\tau, 15\tau]$ occur. Then

$$B = \frac{1}{t_2 - t_1} \int_{t_1}^{t_2} \tilde{x}(t)\, dt \tag{6.44}$$

$$A = \max_{t \in [t_1, t_2]} |\tilde{x}(t)| - B \tag{6.45}$$

$$\omega = \frac{2\pi}{t_2 - t_1} \tag{6.46}$$

The comparison between the harmonic balance approximation and numerical simulations is shown in Figure 6.2. The agreement is excellent. Unfortunately, the method of Harmonic Balance is known to yield spurious solutions (or no solutions at all) and it can not provide information about stability. Also, making the derivation rigorous for equation (6.29) and proving convergence is not an easy task. Since we want to establish the presence of Hopf bifurcation rigorously, we turn to Center Manifold Theory (for a modern treatment on ODEs see Rand and Armbruster (1987), Guckenheimer and Holmes (1992) and Wiggins (1996)).

6.4 Operator Differential Equation Formulation

In order to study the *critical* infinite dimensional problem on a two-dimensional center manifold we need the operator differential equation representation of equation (6.13).

This delay-differential equation can be expressed as the abstract evolution equation (Campbell et al., 1995; Hale, 1977; Kuang, 1993) on the Banach space $\mathcal{H}$ of continuously differentiable functions $\mathbf{u}\colon [-\tau, 0] \to \mathbb{R}^2$

$$\dot{\mathbf{x}}_t = \mathcal{A}\mathbf{x}_t + \mathcal{F}(\mathbf{x}_t) \tag{6.47}$$

Here $\mathbf{x}_t(\varphi) \in \mathcal{H}$ is defined by the shift of time

$$\mathbf{x}_t(\varphi) = \mathbf{x}(t + \varphi)\,, \quad \varphi \in [-\tau, 0] \tag{6.48}$$

The linear operator $\mathcal{A}$ at the critical value of the bifurcation parameter assumes the form (see Chapter 4)

$$\mathcal{A}\mathbf{u}(\vartheta) = \begin{cases} \frac{\mathrm{d}}{\mathrm{d}\vartheta}\mathbf{u}(\vartheta) & \vartheta \in [-\tau, 0) \\ \mathbf{L}\mathbf{u}(0) + \mathbf{R}\mathbf{u}(-\tau) & \vartheta = 0 \end{cases} \tag{6.49}$$

while the nonlinear operator $\mathcal{F}$ can be written as

$$\mathcal{F}(\mathbf{u})(\vartheta) =$$

$$= \begin{cases} \mathbf{0} & \vartheta \in [-\tau, 0) \\ \frac{3p}{10} \begin{pmatrix} 0 \\ (u_1(0) - u_1(-\tau))^2 - (u_1(0) - u_1(-\tau))^3 \end{pmatrix} & \vartheta = 0 \end{cases} \tag{6.50}$$

where $\mathbf{u} \in \mathcal{H}$ (compare with equation (6.14)).

The adjoint space $\mathcal{H}^*$ of continuously differentiable functions $\mathbf{v}\colon [0, \tau] \to \mathbb{R}^2$ with the adjoint operator

$$\mathcal{A}^*\mathbf{v}(\sigma) = \begin{cases} -\frac{\mathrm{d}}{\mathrm{d}\sigma}\mathbf{v}(\sigma) & \sigma \in (0, \tau] \\ \mathbf{L}^*\mathbf{v}(0) + \mathbf{R}^*\mathbf{v}(\tau) & \sigma = 0 \end{cases} \tag{6.51}$$

is also needed as well as the bilinear form $(\ ,\ )\colon \mathcal{H}^* \times \mathcal{H} \to \mathbb{R}$ defined by

$$(\mathbf{v}, \mathbf{u}) = \mathbf{v}^*(0)\mathbf{u}(0) + \int_{-\tau}^{0} \mathbf{v}^*(\xi + \tau)\mathbf{R}\mathbf{u}(\xi)\mathrm{d}\xi \tag{6.52}$$

For a heuristic argument of how these operators and bilinear form arise, see Section 4.5.

Since the critical eigenvalues of the linear operator $\mathcal{A}$ just coincide with the critical characteristic roots of the characteristic function $D(\lambda, p)$, the Hopf bifurcation arising at the degenerate trivial solution can be studied on a 2 dimensional center manifold embedded in the infinite dimensional phase space.

A first order approximation to this center manifold can be given by the center subspace of the associated linear problem, which is spanned by the real and imaginary parts $\mathbf{s}_1$, $\mathbf{s}_2$ of the *complex* eigenfunction $\mathbf{s}(\vartheta) \in \mathcal{H}$ corresponding to the critical characteristic root $i\omega$. This eigenfunction satisfies

$$\mathcal{A}\mathbf{s}(\vartheta) = i\omega\mathbf{s}(\vartheta) \tag{6.53}$$

that is

$$\mathcal{A}\left(\mathbf{s}_1(\vartheta) + i\mathbf{s}_2(\vartheta)\right) = i\omega\left(\mathbf{s}_1(\vartheta) + i\mathbf{s}_2(\vartheta)\right) \tag{6.54}$$

Separating the real and imaginary parts yields

$$\mathcal{A}\mathbf{s}_1(\vartheta) = -\omega\mathbf{s}_2(\vartheta) \tag{6.55}$$

$$\mathcal{A}\mathbf{s}_2(\vartheta) = \omega\mathbf{s}_1(\vartheta) \tag{6.56}$$

Using the definition of $\mathcal{A}$ results in the following boundary value problem

$$\begin{aligned} \tfrac{\mathrm{d}}{\mathrm{d}\vartheta}\mathbf{s}_1(\vartheta) &= -\omega\mathbf{s}_2(\vartheta) \\ \tfrac{\mathrm{d}}{\mathrm{d}\vartheta}\mathbf{s}_2(\vartheta) &= \omega\mathbf{s}_1(\vartheta) \end{aligned} \tag{6.57}$$

$$\begin{aligned} \mathbf{L}\mathbf{s}_1(0) + \mathbf{R}\mathbf{s}_1(-\tau) &= -\omega\mathbf{s}_2(0) \\ \mathbf{L}\mathbf{s}_2(0) + \mathbf{R}\mathbf{s}_2(-\tau) &= \omega\mathbf{s}_1(0) \end{aligned} \tag{6.58}$$

The general solution to the differential equation (A.3) is

$$\begin{aligned} \mathbf{s}_1(\vartheta) &= \cos(\omega\vartheta)\,\mathbf{c}_1 - \sin(\omega\vartheta)\,\mathbf{c}_2 \\ \mathbf{s}_2(\vartheta) &= \sin(\omega\vartheta)\,\mathbf{c}_1 + \cos(\omega\vartheta)\,\mathbf{c}_2 \end{aligned} \tag{6.59}$$

The boundary conditions (6.58) result in a system of linear equations for some of the unknown coefficients:

$$\begin{pmatrix} \mathbf{L} + \cos(\omega\tau)\mathbf{R} & \omega\mathbf{I} + \sin(\omega\tau)\mathbf{R} \end{pmatrix} \begin{pmatrix} \mathbf{c}_1 \\ \\ \mathbf{c}_2 \end{pmatrix} = \mathbf{0} \tag{6.60}$$

The center manifold reduction also requires the calculation of the 'left-hand-side' critical real eigenfunctions $\mathbf{n}_{1,2}$ of $\mathcal{A}$ that satisfy the adjoint problem

$$\mathcal{A}^*\mathbf{n}_1(\sigma) = \omega\mathbf{n}_2(\sigma) \tag{6.61}$$

$$\mathcal{A}^*\mathbf{n}_2(\sigma) = -\omega\mathbf{n}_1(\sigma) \tag{6.62}$$

This boundary value problem has the general solution

$$\mathbf{n}_1(\sigma) = \cos(\omega\sigma)\,\mathbf{d}_1 - \sin(\omega\sigma)\,\mathbf{d}_2 \tag{6.63}$$

$$\mathbf{n}_2(\sigma) = \sin(\omega\sigma)\,\mathbf{d}_1 + \cos(\omega\sigma)\,\mathbf{d}_2 \tag{6.64}$$

while the boundary conditions simplify to

$$\begin{pmatrix} \mathbf{L}^{\mathrm{T}} + \cos(\omega\tau)\mathbf{R}^{\mathrm{T}} & -\omega\mathbf{I} - \sin(\omega\tau)\mathbf{R}^{\mathrm{T}} \end{pmatrix} \begin{pmatrix} \mathbf{d}_1 \\ \mathbf{d}_2 \end{pmatrix} = \mathbf{0} \tag{6.65}$$

With the help of the bilinear form (6.52), the 'orthonormality' conditions

$$(\mathbf{n}_1, \mathbf{s}_1) = 1\,, \quad (\mathbf{n}_1, \mathbf{s}_2) = 0 \tag{6.66}$$

provide two more equations.

Since equations (6.60, 6.65, 6.66) do not determine the unknown coefficients uniquely (8 unknowns and 6 equations) we can choose two of them freely (so that the others will be of simple form)

$$c_{11} = 1, \quad c_{21} = 0 \tag{6.67}$$

Then

$$\mathbf{c}_1 = \begin{pmatrix} 1 \\ 0 \end{pmatrix}, \qquad \mathbf{c}_2 = \begin{pmatrix} 0 \\ \omega \end{pmatrix} \tag{6.68}$$

$$\mathbf{d}_1 = 2\gamma \begin{pmatrix} 2\zeta^2 + 2\zeta + 1 \\ \zeta \end{pmatrix}, \qquad \mathbf{d}_2 = 2\gamma\omega \begin{pmatrix} \zeta \\ 1 \end{pmatrix} \tag{6.69}$$

Let us decompose the solution $\mathbf{x}_t(\vartheta)$ of equation (6.47) into two components $y_{1,2}$ lying in the center subspace and into the infinite dimensional component $\mathbf{w}$ transverse to the center subspace:

$$\mathbf{x}_t(\vartheta) = y_1(t)\mathbf{s}_1(\vartheta) + y_2(t)\mathbf{s}_2(\vartheta) + \mathbf{w}(t)(\vartheta) \tag{6.70}$$

where

$$y_1(t) = (\mathbf{n}_1, \mathbf{x}_t)\,|_{\vartheta=0}\ , \quad y_2(t) = (\mathbf{n}_2, \mathbf{x}_t)\,|_{\vartheta=0} \tag{6.71}$$

With these new coordinates the operator differential equation (6.47) can be transformed into a 'canonical form' (see the Appendix)

$$\dot{y}_1 = (\mathbf{n}_1, \dot{\mathbf{x}}_t) = \omega y_2 + \mathbf{n}_1^{\mathrm{T}}(0)\,\mathbf{F} \tag{6.72}$$

$$\dot{y}_2 = (\mathbf{n}_2, \dot{\mathbf{x}}_t) = -\omega y_1 + \mathbf{n}_2^{\mathrm{T}}(0)\,\mathbf{F} \tag{6.73}$$

$$\dot{\mathbf{w}} = \mathcal{A}\mathbf{w} + \mathcal{F}(\mathbf{x}_t) - \mathbf{n}_1^{\mathrm{T}}(0)\,\mathbf{F}\mathbf{s}_1 - \mathbf{n}_2^{\mathrm{T}}(0)\,\mathbf{F}\mathbf{s}_2 \tag{6.74}$$

where

$$\mathbf{F} = \mathcal{F}(y_1(t)\mathbf{s}_1(0) + y_2(t)\mathbf{s}_2(0) + \mathbf{w}(t)(0)) \tag{6.75}$$

and in equation (6.74) the decomposition (6.70) should be substituted for $\mathbf{x}_t$. Equations (6.13, 6.14) give rise to the nonlinear operator

$$\mathcal{F}(\mathbf{w} + y_1\mathbf{s}_1 + y_2\mathbf{s}_2)(\vartheta) =$$

$$= \begin{cases} \mathbf{0} & \vartheta \in [-\tau, 0) \\ \frac{3}{5}\zeta z \begin{pmatrix} 0 \\ \frac{z}{1+\zeta} + 2\left(w_1(0) - w_1(-\tau)\right) - \left(\frac{z}{1+\zeta}\right)^2 \end{pmatrix} & \vartheta = 0 \end{cases} \tag{6.76}$$

where $z = y_1 - \omega y_2$ and the terms of fourth or higher order were neglected (since $\mathbf{w}(y_1, y_2)$ is second order in equation (6.77) and the normal form (6.100) will only contain terms up to third order).

6.5 Two-Dimensional Center Manifold

The center manifold is tangent to the plane (y_1, y_2) at the origin, and it is locally invariant and attractive to the flow of system (6.47). Since the nonlinearities considered here are non-symmetric, we have to compute the second order Taylor-series expansion of the center manifold. Thus, its equation can be assumed in the form of the truncated power series

$$\mathbf{w}(y_1, y_2)(\vartheta) = \frac{1}{2}(\mathbf{h}_1(\vartheta)y_1^2 + 2\mathbf{h}_2(\vartheta)y_1y_2 + \mathbf{h}_3(\vartheta)y_2^2) \tag{6.77}$$

The time derivative of $\mathbf{w}$ can be expressed both by differentiating the right-hand-side of equation (6.77) via substituting the equations (6.72, 6.73)

$$\begin{gathered}\dot{\mathbf{w}} = \mathbf{h}_1y_1\dot{y}_1 + \mathbf{h}_2y_2\dot{y}_1 + \mathbf{h}_2y_1\dot{y}_2 + \mathbf{h}_3y_2\dot{y}_2 = \\ = \dot{y}_1\left(\mathbf{h}_1y_1 + \mathbf{h}_2y_2\right) + \dot{y}_2\left(\mathbf{h}_2y_1 + \mathbf{h}_3y_2\right) = \\ = \left(\omega y_2 + d_{12}\mathrm{f}\right)\left(\mathbf{h}_1y_1 + \mathbf{h}_2y_2\right) + \left(-\omega y_1 + d_{22}\mathrm{f}\right)\left(\mathbf{h}_2y_1 + \mathbf{h}_3y_2\right) = \\ = -\omega\mathbf{h}_2y_1^2 + \omega\left(\mathbf{h}_1 - \mathbf{h}_3\right)y_1y_2 + \omega\mathbf{h}_2y_2^2 + o\left(y^3\right)\end{gathered} \tag{6.78}$$

where $\mathrm{f} = \begin{pmatrix} 0 & 1 \end{pmatrix}.\mathbf{F}$ and also by calculating equation (6.74)

$$\frac{d\mathbf{w}}{dt} = \mathcal{A}\mathbf{w} + \mathcal{F}(\mathbf{w} + y_1\mathbf{s}_1 + y_2\mathbf{s}_2) - \left(d_{12}\mathbf{s}_1 + d_{22}\mathbf{s}_2\right)\mathrm{f} \tag{6.79}$$

where

$$\mathcal{A}\mathbf{w} = \begin{cases} \frac{1}{2}(\dot{\mathbf{h}}_1y_1^2 + 2\dot{\mathbf{h}}_2y_1y_2 + \dot{\mathbf{h}}_3y_2^2) & \vartheta \in [-\tau, 0) \\ \mathbf{L}\mathbf{w}\left(0\right) + \mathbf{R}\mathbf{w}\left(-\tau\right) & \vartheta = 0 \end{cases} \tag{6.80}$$

$$\begin{gathered}\mathbf{L}\mathbf{w}\left(0\right) + \mathbf{R}\mathbf{w}\left(-\tau\right) = \frac{1}{2}y_1^2\left(\mathbf{L}\mathbf{h}_1\left(0\right) + \mathbf{R}\mathbf{h}_1\left(-\tau\right)\right) + \\ + y_1y_2\left(\mathbf{L}\mathbf{h}_2\left(0\right) + \mathbf{R}\mathbf{h}_2\left(-\tau\right)\right) + \frac{1}{2}y_2^2\left(\mathbf{L}\mathbf{h}_3\left(0\right) + \mathbf{R}\mathbf{h}_3\left(-\tau\right)\right)\end{gathered} \tag{6.81}$$

Equating like coefficients of the second degree expressions $y_1^2,\ y_1y_2,\ y_2^2$ we obtain a 6 dimensional linear boundary value problem for the unknown coefficients $\mathbf{h}_1,\ \mathbf{h}_2,\ \mathbf{h}_3$

$$\begin{aligned}
\frac{1}{2}\dot{\mathbf{h}}_1 &= -\omega\mathbf{h}_2 + \mathrm{f}_{11}\left(d_{12}\mathbf{s}_1(\vartheta) + d_{22}\mathbf{s}_2(\vartheta)\right) \\
\dot{\mathbf{h}}_2 &= \omega\mathbf{h}_1 - \omega\mathbf{h}_3 + \mathrm{f}_{12}\left(d_{12}\mathbf{s}_1(\vartheta) + d_{22}\mathbf{s}_2(\vartheta)\right) \\
\frac{1}{2}\dot{\mathbf{h}}_3 &= \omega\mathbf{h}_2 + \mathrm{f}_{22}\left(d_{12}\mathbf{s}_1(\vartheta) + d_{22}\mathbf{s}_2(\vartheta)\right)
\end{aligned} \tag{6.82}$$

$$\begin{aligned}
\frac{1}{2}\left(\mathbf{L}\mathbf{h}_1(0) + \mathbf{R}\mathbf{h}_1(-\tau)\right) &= -\omega\mathbf{h}_2(0) + \mathrm{f}_{11}\left(d_{12}\mathbf{s}_1(0) + d_{22}\mathbf{s}_2(0)\right) \\
\mathbf{L}\mathbf{h}_2(0) + \mathbf{R}\mathbf{h}_2(-\tau) &= \omega\mathbf{h}_1(0) - \omega\mathbf{h}_3(0) + \mathrm{f}_{12}\left(d_{12}\mathbf{s}_1(0) + d_{22}\mathbf{s}_2(0)\right) \\
\frac{1}{2}\left(\mathbf{L}\mathbf{h}_3(0) + \mathbf{R}\mathbf{h}_3(-\tau)\right) &= \omega\mathbf{h}_2(0) + \mathrm{f}_{22}\left(d_{12}\mathbf{s}_1(0) + d_{22}\mathbf{s}_2(0)\right)
\end{aligned} \tag{6.83}$$

Where the f_{ij}'s denote the partial derivatives of f (with the appropriate multiplier) evaluated at $y_1 = y_2 = 0$ (thus giving the coefficient of the corresponding quadratic term)

$$\mathrm{f}_{11} = \frac{1}{2}\frac{\partial^2 \mathrm{f}}{\partial y_1^2}\bigg|_{\mathbf{0}} \quad \mathrm{f}_{12} = \frac{\partial^2 \mathrm{f}}{\partial y_1 y_2}\bigg|_{\mathbf{0}} \quad \mathrm{f}_{22} = \frac{1}{2}\frac{\partial^2 \mathrm{f}}{\partial y_2^2}\bigg|_{\mathbf{0}} \tag{6.84}$$

Introducing the following notation

$$\mathbf{h} := \begin{pmatrix} \mathbf{h}_1 \\ \mathbf{h}_2 \\ \mathbf{h}_3 \end{pmatrix} \qquad \mathbf{C}_{6\times 6} = \omega \begin{pmatrix} \mathbf{0} & -2\mathbf{I} & \mathbf{0} \\ \mathbf{I} & \mathbf{0} & -\mathbf{I} \\ \mathbf{0} & 2\mathbf{I} & \mathbf{0} \end{pmatrix} \tag{6.85}$$

$$\mathbf{p} = \begin{pmatrix} \mathrm{f}_{11}\mathbf{p}_0 \\ \mathrm{f}_{12}\mathbf{p}_0 \\ \mathrm{f}_{22}\mathbf{p}_0 \end{pmatrix} \qquad \mathbf{q} = \begin{pmatrix} \mathrm{f}_{11}\mathbf{q}_0 \\ \mathrm{f}_{12}\mathbf{q}_0 \\ \mathrm{f}_{22}\mathbf{q}_0 \end{pmatrix} \tag{6.86}$$

$$\mathbf{p}_0 = \begin{pmatrix} d_{12} \\ c_{22}d_{22} \end{pmatrix} \qquad \mathbf{q}_0 = \begin{pmatrix} d_{22} \\ -c_{22}d_{12} \end{pmatrix} \tag{6.87}$$

equation (6.82) can be written as the inhomogeneous differential equation

$$\frac{\mathrm{d}}{\mathrm{d}\vartheta}\mathbf{h} = \mathbf{C}\mathbf{h} + \mathbf{p}\,\cos(\omega\vartheta) + \mathbf{q}\sin(\omega\vartheta) \tag{6.88}$$

The general solution of equation (6.88) assumes the usual form

$$\mathbf{h}(\vartheta) = \mathrm{e}^{\mathbf{C}\vartheta}\mathbf{K} + \mathbf{M}\cos(\omega\vartheta) + \mathbf{N}\sin(\omega\vartheta) \tag{6.89}$$

The coefficients $\mathbf{M}$, $\mathbf{N}$ of the non-homogeneous part are obtained after substituting this solution back to equation (6.88) resulting in a 12 dimensional inhomogeneous linear algebraic system

$$\begin{pmatrix} \mathbf{C}_{6\times6} & -\omega\mathbf{I}_{6\times6} \\ \omega\mathbf{I}_{6\times6} & \mathbf{C}_{6\times6} \end{pmatrix}\begin{pmatrix} \mathbf{M} \\ \mathbf{N} \end{pmatrix} = -\begin{pmatrix} \mathbf{p} \\ \mathbf{q} \end{pmatrix} \tag{6.90}$$

Since we will only need the first component w_1 of $\mathbf{w}(y_1, y_2)(\vartheta)$ (see equation (6.76)) we have to calculate only the 1st, 3rd and 5th component of $\mathbf{M}$, $\mathbf{N}$, $\mathbf{K}$. From equation (6.90)

$$\begin{pmatrix} M_1 \\ M_3 \\ M_5 \end{pmatrix} = \frac{-5\,(1+\zeta)\,\omega}{4\zeta\gamma}\begin{pmatrix} \omega\,(3+2\zeta) \\ 2\zeta^2+2\zeta+1 \\ \omega\,(3+4\zeta) \end{pmatrix} \tag{6.91}$$

$$\begin{pmatrix} N_1 \\ N_3 \\ N_5 \end{pmatrix} = \frac{5\,(1+\zeta)\,\omega}{4\zeta\gamma}\begin{pmatrix} 2+7\zeta+4\zeta^2 \\ -\zeta\omega \\ 2\zeta^2-\zeta-2 \end{pmatrix} \tag{6.92}$$

The boundary condition for $\mathbf{h}$ associated with equation (6.88) comes from those parts of equation (6.74) where $\mathcal{A}$, $\mathcal{F}$ are defined at $\vartheta = 0$. It is

$$\mathbf{P}\mathbf{h}(0) + \mathbf{Q}\mathbf{h}(-\tau) = \mathbf{p} + \mathbf{r} \tag{6.93}$$

with

$$\mathbf{P}_{6\times6} = \begin{pmatrix} \mathbf{L} & \mathbf{0} & \mathbf{0} \\ \mathbf{0} & \mathbf{L} & \mathbf{0} \\ \mathbf{0} & \mathbf{0} & \mathbf{L} \end{pmatrix} - \mathbf{C}_{6\times6}\,, \quad \mathbf{Q}_{6\times6} = \begin{pmatrix} \mathbf{R} & \mathbf{0} & \mathbf{0} \\ \mathbf{0} & \mathbf{R} & \mathbf{0} \\ \mathbf{0} & \mathbf{0} & \mathbf{R} \end{pmatrix}, \tag{6.94}$$

$$\mathbf{r} = -\begin{pmatrix} 0 & \mathrm{f}_{11} & 0 & \mathrm{f}_{12} & 0 & \mathrm{f}_{22} \end{pmatrix}^{\mathrm{T}} \tag{6.95}$$

$\mathbf{K}$ is found by substituting the general solution (6.89) into equation (6.93)

$$\left(\mathbf{P} + \mathbf{Q}\mathrm{e}^{-\tau\mathbf{C}}\right)\mathbf{K} = \mathbf{r} + \mathbf{p} - \mathbf{P}\mathbf{M} - \mathbf{Q}\left(\cos(\omega\tau)\mathbf{M} - \sin(\omega\tau)\mathbf{N}\right) \tag{6.96}$$

Despite its hideous look equation (6.96) simplifies, because

$$\mathbf{p} - \mathbf{P}\mathbf{M} - \mathbf{Q}\left(\cos(\omega\tau)\mathbf{M} - \sin(\omega\tau)\mathbf{N}\right) = \mathbf{0} \tag{6.97}$$

For our system

$$\begin{pmatrix} K_1 \\ K_3 \\ K_5 \end{pmatrix} = \frac{6\zeta}{5\left(9 + 33\zeta + 32\zeta^2\right)} \begin{pmatrix} 9 + 32\zeta + 32\zeta^2 \\ \omega\left(3 + 4\zeta\right) \\ 9 + 34\zeta + 32\zeta^2 \end{pmatrix} \tag{6.98}$$

Finally, equations (6.91, 6.92, 6.98) are substituted into equation (6.89) resulting in the second order approximation of the center manifold (6.77). It is not necessary to express the center manifold approximation in its full form, since we only need the values of its components at $\vartheta = 0$ and $-\tau$ in the transformed operator equation (6.72, 6.73, 6.74). For example,

$$w_1(0) = \frac{1}{2}\left(\left(M_1 + K_1\right)y_1^2 + 2\left(M_3 + K_3\right)y_1y_2 + \left(M_5 + K_5\right)y_2^2\right) \tag{6.99}$$

while the expression for $w_1(-\tau)$ is somewhat more lengthy.

6.6 The Hopf Bifurcation

In order to restrict a third order approximation of system (6.72, 6.73, 6.74) to the two-dimensional center manifold calculated in the previous section, the second order approximation $\mathbf{w}(y_1, y_2)$ of the center manifold has to be substituted into the 2 scalar equations (6.72, 6.73). Then these equations will assume the form

$$\begin{aligned}\dot{y}_1 = &\quad \omega y_2 + a_{20}y_1^2 + a_{11}y_1y_2 + a_{02}y_2^2 + a_{30}y_1^3 + a_{21}y_1^2y_2 + a_{12}y_1y_2^2 + a_{03}y_2^3 \\ \dot{y}_2 = &-\omega y_1 + b_{20}y_1^2 + b_{11}y_1y_2 + b_{02}y_2^2 + b_{30}y_1^3 + b_{21}y_1^2y_2 + b_{12}y_1y_2^2 + b_{03}y_2^3 \end{aligned} \quad (6.100)$$

Using 10 out of these 14 coefficients a_{jk}, b_{jk}, the so-called Poincaré-Lyapunov constant Δ can be calculated as shown in Guckenheimer and Holmes (1986) or Hassard, Kazarinoff and Wan (1981)

$$\begin{aligned}\Delta = \frac{1}{8\omega}\left[(a_{20}+a_{02})(-a_{11}+b_{20}-b_{02}) + (b_{20}+b_{02})(a_{20}-a_{02}+b_{11})\right] + \\ + \frac{1}{8}\left(3a_{30}+a_{12}+b_{21}+3b_{03}\right)\end{aligned} \quad (6.101)$$

The negative/positive sign of Δ determines if the Hopf bifurcation is supercritical or subcritical. Despite the above described tedious calculations Δ is quite simple:

$$\Delta = \frac{9\zeta\gamma}{50}\frac{45+177\zeta+196\zeta^2+24\zeta^3}{9+33\zeta+32\zeta^2} > 0 \quad (6.102)$$

This means that the Hopf bifurcation is *subcritical*, that is a family of *unstable periodic motions* exists around the stable steady state cutting for cutting coefficients p which are somewhat smaller than the critical value p_{cr} (this is also true for all softening power law cutting force relations and everywhere along the stability boundary, see Kalmár-Nagy et al. (2002)). The estimation of the vibration amplitude has the simple form

$$A = \sqrt{-\frac{\gamma}{\Delta}(p-p_{cr})} = \sqrt{\frac{\gamma p_{cr}}{\Delta}}\sqrt{1-\frac{p}{p_{cr}}} \quad (6.103)$$

The approximation of the corresponding periodic solution of the original operator differential equation (6.47) can be obtained from the definition (6.48) of $\mathbf{x}_t$ as

$$\mathbf{x}_t(\vartheta) = \mathbf{x}(t+\vartheta) = y_1(t)\mathbf{s}_1(\vartheta) + y_2(t)\mathbf{s}_2(\vartheta) + \mathbf{w}(t)(\vartheta) \approx$$
$$\approx A(\cos(\omega t)\mathbf{s}_1(\vartheta) - \omega \sin(\omega t)\mathbf{s}_2(\vartheta)) \tag{6.104}$$

Note that this approximation does not include p-dependent translational term (like B in the Harmonic Balance approximation). The periodic solution of the delay-differential equation (6.13) can then be obtained in the form

$$\mathbf{x}(t) = \mathbf{x}_t(0) \approx y_1(t)\mathbf{s}_1(0) + y_2(t)\mathbf{s}_2(0) =$$
$$= A \begin{pmatrix} \cos(\omega t) \\ -\omega \sin(\omega t) \end{pmatrix} \tag{6.105}$$

The vibration amplitude for general α (general power cutting force law) and ω (anywhere along the stability boundary) is obtained in Kalmár-Nagy et al. (1999) and Kalmár-Nagy et al. (2002). The approximation of the vibration amplitude is still as in (6.103), but

$$\gamma = \frac{p\tau\left(\omega^2-1\right)+2\zeta\left(\omega^2+1\right)}{p\left(\left(2\zeta+p\tau\right)^2+4\zeta\tau\left(\omega^2+1\right)+4\omega^2\right)} \tag{6.106}$$

$$\Delta = \frac{q\delta\left(\omega^2-1\right)}{4p^2}\left(3p\tau\left(\omega^2-1+2p\sigma\left(1+2p-\omega^2\right)\right)+\right. \tag{6.107}$$
$$2\zeta\left(3\left(\omega^2-1\right)+\right.$$
$$\left.\left.+2\sigma\left(2+7p+6p^2+\left(4+11p\right)\omega^2-2\omega^2-4\omega^6\right)\right)\right)$$

with

$$q = \frac{3p\left(1-\alpha\right)}{2\left(2-\alpha\right)}, \qquad \sigma = \frac{2q\left(\omega^2-1\right)}{p\left(4+9p-12\omega^4+8\omega^6\right)} \tag{6.108}$$

and

$$\delta = \frac{4}{2\omega^2\left(1+\zeta\tau\right)^2+\left(2\zeta+\tau\left(1+p-\omega^2\right)\right)^2} \tag{6.109}$$

In our case ($\alpha = 3/4$, $\omega = \sqrt{1+2\zeta}$) the vibration amplitude is

$$A = \frac{10}{3}\sqrt{\frac{(1+\zeta)\,(9+33\zeta+32\zeta^2)}{45+177\zeta+196\zeta^2+24\zeta^3}}\sqrt{1-\frac{p}{p_{cr}}} \tag{6.110}$$

Since the relative damping factor ζ is usually far less than 1 in realistic machine tool structures, the first order Taylor expansion of the amplitude A with respect to ζ is also a good approximation

$$A \approx \frac{30+11\zeta}{9\sqrt{5}}\sqrt{1-\frac{p}{p_{cr}}} \tag{6.111}$$

Let us transform the nondimensional time and displacement back to the original ones. Selecting the first coordinate of equation (6.105), we obtain the approximate form of the unstable periodic motion embedded in the regenerative machine tool vibrations for $p < p_{cr}$

$$x(t) \approx \frac{4}{15\sqrt{5}}\frac{30+11\zeta}{f_0}\sqrt{1-\frac{p}{p_{cr}}}\cos(\omega_n\sqrt{1+2\zeta}t) \tag{6.112}$$

6.7 Numerical Results

The results of the above sections were confirmed numerically. Simulations with

$$\zeta = 0.1, \quad j = 1 \tag{6.113}$$

were carried out (see equations (6.25)). The full delay equation (6.13, 6.14) was integrated in Mathematica.To find the amplitude of the unstable limit cycles the procedure described in Section 6.3 is employed (A is calculated by equation (6.45)). The bifurcation diagram (presenting the amplitude of the unstable limit cycle vs. the normalized bifurcation parameter) is shown in Figure 6.3, together with the analytical approximation (6.110) (solid line). The agreement is excellent. Comparing the results obtained from Center Manifold Theory with those obtained by

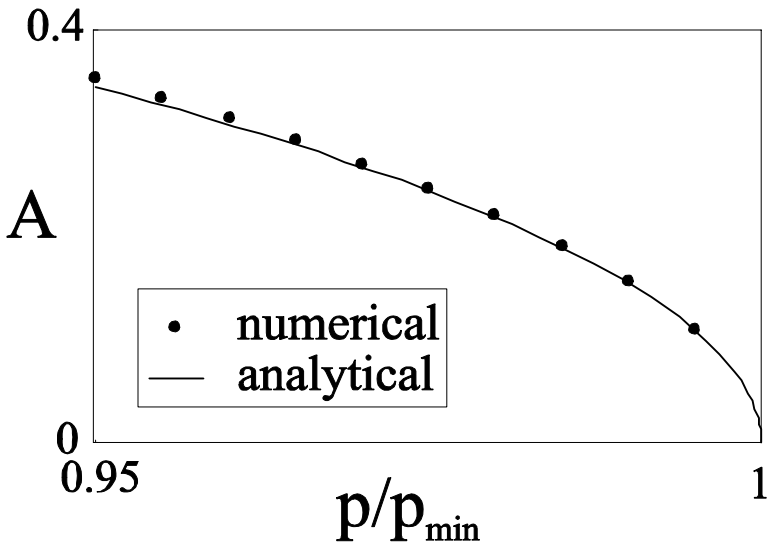

Figure 6.3: Bifurcation diagram.

a simple Harmonic Balance approximation (Figure 6.2) we note that both provide very good approximations. While the Harmonic Balance calculations were extremely simple, the application of the Center Manifold Theory provides rigorous proof of these results.

Numerical solutions displayed only two kinds of behavior. They either converged to the stable trivial solution or they were unbounded. This suggests that some other nonlinearity is needed to stabilize the system. Structural nonlinearity (as in Johnson, 1996; Nayfeh, Chin, Pratt, 1999) has been suggested to provide a mechanism that bounds the motions. However, these nonlinearities are usually negligible (Shi and Tobias, 1984), so instead of using these we focus our attention on the multiple regenerative effect.

6.8 Multiple Regenerative Effect

When the chatter amplitude exceeds a certain value, the contact ceases between the tool and the workpiece and the tool starts a damped vibration until it comes in contact with the workpiece again. When this happens, the uncut chip thickness is affected by the trace of the tool motion even from two or more previous turns before. This phenomenon is called the multiple regenerative effect. This effect has been studied by many researchers (Shi and Tobias, 1984; Kondo et al., 1981; Batzer et al., 1999; Balachandran, 2001). Tlusty and Ismail (1981) refer to this effect as to the 'basic non-linearity' in machining.

6.8.1 Linear Cutting Force

In the following we use a linear cutting force to gain insight into the dynamics related to repeated impacts between tool and workpiece. The cutting force is

$$F_x(f) = \begin{cases} Kwf & f > 0 \\ 0 & f \leq 0 \end{cases} \tag{6.114}$$

where w is the width of cut and the parameter K depends on further technological parameters. The case $f \leq 0$ corresponds to zero cutting force as the tool leaves the material. Then

$$\Delta F_x = \begin{cases} Kw\,(f - f_0) & f > 0 \\ -Kwf_0 & f \leq 0 \end{cases} \tag{6.115}$$

The chip thickness f is expressed as the difference of the present tool edge position $x(t)$ and the delayed one $x(t-\tau)$

$$f = f_0 + x(t) - x(t-\tau) = f_0 + x - x_\tau$$

The equation of motion becomes

$$\ddot{x} + 2\zeta\omega_n\dot{x} + \omega_n^2 x = \begin{cases} -\frac{Kw}{m}(x - x_\tau) & f_0 + x > x_\tau \\ \frac{Kw}{m} f_0 & f_0 + x \leq x_\tau \end{cases} \tag{6.116}$$

Introducing the dimensionless displacement $\widetilde{x}$ and time $\tilde{t}$ and a dimensionless parameter $\tilde{p}$

$$x = f_0\widetilde{x} \quad t = \tfrac{1}{\omega_n}\tilde{t} \quad \tilde{p} = \tfrac{Kw}{\omega_n^2 m} \tag{6.117}$$

(note that $\tilde{\tau} = \omega_n\tau$) and dropping the tilde immediately transforms (6.116) into

$$\ddot{x} + 2\zeta\dot{x} + x = \begin{cases} p\,(x(t-\tau) - x) & x > x(t-\tau) - 1 \\ p & x \leq x(t-\tau) - 1 \end{cases} \tag{6.118}$$

The solution to the damped vibration

$$\ddot{x} + 2\zeta\dot{x} + x = p \tag{6.119}$$

can be obtained analytically (see Appendix A) as

$$x = p + e^{-\zeta t}\left(A\cos\left(\sqrt{1-\zeta^2}t\right) + B\sin\left(\sqrt{1-\zeta^2}t\right)\right) \tag{6.120}$$

$$A = x_0 - p, \quad B = \frac{v_0 + \zeta\,(x_0 - p)}{\sqrt{1-\zeta^2}} \tag{6.121}$$

Numerical simulations show that stable limit cycles appear for values of p over the critical value, i.e. where the trivial solution is unstable (the amplitude is nonzero when $p = p_{cr}$). However, the stable region appears to be globally stable! Thus the contact-loss nonlinearity is not enough in itself to sustain periodic motions below the stability boundary.

Next, the cutting force and contact-loss nonlinearities are combined.

6.8.2 Cutting Force and Motion Limiting Nonlinearities

In the following calculations we will use the general power law (to get results comparable to those from the NIST experiments)

$$F_x(f) = \begin{cases} 0 & f \leq 0 \\ Kwf^a & f > 0 \end{cases} \tag{6.122}$$

where $\alpha < 1$ is the cutting force exponent. When $f \leq 0$ there is no contact between the tool and the workpiece.

Then cutting force variation can then be expressed as

$$\Delta F_x(f) = F_x - F_x(f_0) = \begin{cases} -F_x(f_0) & \Delta f \leq -f_0 \\ Kw\left(f^a - f_0^\alpha\right) & \Delta f > -f_0 \end{cases} \tag{6.123}$$

where f_0 is the nominal chip thickness (feed) in steady state cutting. The chip thickness variation Δf can be expressed as

$$\Delta f = f - f_0 = x(t) - x(t-\tau) = x - x_\tau \tag{6.124}$$

Let us also define

$$\Delta x = -\Delta f = x_\tau - x \tag{6.125}$$

The slope of the power-law curve at the nominal chip thickness f_0 is called the *cutting force coefficient* and usually denoted by k_1 ($k_1 = \frac{\partial F_x}{\partial f}\Big|_{f=f_0} = \alpha K w f_0^{\alpha-1}$).

Expressing $\Delta F_x(f)$ in terms of k_1 yields the following equation of motion

$$\ddot{x} + 2\zeta\omega_n\dot{x} + \omega_n^2 x = \begin{cases} \frac{k_1 f_0}{m\alpha} & \Delta f \leq -f_0 \\ \frac{k_1 f_0}{m\alpha}\left(1 - \left(\frac{f}{f_0}\right)^\alpha\right) & \Delta f > -f_0 \end{cases} \tag{6.126}$$

Let us introduce the nondimensional time $\tilde{t}$ and displacement $\widetilde{x}$

$$\tilde{t} = \omega_n t \quad \widetilde{x} = \frac{x}{X} \tag{6.127}$$

where X is a lengthscale chosen later. The nondimensional equation of motion is then

$$\tilde{x}'' + 2\zeta\tilde{x}' + \tilde{x} = \begin{cases} \frac{k_1 f_0}{\alpha m\omega_n^2 X} & \Delta\tilde{x} \geq \frac{f_0}{X} \\ \frac{k_1 f_0}{\alpha m\omega_n^2 X}\left(1 - \left(1 - \frac{X}{f_0}\Delta\tilde{x}\right)^{\alpha}\right) & \Delta\tilde{x} < \frac{f_0}{X} \end{cases} \tag{6.128}$$

where $'$ denotes time derivative w.r.t the nondimensional time. Expanding the RHS about $\Delta\tilde{x} = 0$ yields

$$\frac{k_1}{m\omega_n^2}\Delta\tilde{x} + \frac{k_1 X\left(\alpha-1\right)}{2f_0 m\omega_n^2}\Delta\tilde{x}^2 + \frac{k_1 X^2\left(\alpha-1\right)\left(\alpha-2\right)}{6f_0^2 m\omega_n^2}\Delta\tilde{x}^3 + O\left(\Delta\tilde{x}^4\right) \tag{6.129}$$

Let us choose $X > 0$ in such a way that the absolute value of the coefficients of the second and the third order terms are equal, i.e.

$$\left|\frac{k_1 X\left(\alpha-1\right)}{2f_0 m\omega_n^2}\right| = \left|\frac{k_1 X^2\left(\alpha-1\right)\left(\alpha-2\right)}{6f_0^2 m\omega_n^2}\right| \tag{6.130}$$

This gives $X = \frac{3f_0}{2-\alpha}$. Introducing the nondimensional bifurcation parameter $p = \frac{k_1}{m\omega_n^2}$ and dropping the tilde results in the full nondimensional equation of motion

$$x'' + 2\zeta x' + x = \begin{cases} \frac{p(2-\alpha)}{3\alpha} & \Delta x \geq \frac{2-\alpha}{3} \\ \frac{p(2-\alpha)}{3\alpha}\left(1 - \left(1 - \frac{3}{2-\alpha}\Delta x\right)^{\alpha}\right) & \Delta x < \frac{2-\alpha}{3} \end{cases} \tag{6.131}$$

However, here the definition of Δx must be modified according to

$$\Delta x = \min\left(x_\tau - x, \frac{2-\alpha}{3}\right), \tag{6.132}$$

because when the tool is not in contact with the workpiece, the chip thickness will not be affected. To find an approximation to the vibration amplitude at which the tool leaves the workpiece, the following approximation is employed. The tool leaves the material when

$$x_\tau - x = \frac{2-\alpha}{3} \tag{6.133}$$

Assuming the solution in the following form

$$x = A\cos(\omega t) + B \tag{6.134}$$

we have

$$A\left[\cos\left(\omega\left(t-\tau\right)\right) - \cos\left(\omega t\right)\right] = \frac{2-\alpha}{3} \tag{6.135}$$

which can be written as

$$A = \frac{2-\alpha}{6\sin\left(\frac{\tau\omega}{2}\right)\sin\left(\omega\left(t-\frac{\tau}{2}\right)\right)} \tag{6.136}$$

A is minimal where the time-dependent term $\sin\left(\omega\left(t-\frac{\tau}{2}\right)\right)$ is maximal ($=1$). Thus the minimum vibration amplitude for contact loss is

$$A^{cl} = \frac{2-\alpha}{6\sin\left(\frac{\tau\omega}{2}\right)} \tag{6.137}$$

6.9 Comparison with Experimental Data

To numerically solve system (6.131) the following parameters (as identified in Chapter 5) were used

$$\alpha = 0.41,\ \zeta = 0.0136 \tag{6.138}$$

To find the analytical approximation for the vibration amplitude (6.110) equations (6.106-6.109) were used with the approximation (since the experiments were performed near the notch of a lobe)

$$\omega = \sqrt{1+2\zeta} \tag{6.139}$$

The result is

$$A \approx 1.1\sqrt{1-\frac{p}{p_{cr}}} \tag{6.140}$$

where the critical value of the nondimensional cutting force coefficient is

$$p_{cr} = 0.23 \tag{6.141}$$

The dimensional rms vibration amplitude is found from the following considerations. The experimental bifurcation diagram was obtained at

$$\Omega = 836 \text{ rpm} = 13.93 \frac{\text{rot}}{\text{s}} \tag{6.142}$$

with a feedrate $s = 508$ μm/s. Thus

$$\tau = 1/\Omega = 0.072s, \; f_0 = s\tau = 36.6 \; \mu\text{m} \tag{6.143}$$

The lengthscale is

$$X = \frac{3f_0}{2-\alpha} = 68.8 \; \mu\text{m} \tag{6.144}$$

and the rms lengthscale is (the vibration is sinusoidal)

$$X_{rms} = \frac{\sqrt{2}}{2} X = 48.6 \; \mu\text{m} \tag{6.145}$$

Hence

$$A_{rms} = X_{rms} A \approx 53.4 \sqrt{1 - \frac{p}{0.23}} \tag{6.146}$$

To compute the vibration amplitude for contact loss, the approximation

$$\sin\left(\frac{\tau\omega}{2}\right) = \frac{1}{\sqrt{2\left(1+\zeta\right)}} \tag{6.147}$$

is used (by using (6.139) with (6.22)). The rms contact loss vibration amplitude is then

$$A^{cl}_{rms} = X_{rms} \frac{(2-\alpha)\sqrt{2\left(1+\zeta\right)}}{6} \approx 18.4 \; \mu\text{m} \tag{6.148}$$

Figure 6.4 compares the experimental results with the analytical and numerical solutions. The black and white circles represent rms vibration amplitudes for

forward and backwards sweeps, respectively. As the Figure shows, hysteresis is present, which corresponds to the subcritical Hopf bifurcation. The solid line corresponds to the analytical solution (6.146). The dashed line shows the amplitude A_{rms}^{cl} at which the tool leaves the material. Since the analytical solution is based on a series expansion of the power law cutting force expression, a good match between simulation and the analytical solution is expected around the bifurcation point. This is indeed the case. Also, the graph strongly suggest that the contact-loss nonlinearity is the mechanism responsible for the stable upper branch. The analytical solution overestimates the occurrence for contact loss.

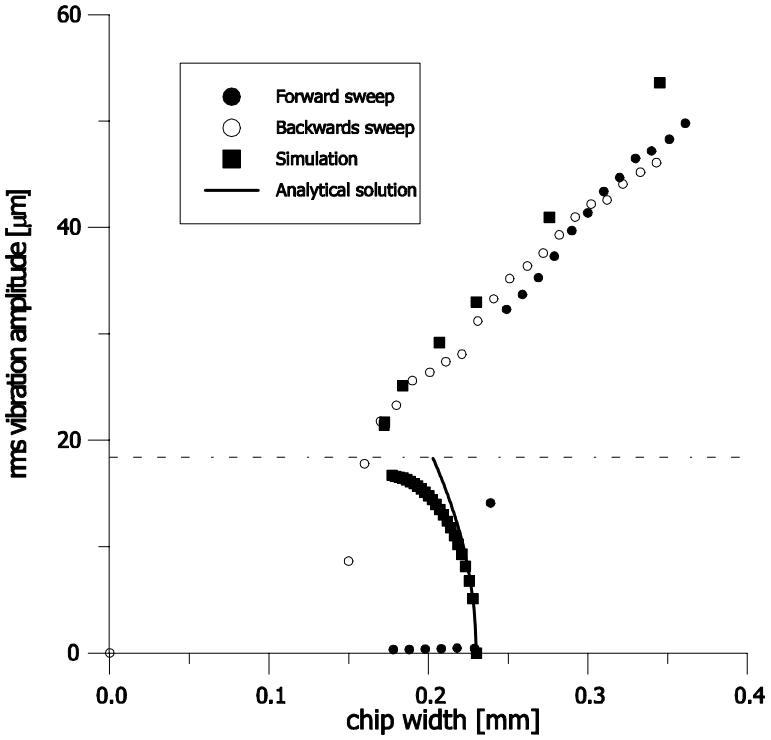

Figure 6.4: Comparison of experiments, analytical and numerical solutions.

6.10 Conclusions

The existence and nature of a Hopf bifurcation in the delay-differential equation for self-excited tool vibration is presented and proved analytically with the help of the Center Manifold and Hopf Bifurcation Theory. The simple results are due to the special structure of the nonlinearities considered in the cutting force dependence on the chip thickness. On the other hand this analysis is local in the sense that it does not account for nonlinear phenomena as the tool leaves the material. In this case the regenerative effect disappears, and the result of the local analysis is not valid anymore (see Doi and Kato, 1956; Kalmár-Nagy et al., 1999).

The semi-analytical and numerical results of Nayfeh, Chin and Pratt (1997) show some cases where a slight supercritical bifurcation appears before the birth of the unstable limit cycle, and they also present some robust supercritical Hopf bifurcations. These results were calculated at critical parameter values somewhat away from the 'notches' of the stability chart chosen in this study. The model considered there also contained structural nonlinearities (both quadratic and cubic terms).

We have also shown in this Chapter that the multiple regenerative effect combined with a linear cutting force is not enough to produce a subcritical instability, for this the cutting force has to be nonlinear. On the other hand, with only cutting force nonlinearity, a stable family of periodic orbits does not exist. This can only be produced by a motion limiting nonlinearity. This nonlinearity can be structural (Hanna and Tobias, 1974; Johnson, 1996; Nayfeh, Chin and Pratt, 1997) or it can be due to the multiple regenerative effect. Assuming the latter in conjunction with a power law cutting force, excellent agreement was achieved between experimental results described in Chapter 5 and simulations.

Chapter 7

Single DOF Models with Delay: Forcing and Hysteresis

The machining tool can be subject to different kinds of excitations. The forcing may have external sources (such as rotating imbalance or misalignment of the workpiece) or it can arise from the cutting process itself (e.g. chip formation, see Section 2.7). We start this Chapter with investigating the classical tool vibration model with cutting force nonlinearity and periodic forcing. The second phenomenon that will be studied here is the presence of active hysteresis in the cutting force (see Section 2.1). We present models that have some characteristics of rate-independent plasticity.

7.1 A Harmonically Forced Nonlinear Delay-Differential Equation

To date there have only been a few studies on forced nonlinear delay-differential equations. These kind of equations arise for example in active vehicle suspension systems when the nonlinearity in tires is taken into account (Palkovics and Venhovens, 1992). Hu, Dowell and Virgin (1998) investigated resonances of a harmonically forced Duffing oscillator with time-delay state feedback (both primary and 1/3 subharmonic resonance).

The goal of this Section is to analyze the dynamics of the system that describes vibrations of a machine tool (see Chapter 6) under periodic forcing. The equation of motion is the forced nonlinear delay equation (also see equation 6.10)

$$\ddot{x} + 2\zeta\dot{x} + x = p\left(x_\tau - x\right) + q\left(\left(x - x_\tau\right)^2 - \left(x - x_\tau\right)^3\right) + A\cos\left(\omega t\right) \tag{7.1}$$

where x is the tool displacement ($x_\tau = x\left(t - \tau\right)$ is its delayed value), ζ is the relative damping factor, p is the nondimensional cutting force, q is the coefficient of nonlinearity, A is the amplitude of the forcing and ω is its frequency. As mentioned earlier, this forcing could be produced by the rotation of the workpiece (the resulting excitation frequency is an order of 1 kHz) or by periodic chip formation (frequencies up to 100 kHz).

Perturbation methods were successfully applied to delay-differential equations (such as the Linstedt-Poincaré method (Casal and Freedman, 1980) or the method of multiple scales (Nayfeh, Chin and Pratt, 1997)). In the following we present the analysis of the primary resonance of (7.1) by the method of multiple scales (see Appendix C).

7.1.1 Primary Resonance

In order to be able to use multiple scales, we need an ordering of the terms. We will assume that damping is small, the nonlinearity and forcing are weak. In particular

$$\zeta,\, p,\, q,\, A \sim O(\varepsilon) \qquad \omega = 1 + \varepsilon\sigma \tag{7.2}$$

where $\varepsilon \ll 1$ and σ is the detuning frequency. We also assume that the solution can be well approximated by the two-scale expansion

$$x(t) = x_0(t_0, t_1) + \varepsilon x_1(t_0, t_1) + O\left(\varepsilon^2\right) \tag{7.3}$$

where both t_0, t_1 are timescales, defined as

$$t_0 = t, \quad t_1 = \varepsilon t \tag{7.4}$$

With the differential operators

$$D_0 = \frac{\partial}{\partial t_0}, \quad D_1 = \frac{\partial}{\partial t_1} \tag{7.5}$$

time differentiation can be written as

$$\frac{d}{dt} = D_0 + \varepsilon D_1 + O\left(\varepsilon^2\right) \tag{7.6}$$

and similarly

$$\frac{d^2}{dt^2} = D_0^2 + 2\varepsilon D_0 D_1 + O\left(\varepsilon^2\right) \tag{7.7}$$

Substituting (7.6) and (7.7) into (7.1) and equating like powers of ε one obtains

$$D_0^2 x_0(t_0, t_1) + x_0(t_0, t_1) = 0 \tag{7.8}$$

$$D_0^2 x_1(t_0, t_1) + x_1(t_0, t_1) = -2D_0 D_1 x_0(t_0, t_1) - 2\zeta D_0 x_0(t_0, t_1) +$$

$$+p\left[x_0(t_0 - \tau, t_1) - x_0(t_0, t_1)\right] + q\left[x_0(t_0 - \tau, t_1) - x_0(t_0, t_1)\right]^2 +$$

$$+q\left[x_0\left(t_0-\tau,t_1\right)-x_0\left(t_0,t_1\right)\right]^3+A\cos\left(t_0+\sigma t_1\right) \tag{7.9}$$

Solving (7.8) for $x_0\left(t_0,t_1\right)$ yields

$$x_0\left(t_0,t_1\right)=a\left(t_1\right)e^{it_0}+\bar{a}\left(t_1\right)e^{-it_0} \tag{7.10}$$

Then we substitute this solution into (7.9) and eliminate the secular terms which would give rise to nonperiodic terms

$$-\frac{1}{2}e^{i\sigma t_1}+a\left(t_1\right)\left[p-e^{-i\tau}p+2i\zeta-3e^{-2i\tau}\left(e^{i\tau}-1\right)^3qa\left(t_1\right)\bar{a}\left(t_1\right)\right]+2i\bar{a}\left(t_1\right)=0 \tag{7.11}$$

Writing $a\left(t_1\right)$ in a polar form (where $\alpha\left(t_1\right)$ is the amplitude and $\beta\left(t_1\right)$ is the phase)

$$a\left(t_1\right)=\frac{1}{2}\alpha\left(t_1\right)e^{i\beta(t_1)}\qquad\bar{a}\left(t_1\right)=\frac{1}{2}\alpha\left(t_1\right)e^{-i\beta(t_1)} \tag{7.12}$$

then substituting into (7.11) and separating the real and imaginary parts results in two ordinary differential equations describing the evolution of the amplitude and phase

$$D_1\alpha=-\left(\zeta+\frac{p}{2}\sin\tau\right)\alpha-3q\cos\frac{\tau}{2}\sin^3\frac{\tau}{2}\alpha^3+\frac{A}{2}\sin\phi \tag{7.13}$$

$$\alpha D_1\phi=\frac{1}{2}\left(p\cos\tau+2\sigma-p\right)\alpha-3q\sin^4\frac{\tau}{2}\alpha^3+\frac{A}{2}\cos\phi \tag{7.14}$$

where

$$\phi\left(t_1\right)=\sigma t_1-\beta\left(t_1\right) \tag{7.15}$$

To get the amplitude of the steady-state primary resonance we set the left-hand sides of (7.13) and (7.14) to zero and solve the resulting algebraic equations (by eliminating the trigonometric terms from them)

$$\left[\frac{1}{2}\left(p\left(1-\cos\tau\right)-2\sigma+6q\alpha^2\sin^4\frac{\tau}{2}\right)^2+\left(\zeta+\frac{p}{2}\sin\tau+3q\alpha^2\cos\frac{\tau}{2}\sin^3\frac{\tau}{2}\right)^2\right]\alpha^2-$$

$$-\frac{A^2}{4}=0 \tag{7.16}$$

Response curves were calculated in the asymptotically stable region of the unforced equation (7.1). A stability chart (Figure 7.1) shows the location of the first stability lobe in the (τ, p) plane. The nondimensional cutting force coefficient was

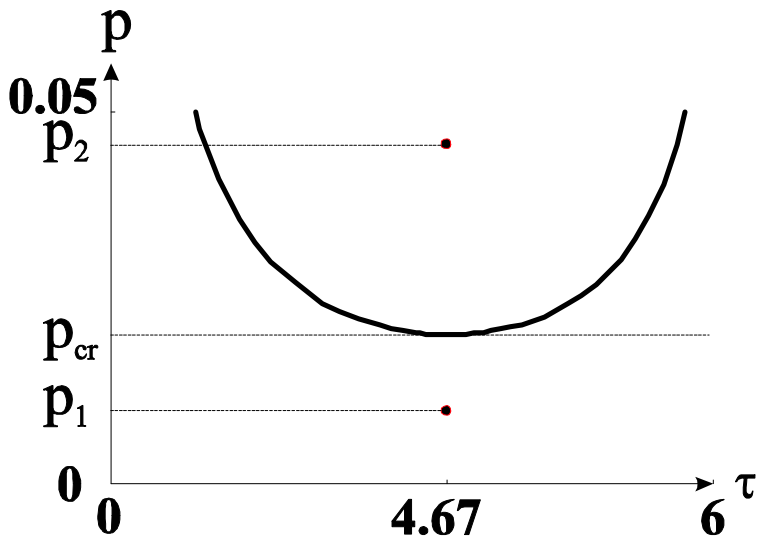

Figure 7.1: The first lobe of the stability chart of the classical model.

taken to be $p = p_1 = 0.01$, which is well below the minimal value $p_{cr} = 0.0202$ (corresponding to $\zeta = 0.01$). The time delay τ was set to 4.67 which is where the minimal p occurs. The coefficient of nonlinearity $q = 0.003$ is the same as used in the simulations of Chapter (6).

Figure 7.2 shows the amplitude as a function of forcing frequency for $A = 0.01$ (the solid line). Results of numerical simulations are also shown on this Figure (dots).

The resonance curves are similar to those found for the Duffing-equation (Nayfeh and Mook, 1979), having a hardening characteristic. These results may not always be valid because equation (7.1) without forcing admits a subcritical Hopf bifurcation and the interaction of forcing and Hopf bifurcation may lead to incredibly

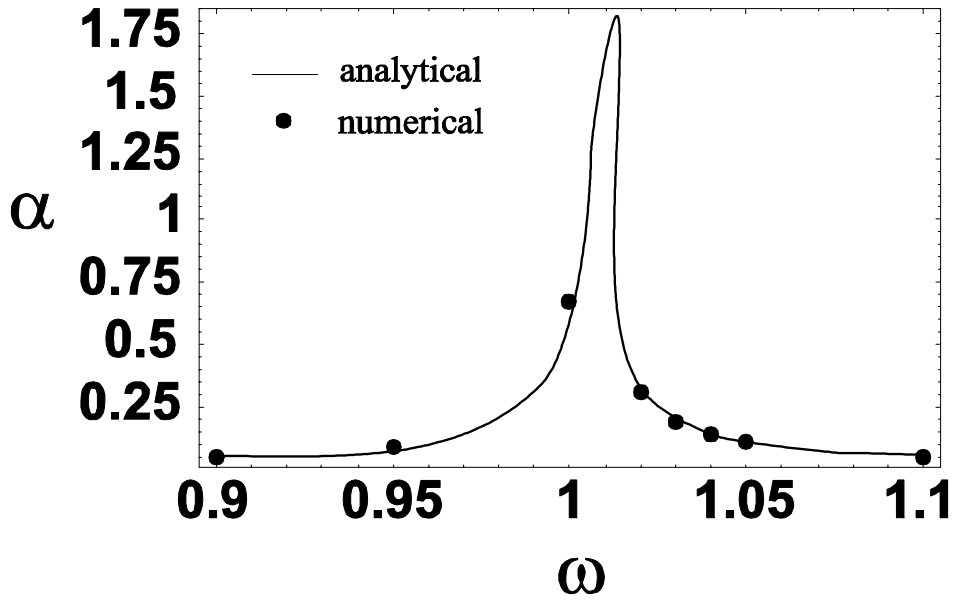

Figure 7.2: Primary resonance curve.

complex phenomena (Gambaudo, 1985). Plaut and Hsieh (1986) studied a one-DOF mechanical system with delay and excitation and found periodic, chaotic and unbounded responses. Forcing of a Duffing-type equation without delay can also result in complicated bifurcation structure (Sanchez and Nayfeh, 1990; Zavodney, Nayfeh and Sanchez, 1990). We also note that even for weak forcing, the response amplitude can be large enough for contact loss to occur. In the following Section we incorporate this global nonlinearity into the model and investigate its effect.

7.1.2 Forcing with Global Nonlinearity

It is well known that oscillators with piecewise linear stiffness under periodic forcing can exhibit chaotic behavior (Shaw and Holmes, 1983, Mahfouz and Badrakhan, 1990a, 1990b). Numerical simulations of (7.1) were performed with the addition of the multiple regenerative effect (see Sections 2.3 and 6.8). These numerical exper-

iments showed (Figure 7.3) that forcing together with a contact loss nonlinearities may result in chaotic attractors. Here the value of the nondimensional parameter

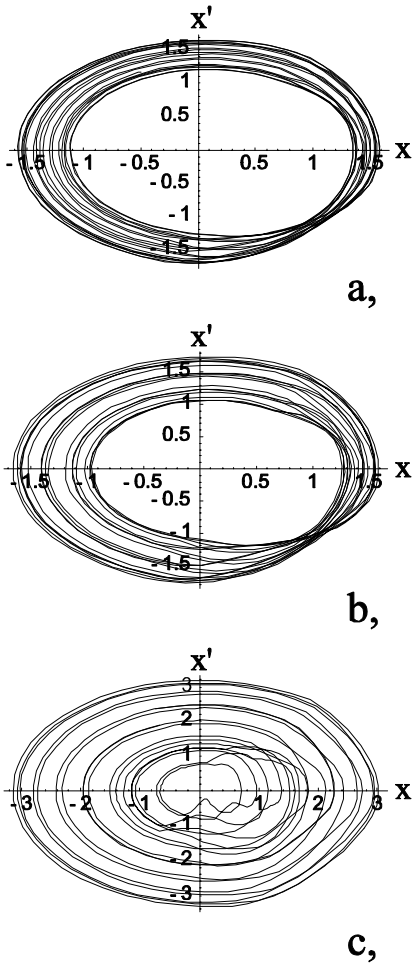

Figure 7.3: Forcing of the nonlinear DDE (7.1) with contact loss nonlinearity ($\omega = 3$). a, $A = 0.3$ b, $A = 0.5$ c, $A = 1$.

p was chosen such that the unforced system is in the unstable region ($p_2 = 4p_{cr}$, shown in Figure 7.1). The other parameters were the same used in the previous Section. The amplitude of forcing A is 0.3, 0.5, 1 in Figure 7.3a, b, c, respectively. The forcing frequency is $\omega = 3$.

7.2 Hysteresis

Most of the theoretical analyses of machine tool vibrations employ force laws that are based on the assumption that cutting is steady state. However, cutting is a dynamic process and experimental results show differences between steady state and dynamic cutting (see Section 2.1). Many other physical systems exhibit hysteresis. This nonlinear phenomenon may be due to Coulomb friction or elastoplastic behavior of the material. Hysteresis has been studied in fields as diverse as soil mechanics (Fu, 1969) and superconducting levitation (Hikihara and Moon, 1994). Theoretical studies have also been conducted (Block, 1960; Krasnoselskii and Pokrovskii, 1989). The civil engineering community generated a vast literature of hysteretic systems, mainly in the context of the stability of structures under earthquake-type loadings (Rahman, 1991). A good survey of hysteretic models can be found in Otani (1981).

7.2.1 Oscillators with Hysteretic Restoring Force

In a hysteretic system, the evolution has a functional dependence on the past history. First we consider a simple harmonic oscillator with hysteretic restoring force. The (nondimensional) equation of motion is given by

$$\ddot{x} + g\left(x, \dot{x}\right) = F(t) \tag{7.17}$$

where $F\left(t\right)$ is the forcing and the restoring force g admits an additive decomposition of a hysteretic and nonhysteretic component

$$g\left(x, \dot{x}\right) = g_{nh}\left(x, \dot{x}\right) + g_{h}\left(x_t, \dot{x}_t\right) \tag{7.18}$$

Here $x_t(\varphi)$ represents the 'memory' of the system (not to be confused with the delay in (7.1))

$$x_t(\varphi) = x(t+\varphi)\,, \quad \varphi \in [0,t] \tag{7.19}$$

The nonhysteretic component is given by

$$g_{nh}\,(x,\dot{x}) = 2\zeta\dot{x} + \alpha x \tag{7.20}$$

and the hysteretic force is specified by

$$g_h\,(x_t,\dot{x}_t) = (1-\alpha)\,z \tag{7.21}$$

where α is the measure of the relative importance of the hysteresis effect and z is the hysteretic state variable, whose evolution can be modeled by a first-order equation

$$\dot{z} = f\,(x,\dot{x},z,t) \tag{7.22}$$

7.2.2 Bilinear Elastoplastic Model

The bilinear hysteretic model has been extensively used to model elastoplastic structural behavior. Tanabashi (1956) studied the response of a two-DOF system under earthquake-type loading. Transient and steady-state response of a SDOF system under sinusoidal excitation was studied by Caughey (1960). Ballio (1968, 1970) conducted experimental as well as theoretical studies on a beam column subjected to a static axial load, and a periodic transverse load in resonance with the structure in the elastic range. Reddy and Pratap (2000) showed that for certain loads and viscous damping the frequency response of a SDOF damped bilinear hysteretic oscillator under harmonic excitation can be represented exactly by a simple harmonic oscillator with a variable equivalent viscous damping.

The bilinear elastic-perfectly-plastic model is described by the evolution equation (Kobori, Minai and Suzuki, 1976)

$$\dot{z} = \dot{x}\left[1 - \mathrm{H}\left(\dot{x}\right)\mathrm{H}\left(z-1\right) - \mathrm{H}\left(-\dot{x}\right)\mathrm{H}\left(-z-1\right)\right] \tag{7.23}$$

where H is the unit step (Heaviside) function. A simpler form of this equation is

$$\dot{z} = \dot{x}\left[1 - \mathrm{H}\left(\dot{x}z - |\dot{x}|\right)\right] \tag{7.24}$$

Figure 7.4 shows z as a function of time as well as the hysteresis loop (z versus x) for $x = 2\cos t$ and $z\left(0\right) = 1$. An evolution equation can similarly be given for the

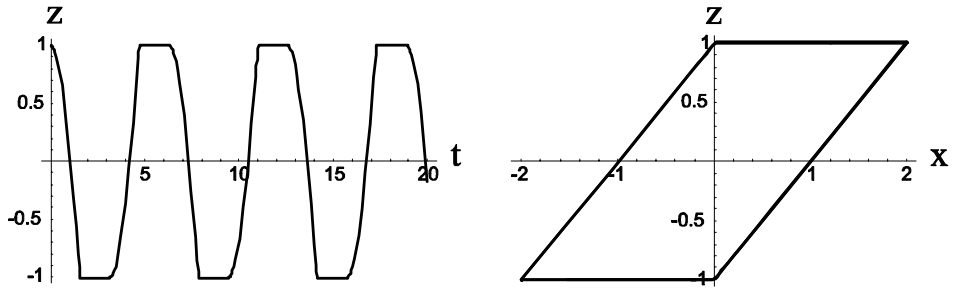

Figure 7.4: Elastic-perfectly-plastic hysteresis. a, $z(t)$ b, hysteresis loop.

case of elastic-plastic hysteresis

$$\dot{z} = \dot{x}\left[1 + \left(k-1\right)\mathrm{H}\left(\dot{x}\left(z - kx + \left(k-1\right)\operatorname{sgn}\dot{x}\right)\right)\right] \tag{7.25}$$

where k is the kinematic hardening parameter ($k = 0$ corresponds to the perfectly plastic case, while $k = 1$ corresponds to perfectly elastic behavior). For $k = 0.5$ Figure 7.5 shows $z\left(t\right)$ and the hysteretic force z as a function of x (and $\dot{x}$). Again $x = 2\cos t$ was used and $z\left(0\right) = 1.5$.

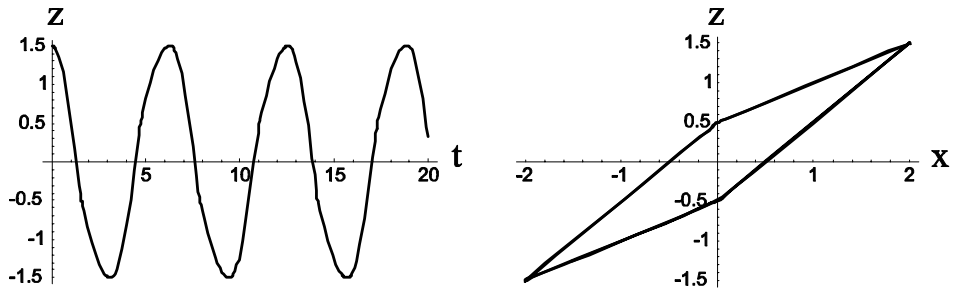

Figure 7.5: Elastic-plastic hysteresis for $k = 0.5$. a, $z(t)$ b, hysteresis loop.

7.2.3 Smooth Hysteresis

Badrakhan (1988) proposed an approximation to hysteretic systems which results in a Duffing equation with amplitude-dependent coefficients.

A smooth hysteretic model proposed by Bouc (1967) is

$$\dot{z} = \dot{x} \left(\beta - \gamma z \operatorname{sgn} \dot{x} - \delta \left| z \right| \right) \tag{7.26}$$

where the parameters β, γ, δ control the amplitude and shape of the hysteretic loops.

The drawbacks of this model are the anomalous behavior during cycles without load reversal and the openness of the hysteresis loops (this latter can be avoided by a judicious choice of parameters). Figures 7.6, 7.7 and 7.8 depict the shapes of various hysteresis loops for different parameter values and for sinusoidally varying x ($x = 2 \sin t$). First β and γ were kept constant (0.1), while δ varied (0.5, 1, 2) (Figure 7.6). For Figure 7.7 β and δ were kept constant (0.1), while γ varied (0.5, 1, 2). And finally, Figure 7.8 shows hysteretic loops where γ and δ are kept constant (0.1), and β is varied (0.2, 0.5, 1).

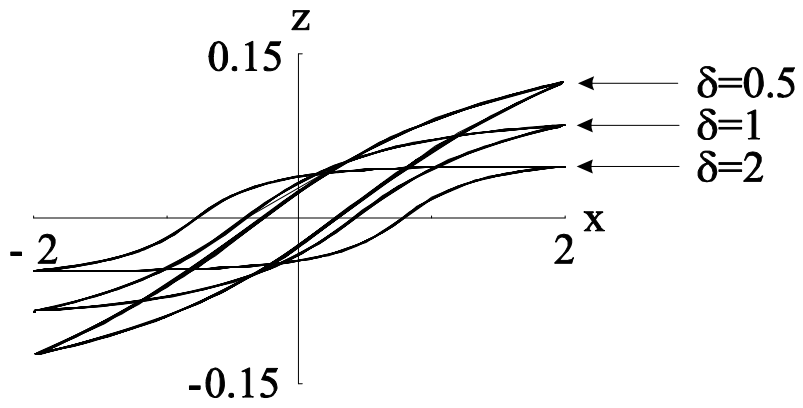

Figure 7.6: Smooth hysteresis loop, Bouc's model ($\beta = \gamma = 0.1$, $\delta = 0.5$, 1, 2).

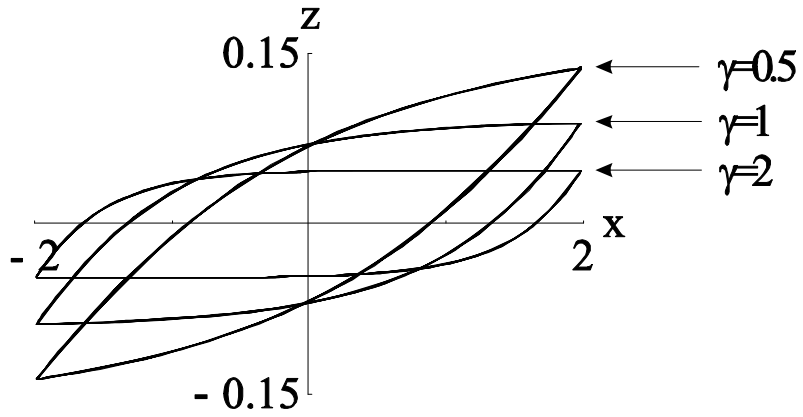

Figure 7.7: Smooth hysteresis loop, Bouc's model ($\beta = \delta = 0.1$, $\gamma = 0.5$, 1, 2).

7.3 Models Described by Third Order DDEs

In the following we describe two models that lead to a third order DDE. Both models are generalizations of the second order classical model (3.28). The first one also shows how a finite hysteresis effect (described by an integro-differential equation) can result a differential model. The second arrives at a similar (but more general) equation by assuming a viscoelastic constitutive law for the cutting force.

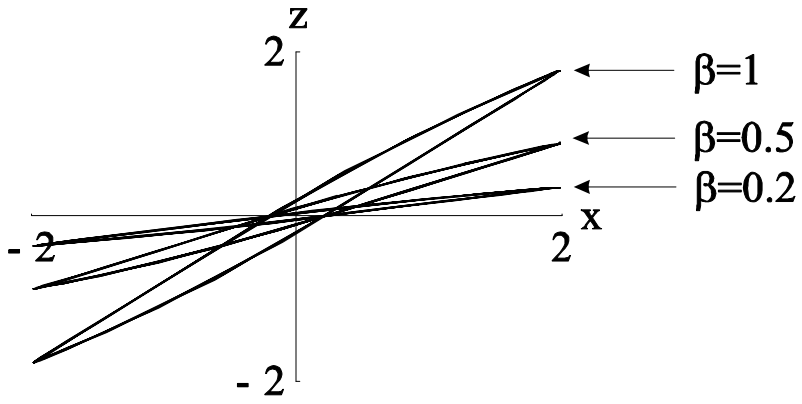

Figure 7.8: Smooth hysteresis loop, Bouc's model ($\gamma = \delta = 0.1$, $\delta = 0.2$, 0.5, 1)

7.3.1 Distributed Cutting Force

Stépán (1998) derived a model which takes the distributed characteristic of the cutting force into account (see Section 3.5) by means of a shape function $w(\theta)$.

We examine his results here because we will show in section (7.3.2) that this problem is equivalent to a linear viscoelastic relation between cutting force ΔF and chip thickness Δf. The equation of motion is the linear DDE

$$\ddot{x}(t) + 2\zeta\dot{x}(t) + x(t) = p\int_0^h x(t-\theta)w(\theta)\mathrm{d}\theta - p\int_{-\tau-h}^{-\tau} x(t+\theta)w(\tau+\theta)\mathrm{d}\theta \quad (7.27)$$

If the shape of the distributed cutting force system is approximated by the exponential function

$$w(\theta) = \frac{v_{chip}}{l_0}\exp\left(\frac{v_{chip}}{l_0}\theta\right) = \frac{1}{q_0\tau}\exp\frac{\theta}{q_0\tau}\,,\ \theta \in (-\infty, 0] \quad (7.28)$$

where l_0 is the effective contact length and q_0 is the ratio of the short and regenerative delay, then equation (7.27) can be transformed into a third order system

having only a discrete delay τ (Stépán, 1998)

$$q_0\tau\frac{\mathrm{d}^3x}{\mathrm{d}t^3}(t) + (1+2\zeta q_0\tau)\frac{\mathrm{d}^2x}{\mathrm{d}t^2}(t) + (2\zeta + q_0\tau)\frac{\mathrm{d}x}{\mathrm{d}t}(t) + (1+p)x(t) - px(t-\tau) = 0\,. \tag{7.29}$$

For $q_0 = 0$ the classical linear model

$$\ddot{x}(t) + 2\zeta\dot{x}(t) + x(t) = p\left(x(t-\tau) - x\left(t\right)\right) \tag{7.30}$$

is recovered. The D-curves are (see Chapter 4)

$$R_0(\psi) = \frac{1-\cos\psi + q_0\psi\sin\psi}{1+q_0^2\psi^2}\,, \quad S_0(\psi) = \frac{\sin\psi - q_0\psi(1-\cos\psi)}{1+q_0^2\psi^2} \tag{7.31}$$

With these the stability chart of (7.29) can be drawn (Figure 7.9). The so-called *process damping* effect can be observed at low rpms of the stability chart. Experiments also show that the chatter threshold is higher for lower cutting speeds than for higher speeds. Thus the model clearly shows a good qualitative agreement with the experimental observations.

7.3.2 Viscoelastic Model

Here we derive a delay-differential equation model that includes hysteretic effects via a constitutive relation (Moon and Kalmár-Nagy, 2001).

To describe elastoplastic materials the Kelvin-Voigt model (Figure 7.10) is often used. This model describes solid-like behavior with delayed elasticity (instantaneous elastic deformation and delayed elastic deformation) via a constitutive relation that is linear in stress, rate of stress, strain and strainrate.

The constitutive equation of this kind of material is given by

$$\sigma + \frac{\eta_1}{R_1+R_2}\dot{\sigma} = \frac{R_1R_2}{R_1+R_2}\varepsilon + \frac{R_2\eta_1}{R_1+R_2}\dot{\varepsilon} \tag{7.32}$$

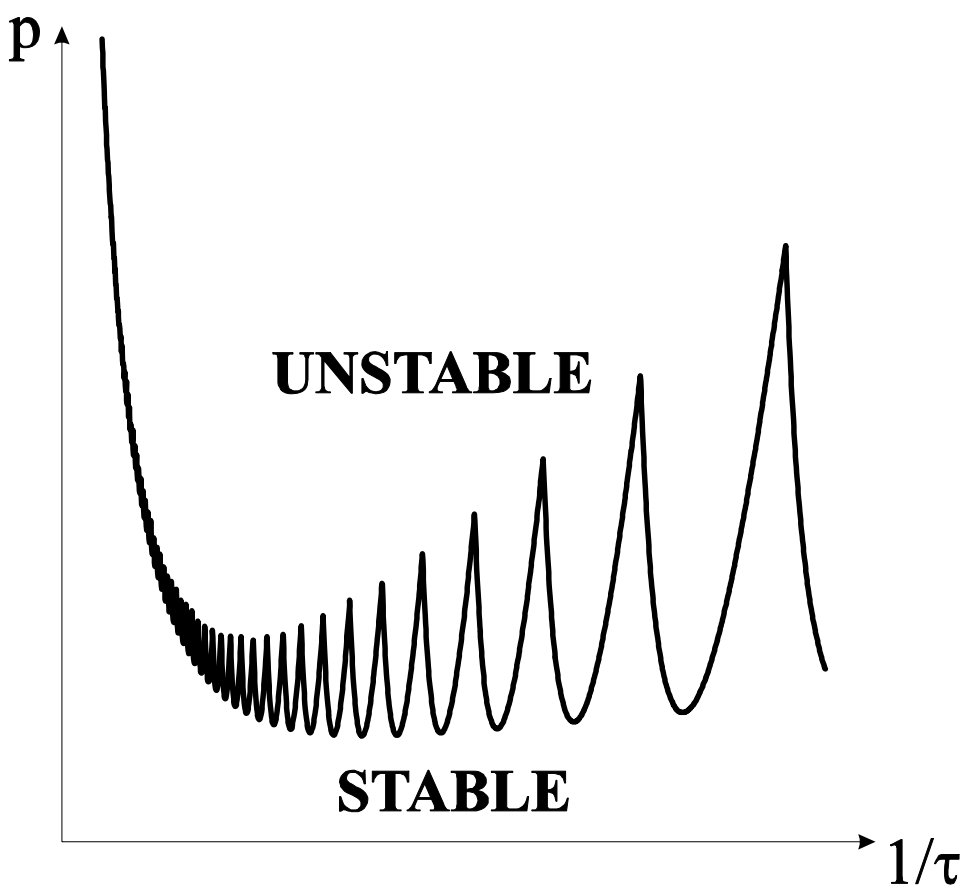

Figure 7.9: Stability chart for exponential stress distribution (Stépán, 1998).

where R_1, R_2 are the spring constants and η_1 is the coefficient of viscosity.

We assume that a similar relation between cutting force and chip thickness holds, where the coefficients of the rates depend on the cutting speed (through the time delay, using $\Delta f = x - x_\tau$)

$$\Delta F + q_0 \tau \Delta \dot{F} = k_1 \Delta f + q_1 \tau \Delta \dot{f} \tag{7.33}$$

The usual 1 DOF model is

$$\ddot{x} + 2\zeta\omega_n \dot{x} + \omega_n^2 x = -\frac{1}{m}\Delta F \tag{7.34}$$

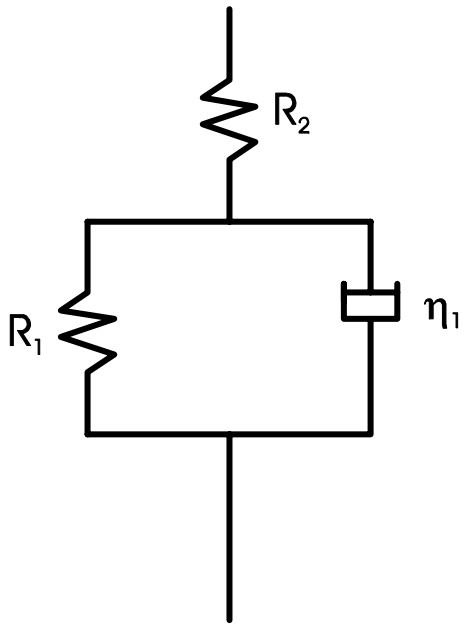

Figure 7.10: Kelvin-Voigt Model.

Multiplying the time derivative of (7.34) by $q_0\tau$ and adding it to (7.34) gives

$$\ddot{x} + 2\zeta\omega_n\dot{x} + \omega_n^2 x + q_0\tau\left(\dddot{x} + 2\zeta\omega_n\ddot{x} + \omega_n^2\dot{x}\right) = -\frac{1}{m}\left(\Delta F + q_0\tau\Delta\dot{F}\right) \tag{7.35}$$

which can be rewritten using (7.33) and the relation for chip thickness variation $\Delta f = x - x_\tau$ as

$$\begin{aligned} q_0\tau\dddot{x} + \left(1 + 2\zeta q_0\tau\omega_n\right)\ddot{x} + \left(2\zeta\omega_n + q_0\tau\omega_n^2 + \tfrac{q_1\tau}{m}\right)\dot{x} + \\ + \left(\omega_n^2 + \tfrac{k_1}{m}\right)x - \tfrac{k_1}{m}x_\tau - \tfrac{q_1\tau}{m}\dot{x}_\tau = 0 \end{aligned} \tag{7.36a}$$

The characteristic equation of (7.36a) is

$$\begin{aligned} &D(\lambda) = q_0\tau\lambda^3 + \left(1 + 2\zeta q_0\tau\omega_n\right)\lambda^2 + \left(2\zeta\omega_n + q_0\tau\omega_n^2 + \tfrac{q_1\tau}{m}\right)\lambda + \\ &+ \left(\omega_n^2 + \tfrac{k_1}{m}\right)\lambda - -\tfrac{k_1}{m}e^{-\lambda\tau} - \tfrac{q_1\tau}{m}\lambda e^{-\lambda\tau} \end{aligned} \tag{7.37}$$

The stability boundaries can be found by solving $D(i\omega) = 0$.

$$\operatorname{Re} D(i\omega) = -\omega^2 + \alpha_1\omega + \alpha_2 + \alpha_3 k_1 = 0 \tag{7.38}$$

$$\operatorname{Im} D(i\omega) = -\omega^2 + \beta_1\omega + \beta_2 + \beta_3 k_1 = 0 \tag{7.39}$$

Defining $\psi = \omega\tau$, the coefficients $\alpha_i(\psi)$, $\beta_i(\psi)$ can be expressed as

$$\alpha_1 = -2q_0\zeta\psi\omega_n \quad \alpha_2 = \omega_n^2 - \frac{q_1\psi\sin\psi}{m} \quad \alpha_3 = \frac{1-\cos\psi}{m} \tag{7.40}$$

$$\beta_1 = \frac{2\zeta\omega_n}{q_0\psi} \quad \beta_2 = \omega_n^2 + \frac{q_1(1-\cos\psi)}{mq_0} \quad \beta_3 = \frac{\sin\psi}{mq_0\psi} \tag{7.41}$$

One can eliminate k_1 from (7.38, 7.39) to get

$$\omega^2 + 2\gamma\omega - \delta^2 = 0 \tag{7.42}$$

where

$$\gamma = \frac{\alpha_1\beta_3 - \alpha_3\beta_1}{2(\alpha_3 - \beta_3)} = \frac{\zeta\omega_n(1-\cos\psi + q_0\psi\sin\psi)}{q_0\psi(\sin\psi - q_0\psi(1-\cos\psi))} \tag{7.43}$$

$$\delta^2 = \frac{\alpha_2\beta_3 - \alpha_3\beta_2}{\beta_3 - \alpha_3} = \omega_n^2 - \frac{2q_1\psi(1-\cos\psi)}{m(\sin\psi - q_0\psi(1-\cos\psi))} \tag{7.44}$$

Equation (7.42) can then be solved

$$\omega(\psi) = \sqrt{\gamma^2 + \delta^2} - \gamma \tag{7.45}$$

And finally τ (thus Ω) and k_1 can be expressed as functions of ω and ψ

$$\tau(\psi) = \frac{\psi}{\omega(\psi)} \Rightarrow \Omega(\psi) = \frac{2\pi\omega(\psi)}{\psi} \tag{7.46}$$

$$k_1(\psi) = \frac{1}{\alpha_3}\left(\omega^2 - \alpha_1\omega - \alpha_2\right) \tag{7.47}$$

The stability chart can be drawn as a function of the real parameter ψ. If $q_1 = 0$ equation (7.36a) is equivalent to that obtained by Stépán (see equation (7.29)) who calculated the cutting force by integrating an exponentially distributed force system on the rake face. The stability chart for this case is shown in Figure 7.9. Small values of q_1 do not seem to influence this chart, however, for higher values of this variable the minima of the lobes in the low speed region decrease (in contrast to the experimental observations).

7.4 Piecewise Linear Hysteretic Cutting Force Models

The model presented here was inspired by research at Cornell on chaos in elastoplastic structures (Poddar et al., 1988; Pratap et al., 1994; Moon and Kalmár-Nagy, 2001).

The idea of cutting force hysteresis is based on the fact that the cutting force is an elastoplastic process in many materials. In such behavior, the stress follows a work hardening rule for positive strain rate but reverts to a linear elastic rule for decreasing strain rate. A possible macroscopic model of such behavior is shown in Figure 7.11 (here RHS corresponds to the right hand side of (7.34)).

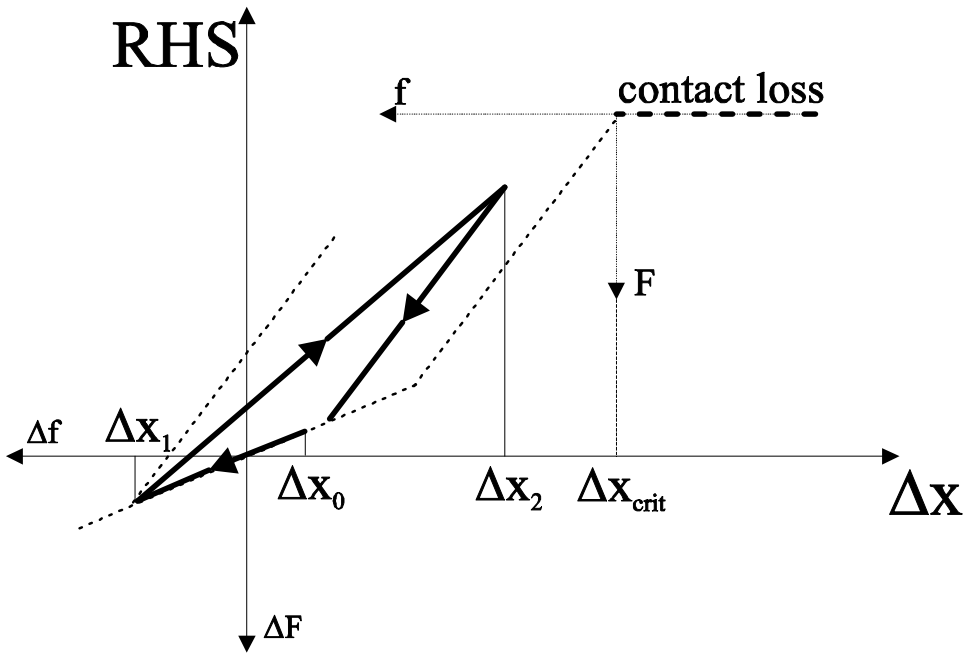

Figure 7.11: Piecewise linear hysteretic cutting force model.

Here the power-law curve has been replaced with a piecewise-linear function, where the lower line is tangent to the nonlinear cutting force relation at $\Delta x = 0$ (Figure 7.12). The loading line and the unloading line can have different slopes

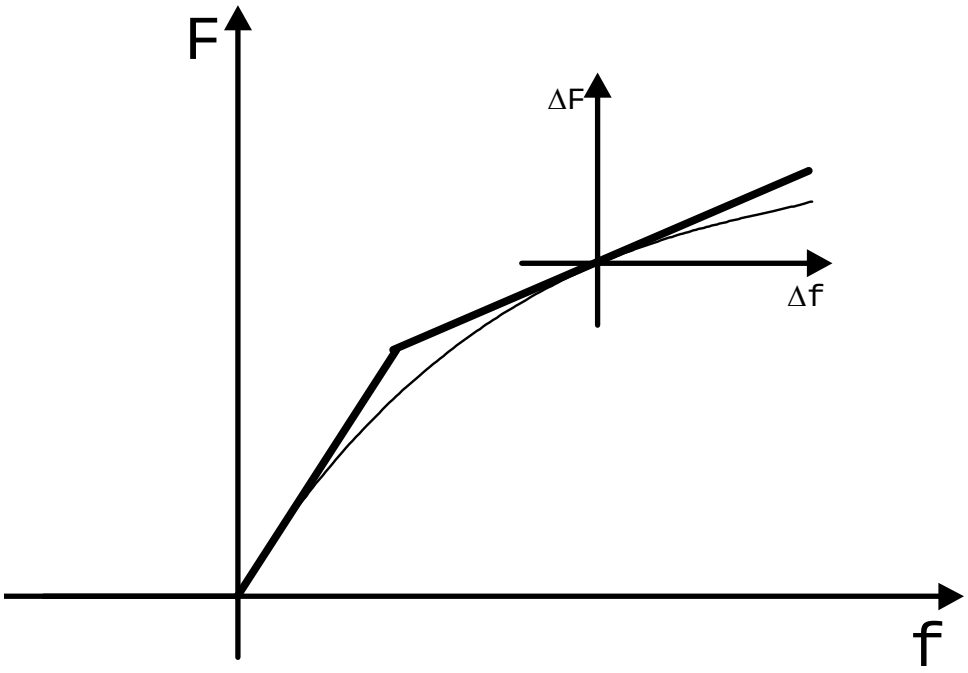

Figure 7.12: Bilinear cutting force law.

(Figure 7.13 shows possible loading-unloading paths). This model also includes separation of the tool and workpiece. An interesting feature of this model is the coexistence of periodic and quasiperiodic attractors below the linear stability boundary. As shown in Figure 7.14 there exists a torus 'inside' of the stable limit cycle. This could explain the experimental observation of the sudden transition of periodic tool vibration into complex motion. Figure 7.15 shows hysteresis loops for the observed behavior.

7.5 Bilinear Hysteresis

This Section is based on Caughey (1960) and Iwan (1965). Here we consider the forced vibration of an undamped pendulum with hysteretic restoring force. The

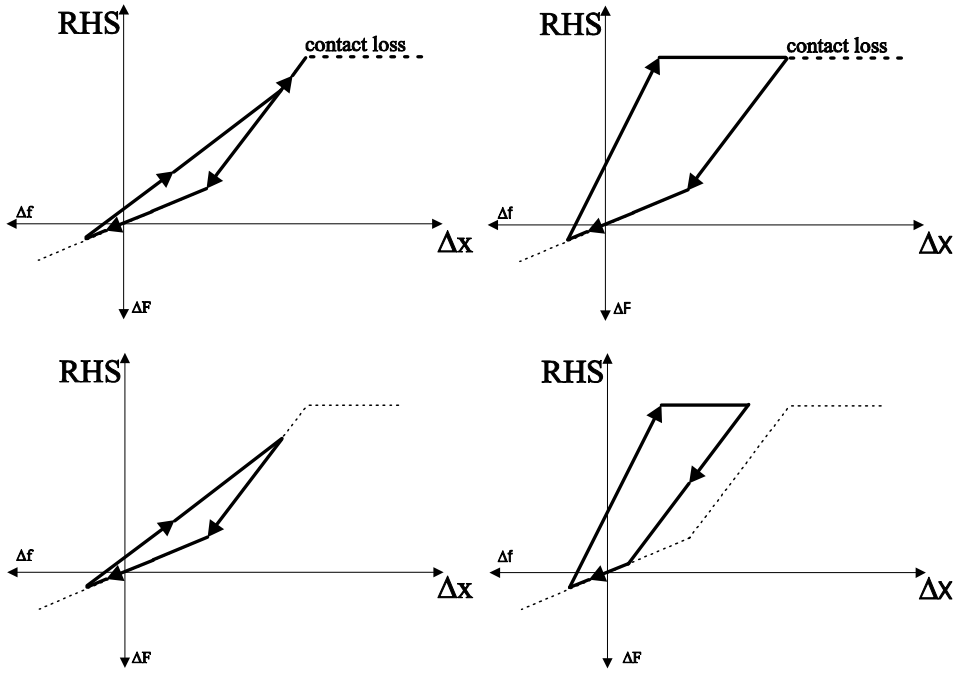

Figure 7.13: Loading-unloading paths.

nondimensional equation of motion of the system is

$$\ddot{x} + G(x, \varepsilon) = A\cos(\omega t) \tag{7.48}$$

where $G(x, \varepsilon)$ is the hysteretic restoring force shown in Figure 7.16.

The line segments are described by

$$\begin{aligned} &\text{I} && G_I = x - \varepsilon(r-1) \\ &\text{II} && G_{II} = (1-\varepsilon)x - \varepsilon \\ &\text{III} && G_{III} = x + \varepsilon(r-1) \\ &\text{IV} && G_{IV} = (1-\varepsilon)x + \varepsilon \end{aligned} \tag{7.49}$$

In the limit $\varepsilon \to 0$ the simple harmonic oscillator is recovered. Equation (7.48) can easily be put in the standard form

$$\ddot{x} + x = F(x, \varepsilon) + A\cos(\omega t) \tag{7.50}$$

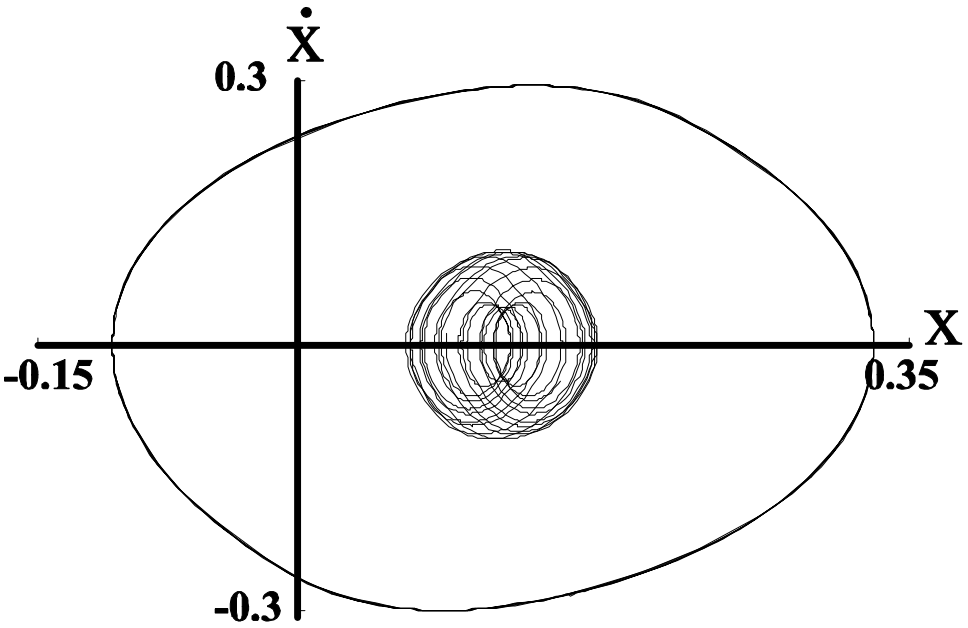

Figure 7.14: Torus 'inside' the stable limit cycle.

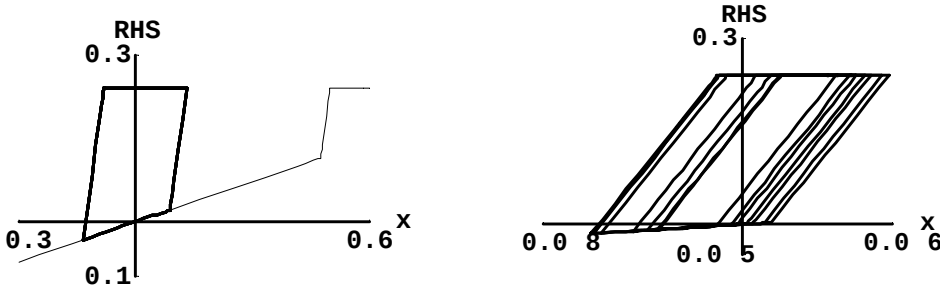

Figure 7.15: Hysteresis loops for periodic and quasiperiodic motions.

with

$$F(x,\varepsilon) = x - G(x,\varepsilon) \tag{7.51}$$

The solution is based on the averaging method (see Appendix C). The solution is assumed to have the form

$$x(t) = r(t)\cos(\omega t + \phi(t)) \tag{7.52}$$

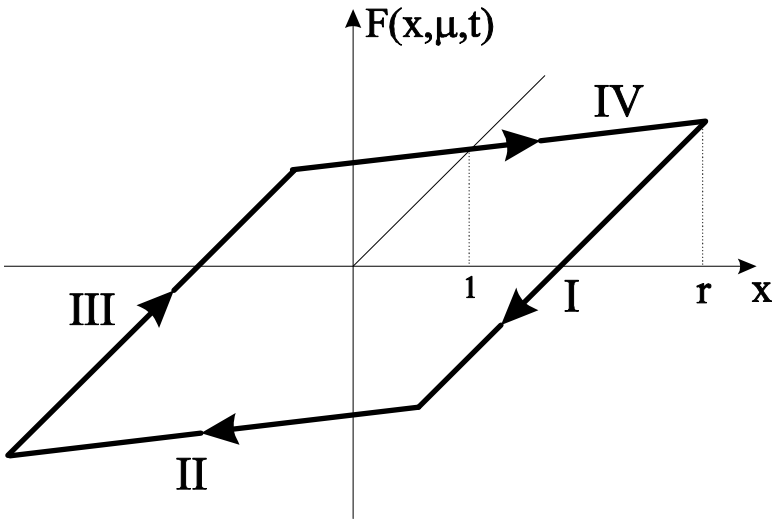

Figure 7.16: Bilinear hysteresis.

where r and ϕ are slowly varying functions of t. The averaged equations are

$$-\omega\dot{r} - S(r) = \frac{A}{2}\sin\phi \tag{7.53}$$

$$\frac{r}{2}\left(1-\omega^2\right) - \omega r\dot{\phi} - C(r) = \frac{A}{2}\cos\phi \tag{7.54}$$

where

$$S(r) = \frac{1}{2\pi}\int_0^{2\pi} F(r\cos\theta,\varepsilon)\sin\theta d\theta \tag{7.55}$$

$$C(r) = \frac{1}{2\pi}\int_0^{2\pi} F(r\cos\theta,\varepsilon)\cos\theta d\theta \tag{7.56}$$

Here $\theta = x/r$. The quantities $S(r)$ and $C(r)$ are evaluated next. Line segment I is characterized by

$$r-2 < x < r \tag{7.57}$$

Dividing by r we have

$$\psi < \theta < 1 \tag{7.58}$$

where

$$\psi = \arccos\left(\frac{r-2}{r}\right) \tag{7.59}$$

Hence

$$S(r) = \frac{1}{2\pi}\left(\int_0^{\psi} F_I \sin\theta d\theta + \int_{\psi}^{\pi} F_{II} \sin\theta d\theta + \int_{\pi}^{\pi+\psi} F_{III} \sin\theta d\theta + \int_{\pi+\psi}^{2\pi} F_{IV} \sin\theta d\theta\right) \tag{7.60}$$

$$C(r) = \frac{1}{2\pi}\left(\int_0^{\psi} F_I \cos\theta d\theta + \int_{\psi}^{\pi} F_{II} \cos\theta d\theta + \int_{\pi}^{\pi+\psi} F_{III} \cos\theta d\theta + \int_{\pi+\psi}^{2\pi} F_{IV} \cos\theta d\theta\right) \tag{7.61}$$

Because of symmetry

$$\begin{aligned} \int_0^{\psi} F_I \cos\theta d\theta &= \int_{\pi}^{\pi+\psi} F_{III} \cos\theta d\theta, & \int_0^{\psi} F_I \sin\theta d\theta &= \int_{\pi}^{\pi+\psi} F_{III} \sin\theta d\theta \\ \int_{\psi}^{\pi} F_{II} \cos\theta d\theta &= \int_{\pi+\psi}^{2\pi} F_{IV} \cos\theta d\theta, & \int_{\psi}^{\pi} F_{II} \sin\theta d\theta &= \int_{\pi+\psi}^{2\pi} F_{IV} \sin\theta d\theta \end{aligned} \tag{7.62}$$

So

$$S(r) = \frac{1}{\pi}\left(\int_0^{\psi} F_I(r\cos\theta, \varepsilon)\sin\theta d\theta + \int_{\psi}^{\pi} F_{II}(r\cos\theta, \varepsilon)\sin\theta d\theta\right) \tag{7.63}$$

$$C(r) = \frac{1}{\pi}\left(\int_0^{\psi} F_I(r\cos\theta, \varepsilon)\cos\theta d\theta + \int_{\psi}^{\pi} F_{II}(r\cos\theta, \varepsilon)\cos\theta d\theta\right) \tag{7.64}$$

And finally, substituting the equations of the line segments (7.49)

$$S(r) = \begin{cases} \frac{\varepsilon r \sin^2\psi}{\pi} & r > 1 \\ 0 & r \leq 1 \end{cases} \tag{7.65}$$

$$C(r) = \begin{cases} \frac{r\varepsilon}{2\pi}\left[\pi - \psi + \frac{1}{2}\sin 2\psi\right] & r > 1 \\ r & r \leq 1 \end{cases} \tag{7.66}$$

7.6 Steady-State Response

The system is in steady-state when $\dot{r} = \dot{\phi} = 0$. The equations (7.53, 7.54) become

$$-S(\bar{r}) = \frac{A}{2}\sin\bar{\phi} \tag{7.67}$$

$$\frac{\bar{r}}{2}\left(1-\omega^2\right) - C(\bar{r}) = \frac{A}{2}\cos\bar{\phi} \tag{7.68}$$

where the barred quantities denote steady-state values. We can eliminate the trigonometric terms from (7.67, 7.68) by squaring and adding them

$$\left(\frac{\bar{r}}{2}\left(1-\omega^2\right) - C(\bar{r})\right)^2 + S^2(\bar{r}) = \frac{A^2}{4} \tag{7.69}$$

Solving (7.69) for ω^2

$$\omega^2 = 1 - 2\left(\frac{C(\bar{r})}{\bar{r}} \pm \sqrt{\left(\frac{A}{2\bar{r}}\right)^2 - \left(\frac{S(\bar{r})}{\bar{r}}\right)^2}\right) \tag{7.70}$$

or with (7.66, 7.65)

$$\omega^2 = 1 - 2\varepsilon\left(\frac{1}{2} - \frac{\psi}{2\pi} + \frac{1}{4\pi}\sin 2\psi \pm \sqrt{\frac{A^2}{4\varepsilon^2\bar{r}^2} - \frac{\sin^4\psi}{\pi^2}}\right) \tag{7.71}$$

Introducing the new variables

$$\Omega = 1 + \frac{\omega^2 - 1}{\varepsilon}, \qquad f = \frac{A}{2\varepsilon} \tag{7.72}$$

this can also be written as

$$\Omega = \frac{1}{\pi}\left(\psi - \frac{1}{2}\sin 2\psi\right) \pm \sqrt{\left(\frac{f}{\bar{r}}\right)^2 - \frac{\sin^4\psi}{\pi^2}} \tag{7.73}$$

The maximum amplitude will occur at the point where Ω has a double root, that is where

$$\frac{f}{\bar{r}_{\max}} = \frac{\sin^2\psi}{\pi} = \frac{4\left(\bar{r}_{\max} - 1\right)}{\bar{r}_{\max}^2\pi} \tag{7.74}$$

Here

$$\bar{r}_{\max} = \frac{4}{4 - \pi f} \tag{7.75}$$

Since $\bar{r}_{\max} > 0$ the following has to hold

$$f < \frac{4}{\pi} \sim 1.27 \tag{7.76}$$

to have a bounded response.

The steady-state phase can be found from equations (7.67, 7.68) as

$$\bar{\phi} = \arctan \frac{S(\bar{r})}{C(\bar{r}) - \frac{\bar{r}}{2}(1 - \omega^2)} \tag{7.77}$$

Substituting for $C(r)$ and $S(r)$ results

$$\bar{\phi} = \arctan \frac{\sin^2 \psi}{\pi\Omega - \psi + \frac{1}{2}\sin 2\psi} \tag{7.78}$$

Note that at peak response, the denominator vanishes, resulting

$$\bar{\phi}_{\max} = \frac{\pi}{2} \tag{7.79}$$

Thus for this system, phase and amplitude resonance occur at the same frequency.

To check the results of the analysis, direct numerical integration was performed in Mathematica. For the simulations $\varepsilon = 0.5$ was specified (so the forcing amplitude was $A = f$). For initial conditions the approximate-solution amplitude and phase was used and the equation of motion was integrated for 100 time units. Steady-state was reached in every test case. The last extremal value of x was taken as the steady state amplitude. Figure 7.17 shows the frequency response function for different values of the forcing f (0.2, 0.5, 0.7, 1) as a function of Ω. The dots represent simulation results. Note the softening characteristic of the response function. The solutions are always stable (Caughey, 1960).

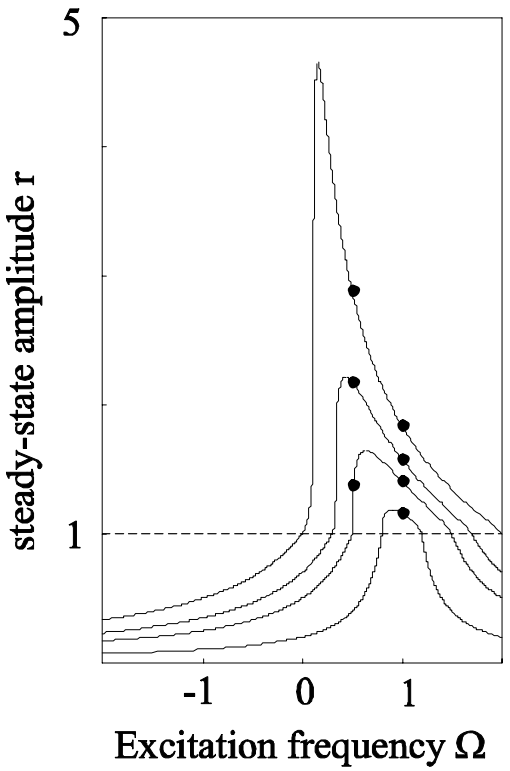

Figure 7.17: Response function for (7.48).

7.7 A Simple DDE with Bilinear Hysteresis

Here the forced vibration of an undamped pendulum with hysteretic restoring force is considered (note the similarity with the classical cutting model). The nondimensional equation of motion of the system is

$$\ddot{x} + x = pF\left(x_\tau - x, \varepsilon\right) + A\cos\left(\omega t\right) \tag{7.80}$$

where $F\left(x, \varepsilon\right) = x - G\left(x, \varepsilon\right)$ and $G\left(x, \varepsilon\right)$ is the hysteretic force specified by (7.49). The ε-dependence of F will not be shown for brevity.

Again, the averaging method is used. The averaged equations are

$$-\omega\dot{r} - p\left(S_\tau\left(r, \omega\right) - S\left(r\right)\right) = \frac{A}{2}\sin\phi \tag{7.81}$$

$$\frac{r}{2}\left(1-\omega^2\right)-\omega r\dot{\phi}-p\left(C_\tau\left(r,\omega\right)-C\left(r\right)\right)=\frac{A}{2}\cos\phi \tag{7.82}$$

where $S\left(r\right)$, $C\left(r\right)$ are given by (7.65, 7.66) and

$$S_\tau\left(r,\omega\right)=\frac{1}{2\pi}\int_0^{2\pi}F\left(r\cos\left(\theta-\omega\tau\right)\right)\sin\theta d\theta \tag{7.83}$$

$$C_\tau\left(r,\omega\right)=\frac{1}{2\pi}\int_0^{2\pi}F\left(r\cos\left(\theta-\omega\tau\right)\right)\cos\theta d\theta \tag{7.84}$$

Note that these quantities are functions of ω! They are evaluated as follows

$$S_\tau\left(r,\omega\right)=\frac{1}{2\pi}\left(\int_{\omega\tau}^{\psi+\omega\tau}F_I\left(r\cos\left(\theta-\omega\tau\right)\right)\sin\theta d\theta+\int_{\psi+\omega\tau}^{\pi+\omega\tau}F_{II}\left(r\cos\left(\theta-\omega\tau\right)\right)\sin\theta d\theta+\right. \tag{7.85}$$

$$\left.\int_{\pi+\omega\tau}^{\pi+\psi+\omega\tau}F_{III}\left(r\cos\left(\theta-\omega\tau\right)\right)\sin\theta d\theta+\int_{\pi+\psi+\omega\tau}^{2\pi+\omega\tau}F_{IV}\left(r\cos\left(\theta-\omega\tau\right)\right)\sin\theta d\theta\right) \tag{7.86}$$

$$C_\tau\left(r,\omega\right)=\frac{1}{2\pi}\left(\int_{\omega\tau}^{\psi+\omega\tau}F_I\left(r\cos\left(\theta-\omega\tau\right)\right)\cos\theta d\theta+\int_{\psi+\omega\tau}^{\pi+\omega\tau}F_{II}\left(r\cos\left(\theta-\omega\tau\right)\right)\cos\theta d\theta+\right. \tag{7.87}$$

$$\left.\int_{\pi+\omega\tau}^{\pi+\psi+\omega\tau}F_{III}\left(r\cos\left(\theta-\omega\tau\right)\right)\cos\theta d\theta+\int_{\pi+\psi+\omega\tau}^{2\pi+\omega\tau}F_{IV}\left(r\cos\left(\theta-\omega\tau\right)\right)\cos\theta d\theta\right) \tag{7.88}$$

Substituting the equations of the line segments (7.49)

$$S_\tau\left(r,\omega\right)=\begin{cases}\frac{r}{2\pi}\left[\pi\sin\omega\tau+\varepsilon\left(\left(\psi-\pi\right)\sin\omega\tau-\sin\psi\sin\left(\psi+\omega\tau\right)\right)\right] & r>1\\ 0 & r\leq 1\end{cases} \tag{7.89}$$

$$C_\tau\left(r,\omega\right)=\begin{cases}\frac{r}{2\pi}\left[\pi\cos\omega\tau+\varepsilon\left(\left(\psi-\pi\right)\cos\omega\tau-\sin\psi\cos\left(\psi+\omega\tau\right)\right)\right] & r>1\\ r & r\leq 1\end{cases} \tag{7.90}$$

7.8 Steady-State Response

The steady-state averaged equations are

$$-p\left(S_\tau\left(\bar{r},\omega\right)-S\left(\bar{r}\right)\right)=\frac{A}{2}\sin\bar{\phi} \tag{7.91}$$

$$\frac{\bar{r}}{2}\left(1-\omega^2\right)-p\left(C_\tau\left(\bar{r},\omega\right)-C\left(\bar{r}\right)\right)=\frac{A}{2}\cos\bar{\phi} \tag{7.92}$$

where the barred quantities denote steady-state values. We can eliminate the trigonometric terms by squaring and adding these equations

$$\left(\frac{\bar{r}}{2}\left(1-\omega^2\right)-p\left(C_\tau\left(\bar{r},\omega\right)-C\left(\bar{r}\right)\right)\right)^2+p^2\left(S_\tau\left(\bar{r},\omega\right)-S\left(\bar{r}\right)\right)^2=\frac{A^2}{4} \tag{7.93}$$

This equation can numerically be solved to find $\bar{r}$ as a function of ω. It seems however, that replacing $C_\tau\left(\bar{r},\omega\right)$ and $S_\tau\left(\bar{r},\omega\right)$ by $C_\tau\left(\bar{r},1\right)$ and $S_\tau\left(\bar{r},1\right)$ and solving (7.69) for ω

$$\omega=\sqrt{1-2p\left(\frac{C_\tau\left(\bar{r},1\right)-C_\tau\left(\bar{r}\right)}{\bar{r}}\pm\sqrt{\left(\frac{A}{2\bar{r}p}\right)^2-\left(\frac{S\left(\bar{r}\right)-S_\tau\left(\bar{r},1\right)}{\bar{r}}\right)^2}\right)} \tag{7.94}$$

provides a very good approximation in a fairly large parameter regime. Figure 7.18 shows the influence of various parameters on the frequency response of the system. Figure a, shows that increasing p results larger vibration amplitudes. Figure b, shows the effect of ε on the response. As expected, ε acts like damping. Figure c, shows that for certain parameter values ($A=0.3$) an unstable branch can appear, unlike in the problem without delay. Finally, Figure c, depicts how the response curves move with varying τ. These phenomena deserve a more detailed analysis.

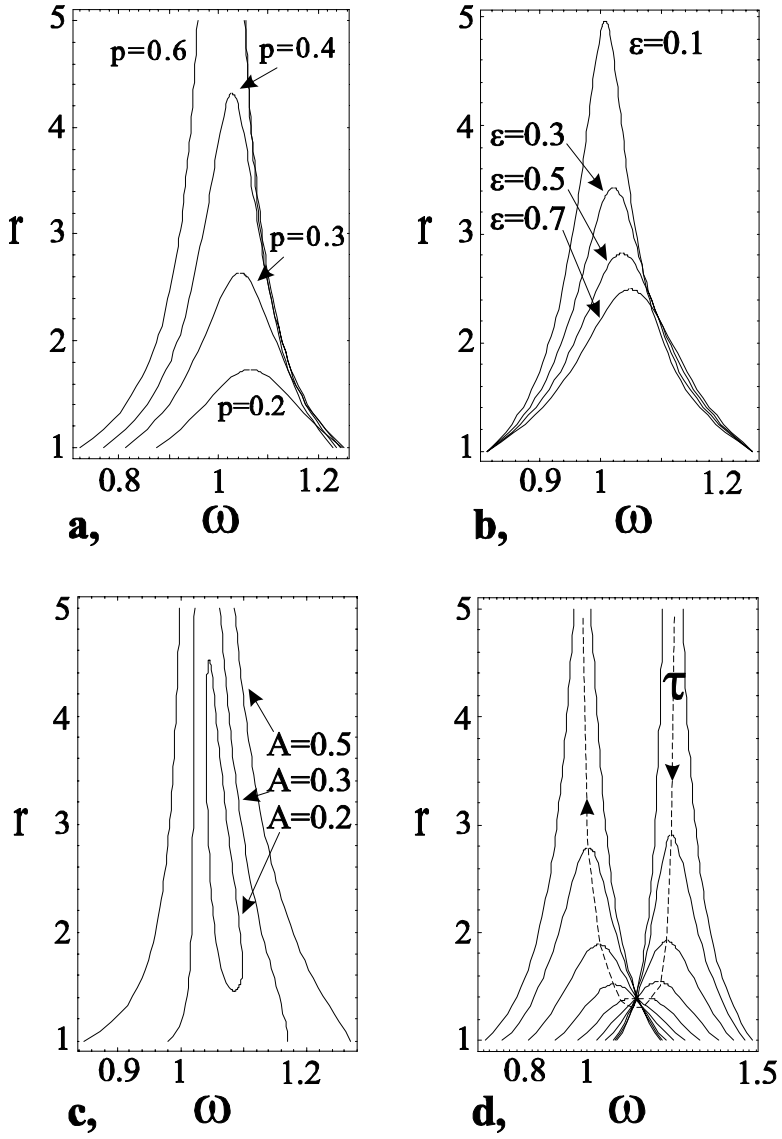

Figure 7.18: Response functions for various parameters. **a,** $\epsilon = 0.2, \tau = 1, A = 0.5$ **b,** $p = 0.5, \tau = 1, A = 0.5$ **c,** $p = 0.48, \epsilon = 0.8, \tau = 5$ **d,** $p = 0.6, \epsilon = 0.2, A = 0.5, \tau = 0.3 \rightarrow 3$

Chapter 8

A New Three Degree-of-Freedom Tool Vibration Model

Real tools have multiple degrees of freedom. In addition to horizontal and vertical displacements, tools can twist and bend. Even though the classical model (3.28) with nonlinear cutting force is quite successful in predicting the experimentally observed subcritical instability, it can not possibly account for all phenomena displayed in real cutting experiments, such as small vibrations below the classical stability boundaries (e.g. Figure 4.2).

In this Chapter we derive a new 3 DOF lumped-parameter delay model for tool vibrations. The three degrees-of-freedom are the horizontal (feed direction) and vertical displacements as well as the rotation of the tooltip. The cutting force acts as a partial follower force resulting in a nonsymmetric stiffness matrix. Linear stability analysis is performed on the model. The possible effects of mode coupling include birth of unstable regions below the minimum value predicted by the single DOF classical model (3.28).

8.1 Oblique Cutting

Although many practical machining processes can adequately be modeled as orthogonal, more accurate models demand a chip formation model in which the cutting velocity is not normal to the cutting edge. Figure 8.1 shows the usual oblique chip formation model, where the inclination angle i (measured between the cutting edge and the normal to the cutting velocity in the plane of the machined surface) is not zero, as in orthogonal cutting. The cutting velocity is denoted by v_C, the chip flow

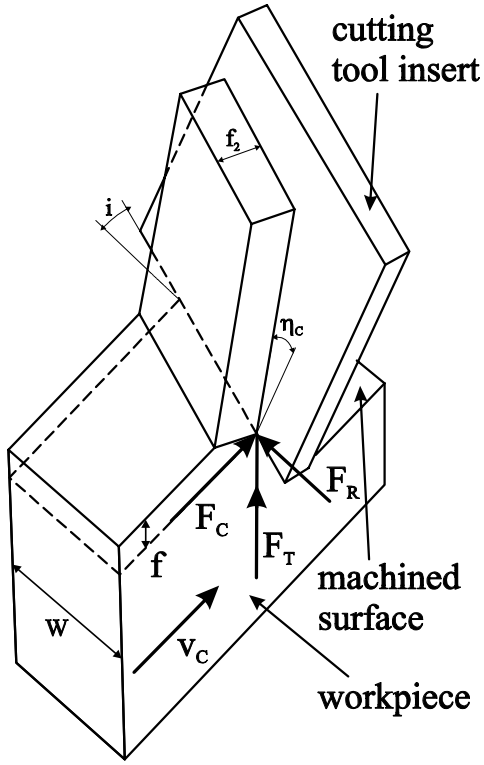

Figure 8.1: Oblique chip formation model.

angle is η_c, the thickness of the undeformed chip is f, the deformed chip thickness is f_2 and the chip width is w. The three dimensional cutting force acting on the tool insert is decomposed into three mutually orthogonal forces: F_C, F_T, F_R. The

cutting force F_C is the force in the cutting direction, the thrust force F_T is the force normal to the cutting direction and machined surface, while the radial force F_R is normal to both F_C and F_T. The difference between orthogonal and oblique cutting is, while the previous can be modeled as a 2-dimensional process, the latter can not. Oblique cutting is a true three-dimensional plastic flow problem.

8.2 3 DOF Model of Metal Cutting

Figure 8.2 shows a tool with a cutting chip (insert) both in undeformed and deformed state of the tool. The three degrees of freedom are horizontal position (x), vertical position (z), and twist (ϕ). In the lumped parameter model (Figure 8.3)

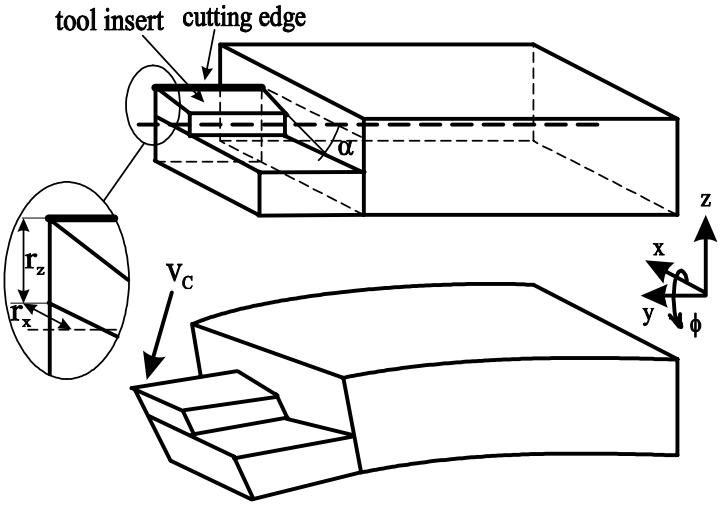

Figure 8.2: 3 DOF metal cutting model.

all the mass m of the beam is placed at its end (this effective mass is equivalent to modal mass for a distributed beam). The equations of motion are the following

$$m\ddot{z} + c_z\dot{z} + k_z z = F_z \tag{8.1}$$

$$m\ddot{x} + c_x\dot{x} + k_x x = F_x \tag{8.2}$$

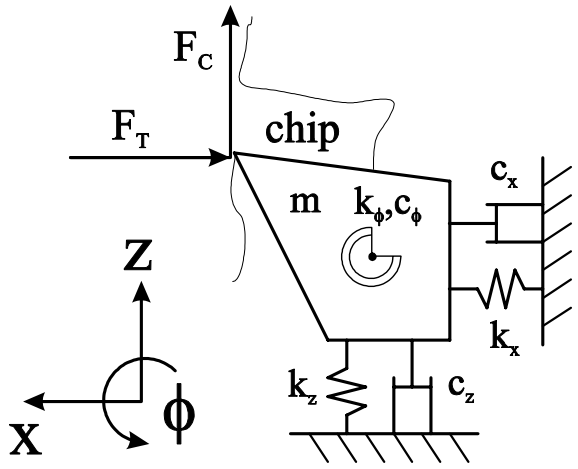

Figure 8.3: 3 DOF lumped-parameter model.

$$I\ddot{\phi} + c_\phi\dot{\phi} + k_\phi\phi = M_y \tag{8.3}$$

Figure 8.4 shows the forces acting on the tooltip.

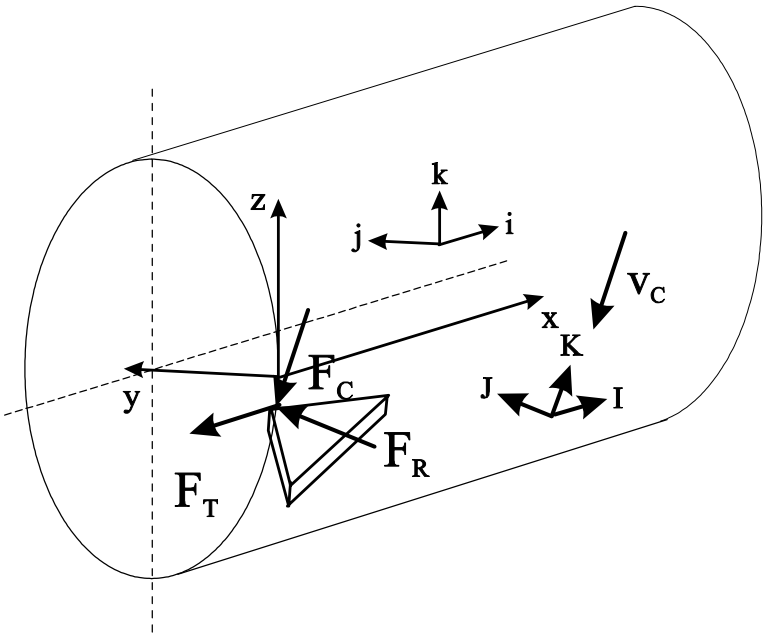

Figure 8.4: Forces on the tooltip.

As the tool bends about the x axis, the direction of the cutting velocity (and

main cutting force) changes, as shown in Figure 8.5.

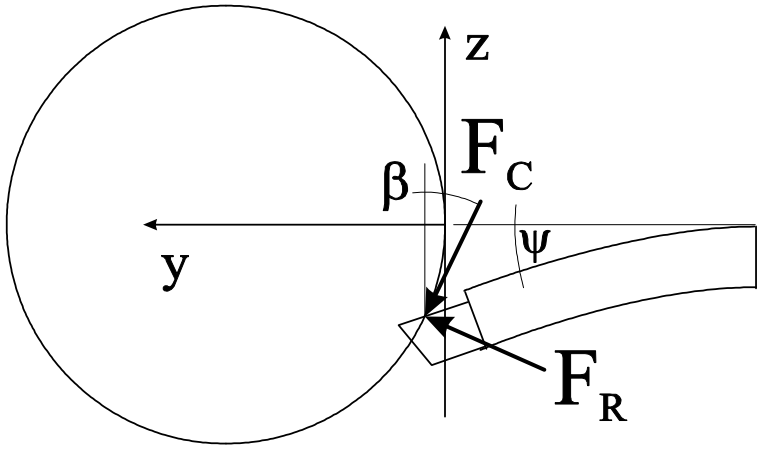

Figure 8.5: Direction of cutting velocity.

The force acting on the insert can be written as

$$\mathbf{F} = -F_T\mathbf{I} + F_R\mathbf{J} - F_C\mathbf{K} \tag{8.4}$$

or

$$\mathbf{F} = F_x\mathbf{i} + F_y\mathbf{j} + F_z\mathbf{k} \tag{8.5}$$

where $\mathbf{i}$, $\mathbf{j}$, $\mathbf{k}$ are unit vectors in the x, y, z directions, respectively.

$$F_x = -F_T \tag{8.6}$$

$$F_y = F_C \sin\beta + F_R \cos\beta \tag{8.7}$$

$$F_z = F_R \sin\beta - F_C \cos\beta \tag{8.8}$$

The bending also results in a pitch ψ (shown in Figure 8.5). This is not a separate degree of freedom, but nonetheless it will influence the inclination angle.

The following assumptions are used in deriving the equations of motion

- The forces that act on the insert are steady state forces

- The width of cut w (y-position) is constant
- All displacements are small
- Yaw is negligible

Next we find the position of the tooltip in the fixed system of the platform.

To do so we have to find the rotation matrix $\mathbf{R}$ that describes the relationship between the moving frame $(\mathbf{i}, \mathbf{j}, \mathbf{k})$ (fixed to the cutting velocity) and the fixed frame $(\mathbf{I}, \mathbf{J}, \mathbf{K})$.

$$\begin{pmatrix} \mathbf{i} & \mathbf{j} & \mathbf{k} \end{pmatrix} = \mathbf{R} \begin{pmatrix} \mathbf{I} & \mathbf{J} & \mathbf{K} \end{pmatrix} \tag{8.9}$$

define angles

Using the set of Euler angles (see for example, Moon, 2000) $\{\psi, \phi\}$ we express $\mathbf{R}$ as a product of two consecutive planar rotations (Pitch-Roll system)

$$\mathbf{R} = \mathbf{R}_2 \mathbf{R}_1 \tag{8.10}$$

The cross section is first rotated about $\mathbf{I}$ by the pitch angle ψ. The corresponding rotation matrix is

$$\mathbf{R}_1 = \begin{pmatrix} 1 & 0 & 0 \\ 0 & \cos\psi & \sin\psi \\ 0 & -\sin\psi & \cos\psi \end{pmatrix} \tag{8.11}$$

The second rotation is about the $\mathbf{J}_2$ (the rotated $\mathbf{J}$) axis through the roll angle ϕ (w.r.t the toolholder)

$$\mathbf{R}_2 = \begin{pmatrix} \cos\phi & 0 & \sin\phi \\ 0 & 1 & 0 \\ -\sin\phi & 0 & \cos\phi \end{pmatrix} \tag{8.12}$$

$\mathbf{R}$ can then be calculated by (8.10)

$$\mathbf{R} = \begin{pmatrix} \mathrm{c}\phi & -\mathrm{s}\phi\mathrm{s}\psi & \mathrm{c}\psi\mathrm{s}\phi \\ 0 & \mathrm{c}\psi & \mathrm{s}\psi \\ -\mathrm{s}\phi & -\mathrm{c}\phi\mathrm{s}\psi & \mathrm{c}\psi\mathrm{c}\phi \end{pmatrix} \tag{8.13}$$

where the abbreviations c = cos, s = sin were used. The position of the tooltip can be expressed in the fixed frame as

$$\mathbf{r}^* = \mathbf{R} \begin{pmatrix} r_x \\ 0 \\ r_z \end{pmatrix} = \begin{pmatrix} r_x\mathrm{c}\phi + r_z\mathrm{c}\psi\mathrm{s}\phi \\ r_z\mathrm{s}\psi \\ r_z\mathrm{c}\psi\mathrm{c}\phi - r_x\mathrm{s}\phi \end{pmatrix} \tag{8.14}$$

The moment that produces roll can then be calculated as

$$M_y = (\mathbf{r}^* \times \mathbf{F}) \cdot \mathbf{j} = F_T \left(r_x\mathrm{s}\phi - r_z\mathrm{c}\phi\mathrm{c}\psi\right) + F_c\mathrm{c}\beta \left(r_x\mathrm{c}\phi + r_z\mathrm{c}\psi\mathrm{s}\phi\right) - \\ -F_R\mathrm{s}\beta \left(r_x\mathrm{c}\phi + r_z\mathrm{c}\psi\mathrm{s}\phi\right) \tag{8.15}$$

In the following we assume small displacements and small angles and neglect non-linear terms. The angle β is taken to be proportional to the vertical displacement, i.e. $\beta = -nz$ and so is the pitch, i.e. $\psi = kz$.

$$m\ddot{z} + c_z\dot{z} + k_z z = -\left(F_C + nz\bar{F}_R\right) \tag{8.16}$$

$$m\ddot{x} + c_x\dot{x} + k_x x = -F_T \tag{8.17}$$

$$I\ddot{\phi} + c_\phi\dot{\phi} + k_\phi\phi = M_y = \phi\left(r_x\bar{F}_T + r_z\bar{F}_C\right) - r_z F_T + r_x F_C - r_x\bar{F}_R\beta \tag{8.18}$$

where $\bar{F}_C$, $\bar{F}_R$, $\bar{F}_T$ denotes the constant term in F_C, F_R and F_T, respectively.

8.3 Cutting Forces

Generally we assume that the cutting forces F_C, F_T, F_R depend only on the rake angle α, the inclination angle i and chip thickness f (see Figure 8.1). We again

emphasize that the chip width w is considered constant in the present analysis. Our hypothesis here is that F_C and F_T depend linearly on both the rake angle and chip thickness (see Section 8.5.2) in the following manner

$$F_C = -l_C\alpha + m_C t_1 + F_{C0} \tag{8.19}$$

$$F_T = -l_T\alpha + m_T t_1 + F_{T0} \tag{8.20}$$

where m_C and m_T are cutting force coefficients (similar to k_1), while l_C and l_T are angular cutting force coefficients (they show how strong the force dependence is on rake angle). F_{C0} and F_{T0} are constant forces, that arise from cutting at a nominal chip thickness.

The radial cutting force can be expressed as (Oxley, 1989)

$$F_R = \sin i \frac{F_C \cos i\,(i - \sin\alpha) - F_T}{\sin^2 i \sin\alpha + \cos^2 i} \tag{8.21}$$

where Stabler's Flow Rule (Stabler, 1964) $\eta_C = i$ was used. The effective rake angle depends on the initial rake angle and the roll

$$\alpha = \alpha_0 - \phi \tag{8.22}$$

while the inclination angle will depend on the pitch

$$i = i_0 - \psi \tag{8.23}$$

The chip thickness depends on the nominal feed and the position of the tooltip (both the present and the delayed ones). The displacement of the tooltip is due to translational and rotational motion as shown in Figure 8.6.

The chip thickness is then given by

$$t_1 = t_{10} + x - x_\tau + r_z \sin(\phi - \phi_\tau) \approx t_{10} + x - x_\tau + r\,(\phi - \phi_\tau) \tag{8.24}$$

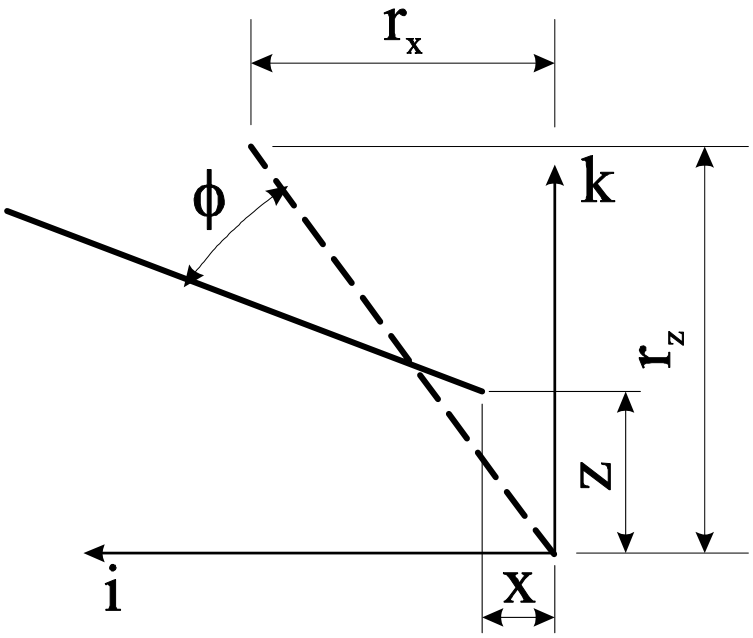

Figure 8.6: Motion of the tooltip.

Then the cutting forces can be written as

$$F_C = m_C\left(x - x_\tau\right) + \left(l_C + r_z m_C\right)\phi - r_z m_C \phi_\tau + \overbrace{m_C t_{10} + F_{C0} - \alpha_0 l_C}^{\bar{F}_C} \tag{8.25}$$

$$F_T = m_T\left(x - x_\tau\right) + \left(l_T + r_z m_T\right)\phi - r_z m_T \phi_\tau + m_T t_{10} + F_{T0} - \alpha_0 l_T \tag{8.26}$$

If the initial inclination angle is assumed to be zero, the expression for F_R will simplify

$$F_R = k\left(\bar{F}_T + \left(\sin\alpha_0 - 1\right)\bar{F}_C + t_{10}\left(m_C\left(1 - \sin\alpha_0\right) - m_T\right)\right) z \tag{8.27}$$

8.4 The Equations of Motion

Equations (8.16-8.18) contain constant terms (the z equation has F_{C0}, the x equation has F_{T0} and the ϕ equation has rF_{T0}). These constant terms can be eliminated

by translating the variables, so that (x, z, ϕ) represent departures from the steady values of these displacements. The new equations of motion are the following

$$m\ddot{z} + c_z\dot{z} + k_z z = -n\bar{F}_R z - m_C\left(x - x_\tau\right) - \left(l_C + r_z m_C\right)\phi + r_z m_C \phi_\tau \tag{8.28}$$

$$m\ddot{x} + c_x\dot{x} + k_x x = -m_T\left(x - x_\tau\right) - \left(l_T + r_z m_T\right)\phi + r_z m_T \phi_\tau \tag{8.29}$$

$$\begin{aligned} I\ddot{\phi} + c_\phi\dot{\phi} + k_\phi\phi = -r_z m_T\left(x - x_\tau\right) - \\ -r_z\left(l_T + r_z m_T - m_C t_{10} - F_{C0} + \alpha_0 l_C\right)\phi + r_z^2 m_T \phi_\tau \end{aligned} \tag{8.30}$$

As we can see, the x and ϕ equations are uncoupled from the z equation, so the stability of the system is determined by (8.29, 8.30) (the coefficient of z in (8.28) is negative).

Equations (8.29, 8.30) can also be written as

$$\ddot{x} + 2\zeta_x\omega_x\dot{x} + \left(\omega_x^2 + \frac{m_T}{m}\right)x + \frac{1}{m}\left(l_T + r_z m_T\right)\phi = \frac{m_T}{m}x_\tau + r_z\frac{m_T}{m}\phi_\tau \tag{8.31}$$

$$\begin{aligned} \ddot{\phi} + 2\zeta_\phi\omega_\phi\dot{\phi} + \frac{r_z m_T}{I}x + \\ + \left(\omega_\phi^2 + \frac{r_z}{I}\left(l_T + r_z m_T - m_C t_{10} - F_{C0} + \alpha_0 l_C\right)\right)\phi = \frac{r_z m_T}{I}x_\tau + r_z^2\frac{m_T}{I}\phi_\tau \end{aligned} \tag{8.32}$$

where

$$\omega_x = \sqrt{\frac{k_x}{m}}, \qquad \omega_\phi = \sqrt{\frac{k_\phi}{I}} \tag{8.33}$$

By introducing the nondimensional time and displacement

$$\hat{t} = t/T \qquad \hat{x} = x/X \tag{8.34}$$

$$\begin{aligned} \hat{x}'' + 2\zeta_x\omega_x T\hat{x}' + \left(\omega_x^2 + \frac{m_T}{m}\right)T^2\hat{x} + \frac{1}{m}\left(l_T + r_z m_T\right)\frac{T^2}{X}\phi = \\ = \frac{m_T}{m}T^2 x_\tau + r_z\frac{m_T}{m}\frac{T^2}{X}\phi_\tau \end{aligned} \tag{8.35}$$

$$\phi'' + 2\zeta_\phi \omega_\phi T \phi' + \frac{r m_T}{I} T^2 X \hat{x} +$$

$$+ \left[\omega_\phi^2 + \frac{r_z}{I} \left(l_T + r_z m_T - F_{C0} - m_C t_{10} + \alpha_0 l_C \right) \right] T^2 \phi = \tag{8.36}$$

$$\frac{r_z m_T}{I} T^2 X x_\tau + r_z^2 \frac{m_T}{I} T^2 \phi_\tau \tag{8.37}$$

With the choice of the following scales

$$T = \frac{1}{\omega_x} \qquad X = \sqrt{\frac{I}{m}} \tag{8.38}$$

the equations assume the form (note that $\hat{\tau} = \omega_x \tau$)

$$\hat{x}'' + 2\zeta_x \hat{x}' + k_{11} \hat{x} + k_{12} \phi = r_{11} \hat{x}_{\hat{\tau}} + r_{12} \phi_{\hat{\tau}} \tag{8.39}$$

$$\phi'' + 2\hat{\zeta}_\phi \phi' + k_{21} \hat{x} + k_{22} \phi = r_{21} \hat{x}_{\hat{\tau}} + r_{22} \phi_{\hat{\tau}} \tag{8.40}$$

where

$$k_{11} = 1 + \frac{m_T}{\omega_x^2 m} \qquad k_{12} = \frac{l_T + r_z m_T}{\omega_x^2 \sqrt{Im}} \tag{8.41}$$

$$k_{21} = \frac{r_z m_T}{\omega_x^2 \sqrt{Im}} \qquad \hat{\zeta}_\phi = \zeta_\phi \frac{\omega_\phi}{\omega_x} \tag{8.42}$$

$$k_{22} = \left(\frac{\omega_\phi}{\omega_x} \right)^2 + \frac{r_z}{\omega_x^2 I} \left(l_T + r_z m_T - m_C t_{10} - F_{C0} + \alpha_0 l_C \right) \tag{8.43}$$

$$r_{11} = \frac{m_T}{\omega_x^2 m} \qquad r_{12} = r_{21} = \frac{r_z m_T}{\omega_x^2 \sqrt{Im}} \tag{8.44}$$

$$r_{22} = \frac{r_z^2 m_T}{\omega_x^2 \sqrt{Im}} \tag{8.45}$$

In the following Section we estimate different terms in (8.41-8.45) to establish their relative strengths in order to simplify the model.

8.5 Estimation of Parameters

8.5.1 Structural Parameters

The toolholder is assumed to be a rectangular steel beam, as shown in Figure 8.7. We consider two cases, a relatively short toolholder (normal cutting) and a longer

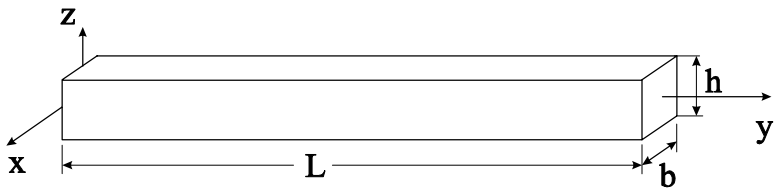

Figure 8.7: The toolholder.

one (corresponding to a boring bar). The geometry is characterized by

$$\text{width } b = 0.01 \text{ m} \tag{8.46}$$

$$\text{height } h = 0.02 \text{ m} \tag{8.47}$$

$$\text{length } l = 0.05 - 0.3 \text{ m} \tag{8.48}$$

The material properties are given by the density, the Young's modulus and the shear modulus. For steel, these are

$$\rho = 7860 \text{ kg/m}^3 \tag{8.49}$$

$$E = 2 * 10^{11} \text{ Pa} \tag{8.50}$$

$$G = 8.3 * 10^{10} \text{ Pa} \tag{8.51}$$

The stiffnesses for a cantilevered beam of rectangular cross-section can be calculated as follows

$$k_x = \frac{3I_x E}{L^3} = \frac{bh^3 E}{4L^3} = 4 * 10^4 - 8 * 10^6 \ \frac{\mathrm{N}}{\mathrm{m}} \tag{8.52}$$

$$k_z = \frac{3I_z E}{L^3} = \frac{b^3 h E}{4L^3} = 1.5 * 10^5 - 3 * 10^7 \ \frac{\mathrm{N}}{\mathrm{m}} \tag{8.53}$$

$$k_\phi = \frac{GJ}{L} = 1300 - 7600 \ \frac{\mathrm{N}}{\mathrm{rad}} \tag{8.54}$$

The torsion constant J is calculated as

$$J = \beta \left(\frac{b}{h}\right) b^3 h \tag{8.55}$$

where β is a width-to-height ratio dependent constant and can be found in tables (Timoshenko, Young and Weaver, 1974). $\beta = 0.23$ was used here.

Since a lumped parameter approximation is used, the mass at the end of the massless beam is assumed to be some equivalent mass (it is basically a modal mass based on vibration of a cantilever beam (Thompson, 1993)). In calculating the longitudinal and transverse vibration frequencies this equivalent mass is

$$m = \frac{33}{140} m_{tool} \tag{8.56}$$

while in torsional vibrations (Sharma, private communication)

$$m = \frac{1}{3} m_{tool} \tag{8.57}$$

The moment of inertia of the beam is assumed to be equal to that of a uniform disk located at the end, with radius r_g (this was taken as 2 cm)

$$I = \frac{1}{2} m r_g^2 \tag{8.58}$$

The vibration frequencies are then

$$\omega_x = \frac{1}{2\pi}\sqrt{\frac{k_x}{m}} \simeq 90 - 3300 \ \frac{\text{rad}}{s} \tag{8.59}$$

$$\omega_z = \frac{1}{2\pi}\sqrt{\frac{k_z}{m}} \simeq 200 - 6600 \ \frac{\text{rad}}{s} \tag{8.60}$$

$$\omega_\phi = \frac{1}{2\pi}\sqrt{\frac{k_\phi}{I}} \simeq 1000 - 6000 \ \frac{\text{rad}}{s} \tag{8.61}$$

The ratio $\frac{\omega_\phi}{\omega_x}$ varies between 2 and 10 (the shorter the tool is the higher the ratio).

8.5.2 Cutting Force Parameters

Experimental and theoretical data are shown in Figures 8.8 and 8.9. They show the forces F_C and F_T during machining of 0.2% carbon steel (Oxley, 1989) for different rake angles (-5° and 5°). The width of cut was 4 mm, while the chip thickness was set to be 0.125 mm, 0.25 mm, and 0.5 mm.

Since our model assumes constant cutting speed, forces were taken from these graphs at the value 200 m/s of the cutting speed and plotted against rake angle (Figure 8.10). The constants l_C and l_T are found as the slope of the lines corresponding to $t_1 = 0.25$ mm

$$l_C = 1580\frac{N}{rad}, \qquad l_T = 3150\frac{N}{rad} \tag{8.62}$$

A linear relationship is assumed between forces at zero rake angle and chip thickness, i.e.

$$F_C = F_{C0} + m_c t_1 \tag{8.63}$$

$$F_T = F_{T0} + m_T t_1 \tag{8.64}$$

where these coefficients were determined to be

$$m_C = 6 * 10^6 \frac{N}{m} \quad F_{C0} = 458N \tag{8.65}$$

$$m_T = 1.65 * 10^6 \frac{N}{m} \quad F_{T0} = 784N \tag{8.66}$$

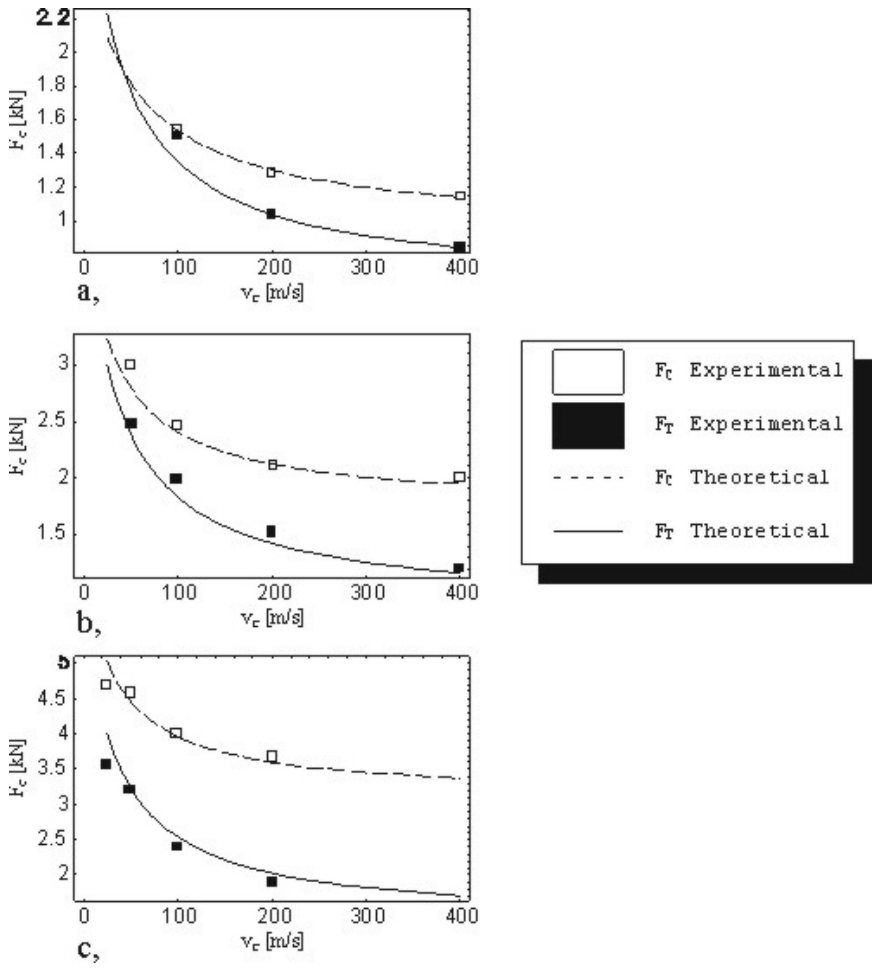

Figure 8.8: Forces in oblique cutting of 0.2% carbon steel. $\alpha = -5°$. After Oxley (1989). **a,** $f = 0.125$ mm **b,** $f = 0.25$ mm **c,** $f = 0.5$ mm

8.5.3 Model Parameters

Since

$$\frac{r_z}{\omega_x^2 I}\left(l_T + r_z m_T - m_C t_{10} - F_{C0} + \alpha_0 l_C\right) \ll \left(\frac{\omega_\phi}{\omega_x}\right)^2 \tag{8.67}$$

this term will be neglected in k_{22}, i.e.

$$k_{22} = \left(\frac{\omega_\phi}{\omega_x}\right)^2 \tag{8.68}$$

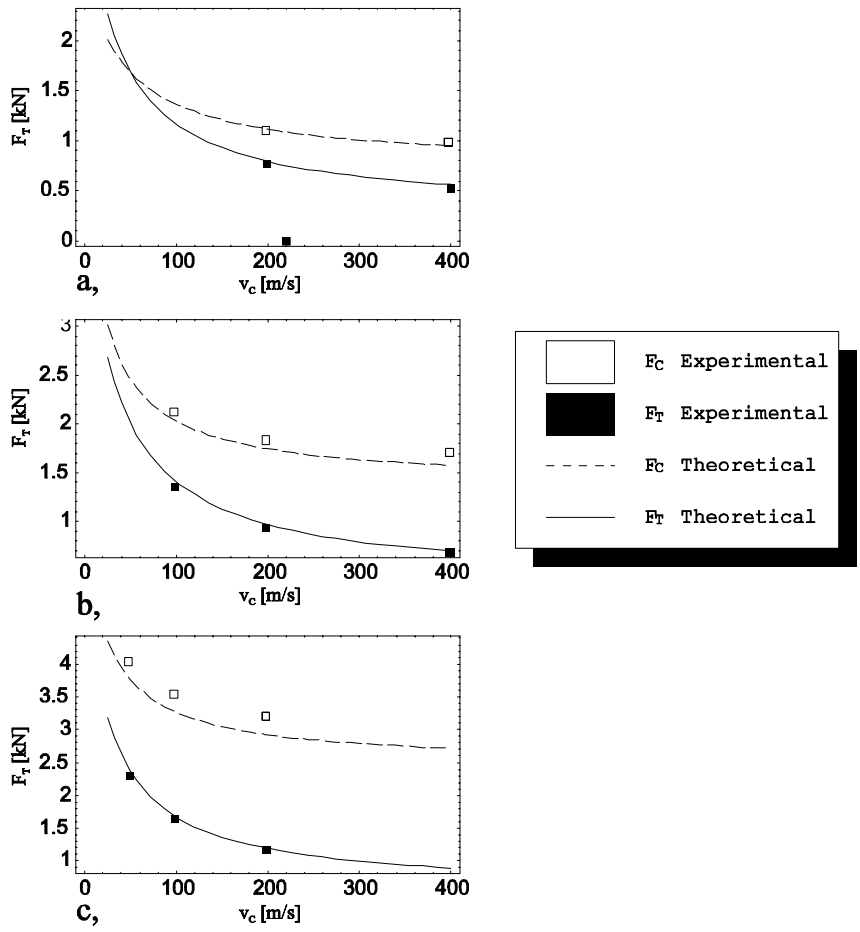

Figure 8.9: Forces in oblique cutting of 0.2% carbon steel. $\alpha = 5°$. After Oxley (1989). **a,** $f = 0.125$ mm **b,** $f = 0.25$ mm **c,** $f = 0.5$ mm

Also, the term r_{22} is very small, so it is neglected

$$r_{22} = 0 \tag{8.69}$$

8.6 Analysis of the Model

With the approximations (8.68, 8.69) the model (8.39, 8.40) can be written as the matrix equation

$$\ddot{\mathbf{x}} + \mathbf{C}\dot{\mathbf{x}} + \mathbf{K}\mathbf{x} = \mathbf{R}\mathbf{x}_\tau \tag{8.70}$$

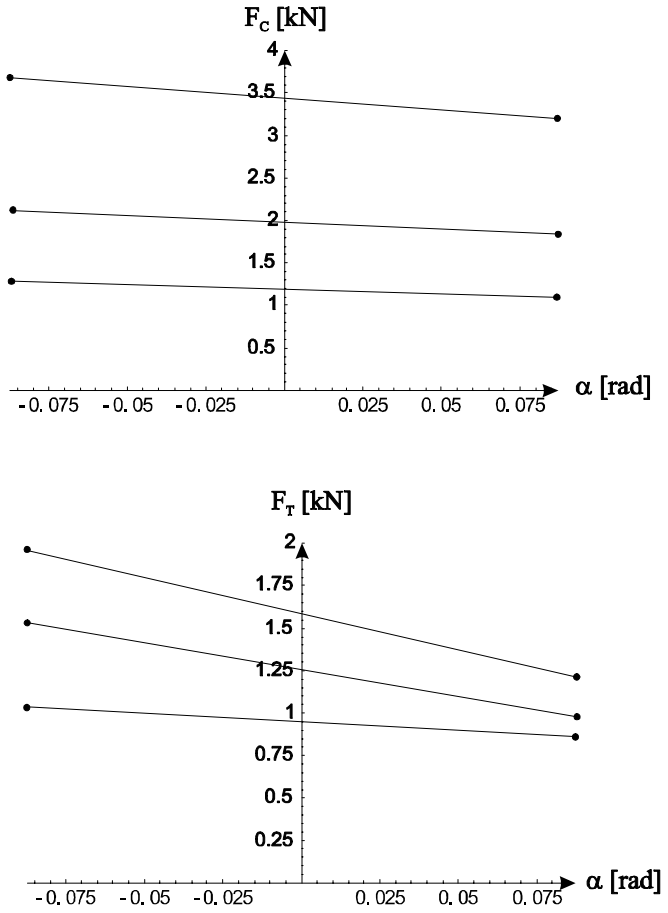

Figure 8.10: Forces vs. rake angle (derived from Oxley (1989)) **a,** cutting force **b,** thrust force.

with

$$\mathbf{C} = \begin{bmatrix} 2\zeta_x & 0 \\ 0 & 2\zeta_\phi \end{bmatrix}, \qquad \mathbf{K} = \begin{bmatrix} 1+p & a+pq \\ pq & k_{22} \end{bmatrix}, \qquad \mathbf{R} = \begin{bmatrix} p & q \\ q & 0 \end{bmatrix} \tag{8.71}$$

Where we introduced the parameters

$$p = \frac{m_T}{\omega_x^2 m}, \qquad q = \frac{r_z}{X} = r_z\sqrt{\frac{m}{I}} \tag{8.72}$$

where constants a and k_{22} are

$$a = \frac{l_T}{\omega_x^2\sqrt{Im}}, \qquad k_{22} = \left(\frac{\omega_\phi}{\omega_x}\right)^2 \tag{8.73}$$

Note that the stiffness matrix is nonsymmetric. Nonconservative systems are discussed in Bolotin (1963, 1964) and in Panovko and Gubanova (1965). It is characteristic of these systems that they can lose stability either by divergence (buckling) or by flutter. Chu and Moon (1983) examined divergence and flutter instabilities in magnetically levitated models. Kiusalaas and Davis (1970) studied stability of elastic systems under retarded follower forces.

8.6.1 Classical Limit

If $q = 0$ (that is the tool is centered) the equations reduce to

$$x'' + 2\zeta_x x' + (1+p)\, x + a\phi = p x_\tau \tag{8.74}$$

$$\phi'' + 2\zeta_\phi \phi' + c\phi = 0 \tag{8.75}$$

The ϕ-equation is uncoupled from the x-equation and reduces to that of a damped oscillator. Its equilibrium $\phi = 0$ is asymptotically stable and thus it does not affect the stability of the x-equation.

In this case we recover the 1 DOF classical model (3.28).

8.7 Stability Analysis of the Undamped System without Delay

First we perform linear stability analysis of the system

$$\ddot{\mathbf{x}} + \mathbf{K}\mathbf{x} = \mathbf{0} \tag{8.76}$$

where the matrix $\mathbf{K}$ is non-symmetric and of the form ($k_{22} > 0$)

$$\mathbf{K} = \begin{bmatrix} k_{11} & k_{12} \\ k_{21} & k_{22} \end{bmatrix} \tag{8.77}$$

Assuming the solutions in the form

$$\mathbf{x} = \mathbf{d}e^{i\omega t} \tag{8.78}$$

we obtain the characteristic polynomials

$$\left(\mathbf{K} - \omega^2\mathbf{I}\right)\mathbf{d} = 0 \tag{8.79}$$

which have nontrivial solution if the determinant is zero

$$\begin{vmatrix} k_{11} - \omega^2 & k_{12} \\ k_{21} & k_{22} - \omega^2 \end{vmatrix} = \left(k_{11} - \omega^2\right)\left(k_{22} - \omega^2\right) - k_{21}k_{12} = 0 \tag{8.80}$$

The characteristic equation for the coupled system becomes

$$\omega^4 - \left(k_{11} + k_{22}\right)\omega^2 + k_{11}k_{22} - k_{21}k_{12} = 0 \tag{8.81}$$

Divergence (static deflection, buckling) occurs when $\omega = 0$, that is when

$$k_{11}k_{22} - k_{21}k_{12} = 0 \tag{8.82}$$

Note that this is equivalent with

$$\det \mathbf{K} = 0 \tag{8.83}$$

If $\omega \neq 0$, then the characteristic equation (8.81) can be solved for ω^2 as

$$\omega^2 = \frac{1}{2}\left(k_{11} + k_{22} \pm \sqrt{\left(k_{11} + k_{22}\right)^2 - 4\left(k_{11}k_{22} - k_{21}k_{12}\right)}\right) \tag{8.84}$$

For stable solutions, both solutions should be positive. Since $k_{22} > 0$, this is the case if

$$0 \leq k_{11}k_{22} - k_{21}k_{12} \leq \left(\frac{k_{11} + k_{22}}{2}\right)^2 \tag{8.85}$$

The two bounds correspond to divergence and flutter boundaries, respectively.

With the stiffness matrix in (8.71)

$$k_{11} = 1 + p, \qquad k_{12} = a + pq \tag{8.86}$$

$$k_{21} = pq \tag{8.87}$$

In the plane of the bifurcation parameters q, p the divergence boundaries are given by

$$p = \frac{1}{2q^2}\left(k_{22} - aq \pm \sqrt{4k_{22}q^2 + (k_{22} - aq)^2}\right) \tag{8.88}$$

and the flutter boundary is characterized by

$$p = \frac{1}{1 + 4q^2}\left(k_{22} - 2aq - 1 \pm 2\sqrt{q\left(a\left(1 - k_{22}\right) + a^2q - q\left(k_{22} - 1\right)^2\right)}\right) \tag{8.89}$$

Figure 8.11 shows these boundaries on the (q, p) parameter plane for $a = 1$, $k_{22} = 2$.

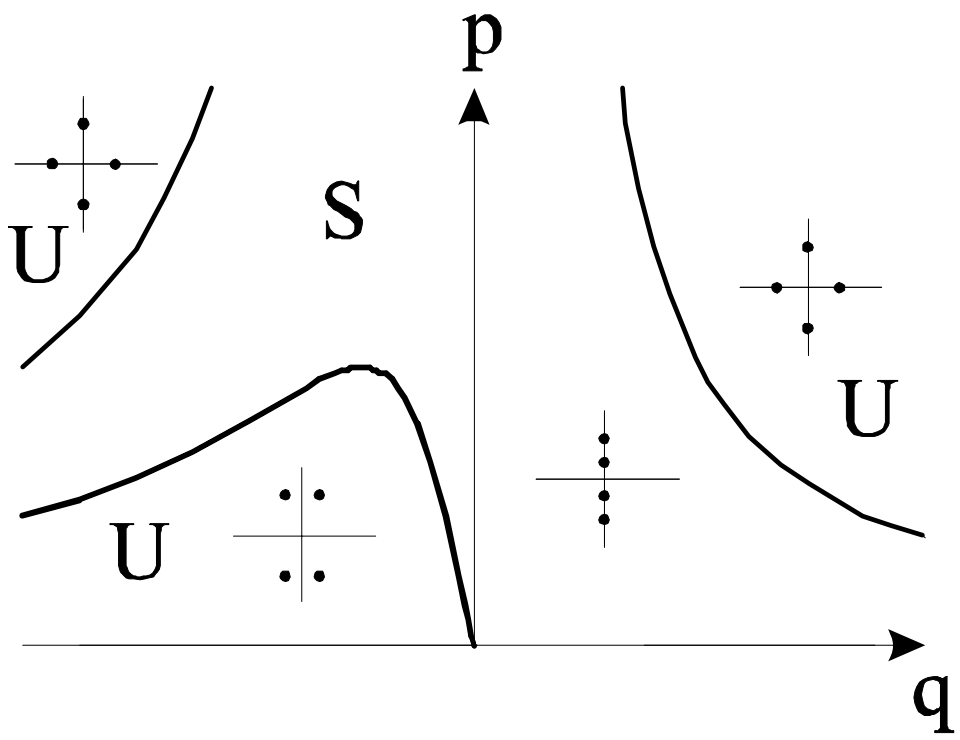

Figure 8.11: Stability boundaries of the 2 DOF model.

The different stability regions are indicated by the root location plots.

8.8 Stability Analysis of the 2 DOF Model with Delay

In this section we include the delay terms in the analysis. However, to be able to study how these terms influence the stability of the system, we introduce a new parameter, similar to the overlap factor mentioned in Chapter 3.

First we analyze the system with no damping:

$$\ddot{\mathbf{x}} + \mathbf{K}\mathbf{x} = \mu \mathbf{R}\mathbf{x}_\tau \tag{8.90}$$

When $\mu = 0$ we recover the previously studied (8.76), while $\mu = 1$ corresponds to equation (8.70) without damping.

The characteristic equation is

$$\det\left(-\lambda^2\mathbf{I} + \mathbf{K} - \mu e^{-\lambda\tau}\mathbf{R}\right) = 0 \tag{8.91}$$

$$\begin{aligned}\lambda^4 + \left(k_{11} + k_{22} - \mu p e^{-\lambda\tau}\right)\lambda^2 + k_{11}k_{22} - k_{12}k_{21} + \\ \mu e^{-\lambda\tau}\left(q\left(k_{12} + k_{21}\right) - pk_{22}\right) - \mu^2 q^2 e^{-2\lambda\tau} = 0\end{aligned} \tag{8.92}$$

Substituting $\lambda = i\omega$, $\omega \geq 0$ yields a complex equation that can be separated into the two real ones (the second equation was divided by $\mu \sin(\tau\omega) \neq 0$)

$$\begin{aligned}\omega^4 - \left(k_{11} + k_{12}\right)\omega^2 + k_{11}k_{22} - k_{12}k_{21} + \\ \mu\cos(\tau\omega)\left(p\omega^2 + q\left(k_{12} + k_{21}\right) - pk_{22}\right) - \mu^2 q^2\cos(2\tau\omega) = 0\end{aligned} \tag{8.93}$$

$$p\omega^2 + q\left(k_{12} + k_{21}\right) - pk_{22} + 2\mu q^2\cos(\tau\omega) = 0 \tag{8.94}$$

We solve the second equation for $\cos(\tau\omega)$

$$\cos(\tau\omega) = \frac{p\omega^2 + q\left(k_{12} + k_{21}\right) - pk_{22}}{-2\mu q^2} \tag{8.95}$$

Using this relation and the identity $\cos(2\tau\omega) = 2\cos(\tau\omega)^2 - 1$ in the real part (8.93) results

$$\omega^4 - (k_{11} + k_{22})\,\omega^2 + k_{11}k_{22} - k_{12}k_{21} + \mu^2 q^2 = 0 \tag{8.96}$$

Divergence occurs where $\omega = 0$, that is where

$$k_{11}k_{22} - k_{12}k_{21} + \mu^2 q^2 = 0$$

Substituting the elements of the stiffness matrix as given in (8.71) yields

$$-\left(q\ (a + q\ (p - \mu))\ (p - \mu)\right) + k_{22}\ (1 + p - p\,\mu) = 0 \tag{8.97}$$

which can be solved for p as

$$\frac{1}{2\,q^2}\left(k_{22}\ (1 - \mu) + q\ (2\,q\,\mu - a) \pm\right. \tag{8.98}$$

$$\left.\sqrt{\left(k_{22}\,(\mu - 1) + q\,(a - 2\mu q)\right)^2 + 4\,q^2\ (k_{22} + q\,\mu\ (a - q\,\mu))}\right) \tag{8.99}$$

The change of the divergence boundary is shown in Figure 8.12 (top, middle, bottom) for $\mu = 0.1$, 0.5 and 1 while the delay was set to 1.

Flutter occurs for $\omega > 0$, and the boundary can be found by numerically solving equations (8.94, 8.96) for p and q for a given μ. Figure 8.13 shows the flutter boundary for a small μ (0.01) together with the flutter boundary (8.89). Figure 8.14 shows how this boundary changes with increasing μ (μ = 0.1, 0.5, 1). And finally, Figure 8.15 shows the full stability chart, complete with both the divergence and flutter boundaries, for $\mu = 1$. Dark dots correspond to stable numerical solutions, while light ones to unstable ones.

This Figure can also explain a practical trick used in machine shops (Harding, private communication): sometimes, to avoid chatter, the tool is placed slightly

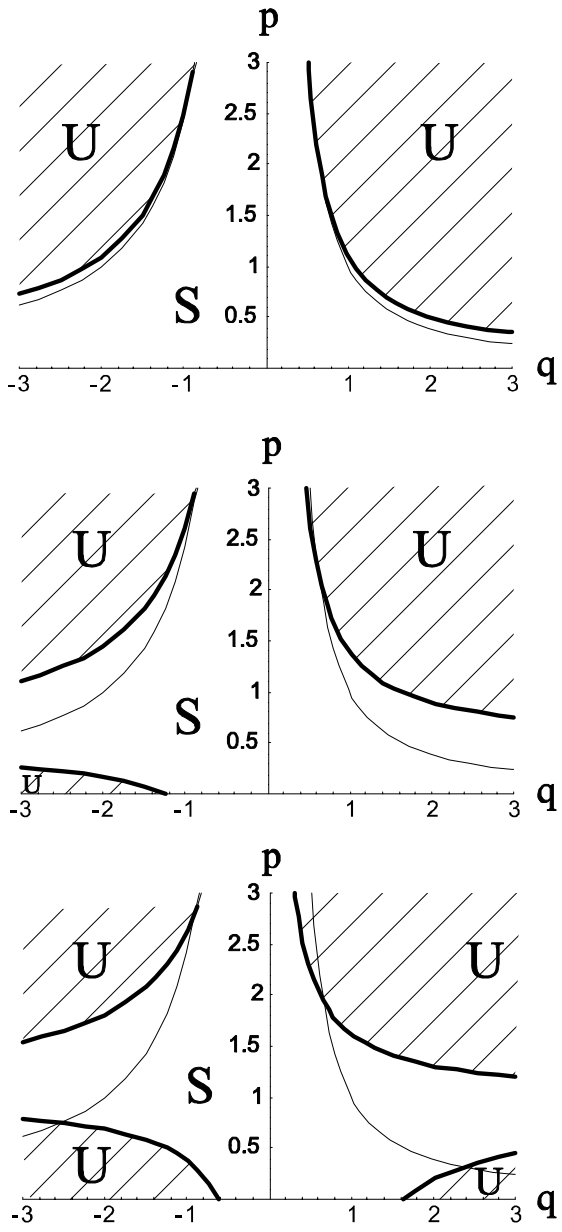

Figure 8.12: The change of the divergence boundary for system (8.89), $\tau = 1$. $\mu = 0.1$, 0.5, 1 for top, middle and bottom Figures, respectively.

ABOVE the centerline. We note that increasing q moves the system into the stable region of the chart.

Now we examine the effect of damping on the size of stability regions. It is

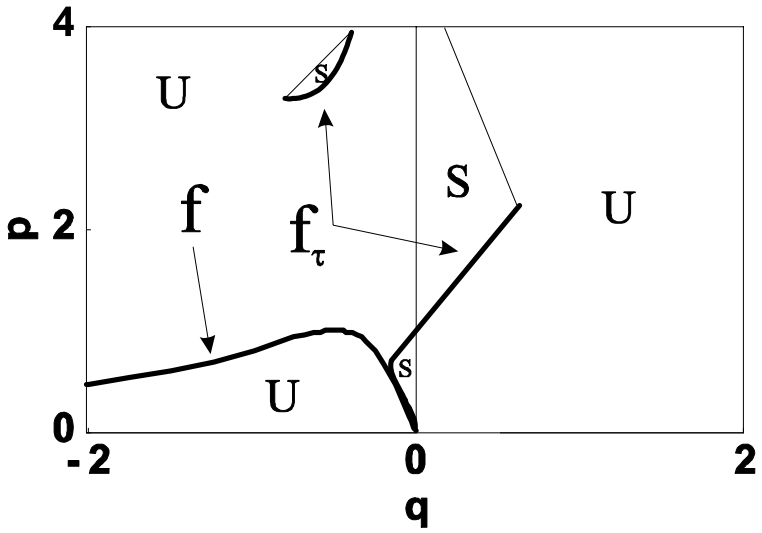

Figure 8.13: Flutter boundary of (8.89) with $\mu = 0.01$.

an important step, as it is known (Herrmann and Jong, 1965) that damping can have a destabilizing effect in nonconservative systems. The damping coefficients ζ_x and ζ_ϕ are taken to be 0.01, while the ratio of frequencies ω_ϕ/ω_x was changed in Figure 8.16 (this is the same as keeping this ratio fixed and increasing ζ_ϕ). As the Figure shows, the size of the stability regions increases with added damping. And finally, we show how the lobes of the conventional stability chart deform with the added parameter q ($0 \leq q \leq 1$). Figure 8.17 shows that increasing q results in the system becoming less stable. It is interesting how unstable regions are born. These upside-down lobes are actually lobes of the classical model for $p < 0$ (recall that $p > 0$ for physical reasons). In our model these lobes become a new source of instability, where the classical model would predict stable behavior.

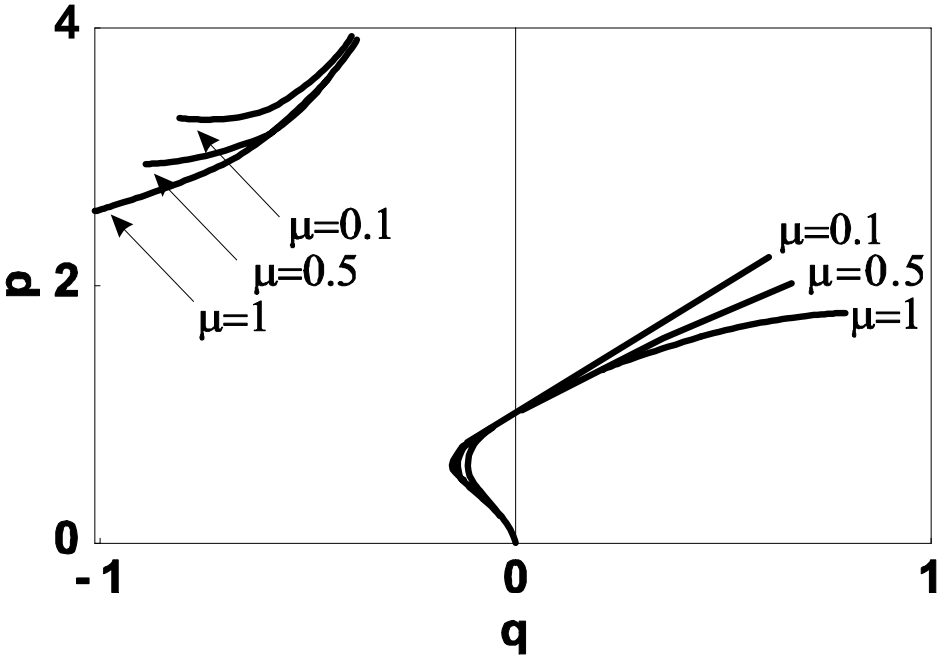

Figure 8.14: Flutter boundary as a function of μ ($\mu = 0.1, 0.5, 1$).

8.9 Conclusions

The new 3 DOF model derived in this Chapter is successful in explaining at least two phenomena. The first is why an off-centered tool might help to avoid chatter.

It can also provide an explanation how vibrations can arise below the classical stability boundary. As shown, the added degrees of freedom result in unstable regions below the one predicted by the one DOF classical model. To summarize the important observations:

- The 3-DOF model results in coupling between twist and lateral bending
- The model can exhibit both divergence and flutter instabilities
- Damping seems to increase the size of stability regions
- The tool offset produces new regions of instability (the upside-down lobes)

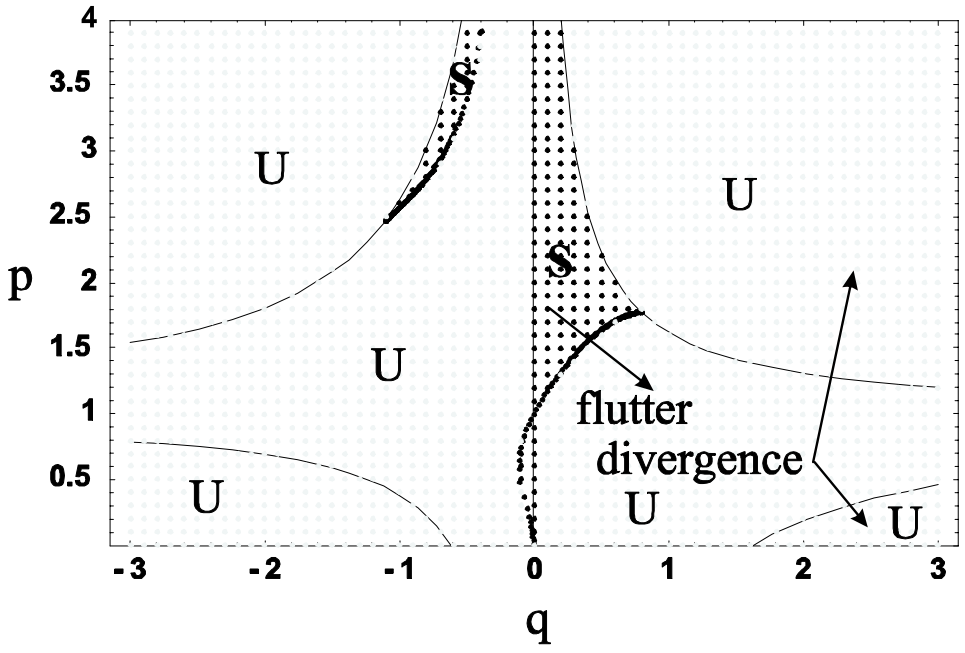

Figure 8.15: Stability chart for the undamped system (8.89), $\mu = 0.1$, $\tau = 1$.

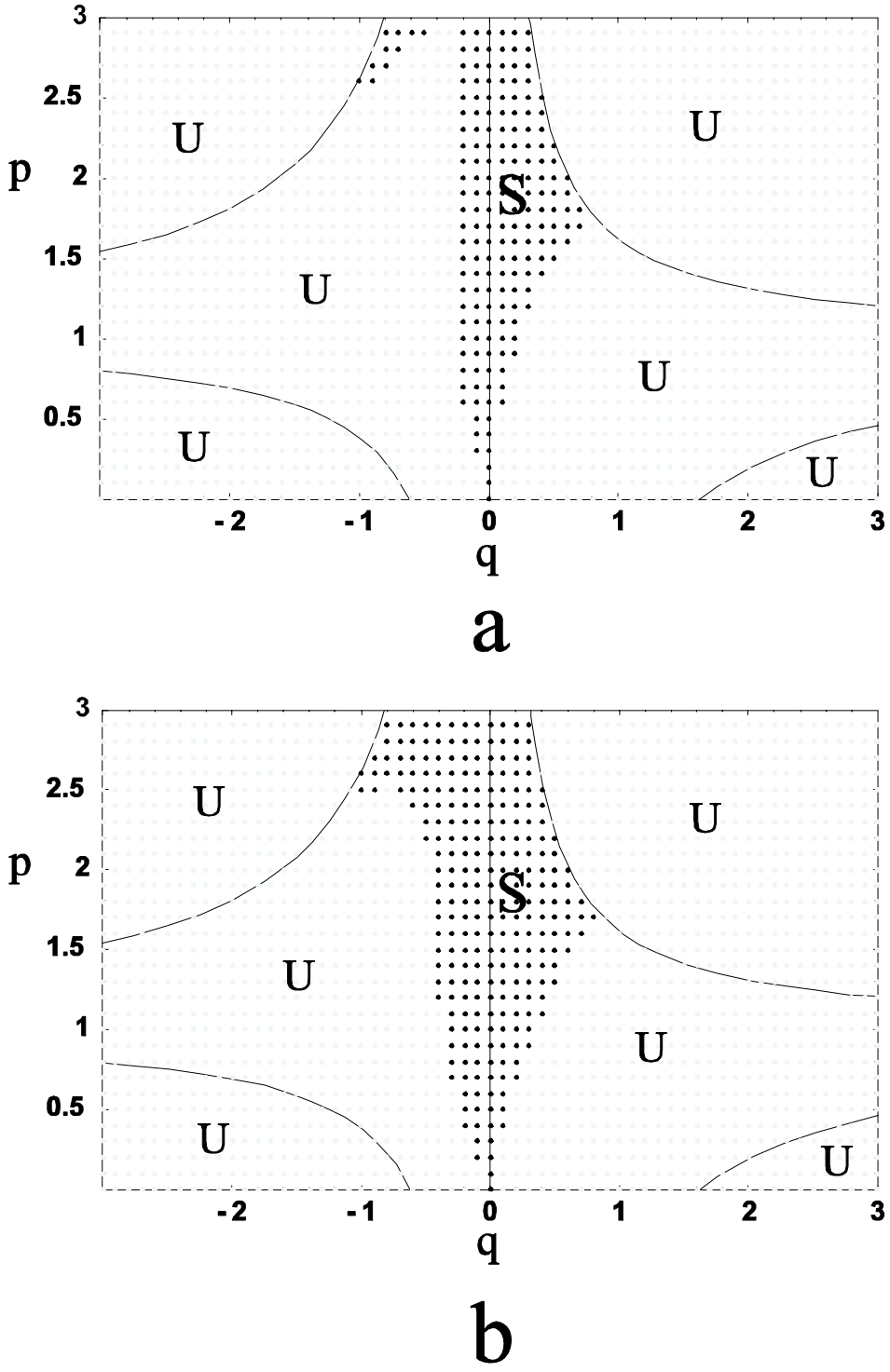

Figure 8.16: Stability chart for the 3 DOF model. **a,** $\omega_\phi/\omega_x = 2$ **b,** $\omega_\phi/\omega_x = 10$.

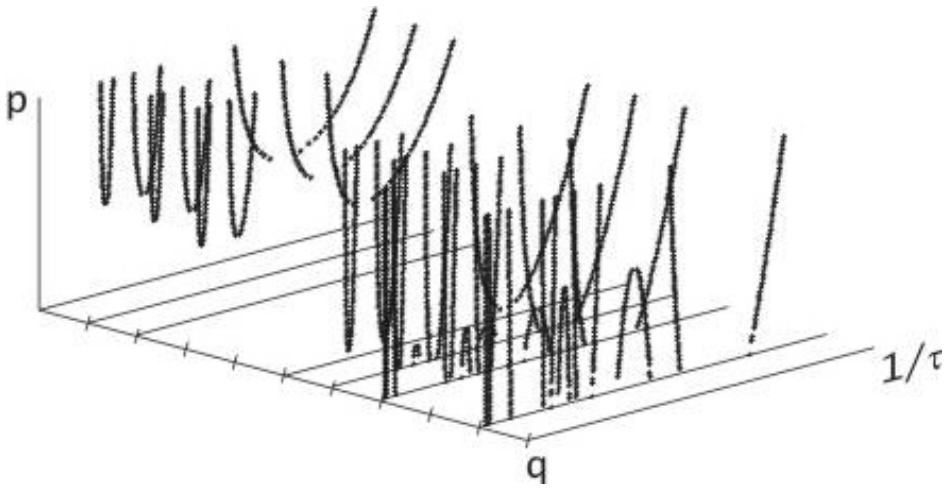

Figure 8.17: 3D stability chart.

Chapter 9

Conclusions and Future Directions

Chatter is most generally defined as unwanted vibrations of the machine tool. Traditional machining research has examined linear theories of chatter (Tobias, 1965; Tlusty, 1978). In the more classical theories the essential dynamic character of material removal processes has not been considered. The result of the analysis of these classical models show that SDOF models without structural nonlinearities but with nonlinear cutting force dependence are fairly successful in predicting the experimentally observed subcritical instability.

In particular, the use of Harmonic Balance and Center Manifold Theory in conjunction with numerical simulations showed the existence of the experimentally observed subcritical phenomenon (namely, a subcritical Hopf bifurcation). The inclusion of tool-workpiece contact loss provided a mechanism to stabilize tool motion and the agreement between theoretical calculations and experimental results are good. On the other hand, it seems that the classical model falls short in exhibiting small amplitude complex vibrations in the pre-chatter regime. One possible

extension could be the analysis of the codimension-two bifurcation present in this model. At the intersection of the stability lobes, two pairs of imaginary roots cross the imaginary axis, giving rise two quasiperiodic oscillations and associated complex phenomena. It is likely, however that single degree-of-freedom (DOF) models are not sufficient to explain all the cutting dynamics phenomena thus more degrees of freedom and/or added state variables such as temperature will be needed.

One way to increase potential complexity of the model is the addition of forcing. Forcing can be due to external sources, such as misalignment of the workpiece, or it can arise from an inherent chip formation process. This latter however has possibly much higher frequency then the natural frequency of the tool. A candidate model for studying the influence of the chip segmentation process on cutting tool dynamics is the one where energy transfer occurs between two widely separated modes (Nayfeh and Nayfeh, 1993). Forcing that has frequency close to the natural tool frequency can result in high amplitude vibrations, making the inclusion of the tool-workpiece contact loss nonlinearity. Preliminary results showed the appearance of chaotic looking vibrations, but this direction has also be investigated.

Another (hidden) state variable could be the hysteretic dependence of cutting force on the tool vibration. As early (Albrecht, 1965) experiments show, the cutting force exhibits well-defined hysteresis. To date, there have only been a few investigations (most notably that of Saravanja-Fabris, 1972) to include such a dynamic effect in a tool vibration model. This Dissertation presents three such models. One is based on a viscoelastic constitutive law (similar to the Kelvin-Voigt model) for the cutting force. The resulting equation is a third-order linear delay-differential equation, whose linear stability was investigated with the help of the D-partition method. This model successfully predicts process damping at low rotational speeds

of the workpiece.

The other model is a piecewise-linear hysteretic cutting force, which can show quasiperiodic motions. The third model is a delay-differential equation with bi-linear hysteresis. Preliminary investigations of this model showed interesting behavior, but a more thorough analysis should be performed. In future research, smooth (Bouc-type) models have to be studied, as they seem to encompass the right characteristics of the observed cutting force hysteresis and their treatment is possible with the methods applied in this Dissertation. Other possibility to predict quasiperiodic or even chaotic vibrations is the extension of the one-DOF models to higher degree-of-freedom ones.

An attempt made here, by deriving a model with three degrees-of-freedom (a horizontal (feed direction), a vertical and a rotational one (twist)). The equations decouple, and the stability is determined by the horizontal and twist modes of motion. Linear stability analysis was performed on this model, showing how the stability boundaries deform by the addition of delay and damping. This model predicts, in accordance with machine shop rules of thumb, that by moving the tool above the centerline can sometimes make the cutting process more stable.

Another interesting phenomenon that occurs in this model is the motion of upside-down lobes in the parameter space, from a region where they are physically impossible to observe (corresponding to negative cutting force coefficients), to the normal parameter regime. These newly born regions of instability might be responsible for pre-chatter vibrations, when the modes of the real tool are coupled. The full analysis (to be undertaken) should include nonlinearities in both the cutting force and structure (at least geometrical nonlinearities).

Appendix A

Linear Vibrations of the Simple Harmonic Oscillator

In this Appendix we summarize the properties of the second order linear differential equation

$$mx''(t) + cx'(t) + kx(t) = A\cos(\omega t + \varphi) \tag{A.1}$$

where x is the position, t is the time and the prime denotes differentiation w.r.t the time. The forcing (the right hand side) is periodic with one dominant frequency $\omega > 0$ with amplitude A and phase φ.

Initial conditions should also be specified. Without losing generality we assume

$$x(0) = R \qquad x'(0) = 0 \tag{A.2}$$

Introducing the the natural angular frequency $\omega_n = \sqrt{k/m}$ and the (nondimensional) relative damping factor $\zeta = c/(2m\omega_n)$ equation (A.1) can be written as

$$x''(t) + 2\zeta\omega_n x'(t) + \omega_n^2 x(t) = \frac{A}{m}\cos(\omega t + \varphi) \tag{A.3}$$

We then introduce the nondimensional length and time scales (another choice of

scaling can be more advantageous when dealing with nonlinear equations)

$$\tilde{x} = \frac{x}{R} \qquad \tilde{t} = \omega_n t \tag{A.4}$$

Then dropping the tildes equation (A.3) together with the initial conditions (A.2) is written as

$$\begin{gathered} \ddot{x}(t) + 2\zeta\dot{x}(t) + x(t) = A\cos(\omega t + \varphi) \\ x(0) = 1 \qquad \dot{x}(0) = 0 \end{gathered} \tag{A.5}$$

where the dots denote differentiation w.r.t the dimensionless time (note that A and ω have been rescaled).

First we study the free vibrations of this system, that is when $A = 0$.

A.1 Free vibrations

When there is no external excitation, equation (A.5) is reduced to the homogeneous differential equation

$$\begin{gathered} \ddot{x}(t) + 2\zeta\dot{x}(t) + x(t) = 0 \\ x(0) = 1 \qquad \dot{x}(0) = 0 \end{gathered} \tag{A.6}$$

Assuming solutions of the form $x(t) = ce^{\lambda t}$ and substituting it into (A.6) we obtain the characteristic equation

$$\lambda^2 + 2\zeta\lambda + 1 = 0 \tag{A.7}$$

with roots

$$\lambda_{1,2} = -\zeta \pm \sqrt{\zeta^2 - 1} \tag{A.8}$$

There are three cases corresponding to the negative, zero and positive values of the discriminant $D = 4(\zeta^2 - 1)$ of the characteristic equation (A.7).

Case 1. $D > 0$ ($|\zeta| > 1$)

The general solution is $x(t) = C_1 e^{\lambda_1 t} + C_2 e^{\lambda_2 t}$. The constants C_1, C_2 can be calculated using the initial conditions in (A.6) as

$$C_1 = \frac{1}{2}\left(1 - \frac{\zeta}{\sqrt{\zeta^2 - 1}}\right) \qquad C_2 = \frac{1}{2}\left(1 + \frac{\zeta}{\sqrt{\zeta^2 - 1}}\right) \tag{A.9}$$

Case 2. $D = 0$ ($|\zeta| = 1$)

The solution satisfying the initial conditions is

$$x(t) = e^{-t} - te^{-t} \tag{A.10}$$

Case 3. $D < 0$ ($|\zeta| < 1$)

The solution to the initial value problem is

$$x(t) = e^{-\zeta t}\left[\cos\left(\sqrt{1-\zeta^2}t\right) + \frac{\zeta}{\sqrt{1-\zeta^2}}\sin\left(\sqrt{1-\zeta^2}t\right)\right] \tag{A.11}$$

This is the case most frequently encountered in applications, so is in the problems considered in this Thesis. Usually $0 < \zeta \ll 1$ also holds, that is the system in question is lightly damped. Equation (A.11) can also be written as

$$x(t) = Ce^{-\zeta t}\cos(\hat{\omega}t + \phi) \tag{A.12}$$

where

$$\begin{aligned} \hat{\omega} &= \sqrt{1-\zeta^2} \\ C &= 1/\hat{\omega} \\ \phi &= -\arccos(\hat{\omega}) \end{aligned} \tag{A.13}$$

This is clearly an oscillation with a slowly decaying amplitude. The timescale corresponding to this decay is ζt (slow timescale), while the oscillation occurs on a much faster timescale characterized by $\hat{\omega}t$. This is a simple example of a system having different timescales. Nonlinear oscillators usually have at least two different timescales and that property will provide the basis of the method of multiple time scales (see Appendix C).

A.2 Forced Vibrations

When the forcing amplitude is not zero, equation (A.5) will become the inhomogeneous differential equation

$$\begin{gathered} \ddot{x}(t) + 2\zeta\dot{x}(t) + x(t) = A\cos(\omega t + \varphi) \\ x(0) = 1 \qquad \dot{x}(0) = 0 \end{gathered} \tag{A.14}$$

The solutions of (A.14) consist of the sum of the solutions of the homogeneous equation (A.6) and a particular solution of (A.14). In other words, the motion of the system is the superposition of the free oscillation and a forced oscillation due to the external force. Assuming small damping and $\omega \neq 1$, these solutions have the form

$$x(t) = De^{-\zeta t}\cos(\hat{\omega}t + \psi) + AM\cos(\omega t + \varphi - \delta) \tag{A.15}$$

where $\hat{\omega}$ is defined in (A.13), while D and ψ has to be calculated from the initial conditions. M is called the *magnification factor*

$$M = \frac{1}{\sqrt{(1-\omega^2)^2 + 4\zeta^2\omega}} > 0 \tag{A.16}$$

If $\zeta > 0$ the amplitude of the oscillation is always finite, however it can be large. The amplitude of the forced oscillation (A.15) is $M|A|$.

The maximum value of the magnification factor M can be obtained from

$$\frac{dM}{d\omega} = 0 \qquad \frac{d^2M}{d\omega^2} < 0 \tag{A.17}$$

If $\zeta < \sqrt{2}/2$ there is a maximum at $\omega = \sqrt{1-2\zeta^2}$ (we require $\omega > 0$). Note that for nonzero values of the damping the frequency that produces the maximum amplitude does not equal to the natural frequency. Figure A.1 shows curves of M as a function of ω for various values of ζ. These curves are called *response curves*,

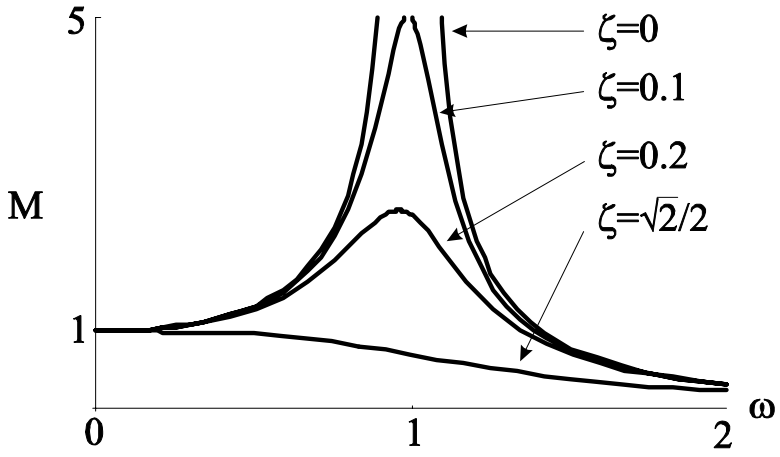

Figure A.1: Response curves for the linear forced oscillator

since they give the response (the amplitude) of the system for an external force of any given frequency.

δ is the *phase shift* relative to that of the external force and satisfies the relations

$$\begin{aligned} \cos\delta &= (1-\omega^2)\,M \\ \sin\delta &= 2\zeta\omega M \end{aligned} \tag{A.18}$$

The phase shift is then

$$\delta = \begin{cases} \arctan\frac{2\zeta\omega}{1-\omega^2} & \omega \le 1 \\ \pi - \arctan\frac{2\zeta\omega}{\omega^2-1} & \omega > 1 \end{cases} \tag{A.19}$$

The phase vs. forcing frequency diagram is shown in Figure A.2. As the Figure shows (and also equation (A.19)), in case of an undamped system ($\zeta = 0$) the phase shift δ is zero for $\omega < 1$ (the forced oscillation is in phase with the external forcing) and $\delta = \pi$ for $\omega > 1$ (the forced oscillation and the forcing are out of phase).

Note that the frequency of the forced oscillation is equal to the frequency of the forcing and that after sufficiently long period of time the free oscillation is damped out and we would only observe the forced vibration.

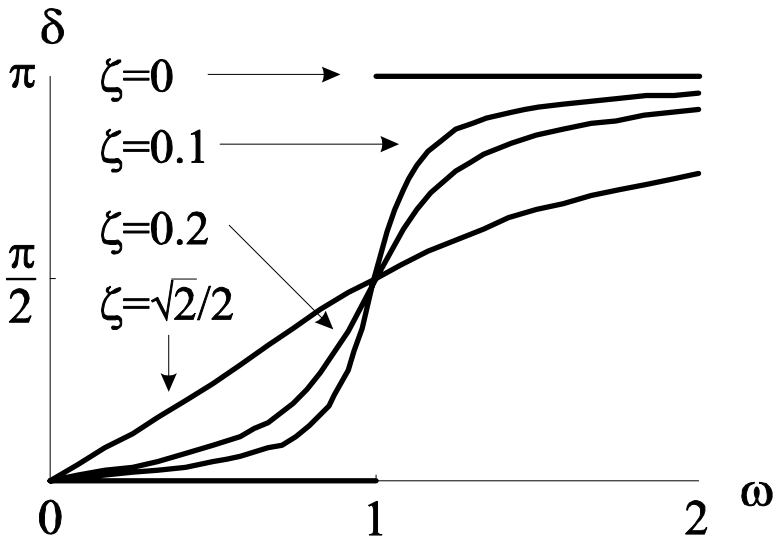

Figure A.2: Phase shift vs. forcing frequency for the simple harmonic oscillator

What happens when the free and the forced oscillations have the same frequency ($\omega = 1$)? This case is called *resonance*. The solution of (A.14) for $\zeta = 0$, $\omega = 1$ will become

$$x(t) = C_1 \cos(t + \psi) + C_2 t \sin(t + \varphi) \tag{A.20}$$

where

$$\begin{aligned} C_1 &= \sqrt{1 + \left(\tfrac{A \sin \varphi}{2}\right)^2} \\ C_2 &= \tfrac{A}{2} \\ \psi &= \arccos(1/C_1) \end{aligned} \tag{A.21}$$

The second term of (A.20) will give rise to unbounded motion as $t \to \infty$. This term is called a *secular* one (or in general terms of the form $t^n \cos t$ or $t^n \sin t$).

Appendix B

The Hopf Bifurcation

By varying a control parameter, periodic solutions might bifurcate from the fixed point of an ODE. This is the so-called Poincaré-Andronov-Hopf bifurcation (or simply Hopf-bifurcation).

B.1 The normal form of the Hopf bifurcation

We start with the analysis of the system (see Kuznetsov, 1998)

$$\dot{r} = r\left(p - ar^2\right) \tag{B.1}$$

$$\dot{\phi} = 1 \tag{B.2}$$

where p is the bifurcation parameter and $a \in \{-1, 1\}$. The bifurcations of system (**??**) can easily be analysed, since its equations are uncoupled. The second equation represents constant rate counterclockwise rotation. The first equation always has the equilibrium $\rho_1 = 0$. It is stable if $p \leq 0$, unstable otherwise. If $p/a > 0$ there

is another equilibrium

$$r_2 = \sqrt{\frac{p}{a}} \tag{B.3}$$

this corresponds to a limit cycle of radius r_2. For $a = 1$ the phase portraits look likeThe limit cycle that exists for $p > 0$ is stable. This is called the *supercritical*

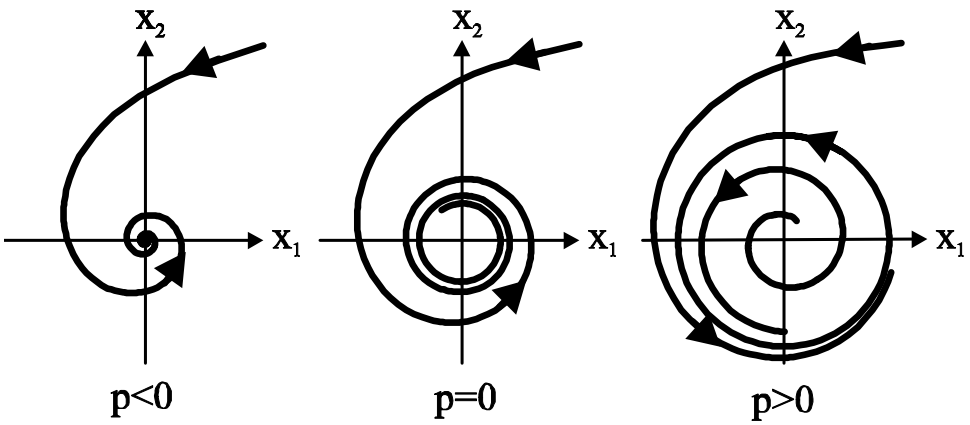

Figure B.1: Supercritical Hopf bifurcation

Hopf bifurcation.

For $a = -1$ the system exhibits an unstable limit cycle, as shown in Figure B.2.This

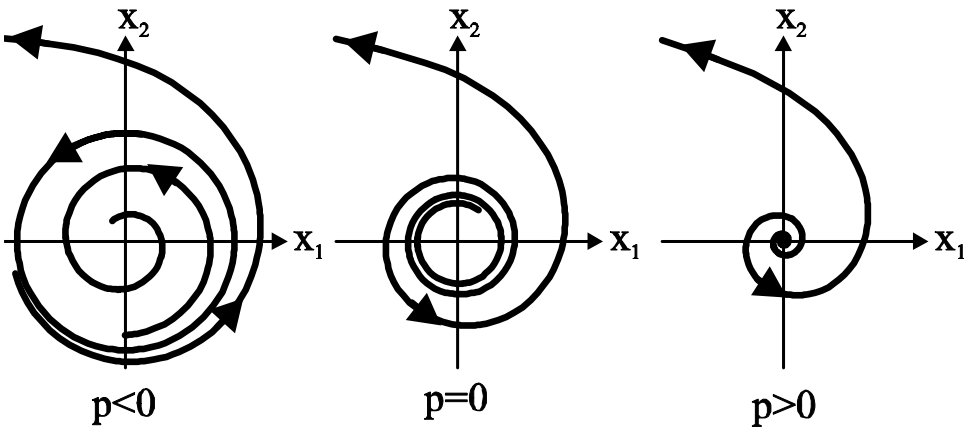

Figure B.2: Subcritical Hopf bifurcation

is a *subcritical* Hopf bifurcation. Introducing the new variables

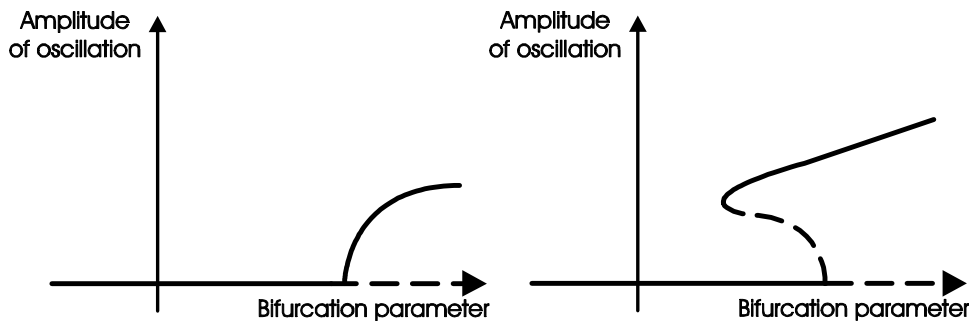

Figure B.3: Supercritical and subcritical Hopf bifurcation

$$x_1 = r\cos\phi \tag{B.4}$$

$$x_2 = r\sin\phi \tag{B.5}$$

equations (C.31, B.2) become

$$\begin{aligned}\dot{x}_1 &= px_1 - x_2 - ax_1\left(x_1^2 + x_2^2\right)\\ \dot{x}_2 &= x_1 + px_2 - ax_2\left(x_1^2 + x_2^2\right)\end{aligned} \tag{B.6}$$

At the equilibrium $x_1 = x_2 = 0$ the Jacobian matrix

$$J = \begin{pmatrix} p & -1 \\ 1 & p \end{pmatrix} \tag{B.7}$$

has eigenvalues $\lambda_{1,2} = p \pm i$. Introducing the complex variable

$$z = x_1 + ix_2 \tag{B.8}$$

system (B.6) can be written in a complex form

$$\begin{aligned}\dot{z} = \dot{x}_1 + i\dot{x}_2 &= p\left(x_1 + ix_2\right) + i\left(x_1 + ix_2\right) - a\left(x_1 + ix_2\right)\left(x_1^2 + x_2^2\right) = \\ &= \left(p + i\right)z + az\left|z\right|^2\end{aligned} \tag{B.9}$$

where

$$\left|z\right|^2 = x_1^2 + x_2^2 \tag{B.10}$$

B.2 Getting to the Normal Form

Consider the following system

$$\dot{\mathbf{y}}(t) = \mathbf{A}(p)\,\mathbf{y}(t) + \mathbf{f}(\mathbf{y}(t), p) \tag{B.11}$$

Without loss of generality we assume that $\mathbf{y} = \mathbf{0}$ is an equilibrium point and at the zero value of the bifurcation parameter p the Jacobian matrix $\mathbf{A}(0)$ has a pair of purely imaginary eigenvalues ($\lambda_{1,2} = \pm i\omega$) while all its other eigenvalues are 'stable' (have real part less than zero). The following analysis is concerned with the $p = 0$ critical case.

Equation (B.11) can be transformed into its canonical form by using the transformation

$$\mathbf{y}(t) = \mathbf{B}\mathbf{x}(t) \tag{B.12}$$

Then equation (B.11) can be rewritten in terms of the new coordinates as

$$\dot{\mathbf{x}} = \mathbf{B}^{-1}\mathbf{A}\mathbf{B}\mathbf{x} + \mathbf{B}^{-1}\mathbf{f}(\mathbf{B}\mathbf{x}) = \underbrace{\begin{pmatrix} 0 & -\omega & \\ \omega & 0 & \mathbf{0} \\ & \mathbf{0} & \mathbf{\Lambda} \end{pmatrix}}_{\mathbf{J}} \mathbf{x} + \mathbf{g}(\mathbf{x}) \tag{B.13}$$

with $\mathbf{\Lambda}$ containing the Jordan blocks corresponding to the stable eigenvalues.

The geometric meaning of Equation (B.12) is to define the new coordinates as projections of $\mathbf{x}$ onto the real and imaginary part of the critical eigenvector of $\mathbf{A}^*$. This eigenvector satisfies

$$\mathbf{A}^*\mathbf{n} = -i\omega\mathbf{n} \tag{B.14}$$

$$\mathbf{n} = \mathbf{n}_1 + i\mathbf{n}_2 \tag{B.15}$$

The projection is achieved with the help of the usual scalar product $(\mathbf{u}, \mathbf{v}) = \mathbf{u}^* \mathbf{v}$ (where $\mathbf{u}^*$ is the complex conjugate transpose (adjoint) of $\mathbf{u}$) as

$$x_i(t) = (\mathbf{n}_i, \mathbf{y}(t)) = \mathbf{n}_i^* \mathbf{y}(t) \tag{B.16}$$

Then the time evolution of a new coordinate can be expressed as

$$\dot{x}_i = (\mathbf{n}_i, \dot{\mathbf{y}}(t)) = (\mathbf{n}_i, \mathbf{A}\mathbf{y} + \mathbf{f}(\mathbf{y})) = (\mathbf{n}_i, \mathbf{A}\mathbf{y}) + (\mathbf{n}_i, \mathbf{f}(\mathbf{y})) =$$

$$= (\mathbf{A}^* \mathbf{n}_i, \mathbf{y}) + (\mathbf{n}_i, \mathbf{f}(\mathbf{y})) = \mathbf{n}_i^* \mathbf{A}\mathbf{y} + \mathbf{n}_i^* \mathbf{f}(\mathbf{y})$$

where we used the linearity of the scalar product and the identity

$$(\mathbf{u}, \mathbf{A}\mathbf{v}) = (\mathbf{A}^* \mathbf{u}, \mathbf{v})$$

This result is equivalent with equation (B.13).

The coordinates $x_1(t)$, $x_2(t)$ of the linear system

$$\dot{\mathbf{x}}(t) = \mathbf{J}\mathbf{x}(t)$$

describe stable (but not asymptotically stable) solutions, while the other coordinates represent exponentially decaying ones. In other words this system has a 2-dimensional attractive invariant subspace (a plane). To obtain the two real vectors that span this plane we first find the two complex conjugate eigenvectors that satisfy

$$\mathbf{J}\mathbf{s} = i\omega\mathbf{s} \tag{B.17}$$

$$\mathbf{J}\overline{\mathbf{s}} = -i\omega\overline{\mathbf{s}} \tag{B.18}$$

These are

$$\mathbf{s} = \begin{pmatrix} 1 \\ -i \\ \mathbf{0} \end{pmatrix}, \quad \overline{\mathbf{s}} = \begin{pmatrix} 1 \\ i \\ \mathbf{0} \end{pmatrix}$$

The two real vectors

$$\mathbf{s}_1 = \mathrm{Re}\,\mathbf{s} = \begin{pmatrix} 1 \\ 0 \\ \mathbf{0} \end{pmatrix} \qquad \mathbf{s}_2 = \mathrm{Im}\,\mathbf{s} = \begin{pmatrix} 0 \\ 1 \\ \mathbf{0} \end{pmatrix}$$

span the plane in question. $\mathbf{s}_1$, $\mathbf{s}_2$ satisfy the orthonormality conditions

$$(\mathbf{n}_1, \mathbf{s}_1) = (\mathbf{n}_2, \mathbf{s}_2) = 1 \tag{B.19}$$

$$(\mathbf{n}_1, \mathbf{s}_2) = (\mathbf{n}_2, \mathbf{s}_1) = 0 \tag{B.20}$$

Note that since $(\mathbf{n}, \mathbf{s}) = (\mathbf{n}_1, \mathbf{s}_1) + (\mathbf{n}_2, \mathbf{s}_2) + i\left((\mathbf{n}_2, \mathbf{s}_1) - (\mathbf{n}_1, \mathbf{s}_2)\right)$ Equations (B.19, B.20) are equivalent to

$$(\mathbf{n}, \mathbf{s}) = \mathbf{n}^* \mathbf{s} = 2$$

Equations (B.17, B.18) can also be written as

$$\mathbf{J}\mathbf{s}_1 = -\omega \mathbf{s}_2$$

$$\mathbf{J}\mathbf{s}_2 = \omega \mathbf{s}_1$$

which can then be solved for the real vectors.

With the decompositions

$$\mathbf{x} = \begin{pmatrix} x_1 \\ x_2 \\ \mathbf{w} \end{pmatrix} \qquad \mathbf{g} = \begin{pmatrix} g_1 \\ g_2 \\ \mathbf{g_w} \end{pmatrix}$$

system (B.13) can be written as

$$\dot{x}_1 = -\omega x_2 + g_1\left(x_1, x_2, \mathbf{w}\right)$$

$$\dot{x}_2 = \omega x_1 + g_2\left(x_1, x_2, \mathbf{w}\right)$$

$$\dot{\mathbf{w}} = \mathbf{\Lambda w} + \mathbf{h}\left(x_1, x_2, \mathbf{x}\right)$$

where

$$g_i\left(x_1, x_2, \mathbf{w}\right) = \left(\mathbf{n}_i, \mathbf{f}\left(\mathbf{y}\right)\right)$$

B.3 Why the Adjoint Eigenvectors?

In this Section we give a simple example to show why the adjoint eigenvectors should be used in the projection described above.

Consider the planar system

$$\dot{\mathbf{x}} = \mathbf{A}\mathbf{x}$$

where the matrix $\mathbf{A}$ has two imaginary eigenvalues $\lambda = \pm i$. We can transform this system into its normal form by introducing the new variables $\mathbf{y}$

$$\mathbf{x} = \mathbf{T}\mathbf{y}, \qquad \mathbf{y} = \mathbf{T}^{-1}\mathbf{x}$$

$$\mathbf{x} = \begin{pmatrix} x_1 \\ x_2 \end{pmatrix}, \qquad \mathbf{y} = \begin{pmatrix} y_1 \\ y_2 \end{pmatrix}$$

To construct the transformation matrix $\mathbf{T}$ we have to find the eigenvector $\mathbf{s}$ corresponding to the eigenvalue i

$$\mathbf{A}\mathbf{s} = i\mathbf{s}$$

$$\mathbf{s} = \begin{pmatrix} s_1 \\ s_2 \end{pmatrix} = \begin{pmatrix} s_{11} + is_{12} \\ s_{21} + is_{22} \end{pmatrix}$$

Then $\mathbf{T}$ can be built as

$$\mathbf{T} = \begin{pmatrix} \operatorname{Re} s & -\operatorname{Im} s \end{pmatrix} = \begin{pmatrix} s_{11} & -s_{12} \\ s_{21} & -s_{22} \end{pmatrix}$$

The determinant of $\mathbf{T}$ is

$$\det \mathbf{T} = s_{21}s_{12} - s_{11}s_{22} \tag{B.21}$$

and its inverse is

$$\mathbf{T}^{-1} = \frac{1}{\det \mathbf{T}} \begin{pmatrix} -s_{22} & s_{12} \\ -s_{21} & s_{11} \end{pmatrix}$$

So the new variables can be calculated from

$$\begin{pmatrix} y_1 \\ y_2 \end{pmatrix} = \frac{1}{\det \mathbf{T}} \begin{pmatrix} -s_{22} & s_{12} \\ -s_{21} & s_{11} \end{pmatrix} \begin{pmatrix} x_1 \\ x_2 \end{pmatrix}$$

as

$$y_1 = \frac{1}{\det \mathbf{T}} \left(-s_{22}x_1 + s_{12}x_2\right) \tag{B.22}$$

$$y_2 = \frac{1}{\det \mathbf{T}} \left(-s_{21}x_1 + s_{11}x_2\right) \tag{B.23}$$

and the new system is

$$\dot{\mathbf{y}} = \mathbf{T}^{-1}\mathbf{A}\mathbf{T}\mathbf{y} = \begin{pmatrix} 0 & -1 \\ 1 & 0 \end{pmatrix} \mathbf{y} \tag{B.24}$$

If we now introduce the complex variable

$$z = y_1 + iy_2 = \begin{pmatrix} 1 & i \end{pmatrix} \mathbf{y}$$

then (B.24) can concisely be written as

$$\dot{z} = \begin{pmatrix} 1 & i \end{pmatrix} \dot{\mathbf{y}} = \begin{pmatrix} 1 & i \end{pmatrix} \begin{pmatrix} 0 & -1 \\ 1 & 0 \end{pmatrix} \mathbf{y} = \begin{pmatrix} i & -1 \end{pmatrix} \mathbf{y} = iz$$

In terms of the old variables

$$\begin{aligned} z = y_1 + iy_2 &= \frac{1}{\det \mathbf{T}} \begin{pmatrix} -(s_{22} + is_{21}) & s_{12} + is_{11} \end{pmatrix} \begin{pmatrix} x_1 \\ x_2 \end{pmatrix} \\ &= \frac{1}{\det \mathbf{T}} \begin{pmatrix} -i\bar{s}_2 & i\bar{s}_1 \end{pmatrix} \begin{pmatrix} x_1 \\ x_2 \end{pmatrix} \end{aligned}$$

Notice that the right-hand side can be written as the scalar product

$$z = (\mathbf{n}, \mathbf{x}) = \mathbf{n}^* \mathbf{x}$$

where n is

$$\mathbf{n} = \frac{1}{\det \mathbf{T}} \begin{pmatrix} is_2 \\ -is_1 \end{pmatrix}$$

Furthermore

$$\mathbf{n}^T \mathbf{s} = 0$$

We see that $\mathbf{n}$ can be taken as the eigenvector of the adjoint problem

$$\mathbf{A}^* \mathbf{n} = \bar{\lambda} \mathbf{n}$$

Also

$$(\mathbf{n}, \mathbf{s}) = \mathbf{n}^* \mathbf{s} = \frac{1}{\det \mathbf{T}} \left(-is_1 \bar{s}_2 + i\bar{s}_1 s_2\right) = 2 \tag{B.25}$$

Appendix C

Analytical Tools for ODE's

The purpose of this Appendix is to give a quick glance at the methods used in this Dissertation.

C.0.1 Method of Multiple Timescales

Here we show another approach to deal with

$$\ddot{x} + x = \varepsilon F\left(x, \dot{x}\right) \tag{C.1}$$

This method is based on the presence of two (slow and fast) timescales in the damped linear oscillator. The exact solution of (here ε takes the role of the damping)

$$\ddot{x} + 2\varepsilon\dot{x} + x = 0 \tag{C.2}$$

is

$$x\left(t\right) = Ce^{-\varepsilon t}\cos\left(\sqrt{1-\varepsilon^2}t + \phi\right) \tag{C.3}$$

The timescale corresponding to the decay of the amplitude is εt (slow timescale), while the fast timescale corresponding to the oscillations is characterized

by $\sqrt{1-\varepsilon^2}t$. Let us introduce the two timescales

$$\hat{t} = \varepsilon t, \qquad t^+ = \sqrt{1-\varepsilon^2}t \tag{C.4}$$

Further it is assumed that a uniformly valid asymptotic expansion for the solution of (C.1) can be written as

$$x\left(t,\varepsilon\right) = \sum_{k=0}^{m-1} \varepsilon^k x_k\left(\hat{t}, t^+\right) + O\left(\varepsilon^m\right) \tag{C.5}$$

where t^+ will be substituted by a series expansion (and neglecting the $O\left(\varepsilon^m\right)$ terms) as

$$t^+ = \left(1 + \sum_{k=1}^{m-1} \varepsilon^k \omega_k\right) t \tag{C.6}$$

where ω_k are constants. The time derivative now becomes

$$\frac{d}{dt} = \varepsilon \frac{\partial}{\partial \hat{t}} + \left(1 + \sum_{k=1}^{m-1} \varepsilon^k \omega_k\right) \frac{\partial}{\partial t^+} \tag{C.7}$$

Equations (C.4, C.5, C.7) transform (C.1) into a partial differential equation. Since the exact solution of the damped harmonic oscillator (C.2) depend explicitly on the variables ε, t, εt, $\varepsilon^2 t$,... another possibility is to consider the new time variables

$$t_k = \varepsilon^k t \qquad k = 0, 1, 2, \ldots \tag{C.8}$$

and a uniformly valid asymptotic expansion

$$x\left(t,\varepsilon\right) = \sum_{k=0}^{m-1} \varepsilon^k x_k\left(t_1, \ldots, t_m\right) + O\left(\varepsilon^m\right) \tag{C.9}$$

and the time derivative

$$\frac{d}{dt} = \sum_{k=0}^{m} \varepsilon^k \frac{\partial}{\partial t_k} \tag{C.10}$$

Now we give details on this last approach considering only two timescales.

C.0.2 Two-scale Expansion

We assume that the solution of (C.1) can be well (uniformly) approximated by the two-scale expansion

$$x(t) = x_0(t_0, t_1) + \varepsilon x_1(t_0, t_1) + O\left(\varepsilon^2\right) \tag{C.11}$$

where both t_0, t_1 are timescales, defined as

$$t_0 = t, \quad t_1 = \varepsilon t \tag{C.12}$$

Now we turn our attention to the time derivatives

$$\begin{aligned} \frac{dx}{dt} &= \frac{\partial x_0}{\partial t_0}\frac{dt_0}{dt} + \frac{\partial x_0}{\partial t_1}\frac{dt_1}{dt} + \varepsilon\left[\frac{\partial x_1}{\partial t_0}\frac{dt_0}{dt} + \frac{\partial x_1}{\partial t_1}\frac{dt_1}{dt}\right] + O\left(\varepsilon^2\right) = \\ &= \left(\frac{\partial x_0}{\partial t_0} + \varepsilon\frac{\partial x_1}{\partial t_0}\right) + \varepsilon\frac{\partial x_0}{\partial t_1} + O\left(\varepsilon^2\right) \end{aligned} \tag{C.13}$$

Using the differential operators

$$D_0 = \frac{\partial}{\partial t_0}, \quad D_1 = \frac{\partial}{\partial t_1} \tag{C.14}$$

time differentiation can be written as

$$\frac{d}{dt} = D_0 + \varepsilon D_1 + O\left(\varepsilon^2\right) \tag{C.15}$$

and similarly

$$\frac{d^2}{dt^2} = D_0^2 + 2\varepsilon D_0 D_1 + O\left(\varepsilon^2\right) \tag{C.16}$$

Substituting (C.15) and (C.16) into (C.1) and equating like powers of ε one obtains

$$D_0^2 x_0(t_0, t_1) + x_0(t_0, t_1) = 0 \tag{C.17}$$

$$D_0^2 x_1(t_0, t_1) + x_1(t_0, t_1) = F(x, \dot{x}) \tag{C.18}$$

Solving (C.17) for $x_0(t_0, t_1)$ yields

$$x_0(t_0, t_1) = A(t_1)\, e^{it_0} + \bar{A}(t_1)\, e^{-it_0} \tag{C.19}$$

Then we substitute this solution into (C.18) and eliminate the secular terms which would give rise to nonperiodic terms. $A(t_1)$ can be expressed in a polar form (where $\alpha(t_1)$ is the amplitude and $\beta(t_1)$ is the phase)

$$A(t_1) = \frac{1}{2}\alpha(t_1)\, e^{i\beta(t_1)} \tag{C.20}$$

then substituting into the equation that would eliminate the secular terms and separating the real and imaginary parts results in two ordinary differential equations describing the evolution of the amplitude and phase.

C.1 Method of Krylov-Bogoliubov-Mitropolsky

Here we introduce a method to get an approximate solution to the second order nonlinear differential equation containing a small parameter ε

$$\ddot{x} + x = F(x, \dot{x}, \varepsilon) \tag{C.21}$$

$$F(x, \dot{x}, 0) = 0 \tag{C.22}$$

The method was developed by Krylov and Bogoliubov (1937) and mathematically justified by Bogoliubov and Mitropolsky (1963). Several examples can be found in Rand (1994), Mickens (1996) and Nayfeh (1981).

When $\varepsilon = 0$ the solution to (C.21) is given by

$$x(t) = r\cos(t + \phi) \tag{C.23}$$

and its derivative

$$\dot{x}(t) = -r\sin(t + \phi) \tag{C.24}$$

For small ε the solution is assumed to have the form

$$x(t) = r(t)\cos(t + \phi(t)) \tag{C.25}$$

where r and ϕ are slowly varying functions of t. Differentiating (C.25) wrt. the nondimensional time and introducing $\theta = t + \phi$ yields

$$\dot{x} = \dot{r}\cos\theta - r\sin\theta - r\dot{\phi}\sin\theta \tag{C.26}$$

Then we impose the condition

$$\dot{r}\cos\theta - r\dot{\phi}\sin\theta = 0 \tag{C.27}$$

so that the derivative has the same form as (C.24)

$$\dot{x} = -r\sin\theta \tag{C.28}$$

and differentiate (C.28) once again

$$\ddot{x} = -\dot{r}\sin\theta - r\cos\theta - r\dot{\phi}\cos\theta \tag{C.29}$$

Substituting into equation (C.21)

$$\dot{r}\sin\theta + r\dot{\phi}\cos\theta = -F\left(r\cos\theta, -r\sin\theta, \varepsilon\right) \tag{C.30}$$

Multiplying (C.27) by $\cos\theta$, equation (C.30) by $\sin\theta$ and adding gives

$$\dot{r} = -F\left(r\cos\theta, -r\sin\theta, \varepsilon\right)\sin\theta \tag{C.31}$$

Similarly, multiplying (C.27) by $\sin\theta$, equation (C.30) by $\cos\theta$ and subtracting gives

$$\dot{\phi} = -\frac{1}{r}F\left(r\cos\theta, -r\sin\theta, \varepsilon\right)\cos\theta \tag{C.32}$$

Since we assumed r and ϕ to be slowly varying, we can average (C.31, C.32) over one cycle as θ goes from 0 to 2π (this also corresponds to replacing $F\cos\theta$ and $F\sin\theta$ with the first term in their Fourier expansion).

With the new quantities

$$S\left(r\right) = \frac{1}{2\pi}\int_0^{2\pi} F\left(r\cos\theta, -r\sin\theta, \varepsilon\right)\sin\theta d\theta \tag{C.33}$$

$$C\left(r\right) = \frac{1}{2\pi}\int_0^{2\pi} F\left(r\cos\theta, -r\sin\theta, \varepsilon\right)\cos\theta d\theta \tag{C.34}$$

equations (C.31, C.32) thus become

$$\dot{r} = -S\left(r\right) \tag{C.35}$$

$$\dot{\phi} = -\frac{C\left(r\right)}{r} \tag{C.36}$$

C.1.1 KBM for Forced Nonlinear Oscillators

Here we consider the forced oscillator

$$\ddot{x} + x = F(x, \dot{x}, \varepsilon) + A\cos\omega t \tag{C.37}$$

$$F(x, \dot{x}, 0) = 0 \tag{C.38}$$

For small ε the solution is assumed to have the form

$$x(t) = r(t)\cos(\omega t + \phi(t)) \tag{C.39}$$

where r and ϕ are again assumed to be slowly varying functions of t. Differentiating (C.39) and introducing $\theta = \omega t + \phi$ yields

$$\dot{x} = -\omega r\sin\theta + \dot{r}\cos\theta - r\dot{\phi}\sin\theta \tag{C.40}$$

Again we impose the condition

$$\dot{r}\cos\theta - r\dot{\phi}\sin\theta = 0 \tag{C.41}$$

and differentiate the resulting

$$\dot{x} = -\omega r\sin\theta \tag{C.42}$$

once again

$$\ddot{x} = -\omega\dot{r}\sin\theta - \omega^2 r\cos\theta - \omega r\dot{\phi}\cos\theta \tag{C.43}$$

Substituting into equation (C.37)

$$\left(1-\omega^2\right) r\cos\theta - \omega\dot{r}\sin\theta - \omega r\dot{\phi}\cos\theta = F(r\cos\theta, -r\sin\theta, \varepsilon) + A\cos(\theta - \phi) \tag{C.44}$$

Multiplying (C.41) by $-\omega\cos\theta$, equation (C.44) by $\sin\theta$ and adding results

$$\left(1-\omega^2\right) r\cos\theta\sin\theta - \omega\dot{r} = F(r\cos\theta, -r\sin\theta, \varepsilon)\sin\theta + A\cos(\theta-\phi)\sin\theta \tag{C.45}$$

while multiplying (C.41) by $\omega \sin\theta$, equation (C.44) by $\cos\theta$ and subtracting yields

$$\left(1-\omega^2\right) r\cos^2\theta - \omega r\dot{\phi} = F\left(r\cos\theta, -r\sin\theta, \varepsilon\right)\cos\theta + A\cos\left(\theta-\phi\right)\cos\theta \quad \text{(C.46)}$$

Averaging equations (C.45, C.46) leads to

$$-\omega\dot{r} - S\left(r\right) = \frac{A}{2}\sin\phi \quad \text{(C.47)}$$

$$\frac{r}{2}\left(1-\omega^2\right) - \omega r\dot{\phi} - C\left(r\right) = \frac{A}{2}\cos\phi \quad \text{(C.48)}$$

where $S\left(r\right)$ and $C\left(r\right)$ are given in (C.33, C.34).

Also note, that (C.47, C.48) reduce to (C.35, C.36) when there is no forcing, that is

$$A = 0, \qquad \omega = 1 \quad \text{(C.49)}$$

Appendix D

Proof of Root Location

First, we recall (see for example Churchill, 1989)

Theorem D.1. *(Rouché): Let $f(\lambda)$ and $g(\lambda)$ be analytic functions in the simply connected domain D. If $f(\lambda)$ has no zeros on a closed simple contour C and the inequality*

$$|f(\lambda) - g(\lambda)| < |g(\lambda)| \tag{D.1}$$

also holds on this contour, then $f(\lambda)$ and $g(\lambda)$ have the same number of zeros inside C (counting multiplicity).

Now we prove

Theorem D.2. *Below the lower envelope of the family of curves (the solid curve in Figure 6.1) given by (6.18, 6.19) the equation $\lambda^2 + 2\zeta\lambda + (1+p) - pe^{-\lambda\tau} = 0$ has no roots in the complex right half plane.*

Proof. We define $f(\lambda) = \lambda^2 + 2\zeta\lambda + (1+p) - pe^{-\lambda\tau}$ and $g(\lambda) = \lambda^2 + 2\zeta\lambda + 1$. $g(\lambda) = 0$ has only two roots (located in the left half plane)

$$\lambda_{1,2} = -\zeta \pm i\sqrt{1-\zeta^2} \tag{D.2}$$

In the following we show that for small p the inequality (D.1), that is

$$\left|p(1-\mathrm{e}^{-\lambda\tau})\right| < \left|\lambda^2 + 2\zeta\lambda + 1\right| \tag{D.3}$$

holds on the contour shown in Figure D.1. To this end we show that $\left|1-\mathrm{e}^{-\lambda\tau}\right|$

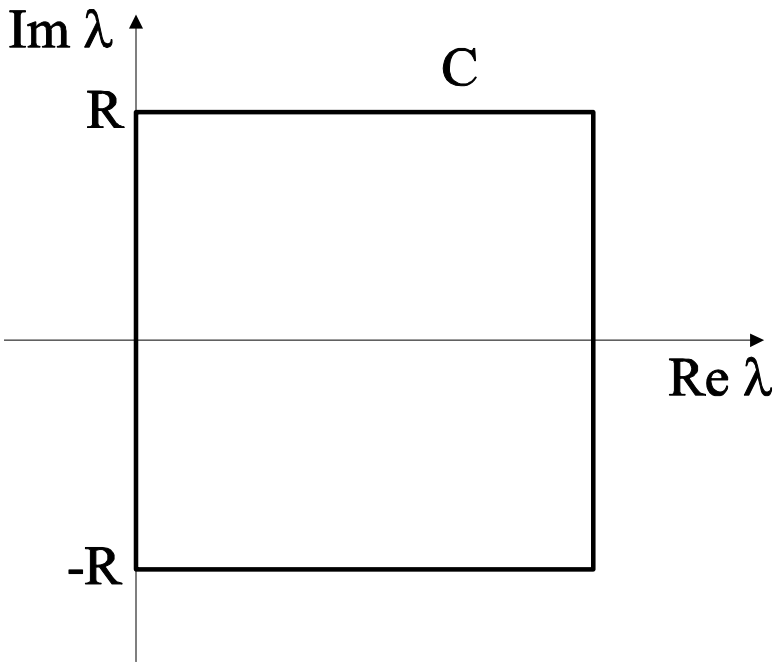

Figure D.1: The closed contour C

has a maximum and $|\lambda^2 + 2\zeta\lambda + 1|$ is strictly positive on C. Then p can be chosen such a way that (D.3) holds.

The vertical lines can be parametrized as

$$V = \{\lambda |\, \lambda = R\,(a + ibt)\,, a \in \{0,1\}\,, b \in \{-1,1\}\,, t \in [0,1]\} \tag{D.4}$$

and the horizontal ones as

$$H = \{\lambda |\, \lambda = R\,(t + ib)\,, b \in \{-1,1\}\,, t \in [0,1]\} \tag{D.5}$$

Then

$$\left|1-e^{\lambda\tau}\right|_H^2=\left(1-e^{-aR\tau}\cos\left(bR\tau t\right)\right)^2+e^{-2aR\tau}\sin^2\left(bR\tau t\right)=$$

$$=1+e^{-2aR\tau}-2e^{-aR\tau}\cos\left(bR\tau t\right) \tag{D.6}$$

and so

$$\max\left|1-\mathrm{e}^{\lambda\tau}\right|_V=\max\sqrt{1+e^{-2aR\tau}+2e^{-aR\tau}}=\max\left(1+e^{-aR\tau}\right)=2 \tag{D.7}$$

Also

$$\left|1-e^{\lambda\tau}\right|_H^2=\left(1-e^{-R\tau t}\cos\left(bR\tau\right)\right)^2+e^{-2R\tau t}\sin^2\left(bR\tau\right)=$$

$$=1+e^{-2R\tau t}-2e^{-R\tau t}\cos\left(bR\tau\right) \tag{D.8}$$

and

$$\max\left|1-\mathrm{e}^{\lambda\tau}\right|_H=\max\sqrt{1+e^{-2R\tau t}+2e^{-R\tau t}}=\max\left(1+e^{-R\tau t}\right)=2 \tag{D.9}$$

Now we show that $|\lambda^2+2\zeta\lambda+1|$ is positive on C as $R\to\infty$. On the vertical lines

$$\left|\lambda^2+2\zeta\lambda+1\right|_V^2=\left(1+R^2\left(a^2-t^2\right)+2aR\zeta\right)^2+4R^2t^2\left(aR+\zeta\right)^2 \tag{D.10}$$

The second term is zero if $t=0$. But the first term is then

$$\left(1+a^2R^2+2aR\zeta\right)^2>0 \tag{D.11}$$

On the horizontal lines

$$\left|\lambda^2+2\zeta\lambda+1\right|_H^2=\left(1+R^2\left(t^2-1\right)+2R\zeta t\right)^2+4R^2\left(Rt+\zeta\right)^2 \tag{D.12}$$

The second term is zero if $t=-\zeta/R$. In this case, the first term is

$$\left(1-R^2-\zeta^2\right)^2>0 \tag{D.13}$$

Since $\lambda^2 + 2\zeta\lambda + 1$ does not have zeros in the right half plane neither does $\lambda^2 + 2\zeta\lambda + (1 + p) - p\mathrm{e}^{-\lambda\tau}$.

Then by continuity, below the stability boundary all roots are located in the left half complex plane. □

References

Abarbanel, H. D. I. 1996. *Analysis of Observed Chaotic Data*. Springer Verlag.

Albrecht, P. 1961. New Developments in the Theory of the Metal-Cutting Process: Part II The Theory of Chip Formation. *Transactions of the American Society of Mechanical Engineers - Journal of Engineering for Industry*, **83**(4), 557–571.

Albrecht, P. 1965. Dynamics of the Metal-Cutting Process. *Journal of Engineering for Industry*, **87**, 429–441.

Arnold, R. N. 1946. The Mechanism of Tool Vibration in the Cutting of Steel. *Proceedings of The Institution of Mechanical Engineers*, **154**(4), 261–284.

Avellar, K. E., & Hale, J. K. 1980. On the Zeroes of Exponential Polynomials. *Journal of Mathematical Analysis and Applications*, **73**, 434–452.

Badrakhan, F. 1988. Dynamic Analysis of Yielding and Hysteretic Systems by Polynomial Approximation. *Journal of Sound and Vibration*, **125**(1), 24–42.

Balachandran, B. 2001. Nonlinear Dynamics of Milling Processes. *Philosophical Transactions of the Royal Society*, **359**, 793–819.

Ballio, G. 1968. Elastic-Plastic Dynamic Behavior of a Beam Column Model. *Meccanica*, **3**, 177–186.

Ballio, G. 1970. On the Dynamic Behavior of an Elastoplastic Oscillator (Experimental Investigation and Theoretical Developments). *Meccanica*, **5**, 85–97.

Batzer, S. A., Gouskov, A. M., & Voronov, S. A. 1999. Modeling the Vibratory Drilling Process. *Pages 1–8 of: Preceedings of the 17th ASME Biennial Conference on Vibration and Noise.*

Bellman, R., & Cooke, K. L. 1963. *Differential-Difference Equations.* Mathematics in Science and Engineering, vol. 6. Academic Press.

Berger, B. S., Rokni, M., & Minis, I. 1992. The Nonlinear Dynamics of Metal Cutting. *International Journal of Engineering Science*, **30**(10), 1433–1440.

Berger, B. S., Minis, I., Chen, Y. H., Chavali, A., & Rokni, M. 1995. Attractor Embedding in Metal Cutting. *Journal of Sound and Vibration*, **184**(5), 936–942.

Block, H. D. 1960. Periodic Solutions of Forced Systems Having Hysteresis. *IRE Transactions on Circuit Theory*, 423–431.

Bogoliubov, N. N., & Mitropolsky, J. A. 1963. *Asymptotical Methods in the Theory of Nonlinear Oscillations (in Russian).* Moscow: State Press for Physics and Mathematical Literature.

Bolotin, V. V. 1963. *Nonconservative Problems of the Theory of Elastic Stability.* New York: The MacMillan Company.

Bolotin, V. V. 1964. *The Dynamic Stability of Elastic Systems.* San Francisco: Holden-Day, Inc.

Bouc, R. 1967. Forced Vibrations of a Mechanical System with Hysteresis. *Page 315 of: Proceedings of the Fourth Conference on Nonlinear Oscillations.* Prague: Czechoslovak Academy of Sciences.

Bukkapatnam, S. T. S. 1999. Compact Nonlinear Signal Representation in Machine Tool Operations. *In: Proceedings of the 1999 ASME Design Engineering Technical Conferences.*

Bukkapatnam, S. T. S., Lakhtakia, A., & Kumara, S. R. T. 1995a. Analysis of Sensor Signals Shows Turning on a Lathe Exhibits Low-Dimensional Chaos. *Physical Review E*, **52**(3), 2375–2387.

Bukkapatnam, S. T. S., Lakhtakia, A., Kumara, S. R. T., & Satapathy, G. 1995b (November). Characterization of Nonlinearity of Cutting Tool Vibrations and Chatter. *Pages 1207–1223 of: American Society of Mechanical Engineers Symposium on Intelligent Manufacturing and Material Processing*, vol. 69-2.

Burns, T. J., & Davies, M. A. 1997. Nonlinear Dynamics Model for Chip Segmentation in Machining. *Physical Review Letters*, **79**(3), 447–450.

Campbell, S. A., Bélair, J., Ohira, T., & Milton, J. 1995. Complex Dynamics and Multistability in a Damped Oscillator with Delayed Negative Feedback. *Journal of Dynamics and Differential Equations*, **7**, 213–236.

Casal, A., & Freedman, M. 1980. A Poincare-Lindstedt Approach to Bifurcation Problems for Differential-Delay Equations. *IEEE Transactions on Automatic Control*, **AC-25**(5), 967–973.

Caughey, T. K. 1960. Sinusoidal Excitation of a System with Bilinear Hysteresis. *Journal of Applied Mechanics*, **27**, 640–643.

Chen, S.-G., Ulsoy, A. G., & Koren, Y. 1997. Computational Stability Analysis of Chatter in Turning. *Journal of Manufacturing Science and Engineering*, **119**, 457–460.

Chiriacescu, S. T. 1990. *Stability in the Dynamics of Metal Cutting*. Elsevier.

Chu, D., & Moon, F. C. 1983. Dynamic Instabilities in Magnetically Levitated Models. *Journal of Applied Physics*, **54**(3), 1619–1625.

Churchill, R. V., & Brown, J. W. 1989. *Complex Variables and Applications*. McGraw-Hill.

Davies, M. A., & Burns, T. J. 2001. Thermomechanical Oscillations in Material Flow During High-Speed Machining. *Philosophical Transactions of the Royal Society*, **359**, 821–846.

Davies, M. A., Chou, Y. S., & Evans, C. J. 1996. On Chip Morphology, Tool Wear and Cutting Mechanics in Finish Hard Turning. *Annals of the CIRP*, **45**(1).

Doi, M., & Ohhashi, M. 1992. A Study on Parametric Vibration in Machining of Hard Cutting Metals. *International Journal of the Japanese Society of Precision Engineers*, **26**(3), 195–200.

Doi, S., & Kato, S. 1956. Chatter Vibration of Lathe Tools. *Transactions of the American Society of Mechanical Engineers*, **78**(5), 1127–1134.

Driver, R. D. 1977. *Ordinary and Delay Differential Equations*. Springer-Verlag.

El'sgol'ts, L. E., & Norkin, S. B. 1973. *Introduction to the Theory and Application of Differential Equations with Deviating Arguments*. Mathematics in Science and Engineering, vol. 105. Academic Press.

Engelborghs, K., & Roose, D. 1999. Numerical Computation of Stability and Detection of Hopf Bifurcations of Steady State Solutions of Delay Differential Equations. *Advances in Computational Mathematics*, **10**, 271–289.

Ernst, H., & Merchant, M. E. 1941. *Surface Treatments of Metals*. American Society of Metals. Chap. Chip Formation, Friction and High Quality Machined Surfaces, page 299.

Fofana, M. S. 1993. *Delay Dynamical Systems with Applications to Machine-Tool Chatter*. Ph.D. thesis, University of Waterloo, Department of Civil Engineering.

Fu, C. C. 1969. Dynamic Stability of an Impact System Connected with Rock Drilling. *Journal of Applied Mechanics*, 743–749.

Gambaudo, J. M. 1985. Perturbation of a Hopf Bifurcation by an External Time-Periodic Forcing. *Journal of Differential Equations*, **57**, 172–199.

Grabec, I. 1986. Chaos Generated by the Cutting Process. *Physics Letters A*, **117**(8), 384–386.

Grabec, I. 1988. Chaotic Dynamics of the Cutting Process. *International Journal of Machine Tools and Manufacture*, **28**(1), 19–32.

Gradišek, J., Govekar, E., & Grabec, I. 1998. Time Series Analysis in Metal Cutting: Chatter versus Chatter-Free Cutting. *Mechanical Systems and Signal Processing*, **12**(6), 839–854.

Guckenheimer, J., & Holmes, P. J. 1990. *Nonlinear Oscillations, Dynamical Systems, and Bifurcations of Vector Fields*. Applied Mathematical Sciences, vol. 42. Springer-Verlag, NY.

Hahn, R. S. 1953. Metal-Cutting Chatter and Its Elimination. *Transactions of the American Society of Mechanical Engineers*, **75**(August), 1073–1080.

Hale, J. K. 1977. *Theory of Functional Differential Equations*. Applied Mathematical Sciences, vol. 3. New York: Springer-Verlag.

Hale, J. K., & Lunel, S. M. V. 1993. *Introduction to Functional Differential Equations*. Applied Mathematical Sciences, no. 99. New York: Springer Verlag.

Hanna, N. H., & Tobias, S. A. 1969. The Non-Linear Dynamic Behaviour of a Machine Tool Structure. *International Journal of Machine Tool Design Research*, **9**, 293–307.

Hanna, N. H., & Tobias, S. A. 1974. A Theory of Nonlinear Regenerative Chatter. *Transactions of the American Society of Mechanical Engineers - Journal of Engineering for Industry*, **96**(1), 247–255.

Hassard, B. D., Kazarinoff, N. D., & Wan, Y. H. 1981. *Theory and Applications of Hopf Bifurcations*. London Mathematical Society Lecture Note Series, vol. 41.

Hastings, W. F., Mathew, P., & Oxley, P. L. B. 1980. A Machining Theory for Predicting Chip Geometry, Cutting Forces etc. from Work Material Properties and Cutting Conditions. *Proceedings of the Royal Society of London*, **371A**, 569–587.

Herrmann, G., & Jong, I.-C. 1965. On the Destabilizing Effect of Damping in Nonconservative Elastic Systems. *Transactions of the ASME*, 592–597.

Hikihara, T., & Moon, F. C. 1994. Chaotic Levitated Motion of a Magnet Supported by Superconductor. *Physics Letters A*, **191**, 279–284.

Hooke, C. J., & Tobias, S. A. 1963. Finite Amplitude Instability-A New Type of Chatter. *Pages 97–109 of: Proceedings of the Fourth International MTDR Conference*. Manchester: Permagon Press.

Hu, H., Dowell, E. H., & Virgin, L. N. 1998. Resonances of a Harmonically Forced Duffing Oscillator with Time Delay State Feedback. *Nonlinear Dynamics*, **15**, 311–327.

Insperger, T. 1999. *Regenerative Vibrations of Lathes and Their Stability (in Hungarian)*. M.Phil. thesis, Technical University of Budapest.

Iwan, W. D. 1965. The Steady-State Response of a Two-Degree-of-Freedom Bilinear Hysteretic System. *Journal of Applied Mechanics*, 151–156.

Johnson, M., & Moon, F. C. 2001. Nonlinear Techniques to Characterize Prechatter and Chatter Vibrations in the Machining of Metals. *International Journal of Bifurcation and Chaos*, **11**(2), 449–467.

Johnson, M. A. 1996. *Nonlinear Differential Equations with Delay as Models for Vibrations in the Machining of Metals*. Ph.D. thesis, Cornell University.

Johnson, M. A., & Moon, F. C. 1999. Experimental Characterization of Quasiperiodicity and Chaos in a Mechanical System with Delay. *International Journal of Bifurcation and Chaos*, **9**, 49–65.

Kalmár-Nagy, T., Stépán, G., & Moon, F. C. Regenerative Machine Tool Vibrations. *Dynamics of Continuous, Discrete and Impulsive Systems*.

Kalmár-Nagy, T., Pratt, J. R., Davies, M. A., & Kennedy, M. D. 1999. Experimental and Analytical Investigation of the Subcritical Instability in Turning. *In: Proceedings of the 1999 ASME Design Engineering Technical Conferences*. DETC99/VIB-8060.

Kalmár-Nagy, T., Stépán, G., & Moon, F. C. 2001. Subcritical Hopf Bifurcation in the Delay Equation Model for Machine Tool Vibrations. *Nonlinear Dynamics*.

Kalpakjian, S. 1984. *Manufacturing Processes for Engineering Materials*. Second edn. Addison-Wesley.

Kiusalaas, J., & Davis, H. E. 1970. On the Stability of Elastic Systems Under Retarded Follower Forces. *International Journal of Solids and Structures*, **6**(4), 399–409.

Kobori, T., Minai, R., & Suzuki, Y. 1976. Stochastic Seismic Response of Hysteretic Structures. *Bulletin of the Disaster Prevention Research Institute*, **26**(1), 55–70.

Kolmanovskii, V. B., & Nosov, V. R. 1986. *Stability of Functional Differential Equations*. Mathematics in Science and Engineering, vol. 180. Academic Press.

Komanduri, R., & Brown, R. H. 1981. On the Mechanics of Chip Segmentation in Machining. *Journal of Engineering for Industry*, **103**, 33–51.

Kondo, Y., Kawano, O., & Hisayoshi, S. 1981. Behavior of Self-Excited Chatter

Due to Multiple Regenerative Effects. *Transactions of the American Society of Mechanical Engineers - Journal of Engineering for Industry*, **103**(3), 324–329.

Krasnoselskii, M. A., & Pokrovskii, A. V. 1989. *Systems with Hysteresis*. Berlin: Springer-Verlag.

Krylov, N., & Bogoliubov, N. 1943. *Introduction to Nonlinear Mechanics*. Princeton, NJ: Princeton University Press.

Kuang, Y. 1993. *Delay Differential Equations with Applications in Population Dynamics*. Mathematics in Science and Engineering, no. 191. Academic Press.

Kudinov, V. A., Klyuchnikov, A. V., & Shustikov, A. D. 1978. Experimental Investigation of the Non-Linear Dynamic Cutting Process (in Russian). *Stanki i instrumenti*, **11**, 11–13.

Kuznetsov, Y. A. 1998. *Elements of Applied Bifurcation Theory*. New York: Springer.

Landberg, P. 1956. Vibrations Caused by Chip Formation. *Microtecnic*, **10**(5), 219–228.

Lee, E. H., & Shaffer, B. W. 1951. The Theory of Plasticity Applied to a Problem of Machining. *Journal of Applied Mechanics*, **18**(4), 405.

Lin, J. S., & Weng, C. I. 1991. Nonlinear Dynamics of the Cutting Process. *International Journal of Mechanical Sciences*, **33**(8), 645–657.

Litak, G., Warmiński, J., & Lipski, J. 1997. Self-Excited Vibrations in Cutting Process. *Pages 193–198 of: 4th Conference on Dynamical Systems - Theory and Applications*.

Mahfouz, I. A., & Badrakhan, F. 1990a. Chaotic Behavior of some Piecewise-Linear Systems, Part I: Systems with Set-Up Springs or with Unsymmetric Elasticity. *Journal of Sound and Vibration*, **143**, 255–288.

Mahfouz, I. A., & Badrakhan, F. 1990b. Chaotic Behavior of some Piecewise-Linear Systems, Part II: Systems with Clearance. *Journal of Sound and Vibration*, **143**, 289–328.

Merchant, M. E. 1945. Mechanics of the Metal Cutting Process. I. Orthogonal Cutting and a Type 2 Chip. *Journal of Applied Physics*, **16**(5), 267–275.

Mickens, R. E. 1996. *Oscillations in Planar Dynamic Systems*. Singapore: World Scientific Publishing Co.

Milisavljevich, B., Zeljkovic, M., & Gatalo, R. 2000. The Nonlinear Model of a Chatter and Bifurcation. *Pages 391–398 of: Proceedings of the 5th Engineering Systems Design and Analysis Conference*. ASME.

Minis, I., & Berger, B. S. 1998. *Modelling, Analysis, and Characterization of Machining Dynamics*. John Wiley and Sons. Pages 125–163.

Moon, F. C. 1994. Chaotic Dynamics and Fractals in Material Removal Processes. *Pages 25–37 of:* Thompson, J.M.T., & Bishop, S.R. (eds), *Nonlinearity and Chaos in Engineering Dynamics*. John Wiley and Sons.

Moon, F. C. 2000. *Advanced Dynamics*. New York: John Wiley and Sons.

Moon, F. C., & Abarbanel, H. D. I. 1995. Evidence for Chaotic Dynamics in Metal Cutting, and Classification of Chatter in Lathe Operations. *Pages 11–12,28–29 of:* Moon, F. C. (ed), *Summary Report of a Workshop on Nonlinear*

Dynamics and Material Processing and Manufacturing, organized by the Institute for Mechanics and Materials, held at the University of California, San Diego.

Moon, F. C., & Callaway, D. 1997. Chaotic Dynamics in Scribing Polycarbonate Plates with a Diamond Cutter. *In: IUTAM Symp. On New Application of Nonlinear and Chaotic Dynamics.*

Moon, F. C., & Johnson, M. A. 1998. Nonlinear Dynamics and Chaos in Manufacturing Processes. *In:* Moon, F. C. (ed), *Dynamics and Chaos in Manufacturing Processes.* John Wiley and Sons.

Moon, F. C., & Kalmár-Nagy, T. 2001. Nonlinear Models for Complex Dynamics in Cutting Materials. *Philosophical Transactions of the Royal Society*, **359**, 695–711.

Nayfeh, A., Chin, C., & Pratt, J. 1998. Applications of Perturbation Methods to Tool Chatter Dynamics. *In:* Moon, F. C. (ed), *Dynamics and Chaos in Manufacturing Processes.* John Wiley and Sons.

Nayfeh, A. H. 1981. *Introduction to Perturbation Techniques.* New York: John Wiley and Sons.

Nayfeh, A. H., & Mook, D. T. 1979. *Nonlinear Oscillations.* John Wiley and Sons.

Nayfeh, S. A., & Nayfeh, A. H. 1993. Nonlinear Interactions Between Two Widely Spaced Modes - External Excitation. *International Journal of Bifurcation and Chaos*, **3**, 417–427.

Nigm, M. M., Sadek, M. M., & Tobias, S. A. 1977a. Determination of Dynamic

Cutting Coefficients from Steady State Cutting Data. *International Journal of Machine Tool Design Research*, **17**, 19.

Nigm, M. M., Sadek, M. M., & Tobias, S. A. 1977b. Dimensional Analysis of the Steady State Orthogonal Cutting Process. *International Journal of Machine Tool Design Research*, **17**, 1–18.

Otani, S. 1981. Hysteresis Models of Reinforced Concrete for Earthquake Response Analysis. *Journal of the Faculty of Engineering, the University of Tokyo*, **36**, 125–159.

Oxley, P. L. B. 1989. *Mechanics of Machining: An Analytical Approach to Assessing Machinability.* New York: John Wiley and Sons.

Oxley, P. L. B., & Hastings, W. F. 1977. Predicting the Strain Rate in the Zone of Intense Shear in which the Chip is Formed in Machining from the Dynamic Flow Stress Properties of the Work Material and the Cutting Conditions. *Proceedings of the Royal Society of London*, **356A**, 395–410.

Palkovics, L., & Venhovens, P. J. Th. 1992. Investigation on Stability and Possible Chaotic Motions in the Controlled Wheel Suspension System. *Vehicle System Dynamics*, **21**(5), 269–296.

Panovko, Y. G., & Gubanova, I. I. 1965. *Stability And Oscillations of Elastic Systems.* New York: Consultants Bureau.

Peters, J., Vanherck, P., & Van Brussel, H. 1972. The Measurement of the Dynamic Cutting Coefficient. *Annals of the CIRP*, **21**, 129–136.

Piispanen, V. 1937. Lastunmuodostumisen Teoriaa (Theory of Chip Formation). *Teknillinen Aikakauslehti*, **27**(9), 315–322.

Plaut, R. H., & Hsieh, J.-C. 1986. *Chaos in a Mechanism with Time Delays Under Parametric and External Excitation.* Tech. rept. Virginia Polytechnic Institute and State University.

Poddar, B., Moon, F. C., & Mukherjee, S. 1988. Chaotic Motion of an Elastic Plastic Beam. *Journal of Applied Mechanics*, **55**, 185–189.

Pontryagin, L. S. 1955. On the Zeroes of Some Elementary Transcendental Functions. *American Mathematical Society Translations*, **1**, 95–110.

Pontryagin, L. S. 1958. On the Zeroes of Some Transcendental Functions. *American Mathematical Society Translations*, **8**, 19–20.

Pratap, R., Mukherjee, S., & Moon, F. C. 1994a. Dynamic Behavior of a Bilinear Hysteretic Elasto-Plastic Oscillator, Part I: Free Oscillations. *Journal of Sound and Vibration*, **172**(3), 321–337.

Pratap, R., Mukherjee, S., & Moon, F. C. 1994b. Dynamic Behavior of a Bilinear Hysteretic Elasto-Plastic Oscillator, Part II: Oscillations under Periodic Impulse Forcing. *Journal of Sound and Vibration*, **172**(3), 339–358.

Pratt, J. 1996. *Vibration Control for Chatter Suppression with Application to Boring Bars.* Ph.D. thesis, Virginia Polytechnic Institute and State University.

Pratt, J., & Nayfeh, A. H. 1996. Experimental Stability of a Time-Delay System. *In: Proc. 37th AIAA/ASME/ASCE/AHS/ACS Structures, Structural Dynamics, and Materials Conf.*

Pratt, J. R., Davies, M. A., Evans, C. J., & Kennedy, M. D. 1999a. Dynamic Interogation of a Basic Cutting Process. *Annals of the CIRP*, **48**(1), 39–42.

Pratt, J. R., Davies, M. A., Kennedy, M. D., & Kalmár-Nagy, T. 1999b. Predictive Modeling of Nonlinear Regenerative Chatter Via Measurement, Analysis and Simulation. *Pages 1–10 of: Proceedings of ASME-1999 International Mechanical Engineering Conference and Exposition.*

Rahman, S. 1991. *A Markov Model for Local and Global Damage Indices in Seismic Analysis.* Ph.D. thesis, Cornell University.

Rand, R. H. 1994. *Topics in Nonlinear Dynamics with Computer Algebra.* Gordon and Breach Science Publishers.

Rand, R. H., & Armbruster, D. 1987. *Perturbation Methods, Bifurcation Theory and Computer Algebra.* New York: Springer-Verlag.

Reddy, C. K., & Pratap, R. 2000. Equivalent Viscous Damping for a Bilinear Hysteretic Oscillator. *Journal of Engineering Mechanics*, **126**(11), 1189–1196.

Rogers, H. C. 1979. Adiabatic Plastic Deformation. *Ann. Revised Material Sci.*, **9**, 283.

Rubenstein, C. 1983. A Note Concerning the Inadmissibility of Applying the Minimum Work Principle to Metal Cutting. *Journal of Engineering for Industry*, **105**, 294–296.

Saljé, E. 1956. Self-Excited Vibrations of Systems with Two Degrees of Fredom. *Transactions of the ASME*, **78**, 737–748.

Sanchez, N. E., & Nayfeh, A. H. 1990. Prediction of Bifurcations in a Parametrically Excited Duffing Oscillator. *International Journal of Non-linear Mechanics*, **25**(2/3), 163–176.

Saravanja-Fabris, N. 1972. *Nonlinear Stability Analysis of Chatter in Metal Cutting.* M.Phil. thesis, Illinois Institute of Technology.

Saravanja-Fabris, N., & D'Souza, A. F. 1974. Nonlinear Stability Analysis of Chatter in Metal Cutting. *Transactions of the American Society of Mechanical Engineers - Journal of Engineering for Industry*, **96**(2), 670–675.

Shaw, M. C. 1954. *Machining Titanium.* Cambridge, Massachusetts: MIT press.

Shaw, S. W., & Holmes, P. J. 1983. A Periodically Forced Piecewise Linear Oscillator. *Journal of Sound and Vibration*, **90**, 129–155.

Shi, H. M., & Tobias, S. A. 1984. Theory of Finite Amplitude Machine Tool Instability. *International Journal of Machine Tool Design and Research*, **24**(1), 45–69.

Sokolovskii, A. P. 1946. Stiffness in Mechanical Engineering Technology (in Russian). *GNTIML Moscow.*

Stabler, G. V. 1964. *Advances in Machine Tool Design and Research.* Pergamon Press Ltd., Oxford. Chap. The Chip Flow Law and its Consequences, page 243.

Stépán, G. 1989. *Retarded Dynamical Systems: Stability and Characteristic Functions.* Vol. 210. Pitman Research Notes in Mathematics, Longman Scientific and Technical.

Stépán, G. 1997. Delay-Differential Equation Models for Machine Tool Chatter. *Pages 165–191 of:* Moon, F. C. (ed), *Dynamics and Chaos in Manufacturing Processes.* New York: John Wiley and Sons.

Stépán, G. 2001. Modelling Nonlinear Regenerative Effects in Metal Cutting. *Philosophical Transactions of the Royal Society*, **359**, 739–757.

Stépán, G., & Kalmár-Nagy, T. 1997. Nonlinear Regenerative Machine Tool Vibrations. *Pages 1–11 of: Proceedings of the 1997 ASME Design Engineering Technical Conferences, 16th ASME Biennial Conference on Mechanical Vibration and Noise.*

Szakovits, R. J., & D'Souza, A. F. 1976. Metal Cutting Dynamics with Reference to Primary Chatter. *Transactions of the ASME*, **B98**(1), 258–264.

Tanabashi, R. 1956. Studies on the Nonlinear Vibrations of Structures Subjected to Destructive Earthquakes. *In: Proceedings of the Second World Conference on Earthquake Engineering.*

Taylor, F. W. 1907. On the Art of Cutting Metals. *Transactions of the American Society of Mechanical Engineers*, **28**, 31–350.

Tcherniak, D. 1999. The Influence of Fast Excitation on a Continuous System. *Journal of Sound and Vibration*, **227**(2), 343–360.

Thompson, R. A. 1969. The Modulation of Chatter Vibrations. *Journal of Engineering for Industry*, 673–679.

Thompson, W. T. 1993. *Theory of Vibrations with Applications.* Fourth edn. Prentice Hall.

Timoshenko, S., Young, D. H., & Weaver, W. 1974. *Vibration Problems in Engineering.* New York: John Wiley and Sons.

Tlusty, J. 1978. Analysis of the State of Research in Cutting Dynamics. *Annals of the CIRP*, **27**(2), 583–589.

Tlusty, J. 1985. Machine Dynamics. *Chap. 3, pages 48–143 of: Handbook of High-Speed Machining Technology*. London: Chapman and Hall.

Tlusty, J., & Ismail, F. 1981. Basic Non-Linearity in Machining Chatter. *CIRP Annals, Manufacturing Technology*, **30**, 299–304.

Tlusty, J., & Spacek, L. 1954. *Self-Excited Vibrations on Machine Tools (in Czech)*. Prague: Nakl CSAV.

Tobias, S. A. 1965. *Machine Tool Vibration*. London: Blackie and Son Limited.

Tobias, S. A., & Fishwick, W. 1958. The Chatter of Lathe Tools Under Orthogonal Cutting Conditions. *Transactions of the American Society of Mechanical Engineers*, **80**(5), 1079–1088.

Tounsi, N., & Otho, A. 2000. Identification of Machine-Tool-Workpiece System Dynamics. *International Journal of Machine Tools and Manufacture*, **40**, 1367–1384.

Vyas, A., & Shaw, M. C. 1997. Chip Formation When Hard Turning Steel. *Manufacturing Science and Technology*, **2**, 21–28.

Wiercigroch, M., & Budak, E. 2001. Sources of Nonlinearities, Chatter Generation and Suppression in Metal Cutting. *Philosophical Transactions of the Royal Society*, **359**, 663–693.

Wiercigroch, M., & Cheng, A. H-D. 1997. Chaotic and Stochastic Dynamics of Orthogonal Metal Cutting. *Chaos, Solitons & Fractals*, **8**(4), 715–726.

Wiercigroch, M., & Krivtsov, A. M. 2001. Frictional Chatter in Orthogonal Metal Cutting. *Philosophical Transactions of the Royal Society*, **359**, 713–738.

Wiggins, S. 1996. *Introduction to Applied Nonlinear Dynamical Systems and Chaos*. New York: Springer.

Wu, D. W., & Liu, C. R. 1985. An Analytical Model of Cutting Dynamics. Part 1: Model Building. *ASME Journal of Engineering for Industry*, **107**, 107.

Zavodney, L. D., Nayfeh, A. H., & Sanchez, N. E. 1990. Bifurcations and Chaos in Parametrically Excited Sigle-Degree-of-Freedom Systems. *Nonlinear Dynamics*, **1**, 1–21.